PUSHING BOUNDARIES: SPECTRAL IMAGING OF ARCHAEOLOGICAL SMALL FINDS

Heather Robin Christie

BA (Hons.), MA, MLitt

Submitted in fulfilment of the requirements for the

Degree of Doctor of Philosophy

School of Simulation and Visualisation

Glasgow School of Art

January 2019

SCHOOL OF
SIMULATION AND
VISUALISATION
THE GLASGOW
SCHOOL OF ART

ABSTRACT

Archaeologists generally view images and 3D models as objective witnesses to archaeological scholarship and excavation, capturing the subject as seen by human eyes so others can 'see' it for themselves. We employ the newest technology we can afford using prescribed, standardised methods to create as objective an image or visualisation as possible. There is much more to photography and 3D imaging, however, and restricting ourselves in this way severely limits the information we can gather from images. In this thesis, I introduce novel, effective and affordable methods for digitally imaging small, reflective and translucent objects using photography, PTM reflectance transformation imaging, and structure from motion photogrammetry. I focus on glass beads from Iron Age and Early Medieval Scottish contexts. First, I identify regional differences in trade and manufacture of Iron Age and Early Medieval Scottish glass beads using visible-range photographic filters to examine bubble concentrations. Next, I determine the chemical relationships between Iron Age and Early Medieval glass bead collections in Scotland and Anglo-Saxon, Roman, New Kingdom Egyptian, Medieval English, and modern collections using near-ultraviolet and near-infrared photographic filters. Third, I use visible- and non-visible-range filters to greatly increase the success rate of reflectance transformation imaging and structure from motion photogrammetry of glass beads. Finally, I apply all these techniques to non-glass subjects to demonstrate their wider applications. In conclusion, I argue that investigating and deploying novel and affordable imaging techniques in addition to standardised current technologies provides significantly more archaeological data than the current practice of continually adopting new imaging technologies for primarily documentary purposes.

TABLE OF CONTENTS

LIST OF FIGURES

LIST OF TABLES

Thanks are extended to Shinu Abraham, without whom I would not have become interested in beads or archaeology. Thanks in memoriam are due to Alice Pomponio, who taught me so much about anthropology and academia that I continue to hear her advice and enthusiasm. I would not be the archaeologist or academic I am without these two phenomenal women.

Thanks also to colleagues, friends and family who have helped me throughout this process. Elsa Perrucchini, Megan Kasten, Kathleen Clifford, Anouk Busset, Catherine Johnson, Mirian Calvo, Claire Young, Chris Mousdale, Tim Raspin, Chris Stark, Doug Young, Doug MacIntyre, and Gemma Renwick provided immeasurable support, entertainment, and tea, for which I am extremely grateful. I am also grateful to my partner, Jeffrey Lamont, and to George Christie, Lorraine Hurley and the rest of my family for their unending support and advice.

AUTHOR'S DECLARATION

I, Heather Christie declare that the enclosed submission for the degree of Doctor of Philosophy and consisting of a written thesis meets the regulations stated in the handbook for the mode of submission selected and approved by the Research Degrees Sub-Committee.

I declare that this submission:

is my own work, and has not been submitted for any other academic award.
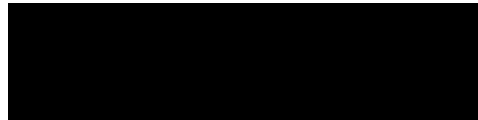
Signed: ████████████████████   Date: 16 May 2019

ACCOMPANYING MATERIALS

USB Drive containing Appendix E: Selection of Example Files and Metadata for this Thesis. This includes 3D models, RTI outputs, and photographs. RTI outputs and 3D models made at certain institutions have been redacted per request.

1   INTRODUCTION

On 19 August 1839, the French government publicly presented Louis Jacques Mandé Daguerre's and Joseph Nicéphore Niépce's technique for permanently fixing images onto copper plates using a camera obscura, one consequence of which was the thorough entanglement of photography-based imaging with the study of the human past (Eder 1945, 227 – 228; Friedman and Ross 2003, 4). Archaeologists first adopted photography in their excavations in the early 1840s and museums quickly joined in, using photography as a method for capturing and displaying pieces that were otherwise inaccessible. Now, little archaeology occurs without photography-based imaging of one kind or another, and there is an increasing emphasis on digital photography and imaging technologies.

The historical entanglement of archaeology and photography has resulted in the limited use of archaeological imaging in the present. Archaeology as a field tends to view most archaeological imaging techniques as documentary tools for recording the archaeological record in a prescribed manner (Boehler and Heinz 1999, 2; Campana 1977, 435; Cookson 1954, 13; Dorrell 1994, 6; Earl et al. 2008; Earl et al. 2010; Howell and Blanc 1995, 1; Mudge et al. 2005; Mudge et al. 2006; Simmons 1969, 2; Wright 1982, 176). Archaeology values apparent objectivity, and champions techniques that it believes result in objective visualisations. These tend to be more expensive, complex technologies that create visualisations closely mimicking that seen by the human eye through standard, prescribed techniques (Conlon 1973, xiii; Cookson 1954, 13; Costall 1997, 50; Dorrell 1989, 7; Howell and Blanc 1995, 1; Shanks 1997; 80; Simmons 1969, 4).

This framing of archaeological imaging as a documentary tool is beneficial to archaeological recording, but it is only a fraction of the possible applications of

archaeological imaging in the field. Photography, reflectance transformation imaging and photogrammetry can support and enhance analysis in addition to serving a purely documentary purpose, for example. Archaeological imaging and its outputs also need not mimic human vision to provide new information about an archaeological subject or collection, as demonstrated in Chapters 4 through 7 of this thesis. We as a discipline have limited our use, and consequently our understanding, of archaeological imaging techniques, largely to our detriment.

This self-imposed limitation contributes to worrying consequences in archaeological imaging. The first is that our over-reliance on standard, objective methodologies often results in a reluctance to explore the full capabilities of the imaging technologies at our disposal. Standard methodologies allow for full comparisons between images or visual representations of archaeological subjects. However, using such techniques on many archaeological subjects does not create informative results due to difficulties such as size, reflection, and diaphaneity. These techniques also fail to realise the full analytical potential of imaging technologies, particularly those seen as less technologically advanced. Our reluctance to deviate from standard techniques therefore often results in a lack of informative visual representations for many objects and ignores the analytical capabilities of archaeological imaging in favour of documentation.

The second worrying by-product of these self-imposed limitations is the privileging of results from projects that can afford the latest new technology over the results of those limited to more affordable techniques (Chapter 2.2.2). Archaeology tends to favour results from techniques seen by the field as more scientific or technologically advanced because we associate those characteristics with objectivity. However, few archaeological project budgets can afford such techniques, or can afford to use such techniques on more than a handful of archaeological subjects. The general bias in

archaeology towards newer and therefore more expensive techniques favours the results of projects with higher budgets and results in the devaluing of research from those without (i.e. the majority of archaeological endeavours).

Perhaps the most concerning consequence of the discipline's current approach to imaging techniques, however, is the omission of certain archaeological subjects from the visual archaeological record because they do not lend themselves well to current imaging methodologies (Chapter 2.2.3). This often includes objects that are small, reflective, translucent, transparent, or a combination of the four. If we do not image these objects, then we do not 'see' them regularly through these images. Consequently, we often unintentionally omit them from our discussions of the past, because we often communicate less about objects without a visual record. Even when such objects are discussed, there is often less available information about them due to a lack of images and visual representations.

In this thesis, I argue for a change in how archaeology uses photography and other digital imaging techniques. First, archaeological imaging is an analytical tool in addition to a documentary one and deviating from standard methods can provide more information than currently available through documentary methods alone. Second, I argue for an increased emphasis on the development of affordable techniques for creating digital representations of archaeological subjects that are otherwise difficult to digitally image. Towards this end, the discipline should strive to exploit readily-available technologies in the search for affordable and informative digital imaging techniques.

To demonstrate the effectiveness of challenging the standards of current imaging techniques, I have conducted four important studies focusing on Iron Age and Early Medieval glass beads found in Scottish contexts. Glass beads are small, reflective, and often translucent or transparent, making them notoriously difficult to photograph or

digitally image (Christie 2014; Dorrell 1994, 216). Iron Age and Early Medieval glass beads from Scottish contexts also form a collection of beads about which archaeology knows relatively little, despite the variety of unique patterns and sophisticated manufacturing techniques found in the Scottish collections (Christie 2014). In the first case study, I analysed visible-range, filtered photographs (400 – 700nm) for differences in bubble concentrations between different bead types and regions within Scotland. In the second case study, data collected from near-ultraviolet (300 – 400nm) and near-infrared (950 – 1000nm) photographs allowed for the identification of chemical differences between Scottish beads and Anglo-Saxon, Roman, New Kingdom Egyptian, medieval English, and modern glass samples. The third case study used visible- and non-visible-range (300 – 1000nm) reflectance transformation imaging and photogrammetry to increase the success rates for digitally imaging and 3D modelling Iron Age and Early Medieval Scottish glass beads, something which is challenging using current methods. The final case study applied the techniques developed in the previous three case studies to a variety of other objects and materials to demonstrate the wide applicability of these techniques, including site trenches, silver brooches, faience and amber beads, and Medieval glazed and unglazed ceramics. These studies demonstrate the benefits of challenging current archaeological perceptions and applications of archaeological imaging and encourage similar investigations in the discipline as a whole.

1.1   DEFINITIONS AND ABBREVIATIONS

There are several phrases and abbreviations throughout this thesis that require definition. First, I often refer to 'higher-' and 'lower-budget projects.' By 'higher-budget projects,' I am referring to archaeological projects that have £5,000 or more dedicated specifically to archaeological imaging in a single season or year. This can come from

private funds or donation, but more often comes from larger research funding bodies like the National Science Foundation in the United States or the Arts and Humanities Research Council in the United Kingdom. 'Lower-budget projects' refers to any project that does not have such dedicated funds. While many archaeological projects have budgets of £5,000 or more, few of those have such a high sum dedicated specifically to visualisation. For perspective, £5,000 is the cost of a short-range, professional-grade laser scanner or a multispectral camera, plus a computer robust enough to process the data (Chapter 8). It is also nearly double the cost of all equipment used in this PhD (Appendix B). The distinction here is important because while significant contributions vital to the field have been made by higher-budget projects, the current attitude towards imaging and objectivity in archaeology has resulted, albeit unintentionally, in a devaluing of the results of lower-budget projects due to their use of technologies the field perceives as less objective (Santana Quintero and Eppich 2016, 3; Zubrow 2006, 14). This is particularly problematic because these projects comprise the majority of current archaeological research.

Additionally, this thesis focuses on experimenting with digital imaging techniques to create informative visual representations of objects that are often notoriously difficult to image. These objects tend to be small, reflective, translucent, transparent, or a combination of these characteristics. Each of these creates problems for digital imaging. Small objects can be difficult for image sensors to detect or render in enough detail to be informative, while reflective materials often produce white or bright patches in an image where the reflection of light was so strong that the image sensor could not detect any data. Transparent or translucent objects scatter light differently than opaque objects in ways that imaging equipment often cannot predict, making these objects difficult to image using laser or structured light scanners. However, referring to these objects as 'small,

reflective, translucent or transparent objects' throughout this thesis would quickly become tedious for the reader, so I will refer to them hereafter as 'SRT objects.' SRT objects include any object that has any one of the above characteristics in addition to objects with multiple.

Throughout this thesis I refer to 'spectral imaging' or 'spectral photography,' which I differentiate from multispectral imaging and hyperspectral imaging. Spectral imaging or spectral photography as used throughout this thesis are defined as the capture, processing and analysis of an object's reactions to visible and non-visible spectra using a standard dSLR camera converted for full spectrum imaging (Chapter 3.2.1). This involves isolating specific wavelengths of light through either digital or physical photographic filters. Multispectral and hyperspectral imaging in this thesis refer to the capture, processing, and analysis of an object's reactions to visible and non-visible spectra using a multispectral or hyperspectral camera, which are specifically designed for that purpose. Hyperspectral cameras capture data for a continuous range of spectra and costs significantly more than a multispectral camera (Chapter 8.10), which captures data for 5 – 10 discrete bands of light (Liang 2012, 309). Both cameras also capture a wider range of spectra and filters and cost significantly more than a dSLR (Chapter 8.10).

There are several abbreviations used to refer to various imaging techniques throughout this thesis. I refer to reflectance transformation imaging as 'RTI,' and focus specifically on polynomial texture mapping within RTI, which I refer to as 'PTM RTI.' Finally, the photogrammetry techniques discussed here focus on structure from motion photogrammetry, for which I have used the common abbreviation of 'SfM photogrammetry.'

Since this thesis is image-based, all images have been created by the author unless otherwise stated. Images featuring specific archaeological subjects include an accession

number or finds number along with an abbreviation of the institution in which it is housed (see below). Some objects have not been accessioned or given a finds number, which is designated in the text as 'Unknown #.'

Finally, there are many museums housing the material used in this study. The name of the museum in which an object is housed is listed in full in Appendix A, but the museum abbreviation also appears at the beginning of the accession or finds number when referring to an object in the main text. Thus, the National Museum of Scotland becomes 'NMS,' the British Museum becomes 'BM,' the Hunterian Museum and Art Gallery becomes 'HMAG,' the Marischal Museum in Aberdeen becomes 'MM,' the Kilmartin House Museum becomes 'KHM,' the Iona Abbey Museum becomes 'IAM' and the National Museum of Ireland becomes 'NMI.' Where certain objects have not been acquired by a museum, I refer to it by the organisation that currently possesses the object. The University of Glasgow therefore becomes 'UG,' the University College London becomes 'UCL,' and Northlight Heritage becomes 'NH.' Finally, there are two replica objects that appear as examples in the text. These are abbreviated as 'RO' (i.e. Replica Object).

1.2 PRESENTATION AND IMAGERY

This thesis is driven by images and imagery, specifically digital photographs, reflectance transformation images, and photogrammetric 3D models. Neither RTI nor 3D models render well in two-dimensional print form, and many of the significant contributions of this thesis would be poorly represented if this were the only medium relied upon. Similarly, there are certain two-dimensional images whose significance to the research presented here is best showcased in a more dynamic fashion. All figures in this thesis that benefit from being viewed on a computer screen rather than paper are

included digitally in Appendix E. The reader is highly encouraged to reference images and models digitally through this appendix whenever mentioned in the text to understand the full benefits of the results.

There are also certain images and models that were pivotal to the research included here. These pieces challenged conventional methods, spurred creative thought in new directions, demonstrated the success of these new techniques and uncovered significant differences between objects that led to the case studies included here. To highlight these pieces and the role they played in the development of this research, I have included a PowerPoint presentation that should be referenced where prompted to do so in the text. All pieces included in the PowerPoint are also included as static images in the text. There is also a PDF file which contains the slides of the PowerPoint for accessibility.

1.3 PRIMARY CASE STUDY MATERIALS: IRON AGE AND EARLY MEDIEVAL GLASS BEADS

The primary SRT objects I focus on in this thesis are glass beads from Iron Age and Early Medieval Scottish contexts (800 BC – AD 800). Beads have been one of the most ubiquitous trade items worldwide for the last 2400 years and the earliest beads found in archaeological contexts date to 135,000 years ago (d'Errico et al. 2008, 2676). Worldwide, glass bead trade mushroomed between 400 BC and AD 500 due to advances in glass bead technology, and many ships sailing along the major trade routes at this time carried glass and beads in addition to spices, metal, and timber (Christie 2011, Abraham and Christie 2010). Most contemporary South, East, and Southeast Asian sites with beads average around 300 per site, which is also true of Anglo-Saxon and Norse sites (Brugmann 2004; Callmer 1977; Christie 2011). We find Roman beads in Indonesian contexts, Indian beads in European contexts, and shipwrecks dating to the early medieval

period (400 – 800 AD) packed full of beads for trade. However, despite being ubiquitous in the archaeological record, particularly in relation to trade, there are very few images of archaeological glass beads and almost no 3D models.

I chose to focus on glass beads in this thesis for two reasons. One is that I have spent a decade studying glass beads, particularly those from contexts dating to the first millennium AD. I began by studying Southeast Asian glass beads with a focus on Indonesian material, then expanded to East and South Asian material for comparison. After five years, I shifted my focus to look at Iron Age and Early Medieval Scotland, using Norse, Anglo-Saxon, Irish, and Roman material as my primary comparative assemblages. I have extensive experience examining and analysing beads across Europe and Asia during the first millennium AD, and I am familiar with the positive and negative aspects of their study. Since this research involved extensive experimentation with imaging techniques, I felt it wise to work with SRT objects with which I was already familiar.

The other, perhaps more important reason for choosing glass beads as the primary focus object is that glass beads are notoriously difficult to image, even among SRT objects. They are highly reflective, often translucent or transparent, and the most popular trade bead in the archaeological record measures no more than 6mm in diameter (Francis 2002, 19). For example, Pattanam in southern India has tens of thousands of glass beads dating to the first millennium AD (Abraham 2013, 241), while Pengkalan Bujang in Malaysia (Basa 1991, 129) and Tounokubi in Japan (Katsuhiko and Gupta 2000, 83) have more than 5,000 beads each. Arikamēḍu, in southern India, has over 27,000 objects classified as glass beads or associated with glass beadmaking (Francis 1991, 28). Of the objects from Arikamēḍu, however, fewer than 20 are directly associated with published photographs, even within Francis's own work (Francis 1991; Francis 2002). European

collections also number in the thousands of objects and are similarly lacking in images. Guido (1978, 1999) describes over 10,000 glass beads across her two works on Iron Age and Roman collections in Britain and Ireland and Anglo-Saxon collections in England, but she provides images for fewer than 200. Of these photographed beads, only 16 were imaged individually and only 6 from more than one angle (Guido 1978, Plate III). The abundance of material, the significant lack of an associated visual record and their general issues of size, reflectiveness, and translucency make glass beads an ideal subject for developing and experimenting with affordable new imaging techniques for SRT objects.

1.3.1 THE CORPUS

Within Scotland, there are at least 4000 beads from over 200 sites possibly dating to the Iron Age and Early Medieval periods (800 BC – AD 800). Culbin Sands on the Murray coast has the largest number of beads in Scotland with roughly 700, while Glenluce Sands (Luce Sands), Newstead, and Traprain Law have roughly 100 beads each. All the other 207 sites have fewer than 65 beads each, and 204 of them have 25 or fewer. Yet, four thousand is a relatively low number when compared to the collections in other countries. For comparison, the average glass bead total for Asian sites active at this time is roughly 310 and the average site totals of glass beads for Anglo-Saxon contexts alone is around 140, while the average site totals for glass beads in Scotland at this time is eight or nine (Brugmann 2004, 112–117; Christie 2011; Christie 2014). Yet, the variety of glass beads in Scotland is impressive. Scottish beads tend to employ design features and manufacturing techniques not often seen elsewhere, including in Anglo-Saxon or Norse contexts, and they range in material from glass to stone, amber, faience, ceramic, shell and bone (Figure 1.1).
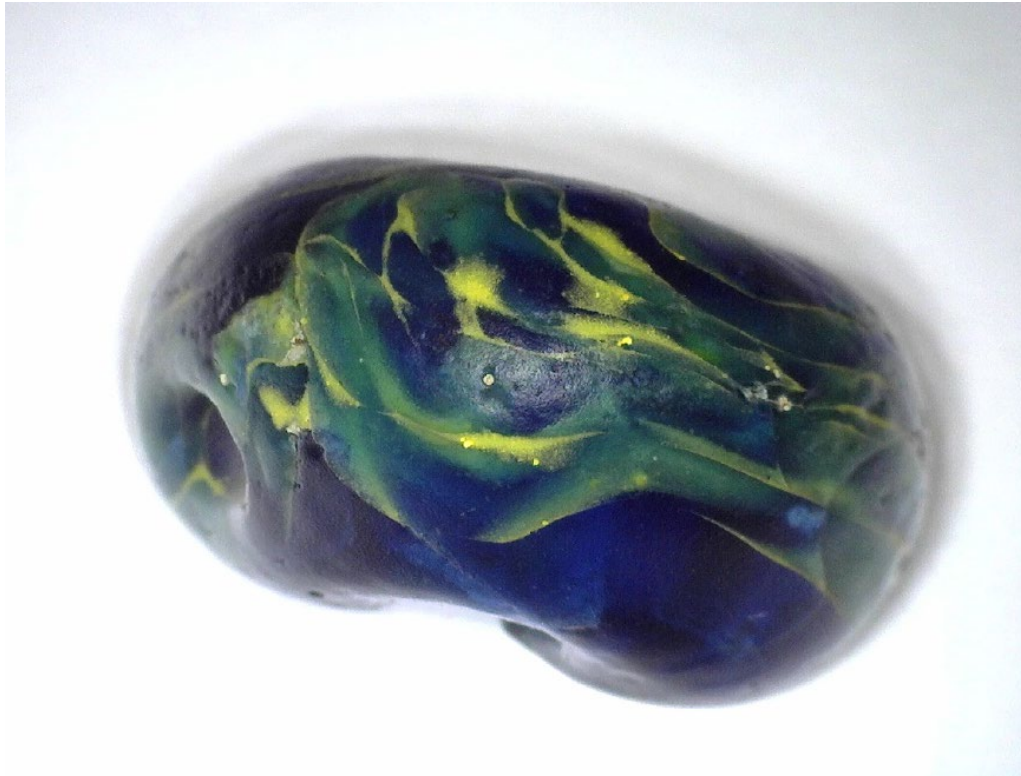
Figure 1.1: Example of a bead type unique to Scotland: that of a translucent base with a single-coloured opaque glass marbled into the surface to form a tri-coloured bead (NMS X.BIB 15).

This thesis examines 400 beads from 48 sites in Scotland (Appendix A). These beads currently reside in the National Museum of Scotland, the Hunterian Museum and Art Gallery, the Marischal Museum, the Kilmartin House Museum, the Iona Abbey Museum, the University of Glasgow's Department of Archaeology, and with Northlight Heritage in Glasgow. Roughly 350 of these beads featured in my master's research in 2014, which focused on analysing the regional distributions of specific colours and shapes of glass beads in Iron Age and Early Medieval Scotland. None of the case studies presented in the following chapters will include all 400 beads, because they focus on the techniques used to acquire the data rather than on the quantity of samples tested and because not all samples lent themselves well to every imaging technique. I also do not include beads from Norse or possible Norse contexts in this thesis, they often are easier to

identify and because the Iron Age and Early Medieval periods in Scotland already span 1600 years.

In addition to 400 beads, I also examined 43 Egyptian glass vessel sherds, 30 Roman-period glass objects, 10 Anglo-Saxon glass vessel sherds, 10 late medieval English window glass sherds, and 56 modern Venetian glass tesserae. These pieces are housed at the British Museum and at University College London. Finally, to demonstrate the use of the techniques developed in this thesis on materials other than glass, I have preliminarily tested my methodologies on a variety of archaeological subjects, including trench sections, glazed ceramics, and amber, faience, copper-alloy and polished metal objects (Appendix A). For each SRT object category, I have demonstrated the benefits of pushing the boundaries of current imaging techniques in uncovering new information. To put these benefits into perspective, let us first examine the current state of glass bead visualisation in archaeology.

1.3.2 VISUALISING GLASS BEADS IN ARCHAEOLOGY

The development of glass bead visualisation followed a similar path to that of archaeological imaging in general, beginning with black and white drawings and continuing with photography (Chapter 2.1). While archaeological imaging developed further with technologies like photogrammetry, laser scanning and RTI, bead visualisation did not. Roughly half of publications at least mentioning beads that I have come across do not employ any form of visualisation technique at all (e.g. Bard et al. 2013; Dussubieux and Gratuze 2002; Hall and Yablonsky 1998; Indraningsih 1985). Generally, publications relying on text alone to describe beads provide little more than a few non-descriptive sentences and rarely go so far as to discuss basic information like design, colour, or size.

Short Chamfered Cylinder	Short Double Chamfered Cylinder	Short Concave.	Short Concave Cone	Short Truncated Concave Cone.	Short Concave Bicone	Short Concave Truncated Bicone	Short Cylinder with one Convex End.	Short Cylinder with two Convex Ends
B.2.b.d	B.2.b.f	B.3.b.	B.3.c	B.3.d	B.3.e.	B.3.f	B 4 d.b	B.4 f b
I.B.2.b.d	I.B.2.b.f	I.B.3.b.	I.B.3.c	I.B.3.d	I.B.3.e	I.B.3.f.	I.B.4.d.b.	I.B.4.f.b.
IX.B.2.b.d	IX.B.2.b.f	IX.B.3.b	IX.B.3.c.	IX.B.3.d.	IX.B.3.e	IX.B.3.f	IX.B.4.d.b	IX.B.4.f.b.

Figure 1.2: Part of Beck's famous set of line drawings (Beck 1926, Plate III).
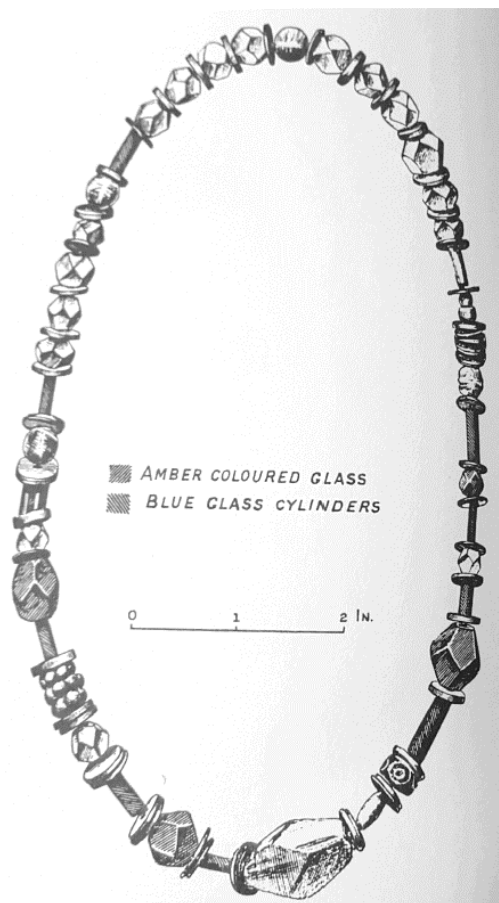
Figure 1.3: Diagram of a necklace from West Africa (van der Sleen 1973).

Illustrations are the most common depiction of beads found in the archaeological record aside from text, most of which do not include colour (Figure 1.2). Roughly a third of sources concerning beads contain black and white drawings, while coloured drawings

appear in fewer than five percent. Coloured drawings are difficult to reproduce, and

publishers often do not accept them due to high printing costs. Some authors use

differential shadings or patterns to indicate colour instead (Figure 1.3) (e.g. Callmer 1977,

van der Sleen 1973). Most simply provide black and white drawings and rely on the text

to convey nuances of colour (e.g. Atkinson 1883; Beck 1926; Jewitt 1870).

One of the earliest uses of photography for beads was Day's work on the

similarities of beads between Ireland and Egypt (1887, Plate 1), in which he illustrated the

beads using a colourised collotype (Figure 1.4). Now, photography is relatively common

in bead studies, with roughly half of publications using photography of some kind.

Published photographs of beads often consist of piles or strings of beads rather than

individual specimens, however, resulting in an image that conveys some information

about many beads, but detailed information about none (Figure 1.5) (e.g. Brugmann 2004;

Francis 2002; Mannion 2015). Roughly half of publications that include photographs of

beads use black and white photographs. Some publications using black and white

photographs also include colour photographs, though it is more common to find one or

the other. Many publications using black and white line drawings to also include

photographs of some kind.

Figure 1.4: Collotype of glass beads (Day 1887, Plate 1).

Figure 1.5: Strings of Indo-Pacific beads, one each from Indonesia, Thailand, and Sri Lanka (Francis 2002, Colour Plate 9).

Unfortunately, this is the extent of visualisation for glass beads in archaeology. Few projects even attempt 3D models of the objects, and none use RTI. Some studies, such as that by Bertini and colleagues (2014, 259; Figure 1.6), have imaged elements of beads using x-ray computed tomography, but few have published the results. Bead visualisation in archaeology has stagnated with photography, the results of which are often uninformative.
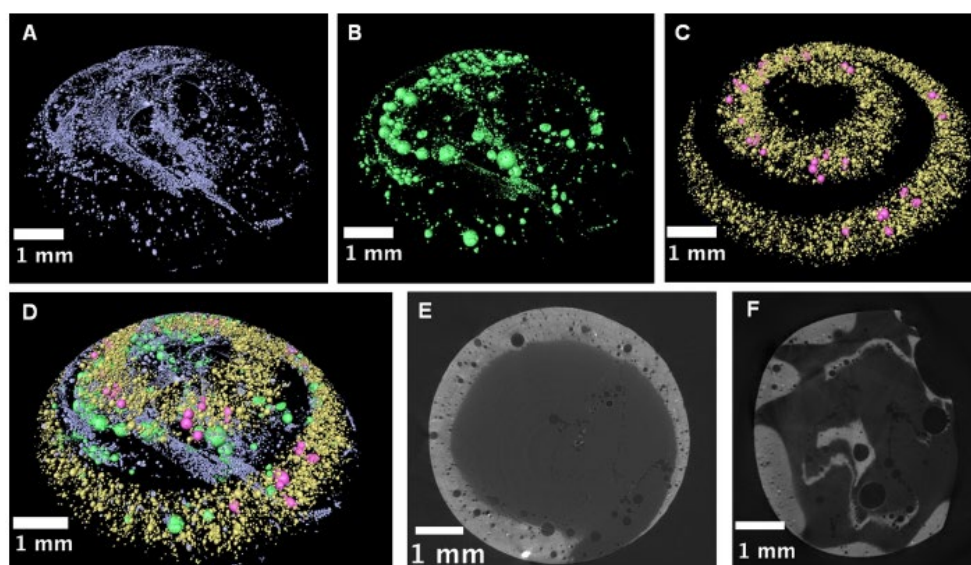
Figure 1.6: 3D images produced by x-ray computed tomographic microscopy (Bertini et al. 2014, 261).

This does not mean bead research has stagnated. On the contrary, bead research has exploded in the last decade or so relative to what it has been in the past. This is particularly true in South, East, and Southeast Asia where excavators recover thousands of beads each season from numerous sites (e.g. Basa 1991; Bellina 2003; Dussubieux 2001; Dussubieux et al. 2008; Dussubieux and Gratuze 2002; Dussubieux et al. 2010; Francis 1988-89; Francis 1990; Francis 1991; Francis 2002; Gan 2009; Gan et al. 2009; Indraningsih 1985; Kanungo 2004; Lankton and Dussubieux 2006; Lankton et al. 2009; Lee 2009). North America and large portions of Africa have also seen a significant expansion of bead studies, and there remains a large emphasis on studies of faience and early glass beads in Egyptian and Roman contexts (e.g. Dussubieux et al. 2008; Rehren 1997; Rehren 2000; Rehren 2001; Robertshaw et al. 2010; Saitowitz and Sampson 1992; Turgeon 2001). Visual records of beads remain scarce, however, making communication and cross-comparison difficult.

1.3.3   Some Problems with Bead Visualisation

There are numerous problems with the current state of bead visualisation. First, there is the severe limitation in the methods specialists can employ. Drawings usually provide more information than purely textual descriptions, but they cannot convey as much detail of the object as other techniques. Many drawings leave out striations or uneven colour mixing (important for identifying recycled glass), bubbles (important for understanding manufacture), or patterns of wear or breakage (important for understanding use and disposal). Illustrators also often draw beads for typological purposes by averaging all beads of a single type together from one site, region, or period, rather than drawing individual beads (e.g. Brugmann 2004; Callmer 1977; Guido 1978; Guido 1999). If they do accurately depict one bead, it is usually one they or a bead specialist has chosen to

represent an entire group of beads, which can range from a few to a few thousand objects, depending on the region.

Unfortunately, current bead photography is equally problematic. While a photograph itself is not an amalgamation of many beads averaged into one, bead publications often select an image of a single bead to represent anywhere from a few to a few thousand objects, as happens with drawings (e.g. Brugmann 2004; Christie 2014; Francis 2002; Guido 1978; Mannion 2015). These photographs can provide detail for the bead depicted, but not the others it represents. Additionally, beads are difficult to photograph and, consequently, images of beads in publications often exhibit patches of high reflection or lack of detail. Thus, even publications with photographs of beads may provide little additional information, depending on the quality of the image.

This discussion of bead imaging would not be complete without a discussion of colour. Colour is an essential element of bead studies, and many reports struggle to communicate vital colour information. Since most journals and publishers require black and white illustrations or photographs, reports usually rely on the text to convey bead colours, if they discuss it at all. This often results in highly subjective (e.g. 'sea-green') or overly specific (e.g. Munsell) phrases. Subjective designations like 'sea-green' could apply to a range of colours; the sea can be any number of different greens depending on location and weather. On the other hand, highly specific categories, like Munsell designations, are problematic because glass changes colour in different light and because the differences between categories are often indistinguishable. Many institutions and researchers also do not have access to the Munsell books of colour, particularly that designated for beads, and therefore cannot use or translate the system. Thus, most publications about archaeological beads do not provide colour images of the object and fail to discuss their colour in meaningful, comparative ways.

The techniques we use to visualise the objects we study will continually limit the research we can engage in and the conclusions we can draw. This is true of bead studies and of archaeology more generally. Additionally, these problems with visualisation are not unique to beads, or even to glass objects. They apply to most SRT objects, including glazed ceramics, precious and semiprecious stones, polished metal, amber, faience, bone, and certain organic materials. A specialism whose best and most published images are often black and white line drawings will not be able to advance in its research as quickly or efficiently as a specialism exploiting as many methods as possible for visualising its subject. Consequently, failing to develop methodologies that provide the best possible visual representation of SRT objects only hinders further research.

1.4 TOWARDS AFFORDABLE ARCHAEOLOGICAL DIGITAL VISUALISATION

The methods discussed and developed in this thesis provide a means through which archaeologists can both document and analyse visible and certain non-visible characteristics of archaeological subjects, particularly SRT objects. These methods are currently more affordable and have a higher success rate for SRT objects than the standard techniques used in archaeology today. They also allow for analysis of these objects that is otherwise difficult or impossible without expensive technological equipment. These techniques were developed by experimenting with current technologies in non-standard ways with aims to maximise affordability, practicality, and effectiveness, They allow for the analysis of SRT objects in new and informative ways and demonstrate the value in applying both these techniques and this approach to archaeology more generally.

Chapter 2 provides a brief history of the development of photography and photographic imaging techniques, particularly in relation to archaeology. It then discusses the connections between current digital imaging practices and prominent theoretical discourses within the discipline. Chapter 3 details the general principles of photography and photography-based imaging used and manipulated throughout this thesis, including photography, spectral photography, PTM RTI, and SfM photogrammetry. Chapter 4 serves as the first of four case studies and uses visible-range photographic filters to examine and analyse relative bubble concentrations between Iron Age and Early Medieval glass beads across Scotland. The results of this study indicate previously unknown differences in the manufacture and long-distance trade of glass beads. In Chapter 5, I use non-visible-range photographic filters to determine relative chemical relationships between glass objects from Iron Age and Early Medieval Scotland and those from Roman, Egyptian, Anglo-Saxon, Medieval English, and modern contexts. Chapter 6 combines visible and non-visible spectral photography with PTM RTI and SfM photogrammetry to improve upon the current techniques used for SRT objects, while Chapter 7 compiles several studies applying the techniques developed in this thesis to non-glass and non-bead subjects (e.g. excavation trenches, brooches, ceramics and lithics. Chapter 8 serves as a comparison of the affordability, practicality, and efficacy of these techniques to that of current standard technologies. Chapter 9 revisits the theoretical discussions from Chapter 2 in light of the results from Chapters 4 through 7, then provides several proposals for future work and a brief conclusion to the thesis.

2   ARCHAEOLOGICAL IMAGING: HISTORY AND THEORY

Archaeology thoroughly became entangled with photography as soon as François Arago made the announcement of the daguerreotype in 1839. Since then, the fields have developed in tandem, each influenced in part by the discourses of the other. This chapter examines the history of archaeological visualisation techniques, beginning with photography and advancing through to laser scanning and x-ray computed tomography. It then identifies and critically examines the theoretical discourses surrounding archaeological imaging before advocating for a change in how we approach the practice.

2.1   A BRIEF HISTORY OF ARCHAEOLOGICAL IMAGING

As often happens with technological innovation, scientists developed many photographic techniques in tandem over a period of roughly a century, which culminated in what we now refer to as the earliest photographs. These early techniques greatly influenced the development of archaeology, and Arago even stated in his announcement that researchers could use the technology "to copy the millions of hieroglyphics which cover the exterior of the great monuments of Thebes, Memphis, Karnak, and others...," (Eder 1945, 234). The inventor of the calotype, William Henry Fox Talbot, had also achieved international recognition for his work in translating Assyrian texts (Lyons 2005, 33). Thus, any theoretical discussion of imaging in archaeology would be incomplete without some consideration of the development of photography more generally.

Photography rests on the principle of the camera obscura, in which a light passing through a pin-sized hole of a box produces an inverted image on any surface opposite the pinhole (Eder 1945, 36; Friedman and Ross 2003, 3). Aristotle briefly mentions the concept and Ibn al Haitam used a camera obscura to study eclipses in the early 11th century (Eder 1945, 36-37). By the 17th century, many artists used a camera obscura to

draw a scene more accurately (Friedman and Ross 2003, 3). Yet, a camera obscura only projects an image onto a surface; it does not capture it.

Photography as a discipline focuses on capturing an image and permanently fixing it to a surface. In 1614, Angelo Sala published his discovery that silver nitrate turns black when exposed to the sun (Eder 1945, 23), and in 1727, Johann Heinrich Schulze confirmed that the sun's light caused the effect, not its heat (Eder 1945, 60-62). If a photographer coated a surface in silver nitrate and exposed it to light via a camera obscura, they could capture a photographic image. However, the capture was not permanent – once the photographer moved the image, the resultant light exposure ruined it (Friedman and Ross 2003, 4).

In 1777, Cal Wilhelm Scheele demonstrated that silver chloride dissolved in ammonia prior to light exposure, but not afterwards (Eder 1945, 97). After numerous experiments, Joseph Nicéphore Niépce successfully recorded images on silver chloride in 1816 (Eder 1945, 195-196). In 1825, he created a fixed image using a pewter plate coated with bitumen of Judea, which hardens when exposed to light (Friedman and Ross 2003, 4). Yet, while Niépce was successful, his process required eight hours of exposure (Friedman and Ross 2003, 4). His new goal was to shorten the time required to capture an image.

Nièpce partnered with Louis Jacques Mandé Daguerre in 1829 (Eder 1945, 215; Friedman and Ross 2003, 4). Daguerre experimented with copper plates, coating them with silver and then treating them with iodine fumes to produce silver iodide (Eder 1945, 223-225). Nièpce unfortunately died in 1833, but his son Isidore took his place in the contract with Daguerre. Daguerre then discovered that he could temporarily fix an image to a copper plate after only half an hour if he exposed the plates to mercury vapour immediately afterwards (Friedman and Ross 2003, 4). As with many discoveries,

Daguerre discovered this rather by accident. He happened to store some of his iodine and silver-coated copper plates in a cupboard that also happened to have a basin of metallic mercury (Eder 1945, 228). When he removed these images after several weeks, the images remained. Daguerre realised something in the cupboard was the answer to capturing a permanent image and removed the items one by one. He did this until he believed there was nothing left and was beginning to consider the cupboard itself may have special properties, having forgotten the open basin of mercury in the back. Eventually, he remembered the mercury and realised it must be the vapours that fixed the images (Eder 1945, 228). In 1837, he discovered that by immediately coating these mercury-treated images in an aqueous salt solution, he could permanently fix the image to the plate (Eder 1945, 227-228; Freidman and Ross 2003, 4). This became the standard process used to make daguerreotypes like the "Boulevard du Temple" (Figure 2.1), which many consider the first photograph of human beings (Frizot 1998, 36).

Figure 2.1: Boulevard du Temple (Daguerre 1838).

On 3 July 1839, Deputy of the East Pyrénées Fraçois Arago presented Daguerre's technique to the French Chamber of Deputies (Eder 1945, 234). In his announcement, he specifically mentioned the use of daguerreotypes in capturing images of the Egyptian hieroglyphs and urged the Chamber to equip the Egyptian Institute with two or three of the machines (Eder 1945, 234 – 235). Within months, daguerreotypists were travelling to Egypt, Greece, Italy, and other ancient sites to photograph everything they could (Lyons 2005, 30; Szegedy-Maszak 2005, 9).

Yet, daguerreotypes proved problematic in the field. Expeditions had difficulty transporting the required equipment safely (Lyons 2005, 34). Perhaps the most vexing problem of the daguerreotype, however, was that the process created a fixed, but unique image. Copying an image from a daguerreotype requires engraving, which inevitably damages or destroys the daguerreotype (Eder 1945, 316; Lyons 2005, 30 – 33; Newhall 2006, 39). These limitations dashed many of the hopes for ease of communication and exchange among scholars, because they could not easily reproduce daguerreotypes in a meaningful way (Lyons 2005, 33).

William Henry Fox Talbot, an Englishman known at the time for his work in physics as well as his assistance in translating Assyrian texts, was working on the photographic problem independently of Daguerre and Nièpce in France (Dorrell 1994, 1; Lyons 2005, 33). In January of 1839, Talbot publicly announced his work and wrote to the Royal Society of London describing his methodology (Eder 1945, 320). By 1840, Talbot had developed a technique for capturing photographic negatives, which he termed 'calotypes' (Eder 1945, 321) This technique shortened the required exposure to less than a minute and allowed for reproduction of multiple positive image copies from the original negative obtained through the camera (Eder 1945, 321 – 323; Lyons 2005, 33). As an antiquarian himself, Talbot urged other scholars to use his machine, and he happily

trained them in its mechanics (Lyons 2005, 33). For these reasons, many early

expeditions of an archaeological or heritage nature preferred the calotype to the

daguerreotype (Dorrell 1994, 4; Lyons 2005, 33). Scholars identify the first use of

photography on an archaeological expedition as that by R. Lepsius to Egypt (1842-1845),

but one of the best known early uses of photography in archaeology is by Tranchand

during the 1852-1855 excavations of Khorsabad, Assyria and subsequent expeditions

through Armenia and Kurdistan (Figure 2.2) (Dorrell 1994, 4).
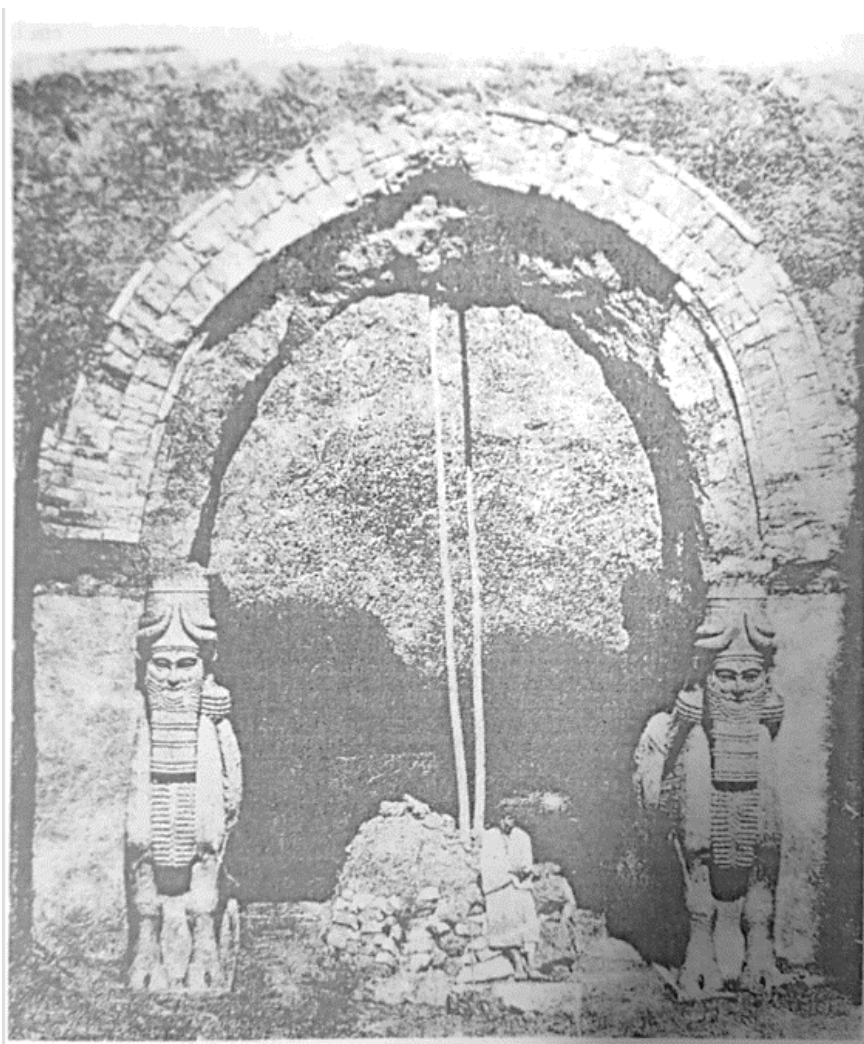
Figure 2.2: The Gate at Khorsabad, by M. Tranchand (from Dorrell 1994, 3).

James Clerk Maxwell developed a method for photographing in colour by 1861,

not long after the invention of photography itself. Working from Young and Helmhotz's

assertions that human retinas have three types of nerves, which, when stimulated, react to red, green, and violet light respectively (von Helmholtz 1896, 364 – 365; Young 1802, 21), Maxwell began to experiment with coloured filters to create colour images (Eder 1945, 640 – 641). In 1861, he took three photographs of a coloured ribbon using three separate coloured light filters. He then combined these photographs to form a coloured image. He stated in a letter to the Royal Institution in London that '…if the red and green images had been as fully photographed as the blue, [it] would have been a truly coloured image of the ribbon,' (Maxwell 1862, 374). The challenge, then, was not to create colour images but to do so using film that was equally sensitive to each of the three primary colours of red, green, and blue (Maxwell 1862, 374).

Another development came in 1925 with the invention of the miniature camera, now known as the 35mm camera (Howell and Blanc 1995, 5). Miniature cameras, while quite familiar to us today, were smaller than roll film cameras and were therefore far more portable (Simmons 1969, 15-16). Researchers could carry them up a mountain or into the desert with relative ease and could capture more accurate photographs with a greater depth of field (Simmons 1969, 16-17). Miniature cameras also had a much shorter exposure times, speeding up the process considerably (Simmons 1969, 16-17). The primary difficulty came in processing the film safely, since any speck of dust on the negative would cause a much larger blemish than it might on the larger roll film (Simmons 1969, 17).

In 1947, Edwin H. Land introduced the Polaroid process of creating a finished photographic print within seconds (Newhall 2006, 281). The primary disadvantage with most polaroid cameras was that they only produced a single copy of the photograph and did not create negatives (Conlon 1973, 8). Polaroids therefore posed similar problems to the daguerreotype in that multiple copies of an image were difficult to obtain. By the

1970s, however, archaeologists could obtain polaroid films that captured a negative *and* generated an immediate, positive print (Conlon 1973, 8).

Despite the developments made in the first century of photographic techniques, many archaeologists did not regard photography as a vital tool for recording an excavation until the 1950s (Cookson 1954, 11). Simmons (1969, 2) noted that many supervisors complained about site photographers for slowing down the excavation. He also noted the change in tune when the same individuals needed to write reports, often long after the dig had concluded (Simmons 1969, 2). By the late 1960s, the general attitude towards archaeological photography had not changed in its purpose; it served as a method of scientific recording, particularly of information lost through excavation (Simmons 1969).

Yet, beginning in the 1950s, photography did become much more prominent in archaeology due to perceptions that it was more objective and truthful than drawings (Bateman 2005, 192; Lyons 2005, 39, 43; Shanks 1997, 74, 82; Walsh 2012, 21). This period marked the rise and prominence of processual archaeology, which argued for the field to become more scientific in its analysis of the past (e.g. Phillips 1955; Phillips and Willey 1953; Willey and Phillips 1955; and Willey and Phillips 1958). It also marked the publication of one of the first archaeological photography manuals, in which M.B. Cookson (photographer to Mortimer Wheeler) described what he felt were the best methods for photographing archaeological subjects (Cookson 1954). The relationship between archaeological photography and archaeological theory is discussed further in Chapter 2.2, but imaging techniques in archaeology developed significantly from this point onwards, and it seems better to discuss them in individual subsections.

2.1.1   PHOTOGRAPHY

During the 1960s and 1970s, the miniature camera, colour film, and polaroid technology finally entered mainstream archaeological photography (Simmons 1969, 11). Yet, even by the late 1960s, colour film was expensive to purchase, expensive to process, and difficult to maintain (Cookson 1954, 106-109; Simmons 1969, 38). Colour films were prone to deterioration in humid areas and tended to fade, complicating their use in the field (Simmons 1969, 38). Publishing in colour was expensive, and scholars opted to use colour images more often for lectures and other situations requiring slide projections (Cookson 1954, 109; Simmons 1969, 37).

Figure 2.3: Glass bead from Glenshee, Scotland in visible light (left) and near-infrared (right) (NH Unknown #).

The mid 1980s saw the advent of image spectrometry, or the capture of many narrow spectral bands of ultraviolet, visible, and infrared light (Goetz et al. 1985, 1147). Visible-range filters for photography had existed since Maxwell's experiments with colour photography in 1861 (Maxwell 1862, 374), but photographers could not capture infrared light and process it together with visible-range data prior to the late 20th century. Multispectral imaging (or image spectrometry) allowed scholars to compare specific reactions of objects and materials to each other to determine similarities or differences

between them. Multispectral imaging has been used extensively in the fields of geology, ecology, and urban planning (e.g. Fischer and Kakouli 2006; Lau et al. 2008; Noordam et al. 2007). Archaeologists use multispectral imaging on paintings and manuscripts (Christens-Barry et al. 2009; Dorrell 1994; Legnaioli et al. 2013; Liang 2012; Padfield et al. 2005). Infrared radiation can penetrate beneath the surface of an object, revealing underdrawings, damage, or other details (Figure 2.3) (Legnaioli et al. 2013, 1; Liang 2012, 313). Ultraviolet light can also reveal areas where paintings have been retouched as well as erased or faded writing on historical manuscripts (Dorrell 1994, 200; Legnaioli et al. 2013, 1; Liang, 2012, 313-314). Multispectral imaging also allows for accurate colour rendering of a painting under any lighting, which highlights conservation efforts and degradation (Liang, 2012, 314-315).

Hyperspectral imaging developed in tandem with multispectral imaging and involves capturing images for the full range of spectra for a single subject (Liang 2012, 309). Multispectral imaging captures discrete bands of spectra (e.g. 560nm (green), 660nm (red), or 800nm (near-infrared)) resulting in 5-10 distinct photographs, while hyperspectral imaging captures data for a continuous range of spectra and stores all the data for each pixel (e.g. 450 – 900nm) (Liang 2012, 309). While hyperspectral imaging has proven useful in geology, astronomy and other related fields (e.g. Baeten et al 2007; Balas et al. 2003; Chabrillat et al. 2002; Dale et al. 2013; Gomez and Del Re 2005; Fischer and Kakouli 2006; Lau et al. 2008; Park and Lu 2015; and Rapantzikos and Balas 2005), it has yet to find much use in archaeological imaging.

A technique related to multispectral and hyperspectral imaging is the creation of false colour images. False colour images involve altering the visible colour of a photograph such that no colour in the image represents that colour in reality (Chapter 5.3). Geologists often use false-colour images combining infrared, red, and green spectra

(represented using red, green, and blue, respectively) to determine the mineral composition of geological formations (Kurz et al. 2012, 417; Kurz et al. 2013, 1799). Astronomy, physics, ecology, and art history use false colour imaging for various purposes, largely to identify differences otherwise invisible to the human eye. Thus far, however, archaeologists have yet to exploit false colour imaging for purposes other than identifying pigments and areas of retouching or conservation (e.g. Pilarska 2016).

2.1.2   REFLECTANCE TRANSFORMATION IMAGING

Reflectance transformation imaging (RTI) captures the reflectance properties of an object to highlight surface and subsurface characteristics. RTI software analyses between 30 and 50 photographs in which the camera and object remain stationary, but the light changes direction (Diaz-Guardamino and Wheatley 2013, 191; Malzbender et al. 2001, 3). The resulting light patterns indicate surface features that may be invisible to the naked eye.

Malzbender and colleagues (2001) developed the technique in the early 21st century to create more photorealistic representations of objects. The resulting visualisation, which many call 2.5D to mark its ambiguity between two and three dimensions, allows for the manipulation of light and the creation and manipulation of artificial lighting scenarios that are difficult if not impossible outside of the software. For example, specular enhancement illuminates the object in a way that maximises pixel brightness, while diffuse gain enhances the representation of surface features on an object, thus making depressions appear deeper (Cultural Heritage Imaging 2010, 12; Diaz-Guardamino and Wheatley 2013, 192). Both techniques reveal information that is not physically accessible to the naked eye.

Reflectance transformation imaging has greatly enhanced the study of paintings and other artworks by providing a better understanding of the brush strokes and other

techniques involved in the creation of the piece (e.g. Giachetti et al. 2017; Tisato and Parraman 2014). In archaeology, RTI has been widely used in the study of rock art and stone sculpture, though some have used it for artefact recording and analysis (e.g. Dellepiane et al., 2006; Diaz-Guardamino and Wheatley 2013; Earl et al. 2008; Earl et al. 2010, Jeffrey 2005; Mudge et al., 2005; Mudge et al., 2006). Yet, RTI has only found significant use in archaeology within the last decade due to its relatively recent development, and archaeologists have yet to exploit it to its fullest extent.

2.1.3 PHOTOGRAMMETRY

The foundational mathematical principle of photogrammetry, or the process of making accurate measurements from drawings, first came into use in the late 18th century to construct plans from hand-drawn landscapes (Eder 1945, 398; Moffitt 1967, 1). Photogrammetry itself did not appear as a scientific method until 1851, however, when Aimé Laussedat began experimenting with photogrammetry to create measured plans of Paris and its surrounding villages (Eder 1945, 398-399). Albrecht Meydenbauer was the first to use the technique for the preservation of historical monuments, and he formed his own photogrammetrical institute in Prussia in 1885 (Eder 1945, 400). Aerial photogrammetry took off during World War I, when plans were of vital importance for the battlefield (Eder 1945, 401).

Dr. Carl Pulfrich was the first to combine stereoscopic imaging with photogrammetry as early as 1901, thus creating stereoscopic photogrammetry (Eder 1945, 402). Stereoscopic imaging was a common practice in the 19th century and stereoscopes often featured in the parlours of wealthier families (Figure 2.4). In principle, stereoscopic imaging involves taking a photograph from one location, moving the camera slightly and taking another photograph of the same subject such that when viewed side-by-side the images are offset to the same degree as a pair of human eyes (Campana 1977, 435-436).

When placed side-by-side in a stereoscope or similar viewer, the images appear to take on a 3-dimensional quality. By 1901, photographers discovered that these 3D viewings of photographs allowed for accurate measurements of the objects in the images (Eder 1945, 402).
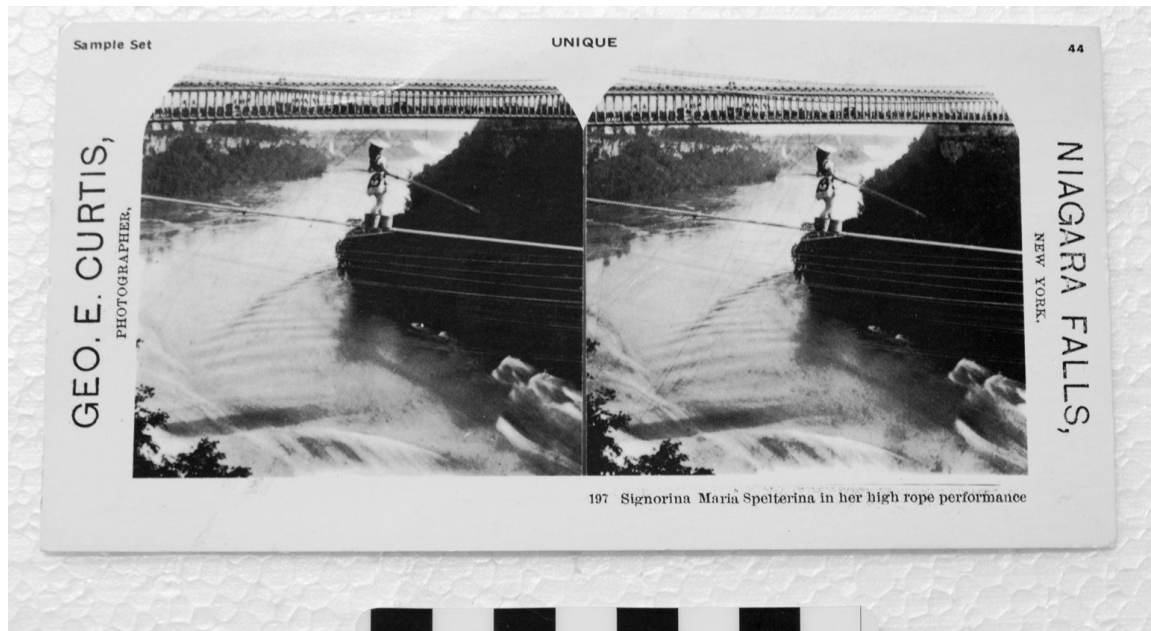
Figure 2.4: Stereoscopic image of Niagara Falls (Mystic Seaport Museum).

Interestingly, archaeology did not find significant use for stereoscopic photogrammetry until the late 1960s, despite the popularity of aerial photography in the field since the early 1900s (Estes et al. 1977, 441). Stereoscopic photogrammetry was a common technique for taking accurate measurements and drawing plans, particularly topographically (Atkinson 1969; Green et al. 1971; McFadgen 1971; Scogings 1978; Whittlesey 1966). One of the first archaeological applications of the technique attempted to measure the building façades in Petra (Atkinson 1969) while others used the technique to document rock art (Scogings 1978). In the late 1970s, archaeologists began using stereo pairs to compare macro and microscopic images of objects, particularly those they could not transport from one location to another (Campana 1977, 435). Some argued stereo pairs were the primary means through which they could document and share

microscopic information, and that they generally captured more detail than standard photographs (Campana 1977, 435).

Photogrammetric software gained popularity in the late 1990s and early 2000s (Boehler and Heinz 1999, 4; Boehler and Marbs 2004, 291; Chandler 1999, 51), when emphasis of photogrammetry shifted from acquiring simple measurements to documenting the object, site, or building in three dimensions with the intent of giving the viewer access to as much information as if they were viewing the object in person (Boehler and Heinz 1999, 2). Photogrammetric software had developed significantly by this time, and it could now create 2D and 3D line drawings of the photographed object (Boehler and Marbs 2004, 294).

At roughly the same time, a new type of photogrammetry emerged. Previous photogrammetric models used a single stereoscopic pair to create a model, as described above. This required knowledge of the 3D positioning of the camera or multiple control points to create a model in 3-dimensional space (Westoby et al. 2012, 301). The new technology, termed Structure from Motion (SfM) photogrammetry, operated on the same principle that overlapping photographs provided the data needed to calculate 3D points, but it used multiple photographs surrounding the object of focus (Doneus et al. 2011, 82; Westoby et al. 2012, 301). The software calculated the digital 3D geometry by matching the overlapping points in each photograph (Westoby et al. 2012, 301; Zhao and Li 2006, 70-71).

Archaeologists generally use photogrammetry for buildings, sites, and aerial photography, though applying the technique to objects is becoming more common (Bernardini et al. 2002; Grün et al. 2004; Koutsoudis et al. 2014; Remondino et al. 2009; Remondino 2011; Salonia et al. 2005). There are also studies comparing the technique to other 3D visualisation methods, particularly laser scanning (Boehler and Marbs 2004;

Doneus et al. 2011; Nylén 2008). Generally speaking, archaeologists widely regard photogrammetry as a relatively simple, affordable mechanism for creating 3D models in archaeology.

2.1.4 LASER AND STRUCTURED LIGHT SCANNING

The 1960s also saw the development of lasers and laser scanning systems (3D Digital 2015; Hecht 2010; Maiman 1960). There were numerous logistical issues with using these technologies in archaeological contexts, not least of which were the relative lack of portability and the time required to complete a scan (3D Digital 2015; Matter and Form 2014). By the 1980s, 3D scanners using structured light or lasers were available for use in scientific research, but they had limited storage space (3D Digital 2015; Matter and Form 2014). By the 1990s, 3D scanners entered the commercial market and storage issues lessened (Matter and Form 2014).

Currently, there are two primary types of 3D scanner on the market: structured light scanners and laser scanners. A structured light scanner creates highly accurate, coloured maps of the object by measuring the way a projected, structured pattern of light changes or distorts as it moves across the surface of a subject (McPherron et al. 2009, 20). The sensor measures these distortions for each pixel, resulting in a point cloud that can be turned into a model. Structured light scanning is often handheld, making it easier to direct and control than laser scans. It can also capture accurate data for objects as small as 1-2cm (McPherron et al. 2009, 20). Within archaeology, structured light scanning has seen a lot of use in underwater archaeology as well as human and faunal skeletal remains (e.g. Niven et al. 2009; Roman et al. 2010).

Laser scanners fire lasers at their current field of view, regardless of what is there (LAGOA 2014). Any time the laser beam touches a surface it reflects back to the scanner,

which records the position and reflective nature of each point the lasers touch on that surface (LAGOA 2014). The laser takes multiple scans from various angles around the subject in question and later joins them using common reference points (LAGOA 2014). These create a point cloud, or a series of points in three-dimensional space that can be joined together to create a 3D model (LAGOA 2014).

Laser scanning has worked wonders in terrestrial imaging and discovery of sites, in part because it can often 'see' around vegetation, which generally blocks normal human vision. It also manages to secure significant detail in objects and buildings, allowing archaeologists to take accurate measurements from the models themselves (Historic Environment Scotland 2018, 31). Yet, archaeologists generally avoid using laser scanners on smaller objects due to either a lack of accuracy or a lack of funds to access the equipment. Laser scanners also do not work well with highly reflective, translucent, or transparent objects (Historic England 2018, 2). While the exact cause for this is unclear, it appears to be a result of the current algorithms being unable to predict the nature of light scatter for such materials.

2.1.5   X-RAY COMPUTED TOMOGRAPHY (CT SCANNING)

X-rays penetrate different materials to varying degrees, a feature that became heavily exploited in scientific applications shortly after the discovery of this type of radiation (Cnudde and Boone 2013, 2). The difficulty with this technique was the representation of three-dimensional data in two dimensions, resulting in a loss of depth information for the imaged subject. Computerised transverse axial tomography was developed in the early 1970s to combat this issue by creating projection images from different directions and reconstructing the 3D volume using complex algorithms (Cnudde and Boone 2013, 2; Hounsfield 1973, 1016). The technique was used almost immediately in the medical field, and soon found use in palaeontology, marine science, soil science,

geosciences and industrial applications (e.g. Boespflung et al. 1995; Gawler et al. 1974; Ledley et al. 1974; Petrovic et al. 1982; Vinegar and Wellington 1987; Zollikofer et al. 1998). X-ray computed tomography grew in popularity within archaeology in the mid-1990s and has since been applied to wooden statues, glass, lithics, ceramics, and other finds (e.g. Anderson and Fell 1995; Bertini et al. 2014; Casali 2006; Morigi et al. 2007; Morigi et al. 2010).

Current archaeological imaging techniques have developed significantly since their beginnings in 1839, ranging from photography to RTI, photogrammetry, laser and structured light scanning, multi- and hyperspectral imaging and x-ray computed tomography. Each of these techniques forms a specialism in itself, but all currently strive to maximise the efficiency of, and detail acquired through, documentary archaeological imaging.

2.2   ARCHAEOLOGICAL THEORY AND ARCHAEOLOGICAL IMAGING

The previous section described the general history of photography and imaging in archaeology from a primarily technological standpoint, listing when and how certain developments occurred. Technology can never divorce itself fully from the social and scholarly milieu of its development and use, however, and each of the developments in archaeological imaging directly relate to the theoretical leanings of the discipline at the time. It is vital to any study of archaeological imaging, therefore, to address the entanglement of archaeological theory and archaeological photography.

Photography developed and became popular at a time when archaeology was becoming more systematic and recognising that significant information could be gained from studying the material culture of prehistoric peoples. Thomsen had recently refined the Three Age System (i.e. Stone Age, Bronze Age, Iron Age) in Scandinavia and

contacts in Scotland and Switzerland led to its application in those nations as well (Trigger 2006, 133 – 134). This style of archaeology relied on creating relative chronologies of objects found in secure contexts using simple seriation techniques, and is one of the first systematic practices developed in archaeology (Trigger 2006, 135). Yet, these methods were seen as less reliable in England and France, the two loci of the development of Western photography. Archaeology in these nations focused on historical peoples and did not truly begin to examine prehistoric groups until the late 1850s (Trigger 2006, 138). Instead, their principle revelations concerning prehistory came from the fields of geology and palaeontology, such as Lyell's discussion of the uniformity of stratigraphic layers or Boucher de Perthes's conclusions that Lower Paleolithic handaxes associated with extinct species such as mammoths in secure contexts necessarily meant the tools themselves were at least as old as the associated remains (Trigger 2006, 143 – 145). Only after Herbert Spencer's reframing of societal complexity as evolving out of individual efforts and free enterprise in the 1850s did England and France begin to investigate the notion of prehistory in earnest (Trigger 2006, 145 – 6). This change in archaeological thought is important because it marks the point at which archaeological remains became informative in their own right rather than materials requiring explanation from textual sources. It also meant that the material remains and their contexts held important information that would be lost as soon as the remains were separated from that context unless archaeologists recorded that information in some way.

Objectivity has been a hallmark of photography since its announcement in 1839. Two characteristics of early photographs greatly impressed viewers in the 19th century and proceeded to shape the reputation of these images: the exquisite detail of the images and the inherent truth they conveyed (Walsh 2007, 21-22). Samuel Morse, known for bringing the daguerreotype technology to the United States as well as creating Morse

code, marvelled at the detail, noting that letters on shop signs that were invisible to the naked eye appeared crisp and clear when using a hand lens (Walsh 2007, 21). Society saw photographs as more objective than portraits or other art forms because the photographer could not manipulate the result as easily. Photographs captured the truth, and that made them ideal for recording what archaeological excavation necessarily destroyed (Bohrer 2005, 181; Walsh 2007, 22). For decades, antiquarians took photographs for the specific purpose of generating realistic, detailed information of excavations and difficult-to-reach sites to preserve what excavation could not and to allow consultation with as many scholars as possible (Dorrell 1994, 2; Eder 1945, 234 – 235; Lyons 2005, 25; Szegedy-Maszak 2005, 9). The only difficulty was the practical logistics of transporting the equipment and protecting and developing the film (Chapter 2.1). Despite the widespread use of photography in archaeology, however, no manual had been published nor standard practices agreed upon for archaeological photography.

By the early 20th century, certain archaeological institutions were calling for a more systematic approach to the discipline, which led to the development of more systematic means of photographing archaeology. Taylor, for example, noted in the early 1940s that the limited intentions of American culture-historical archaeologists had resulted in the field failing to examine artefacts in detail, particularly those that were considered undiagnostic of a specific people or time (Trigger 2006, 368). Instead, he argued archaeologists should strive to recover as much information as possible from archaeological excavations. By the early 1950s, MB Cookson published one of the first manuals for archaeological photography, in which he laid out specific practices for achieving the most objective representation of the archaeological record (Cookson 1954).

The rise of processual archaeology in the 1960s championed the notion that data acquired through technological means was objective. Processual archaeology argued that

archaeology was more science than history, and that the material remains recovered in excavation should be viewed as representative of the total cultural system in which they were found (Binford 1962, 224; Willey and Phillips 1958, 2). By the late 1960s, archaeological photographers noted that going into the field without photographic knowledge and equipment was unthinkable, and that site directors had come to rely on photographers and their skills for recording excavations in the field (Simmons 1969, 2; South 1968, 73). All archaeological photography manuals available at the time provided very specific techniques and approaches to archaeological photography, both to systematise the field and to help beginners navigate commonly encountered situations (e.g. Cookson 1954; Simmons 1969; South 1968). Each manual described the site photographer as a full-time position in the field, requiring at least one person highly skilled in using a camera.

The 1960s to 1970s was also the point at which humans largely disappeared from archaeological manuals. Cookson (1954) did not speak about humans in photographs directly, admittedly, but this is because his dialogue assumed them to be there. He stated that some photographs in the record should be purely pictorial and that some more formal shots may need faster shutter speeds due to moving figures in the image (Cookson 1954, 46). Similarly, South (1968, 78) argued that the site photographer should record every part of the process, including crews or machinery at work. Simmons, however, appears to mark the beginning of a decline in human subjects in archaeological photography, stating that only some images should include workmen for use in public relations (1969, 10). By the early 1970s, Conlon (1973, 56 – 57) stated that human figures should only be included at a distance for scale purposes and, if they must be included, they should be doing something, such as supporting a ranging rod or pointing at significant features.

The decline of human figures in archaeological photographs mirrored the rise in the desire for archaeological objectivity and in the perception that photographs are objective. While photography was perceived as objective upon its announcement in 1839, it was seen as so subjective by the time Sir Mortimer Wheeler wrote the forward to Cookson's manual that his statement "…the camera is an awful liar," (1954, 5) was widely known and repeated by Simmons over a decade later (1969, 4). These archaeologists knew that photography requires choice at every level, choices largely made by the photographer and the person commissioning the photograph. By contrast, Conlon championed photographs as "dispassionate factual records rather than pleasing illustrations" meant to represent the record as accurately as possible (1973, xiii).

Post-processual archaeology developed in response to processual archaeology in the 1980s and was largely championed by the work of Ian Hodder and his students (Hodder 1982; Trigger 2006, 450). They argued against the notion that archaeology could reach an objective understanding of the past and published studies refuting the idea that material culture necessarily reflects social organisation (e.g. Cannon 1989; Gathercole 1984; Hodder 1982; Huntington and Metcalf 1979). To borrow a phrase from Geertz (1972, 26), burial practices and other means of depositing material culture often reflected the stories a society or group told themselves about themselves rather than reality they practiced. Similarly, archaeology's interpretation of the past is directly affected by the current philosophical leanings of the discipline at the time. The significance of the archaeological record therefore depended on its context both in an archaeological sense and in a cultural or societal one. In Hodder's words, "interpretation [began] at the trowel's edge," (Hodder 1999, 83).

The next archaeological photography manual to be published presented an archaeological photography that mirrored these changes in archaeological thought.

Dorrell reinstated the discussion of cameras as deceptive (1989, ix) and encouraged flexibility on the part of archaeological photographers to capture each image as best they can (1989, 129 – 131). He detailed both the method for and importance of photographing people working on-site (1989, 153 – 154). He also encouraged care and tact in photographing locals, particularly in societies where photographing people may not be welcome (Dorrell 1989, 154).

The multivocality advocated by post-processual archaeology encouraged some individuals to begin examining photography in several veins. One large strand of inquiry and debate has been the perpetuation and spread of colonial practice through photography in the 19th and early 20th centuries, including archaeological photography (e.g. Behdad 2013; Guha 2002; Michels 2018; Pinney 2003; Riggs 2017). Many archaeologists began to debate the authenticity of digital visual representations of the archaeological record and whether they captured and maintained the same aura as the original subject (e.g. Flynn 2007; Jeffrey 2015; Latour and Lowe 2010). Others began to advocate for increasingly technological means of visualising the archaeological record to minimise this subjectivity (e.g. Earl 2006; Moser and Smiles 2005, Shanks 1997; Zubrow 2006), while still others began to caution against engaging in such practices without reason (e.g. Bateman 2005, Huggett 2004). Another strand began to question the objectivity of photography, particularly with the growth of digital photography and the ease with which digital images could be manipulated (e.g. Bohrer 2005; Burke 2001; Earl 2006; Lyons 2005; Moser and Smiles 2005; Papadopoulos 2005; Shanks 1997). Related to this, some archaeologists began exploring the relationship between archaeological photographs and memory, and to question for whom archaeological photographs should be taken (e.g. Bateman 2005; Tringham 2010). Of particular relevance for this thesis are the discussions

concerning the objectivity of archaeological imaging, the push for new technologies, and the relationship between images and memory.

2.2.1   OBJECTIVITY AND ARCHAEOLOGICAL IMAGING

In the mid- to late-1800s, society saw photography as more objective than drawings because it was the medium that captured the unbridled truth in the highest degree of detail possible at the time. Drawings captured what a draughtsperson felt was important, while photographs were unedited records of reality (Walsh 2007, 21). By the mid-1950s, archaeologists knew that cameras 'saw' differently than human eyes and prescribed methods for capturing images as close to human sight as possible (Cookson 1954; Simmons 1969, 4; South 1968, 73). By the 1970s, discourse returned to photography being more objective than drawings because they are unselective in what they capture (Conlon 1973, 55). By the mid-1990s and early 2000s, however, discourse shifted again to acknowledging photography as subjective and possibly misleading (Bohrer 2005, 182; Earl 2006, 197; Moser and Smiles 2005, 1; Shanks 1997, 78).

To combat the subjectivity of digital technologies, the field has developed and prescribed standardised methods for use in archaeological imaging. These have changed with new technological developments and shifts in the discipline's perspective on the technique's inherent objectivity or lack thereof, but there remains a set of standard imaging methods for each imaging technology that exists in archaeology today. Images should be well-lit with a scale provided and a perspective that allows for close measurement of the features in the image (Conlon 1973, 56; Cookson 1954, 75; Dorrell 1989, 123; Howell and Blanc 1995, 51 – 52; Simmons 1969, 30 – 31). Site trenches should be clean and tools removed from the frame to show the highest amount of detail (Conlon 1973, 56; Cookson 1954, 13; Dorrell 1989, 7; Howell and Blanc 1995, 55; Simmons 1969, 48). Artefacts or other objects should have a neutral background and even

lighting that allows the equipment to capture the largest amount of detail (Conlon 1973, 76; Cookson 1954, 75; Dorrell 1989, 162 – 173; Howell and Blanc 1995, 58 – 61; Simmons 1969, 71 - 73). Shadows should be minimised unless their presence reveals further detail not captured under other lighting conditions. Archaeological imaging should recreate the object as close to how the individual saw it at the time and retouching is discouraged if not forbidden (Conlon 1973, xiii; Cookson 1954, 13; Dorrell 1989, 7; Howell and Blanc 1995, 1; Simmons 1969, 4, 13). Such standards of archaeological imaging allow for an increased objectivity in the resulting visualisation and for easier comparison between them.

These standard methods also emphasise the importance of replicating human vision in archaeological images, particularly those standards which discourage manipulation or retouching of photographs (Conlon 1973, xiii; Cookson 1954, 13; Dorrell 1989, 7; Howell and Blanc 1995, 1; Simmons 1969, 4, 13). When discussing objectivity in photography and digital imaging, particularly for archaeology, the discipline often equates objectivity with realism (Bateman 2005, 194; Earl 2006, 194; Shanks 1997, 80). Photography in archaeology is primarily documentary and has been since its incorporation into the field. Consequently, the primary goal of archaeological imaging has been to create visual representations that mimic what human eyes see, and there is currently significant discourse concerning the photorealism of archaeological visualisations (Conlon 1973, xiii; Cookson 1954, 13; Costall 1997, 50; Dorrell 1989, 7; Howell and Blanc 1995, 1; Shanks 1997; 80; Simmons 1969, 4). This debate has risen to prominence with the advent of digital imaging and 3D modelling. Archaeologists – and indeed the public – now question the objectivity of digital images or 3D models because nearly anyone can manipulate them with relative ease to show whatever they wish (Earl 2006, 191; Shanks 1997, 92; Tringham 2010, 72). There is a sense, then, that digital

images require authentication, or at least more authentication than analogue photographs do (Earl 2006, 191). This has only increased the desire for digital visualisations to mimic human eyes, because that is the simplest method for verifying the truthfulness of the image or 3D model (Shanks 1997, 82 - 83).

Yet, no image is ever truly objective, or even mostly so. Capturing an image or creating a visualisation is riddled with choice at least on the part of the photographer or digital imaging specialist. We choose what to image, under specific conditions and lighting and with specific equipment. We choose how to edit the image and how to render the visualisation using specific software and methods we have chosen. Some of these choices are borne out of necessity; laser scanning does not produce informative results for glass objects, for example, and qGIS cannot process photographs into a photogrammetric model. Other choices are purely that, made by the individual to capture the information they seek as best they can. Photographs and other archaeological imagery result from the hundreds or more choices the creator has made, including the choice to image the subject at all. In archaeological imaging, interpretation begins when we decide to pick up the camera or set up the laser scanner. Any representation created by humans is riddled with choice, and archaeological images are far from innocent analogues of the scenes they represent (Bohrer 2005, 182; Earl 2006, 197; Lyons 2005, 25; Moser and Smiles 2005, 2; Papadopoulos 2005, 112; Shanks 1997, 92). In fact, archaeological photographs are considered 'realistic' and 'objective' more because they conform to the canon of realism established through disciplinary discourse rather than because they necessarily have an objective relationship with reality (Lyons 2005, 25; Moser and Smiles 2005, 3; Papadopoulos 2005, 112; Shanks 1997, 82 – 83).

Importantly for this thesis, an image need not be truly objective nor mimic human vision to be archaeologically valuable. There is value in the aesthetic of the image, as

well as the analytical possibilities provided through controlled manipulation. Full discussion of the aesthetic value of archaeological images is outside the scope of this thesis. Both public and academic engagement with heritage and archaeology is mitigated and encouraged through images, however, and there is much to be said for ensuring these images draw people in aesthetically as well as serving as documentation of what once was (Arnold 2005, 92; Bateman 2005, 194; Bohrer 2005, 182; James 1997, 22; Phillips 2005, 72).

There is also significant value in the analytical possibilities for archaeological visual media, particularly those created through controlled manipulation. If all images of an artefact category undergo the same composition, treatment, and processing and use the same equipment, for example, the results still show relative differences and similarities between objects (Chapters 4 through 7). Also, archaeologists can recover significantly more information about a subject by intentionally representing it in a way that is impossible for the human eye to capture, such as using both visible and non-visible light. These assertions serve as the basis for all the case studies in this thesis. Indeed, by limiting informative archaeological imaging to that which appears as closely as possible to human vision, we severely limit the information and insight we can glean from archaeological subjects.

While prescribing standardised methods across the discipline for each imaging technology allows for comparison between visualisations, it discourages deviation from the standard. For SRT objects, this results in a lack of informative or engaging images and visualisations due to the poor results generated by standard imaging techniques. "Our digital paintbox is far more diverse than currently employed, and far less open to diversity than the real canvas of our counterparts," (Earl 2006, 195). Experimenting with techniques outside the prescribed standard can provide more information than previously

acquired through standard means, thereby furthering our understanding of and engagement with the archaeological record.

2.2.2 OLD VERSUS NEW TECHNOLOGIES IN ARCHAEOLOGICAL IMAGING

Many archaeologists embrace technological developments in the field and champion their use in archaeological research (e.g. Dellepiane et al. 2006; Doneus and Briese 2006; Doneus et al. 2011; Earl et al. 2008; Earl et al. 2010; Mudge et al. 2005; Mudge et al. 2006; Nylén 2008; Remondino et al. 2009; Remondino 2011). RTI has proven beneficial for studies of rock art, stone sculpture and artefact recording and analysis (e.g. Bernardini et al. 2002; Diaz-Guardamino and Wheatley 2013; Grün et al. 2004; Kitzler Åhfelt 2002; Kitzler Åhfelt et al. 2015; Koutsoudis et al. 2014; Opitz 2015; Remondino et al. 2009; Remondino 2011; Salonia et al. 2005) while photogrammetry (particularly SfM photogrammetry) is often recommended for recording buildings, sites, and artefacts (e.g. Bernardini et al. 2002; Grün et al. 2004; Koutsoudis et al. 2014; Remondino et al. 2009; Remondino 2011; Salonia et al. 2005). Laser scanning and LiDAR have seen the largest success in aerial archaeology, particularly in uncovering sites and buildings located vegetation-dense regions such as the complex urban landscapes at Angkor Wat (Evans et al. 2013) or the Mayan lowlands of the Yucatan (Canuto et al. 2018). Laser and structured light scanning have also been successful in documenting buildings, sites, and certain artefact categories (e.g. Evans and Donahue 2008; Forte et al. 2012; Grussenmeyer et al. 2008; Lerma et al. 2010; Lin et al. 2010; Lobb et al. 2010; McPherron et al. 2009; Niven et al. 2009; Roman et al. 2010). Multispectral and hyperspectral imaging has uncovered underdrawings and revealed conservation efforts of art historical pieces and has allowed art historians to identify the use of specific pigments (e.g. Christens-Barry et al. 2009; Cosentino 2014; Dorrell 1994; Fischer and Kakoulli 2013; Legnaioli et al. 2013; Liang 2012; Padfield et al. 2005;

Pilarska 2016). Digital technologies have significantly improved archaeological research and documentation and will likely continue to do so in the future.

There has been a slower uptake of these technologies in excavation and contract archaeology, however, largely because doing so creates a wave of required changes across the recording of the site and the process of excavation (Backhouse 2006, 51). New technologies require new methodologies and new metadata, many of which cannot necessarily be predicted until months after the excavation has concluded (Backhouse 2006, 51). Additionally, newer digital technologies create digital data that is less amenable to archival procedures, often because the type of file and metadata required are unlike anything for which there are already current archival practices. There are continual debates in archaeology (and elsewhere) concerning the preservation of digital data, a concern that only increases with the use of newer, and more obscure filetypes containing more and more data. Also, those who work with newer technologies are keenly aware of the frequency with which they require troubleshooting or simply break down. From personal experience, I have yet to be on a dig in Scotland during which the portable GPS unit worked consistently, and I can say the same for magnetometers, electrical resistance meters, laser and white light scanners, and even site laptops and printers. Backhouse (2006, 52) cites a related experience in which his team had a portable computer on-site for less than three days before they needed to return it to the head office due to a broken screen (costing £800 to repair). Electronic equipment in the field often has a high casualty rate in archaeology. Coupled with the high cost of much of the equipment and the requisite changes to recording methods and metadata, it is understandable why commercial units have been hesitant to adopt the newer technologies often championed by the research sector (Backhouse 2006, 53; Bradley 2006, 35).

Despite the large push for new technologies in academic archaeology, there are many who caution against allowing new technologies to become a fetish (Huggett 2004, 82), a type of religious fervour (Zubrow 2006, 15), or more an indication of the social aspirations of the user than the quality of the results (Bateman 2005, 195). Still others argue that while in pursuit of new technologies, we do not discredit or diminish the use of the old (Beale et al. 2013, 240). Many criticising the obsession with new technology in archaeological imaging also posit that use of new technology in archaeology creates a power dynamic which privileges both those who can afford and use the technology over those who cannot (Huggett 2004, 85; Rutsky 1999, 156; Santana Quintero and Eppich 2016, 3; Voorips 1984, 48; Zubrow 2006, 14). This power dynamic becomes so prominent in the field that new technologies often abolish older ones and become so essential themselves that there is little possibility for success without them (Zubrow 2006, 14). In the case of archaeological imaging, older technologies have not been abolished so much as discredited. We know that photography is not entirely objective, so we look to new technologies to create objective representations of archaeological material. There appears to be less room for human intervention, so there is less human input to skew the results. Similarly, more technological methods and equipment provide more distance between the archaeologist and what they are recording, either physically or metaphorically, as highlighted through debates of aura and authenticity (Huggett 2015, 89). This, together with the pre-programmed manner in which the equipment records data, furthers the perceived degree of objectivity for a given technology. Naturally, then, archaeologists wish to use more objective methods to produce more objective results, often at the expense of older techniques.

The discussion of objectivity above applies to all techniques, however. There is always human choice in what to record and how, and even the most technical digital

visualisation tools require significant human input. Furthermore, new technologies are not without their limitations or faults: laser scanners cannot create 3D models of glass objects due to the differences in how the material refracts and reflects the laser's energy back to the sensor while many white light scanners cannot work with small objects due to the inability to detect such objects with enough accuracy to create a model. Finally, most archaeological research and imaging results from lower-budget projects, many of which cannot afford the latest new technology and many of which cannot practically transport the technology to the location in which the images must be created. Consequently, older techniques like photography (both analogue and digital) remain more practical, portable, and affordable than any burgeoning new technology and is therefore the more logistical choice for many projects in the field. Championing new technologies at the expense of the old because they are more objective therefore 1) ignores the inherent subjectivity in imaging of any kind; 2) limits the field to imaging only those object categories falling within the limitations of the newer technologies; and 3) inadvertently predicates the value of a project's results at least in part on the degree to which they can afford to use more technical, but often less practical digital equipment. Furthermore, the limitations imposed on archaeological imaging in our pursuit of new technologies for creating objective, standardised visual records of the archaeological materials limits what we record and the information we gain from it, thereby simultaneously placing limits on what information enters into the archaeological record.

2.2.3   ARCHAEOLOGICAL IMAGING AND THE ARCHAEOLOGICAL RECORD

Archaeological imaging has always served as one of the primary means of creating the archaeological record, and our understanding of the world, and therefore the past, is directly influenced by how we represent it visually (Beale et al. 2013, 243). Since its announcement, photography has been used to document archaeological finds and,

importantly, the archaeological process. Imaging techniques like photography or 3D scanning capture detail that excavators and other specialists may have missed, thereby entering information into the archaeological record for which we do not yet know the value. Consequently, we can argue that the archaeological record has significantly less information pertaining to archaeological material that is not imaged as it does for material that is.

Many would argue, and rightly so, that not everything can enter into the archaeological record to the same degree. We cannot image everything; we must be selective. This selectivity is a problem in archaeology not because it exists, but because we do not apply it equally across the discipline. Instead, we apply standard imaging techniques to the objects for which those techniques work and often neglect those objects for which they do not, SRT objects being one such category. There are many more archaeological photographs of ceramics and standing stones than there are of glass objects, for example, even in locations where glass objects vastly outnumber the other two. Sources discussing imaging even for conservation purposes dedicate dozens of pages to structures, standing stones, human remains and documents, but dedicate less than 10% of their work to imaging objects and usually provide only a few sentences, if any, on the imaging of glass (e.g. Conlon 1973; Cookson 1954; Dorrell 1989; Howell and Blanc 1995; Silver 2016). We therefore privilege certain object categories over others based on the ease with which we can image them using available standardised methods, rather than on the value of the information they provide to our understanding of the past. In so doing, we are omitting or ignoring the possible contributions of vast quantities of material to our collective understanding of humanity.

Our pursuit of new technologies only increases the severity of this problem. Many projects cannot afford such technologies, but archaeological discourse often touts the

results as being more objective and therefore more valuable than those created using more affordable technologies. Archaeology therefore often privileges the results of higher-budget projects that can afford new techniques over the results of those that cannot. Thus, archaeology omits, ignores or devalues possible contributions not only from material that does not lend itself well to current, standardised techniques but also from results created by lower-budget projects.

A further complication is the degree to which these results can be entered and archived into the archaeological record. The prominence of digital technologies and their continual development has led to an explosion of digital data without a similar explosion in techniques for safeguarding and archiving said data. Newer technologies often complicate matters further by storing data in newer and rarer filetypes that often only work with specific software and often only in conjunction with several other files of similarly rare and unique types. The push for newer technologies continues to amass data before the field has fully understood what it is and how to care for it. Archival practices are not discussed in detail in this thesis due to space limitations, but the success of the archaeological record directly corresponds to our ability to archive the data it contains.

The value, creation and maintenance of the archaeological record therefore depends on the information we enter into it and the degree to which we can preserve that data. Focusing our efforts on available, systematic, objective techniques for creating archaeological data therefore omits any data that does not lend itself well to capture through these techniques, including most data for SRT objects. Our privileging of the results of newer technologies over older ones omits or diminishes the value of data created by projects unable to afford such techniques. It also privileges the data for which we are least likely to have developed, standardised archival practices. The result is an

archaeological record for which modern practices and discourses are arguably as much as of a factor in its creation as the value of the archaeological data it contains.

2.3   A NEW TYPE OF ARCHAEOLOGICAL IMAGING

Fortunately, we can change our current practices and discourses. Challenging the standard rules of archaeological photography or finding affordable means of gathering data are both valuable pursuits that would allow us to begin releasing ourselves from the current limitations of archaeological imaging. We must continue to examine and employ new technologies and standard rules of photography to continue capturing valuable archaeological data. However, we must also pursue imaging techniques that challenge these standards, including older technologies we tend to view as less objective. In so doing, we can significantly increase the information gleaned from archaeological materials in practical, portable, and affordable ways.

The remainder of this thesis serves as a demonstration of the value of this approach to archaeological imaging, focusing on visible photography (Chapter 4), non-visible-range photography (Chapter 5), PTM RTI and SfM photogrammetry (Chapter 6). The primary goal was to create affordable, practical, and portable means of digitally imaging SRT objects (primarily glass beads and vessel sherds), but the techniques discussed in the following chapters can be applied to many subjects and materials (Chapter 7), including those outside the discipline of archaeology. It is hoped that this will serve as the impetus for others to begin challenging standard imaging methods for other objects and materials and to enter into this discourse of practical and affordable archaeological imaging techniques.

3 PRINCIPLES AND TECHNIQUES

All the techniques used in this research build off the foundational principles of photography by challenging archaeological photographic standards. While there are some principles and techniques unique to each case study, which are outlined in their respective chapters, there are many that create the foundation for all experimentation in this thesis. This chapter discusses these general principles, beginning with the basic principles of photography and ending with a discussion of photogrammetry and 3D modelling.

3.1 PRINCIPLES OF DIGITAL PHOTOGRAPHY

The basic principle of a camera is the camera obscura discussed in Chapter 2: light passing through a pin-sized hole of a box will produce an inverted image on any surface opposite the pinhole. The most common digital cameras today are dSLRs (digital Single Lens Reflex) likely due to the popularity of the SLR design prior to the invention of digital cameras (Freeman 1985, 10; Johnson 1909, 10). Light entering an SLR camera passes through the lens onto a mirror, which reflects the image up through a pentaprism onto a matte surface (Figure 3.1) (Freeman 1985, 11; Mansurov 2009). This surface reflects the image back through the pentaprism into the viewer's eye (Freeman 1985, 11; Mansurov 2009). This allows the photographer to see the image exactly as the camera will capture it (Freeman 1985, 11). When the photographer presses the shutter release, the bottom of the mirror flips up to reveal the shutter (Freeman 1985, 11; Mansurov 2009; Ward 2015). The shutter opens to allow light through the pinhole and onto the image sensor before it shuts again and the mirror moves back into place.

Lining Up a Shot

Capturing an Image
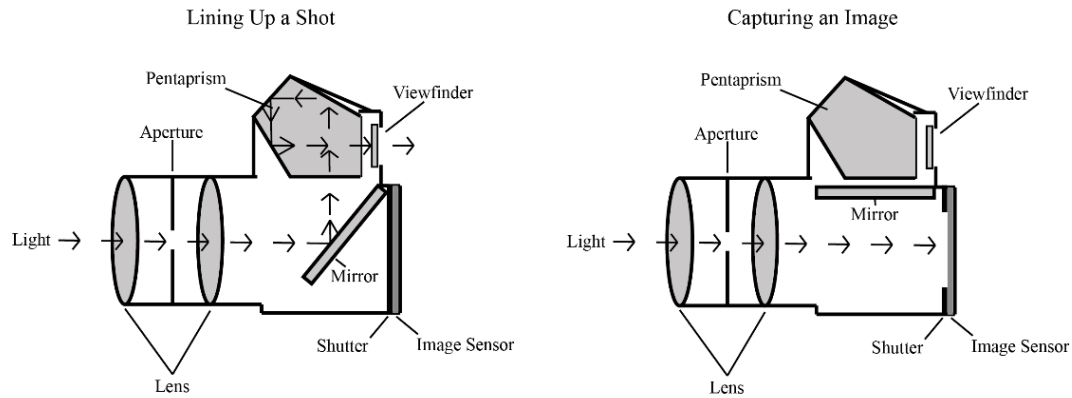
Figure 3.1: Basic workings of a digital Single Lens Reflex camera (dSLR).

In film or analogue cameras, the light passes through to photosensitive film filled

with silver halide crystals and colour couplers, which records a latent image that

photographers can develop into a photograph (Freeman 1985, 98 – 101; Johnson 1909,

10). In a digital camera, however, light passes through onto an image sensor (Mansurov

2009; McDowell 2009; Ward 2015). This sensor contains millions of photo sensors,

which collect data for each pixel in an image. When light hits a photo sensor, it passes

through a coloured filter and registers the light as an electrical charge of red, green, or

blue light in various intensities (Golowzcynski 2016; McDowell 2009; Verhoeven 2016,

146 - 147). The screen in the camera or on a computer can then compile the data for each

pixel to form a digital image.

The camera only records data for red, green, and blue light because any screen

that displays it will only use red, green or blue light to render the image, and because

those are the only colours that human eyes see (Chapter 2.1) (Bayer 1976; Glotzbach et

al. 2001, 141; Golowzcynski 2016; McDowell 2009; Taylor et al. 1991). Both digital

cameras and the screens rendering these images all operate using the RGB colour model

(Figure 3.2) (Taylor et al. 1991). This is an additive colour model with red, green, and

blue as primary colours, and yellow, cyan and magenta as secondary colours (MacLeod

2008, 40; Malpas 2007, 14). Adding primary colours together creates each of the secondary colours, such as red and green for yellow or blue and red for magenta. Thus, when we see an image of a yellow flower on a screen, there are no yellow pixels. Instead, a combination of red and green pixels overlaps to appear yellow.
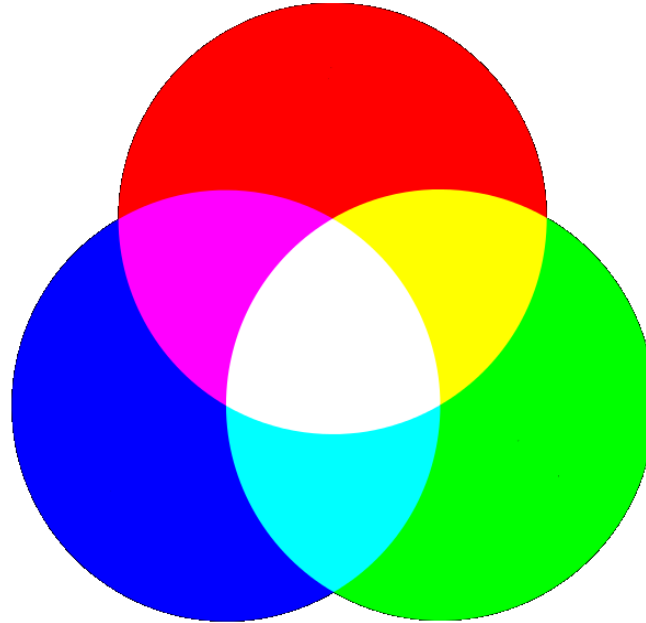
Figure 3.2: The RGB colour model.

3.1.1 SHUTTER SPEED, APERTURE, ISO AND EXPOSURE

Given the mechanics of the camera, there are three factors that determine the exposure of an image: shutter speed, aperture, and ISO. Each of these control different elements of the camera itself, and therefore also control different elements of the resulting image. Shutter speed is the length of time the shutter is open in front of the image sensor to create an image. The longer the shutter speed, the longer the sensor is exposed to light. This can result in lighter or darker images, depending on how fast or slow the shutter speed is (Figure 3.3). It also affects the sharpness of the image. If the camera or subject of the image is moving or unstable, a slower shutter speed will result in a blurry image. Alternatively, a faster shutter speed will result in a sharper image. Scientific imaging

usually requires as sharp an image as possible, but fast shutter speeds may be difficult to achieve in relation to other settings.

Figure 3.3: Comparison of an image taken at shutter speeds of 1/2 second (left), 1/10 second (middle), and 1/40 second (right), processed to have similar exposure.

Aperture is the amount of light reaching the image sensor through the lens, which a photographer controls by widening or narrowing an opening in the lens. Photographers denote the aperture using f/#, which they call the f-stop. The number represents the factor by which we divide the diameter of the lens to create the aperture (Neblette 1952, 29). For example, a 52mm lens with an aperture of f/2.8 has a lens opening 18.57mm in diameter, whereas the same lens using an aperture of f/16 has an opening 3.25mm in diameter. Since the number denotes the factor by which we are dividing the diameter of the lens, the larger the number, the smaller the aperture.

Aperture affects the depth of field in an image, which is the distance between the nearest and farthest elements of the image that are in focus (Neblette 1952, 32). For an object at a fixed distance, a larger aperture (smaller f-stop) results in a shallower the depth of field, while a smaller aperture (larger f-stop) results in a wider depth of field (Figure 3.4). It is important to maintain proper focus across all elements of the image, but the smaller the aperture, the darker the exposure.

Figure 3.4: Comparison of images taken with a larger (f/4.5; left) and smaller (f/9; right) apertures, processed to have similar exposure.

ISO, or film speed, originally described the size of the silver halide crystals on film (Freeman 1985, 96). The larger the grain, the higher its sensitivity to light and therefore the 'faster' the film reacted. In digital cameras, ISO determines the sensitivity of the photo sensors (Figure 3.5) (Rowse 2006; Mansurov 2009). When we overexpose a grain of silver halide or an individual photo sensor, it creates noise or grain in the image. This happens most often at higher ISO settings but can happen at lower ISO settings in digital cameras if we have not been careful with other settings (Figure 3.5).

Figure 3.5: Comparison of images taken with ISO-100 (left), ISO-400 (middle), and ISO-800 (right) (Loch Eriboll; UG F128), processed to have similar exposure.

Ideally, an image would have a low ISO to reduce grain/noise, a small aperture to increase depth of field, and a fast shutter speed to reduce blur. Yet, each of these settings

greatly affects exposure, or the quantity of light reaching and registering on the image sensor. Using low ISO, small aperture, and fast shutter speed allows very little light to reach the sensor, and results in an image that is either very dark or entirely black. The difficulty, then, is balancing each of these factors to minimise error and optimise exposure.

For the scientific photography of objects, we must prioritise aperture and ISO over shutter speed. We can decrease blurriness with relative ease by setting the camera on a tripod and either taking an image on a timer or using a remote, but we cannot easily lessen noise in the image or increase depth of field. If the camera, the object, and the platform(s) upon which they sit remain stationary, the image will remain sharp despite slower shutter speeds. Generally, an ISO of 100 – 200 and an aperture of f/11 – f/22 works well for standard photography of archaeological finds. These two settings will determine the shutter speed, which often falls around 1 second under ambient fluorescent light.

I have found that sometimes capturing slightly underexposed (+1.00 to +3.00) or overexposed (-1.00 to -3.00) images is better in small finds photography than setting the camera to capture perfect exposure (+0.00). Depending on the location, uneven lighting or multicoloured objects can cause an error whereby the camera believes it has captured perfect exposure when it has actually over- or underexposed elements of the object, losing valuable colour and surface information. We can always selectively adjust the exposure in post-processing to brighten darker elements or darken lighter ones. However, the computer cannot recover information that the camera never captured due to overexposure or underexposure (Figure 3.6).
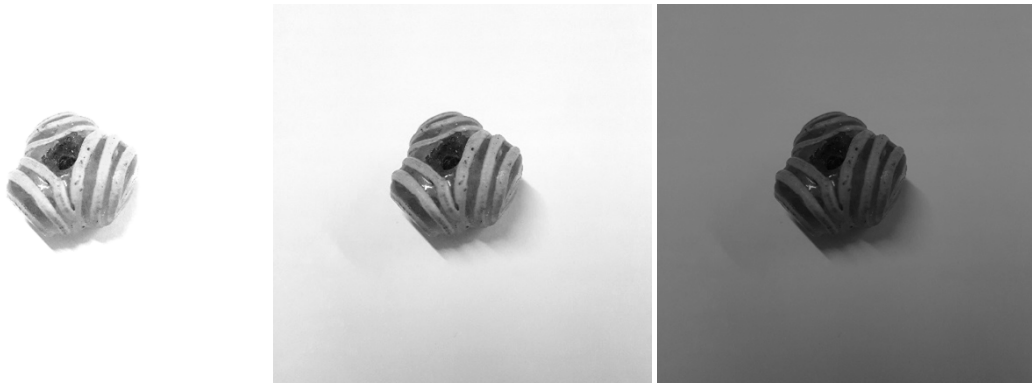
Figure 3.6: Comparison of images that have been overexposed (left), evenly exposed (middle) and underexposed (right) (Loch Eriboll; UG F128).

3.1.2   LENSES AND FOCAL LENGTH

At its most basic, the lens of a camera focuses light through to the sensor. When light interacts with any single point on an object, the light refracts and diverges in different directions. A convex, or converging, lens bends the diverging light back to a single point on any available surface (Freeman 1985, 28; Wheadon 1968, 53–54). The focal length of a lens is the distance at which the light converges to this single point, which varies depending on both the distance between the object and the lens and the structure of the lens itself (Amateur Photography 2013; Neblette 1952, 22). Objects that are closer to a lens have a longer focal length, while those farther away have a shorter focal length. Additionally, a more convex lens will have a shorter focal length than a flatter one (Wheadon 1968, 59; Neblette 1952, 22). When zooming or focusing a camera lens, we are moving the lens closer to or farther away from the sensor and therefore changing the point at which the light converges to form a focused image.

Object photography generally uses at least one of the following three lenses: a zoom lens, a macro lens or a microscope. The first two are attachments for a standard SLR or dSLR camera while the third is a stand-alone unit. Zoom lenses specialise in enlarging the image of an object as it appears on the sensor (Freeman 1985, 34). Most

dSLRs now come with an 18-55mm zoom lens, but 18-200mm lenses are also popular. The range in millimetres denotes the range in focal length; the higher the focal length, the higher the possible magnification of the image (Freeman 1985, 31). While these zoom lenses provide a range of focal lengths, however, this versatility comes at the expense of image resolution, particularly at the extremes of the lens's settings (Freeman 1985, 35). Additionally, many objects are too small even for a highly versatile zoom lens to capture in significant detail, including many beads.

Macro lenses focus the image such that the ratio of the subject to the amount of space it occupies on the image sensor is at least 1:1 (Freeman 1985, 37; Gajski et al. 2016, 263; Meyer 2013; Smith 2009). This means that a 10mm x 10mm object will take up 100mm^2 (or 28%) of the 23.1 x 15.4mm image sensor found in a Nikon D3100. Macro lenses generally have a fixed focal length; the shorter the focal length, the closer the lens must be to the object. Many point-and-shoot cameras have a 'macro' setting (often denoted by a flower), but this is not the same as a macro lens. Macro settings on a point-and-shoot merely optimise the settings to expose and focus on a small object. Most point-and-shoot macro images achieve less than half of the minimum 1:1 ratio of a macro lens, and often fail to capture the same level of detail (Freeman 1985, 288–289; Friedland 2016).

Many archaeological photography manuals discussing photomacrography techniques describe close-up photography instead (Connolly 1953, 12; Dorrell 1994, 177; Fisher 2009, 10). Most recommend using the macro settings on a point-and-shoot camera, while others advocate for using close-up filters (Connolly 1953, 14; Dorrell 1994, 178–179; Fisher 2009, 10). Close-up filters are lenses that screw onto the end of the main lens to decrease the minimum focal length. They can provide useful results and are cheaper

than macro lenses, but they do not capture as much detail and do not achieve the same ratio (Freeman 1985, 288–289).

Many objects are still too small to capture in detail with a good macro lens, especially if we wish to capture surface wear or corrosion. For these objects, a microscope may be the best imaging tool. Handheld digital microscopes use similar optics of focusing light through a lens onto an image sensor, then transferring that image to a computer. These microscopes can magnify the image up to 500x, therefore capturing much more detail than a macro or zoom lens (Absolute Data Services 2017). Microscopes have difficulty capturing a full image of any object over 15mm, however, and image quality suffers in exchange for increased magnification in the more affordable models. Most affordable digital handheld microscopes also do not allow for manual settings of aperture, shutter speed, or ISO, and only capture images as .jpg or .bmp rather than a raw image file.

3.1.3   DEPTH OF FIELD
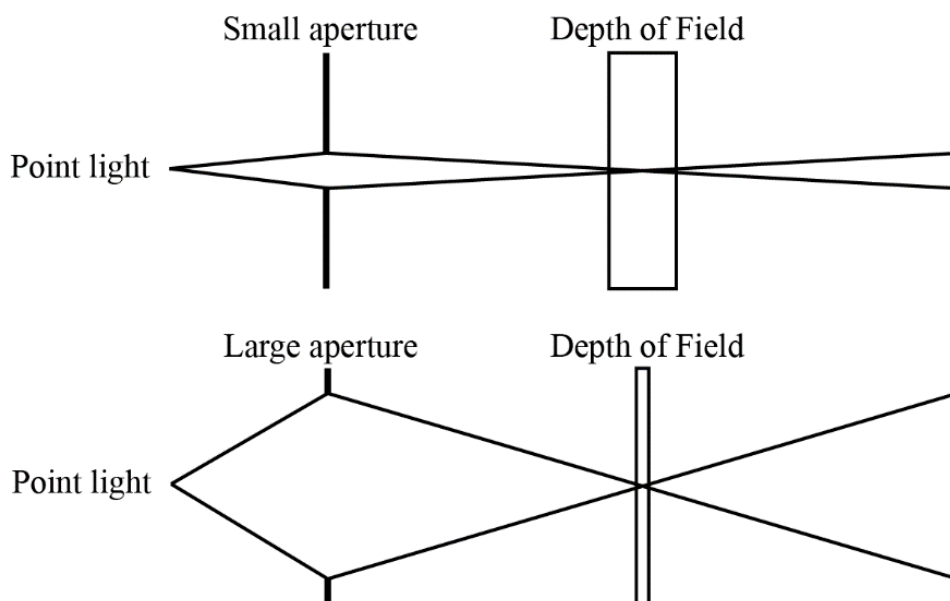
Figure 3.7: Diagram showing depth of field.

Depth of field refers to the distance between the nearest and furthest elements of an image that appear in focus (Neblette 1952, 32). As discussed above, a lens focuses light at a single distance to create a sharp image of the subject of a photograph. Since most images capture three-dimensional subjects, not all points will be in perfect focus. Instead, any point for which light would focus at a different distance will render as a blurry point in the shape of the aperture. If the point is small enough, our human eyes accept it as being 'in focus' and therefore falling within the depth of field (Neblette 1952, 32).The farther away an object is from that focal length, the larger this circle becomes. The circle of confusion is the largest circle our eyes accept as being in focus within an image (Neblette 1952, 31–32). When the aperture is larger, the threshold for the circle of confusion is much lower and the depth if field is smaller (Figure 3.7). When the aperture is smaller, the depth of field is larger. This is because the starting circle size for unfocused points directly correlates to the aperture opening. It is best in object photography to use a smaller aperture (larger f-stop) to maximise depth of field.

3.1.4   Colour Balance

Different temperatures of light cause an object to appear different colours. For example, a white sheet of paper can appear blue, orange, or even green depending on the lighting used to capture the image (Figure 3.8). Images of objects therefore often fail to capture the true colours of the object due to changes in lighting conditions. This creates problems for colour recording, particularly when using specific colour-recording systems like Munsell (Chapter 1.2.3). Consequently, photographers must colour balance their images to display the true colour of an object.

Figure 3.8: Comparison of an image photographed under cooler (left), neutral (middle) and warmer (right) light temperatures (Loch Eriboll; UG F128).

While digital cameras can colour balance when they capture the image, it is easier to control the settings in post-processing. Including an object of known colour in the image helps to ensure colour balancing can occur. This is usually white, black, or a neutral grey, though sometimes includes a combination of the three. A preferable set-up in archaeological photography is to place the object on a neutral (e.g. white, grey or black) background and include a standardised scale. Either the scale or the background can serve as reference for colour balancing, depending on preference. Interestingly, I have found that near-ultraviolet and near-infrared images white balance the same no matter which part of the image acts as the standard, but it is best to continue to use similar backgrounds and scales as visible images to maintain uniformity across images.

3.1.5 IMAGE FILE FORMAT

Cameras capture images in a variety of formats, but most photographers would recommend capturing predominantly or only in the raw format. Raw image files contain the minimally processed raw data from the camera's image sensor rather than a fully formed image, and they are often referred to as digital negatives because of this. Once processed, photographers can save the images as any file type without damaging the original data captured by the camera. Many cameras and software have their own extensions for raw files, which appear in Table 3.1.

Camera	Raw File Extension
Adobe	.dng
Canon	.crw ; .cr2 ; .cr3
Kodak	.dcs ; .dcr ; .drf ; .k25 ; .kdc
Nikon	.nef ; .nrw
Olympus	.orf
Panasonic	.raw ; .rw2
Sony	.arw ; .srf ; .sr2

Table 3.1: Common raw file extensions for common camera models and software.

Most cameras offer the option to capture images as either.jpg, raw files or both. Capturing images in the raw file format is essential, because it allows for a full rendering of the final image. Many .jpg files undergo lossy or irreversible compression, in which the computer discards some data in favour of smaller file size (Verhoeven 2016, 234). There are settings to adjust the degree of compression but saving the image as a .jpg file often results in a loss of data. To ensure high quality photos, it is best to capture a raw file and save it as .tiff or .png rather than capturing the image outright as .jpg. If comparing images captured in different file formats, however, it is better to save all images as the lowest quality format to ensure differences spotted between images are due to actual differences in the object and not to quality of the image itself.

3.1.6 Image Processing

All digital archaeological images must undergo some form of computer processing, at the very least for white balancing, straightening, and possibly cropping. The most popular software for this is the Adobe Suite, using either Adobe Lightroom, Photoshop, or Bridge. In archaeological photography, the primary goal of image processing is to represent the object as it looks to the naked eye and as it looked to the viewer at the time of image capture. To do this, most images only need white or colour

balancing to ensure proper colour representation. Auto tone settings may be useful, and rotation ensures the object is oriented well within the frame.

This thesis challenges the notion that processing should aspire to create images as close to what the eye saw as possible, however, and instead processes images in a systematised manner to highlight information not otherwise visible to the naked eye. Doing so requires more extensive image processing than that required for mimicking human sight and the process differs depending on the desired information. I provide specific details of image processing in each chapter for the case studies included in this thesis, since each study processed the image in different ways.

In all cases, image processing techniques can only work with the data photographers provide. Image processing cannot fix an image that is out of focus, poorly exposed, blurry or noisy. Sharpening an image, for example, will only help so much with blurriness or lack of focus, and often introduces grain into the image. Reducing noise using various settings often introduces blurriness into the image, and only partially reduces noise. It is imperative, then, that the original image be of the best possible quality to ensure a good result.

3.2   PHOTOGRAPHY AND THE PRINCIPLES OF LIGHT

All three case studies in this thesis experiment with spectral photography, or photography that captures reactions to specific wavelengths of light for a given image or subject (Chapter 1.1). This can include the entire visible spectrum, rendering any standard image captured by a digital camera a spectral image, or it can include the non-visible spectra. In this study, I focus on spectra between 300 and 1000nm, ranging from the near-ultraviolet to the near-infrared.

To capture different spectra for a given subject, I attach filters to the lens of my camera. Filters allow specific wavelengths of light through to the lens, thus altering the light a camera can 'see' through its sensor. This section details the principles by which objects interact with light, while the following section describes how we can photograph those interactions using filters and a converted dSLR camera. By understanding the basic principles and behaviours of light and how filters help us isolate that behaviour for specific wavelengths, we can create informative images that reveal and even emphasise previously invisible characteristics of an object.

3.2.1 PRINCIPLES OF LIGHT

A beam of light consists of both electric and magnetic waves. These electromagnetic waves oscillate as the beam of light travels through space (Figure 3.9) (Ditchburn 1991, 10 – 11; Jenkins et al. 1981, 223; Verhoeven 2016, 130; Wheadon 1968, 2). Different types of light oscillate at different rates, and therefore have different wavelengths (Jenkins et al. 1981, 232 – 233; Verhoeven 2016, 130 – 131). The wavelength of a beam of light equals the distance between adjacent peaks or valleys of a wave, often measured in nanometres (10^{-9} m) (Jenkins et al. 1981, 223; Wheadon 1968, 2). The electromagnetic spectrum spans from 1 picometre to 1 megametre (1/1000 to 1e+15 nm) and includes familiar wavelengths like x-rays, gamma rays, radio waves, and visible light (Figure 3.10) (Ditchburn 1991, 13; Wheadon 1968, 3). My research focuses on wavelengths between 300nm and 1000nm, which includes some near-ultraviolet light (300-400nm), the entire visible spectrum (400-700nm), and a portion of near-infrared light (700-1000nm). This is the maximum span of wavelengths detectable by a dSLR camera converted for spectral photography.
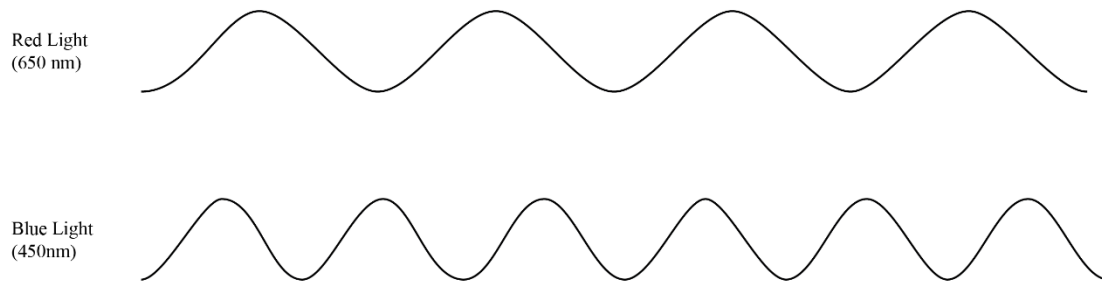
Figure 3.9: Difference in light oscillations/wavelengths.
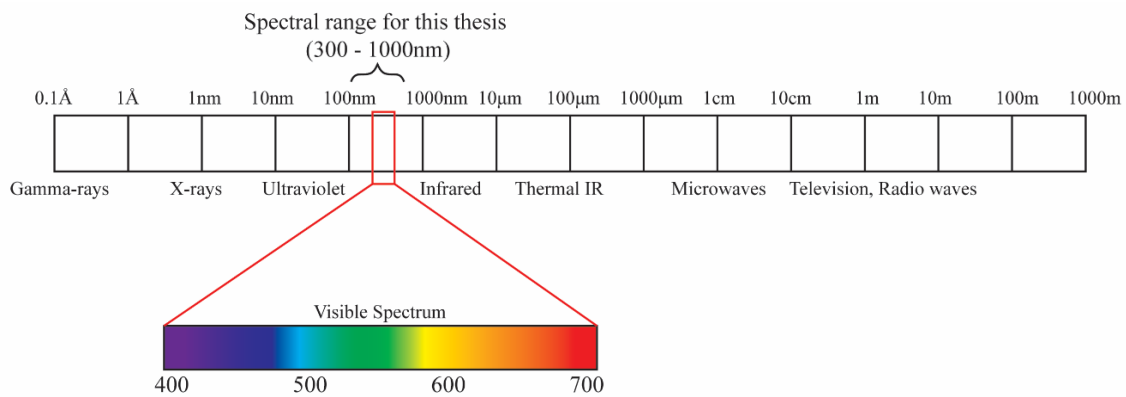
Figure 3.10: The full electromagnetic spectrum and the spectral range employed in this thesis.

Standard dSLR cameras have an internal hot mirror or coating on the image sensor that block extraneous ultraviolet and infrared light from reaching the sensor and ruining images (Tetley and Young 2007, 162; Tetley and Young 2008, 51; Verhoeven 2016, 146 - 148). Consequently, they are sensitive only to wavelengths between roughly 400 and 700nm. To capture images between 300 and 1000nm, we must remove the hot mirror and replace it with a filter of fused silica. Fused silica (also called fused quartz) is a glass made solely of melted silica (Esco Optics 2017; Jenkins et al. 1981, 459; Marshall et al. 1997, 59; Newport Corporation 2017). It does not include other common elements of glass, such as alkalis or colorants or trace elements, which alter the transmittance properties of the glass (Chapter 5.1). Consequently, fused silica is much better at transmitting ultraviolet and infrared light to the camera sensor (Esco Optics 2017; Jenkins et al. 1981, 459; Marshall et al. 1997, 59; Newport Corporation 2017; Phillip 1966, 73).

Attempting the conversion without a specialist is not recommended, as doing so could permanently damage or destroy the camera. Once the camera has been converted, we can begin to examine how light interacts with objects through photographs.

3.2.2 REFLECTION, TRANSMISSION, ABSORPTION, AND FLUORESCENCE

The vibrations of stimulated atoms emit energy at various wavelengths, many of which fall into the spectra of light we can capture with a camera (Jenkins et al. 1981, 215). The wavelength of the emitted energy depends on the wavelength of the original stimulus and on the nature of the atom or molecule in question (Jenkins et al. 1981, 232).

Electrons in atoms all vibrate at a natural frequency, which differ depending on the atom. If energy (e.g. light) hits an atom with the same vibrational frequency, the electrons absorb that energy by transferring it into vibrational motion (i.e. thermal energy) (Chaichian et al. 2014, 193; Wright 1958, 10–11). The atom has absorbed that energy, then, and will not reemit it as light (Figure 3.11). Conversely, an atom stimulated by energy that does not have its same vibrational frequency either reflects it back or transmits it, depending on the nature of the atom and the matter it forms (Gigahertz-Optik 2017; The Physics Classroom 2017a; The Physics Classroom 2017b). Reflection is the return of light from either the surface (surface reflection) or the interior (volume reflection) of a medium, while transmission is the passing of light through a medium to the other side (Gigahertz-Optik 2017; The Physics Classroom 2017a; The Physics Classroom 2017b). In general, opaque objects reflect or absorb light, transparent objects transmit or absorb light, and translucent objects do all three. A medium may selectively reflect, transmit, or absorb any wavelength of light, including those in the non-visible spectra.
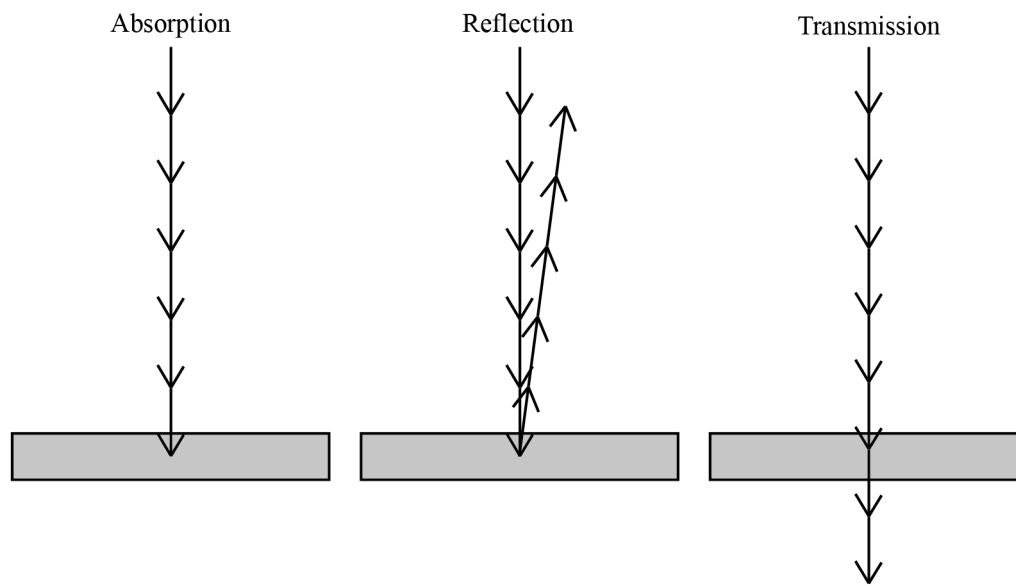
Figure 3.11: Absorption, reflection and transmission of light in a medium.

The selective reflection, transmission, and absorption of various media is what gives objects their colour. When light from the visible range shines on an object, it absorbs certain wavelengths and reflects or transmits others (Jenkins et al. 1981, 458; Optical Society of America et al. 1968, 176). The object appears to be the colour of the reflected or transmitted wavelengths. For example, a red object appears red because the medium has absorbed all other wavelengths of light and is reflecting or transmitting only the red wavelengths. When those wavelengths pass through our eyes, we register the object as red (Figure 3.12).
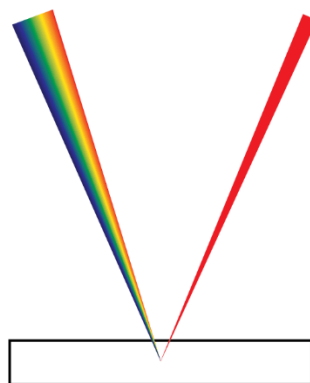
Figure 3.12: Light interacting with a 'red' object.

Fluorescence occurs when energy from one wavelength of light stimulates an atom or molecule and it reflects a longer wavelength of light as a result (Jenkins et al. 1981, 464). An object lit with ultraviolet light may fluoresce in the visible range, for example, while an object lit with visible light may fluoresce in the infrared range. There are many animal species that fluoresce, particularly amphibians, arachnids, and butterflies. Many minerals and gemstones also fluoresce under ultraviolet light, often in different ways depending on the wavelength of the ultraviolet light (Kurz et al. 2012; Kurz et al. 2013; Pirard 2016). Art conservation and art history use a combination of reflection, transmission, absorbance, and fluorescence of visible and non-visible light to identify pigments used in historical paintings(e.g. Cosentino 2014). Infrared fluorescent images can expose underdrawings and other semi-subsurface features in paintings (van Asperen de Boer 1968; Legnaioli et al. 2013; Liang 2012).

While I did test fluorescence on the objects I imaged for this thesis, none of the objects fluoresced in the infrared range and the results of fluorescence from ultraviolet light did not differ enough from ultraviolet reflectance to warrant further study at this time (Figure 3.13). This is an interesting result on its own, particularly given the tendency for certain pigments to fluoresce in various lights as discovered through art conservation research (Cosentino 2014). It is possible that glass objects made with starkly different recipes, such as those made or found outside Europe (Chapter 5.1), may differ in their fluorescence of near-infrared or near-ultraviolet light. It is also likely that different glasses fluoresce in far-infrared light, but capturing such data requires access to a multi- or hyperspectral camera.
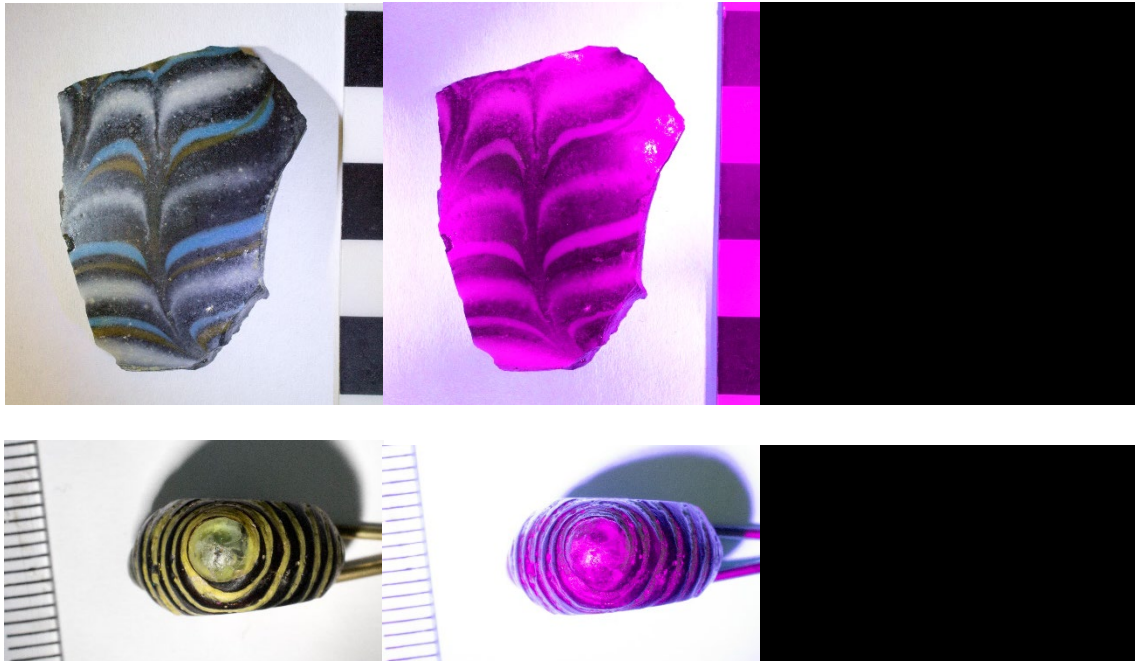
Figure 3.13: Example of visible-range reflection, ultraviolet-visible fluorescence, and visible-infrared fluorescence images (BM 5615 29771 W, top; NMS X.BIB.13, bottom)

Reflection, transmission, and absorption occur with any type of light, not just the visible range. While we cannot always see these reactions with our own eyes, we can capture them using a converted dSLR or multispectral or hyperspectral cameras. Capturing these images requires the use of filters, which isolate specific wavelengths of light much like Maxwell's original coloured solutions (Chapter 2.1).

3.3   VISIBLE-RANGE SPECTRAL PHOTOGRAPHY

Practically, a filter is either 1) a physical attachment to the lens of a camera that only transmits certain wavelengths of light through to the image sensor; or 2) a series of settings applied in photo-editing software to imitate the results of a physical filter. Both work equally well for the visible spectrum, and physical filters can also transmit or absorb ultraviolet and infrared light. Digital filters can only mimic visible-range filters, but they work for any digital image captured in the visible range and can work in tandem with physical filters for producing false colour images (Chapter 2.1.1).

A physical filter is a coloured piece of gel either on its own or placed between two pieces of glass. Both sit in a frame that screws onto the front of a camera lens. Many photographers recommend glass filters, because they are more durable and generally are of a better quality than those without glass (Hermann 2017; Mansurov 2017; Weitz 2015). Some filters are treated pieces of glass mounted on a frame, with no gel involved. These are commonly filters for near-ultraviolet or near-infrared light, either allowing these lights to pass or blocking them from reaching the camera. Filters come in various sizes to fit different size lenses.

 Physical filters for the visible range come in various strengths, denoted by the Wratten number. These codes include both a number (denoting the colour of the filter) and one or more letters (denoting strength) (Peed 1987, 1). Generally, the later a letter is in the alphabet, the stronger the filter. For example, both 80A and 80D are blue filters (as noted by the number 80), but 80D filters more light out of the images than 80A.

Filters can also take the form of digital settings applied in photo-editing software. We can apply these settings to any digital image, regardless of when we took the photograph or whether we intended to use filters originally. We can use a physical filter as the baseline for these settings or simply apply the settings independently of any existing physical filter (Figure 3.14, Appendix E). Images resulting from digital filters are no different from those using physical ones for visible-range photography. Most photo editing software already have greyscale filter presets, which mimic physical filters as well. Results can vary between software when using non-custom presets, however, because the filters each company used to create their presets may differ. Unfortunately, digital settings cannot replicate the results of near-ultraviolet and near-infrared filters. While there are ways of mimicking an infrared image for landscape photography, this is

not a true manipulation of infrared light because the typical dSLR camera cannot capture

infrared light (Chapter 3.2.1).
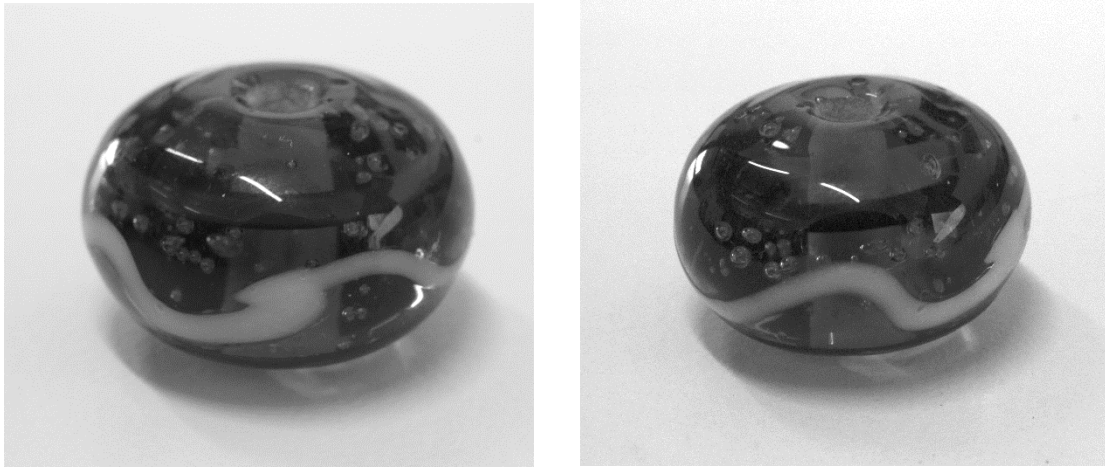
Figure 3.14: Comparison between an image using digital settings derived from a physical filter (left), and an image using a physical filter (right) (Replica bead, RO 002)(Appendix E).

The largest benefit of digital filters is that they can be applied them to any digital

image taken in the visible spectrum. This includes images taken in the past, including

those images taken for other purposes. The only requirement is that the filter be applied to

the original digital image of the object. If applied to a scanned copy of the image, or an

image of the original image (e.g. a photograph of an image in a book), the resulting data

will not necessarily match the original.

Visible-range filters operate using the RBG colour model, just as cameras and

human eyes do (Figure 3.2). Filters of the primary colours will only transmit their own

light and absorb the other two primary colours, so a red filter transmits red light and

absorbs blue and green (Figure 3.15) (Optical Society of America et al. 1968, 172).

Combining a red and green filter therefore does not create a yellow filter, because only

the red light would ever pass through the red filter before being blocked by the green

(Figure 3.16). Filters of the secondary colours transmit two of the primary colours and

absorb the third. Thus, a yellow filter transmits red and green light and absorbs blue

(Figure 3.15). Combining a yellow and a magenta filter could, technically, create a red filter if desired, because the yellow filter allows both red and green light through, while the magenta filter allows blue and red through (Figure 3.16). Since there is no blue to allow through and the magenta filter blocks green light, only the red passes to the camera. This is generally unnecessary, however, as red, green, and blue filters produce better results.
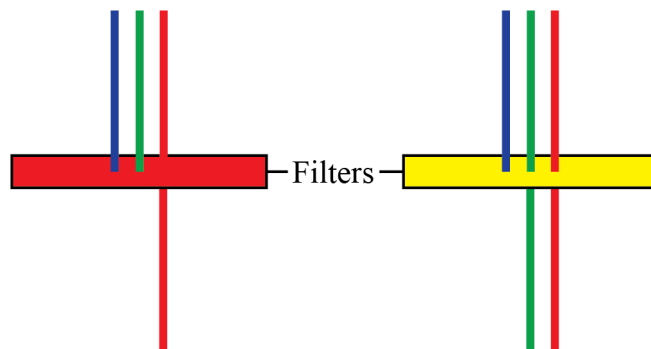
Figure 3.15: A red filter (left) contrasted with a yellow filter (right) in its treatment of light.
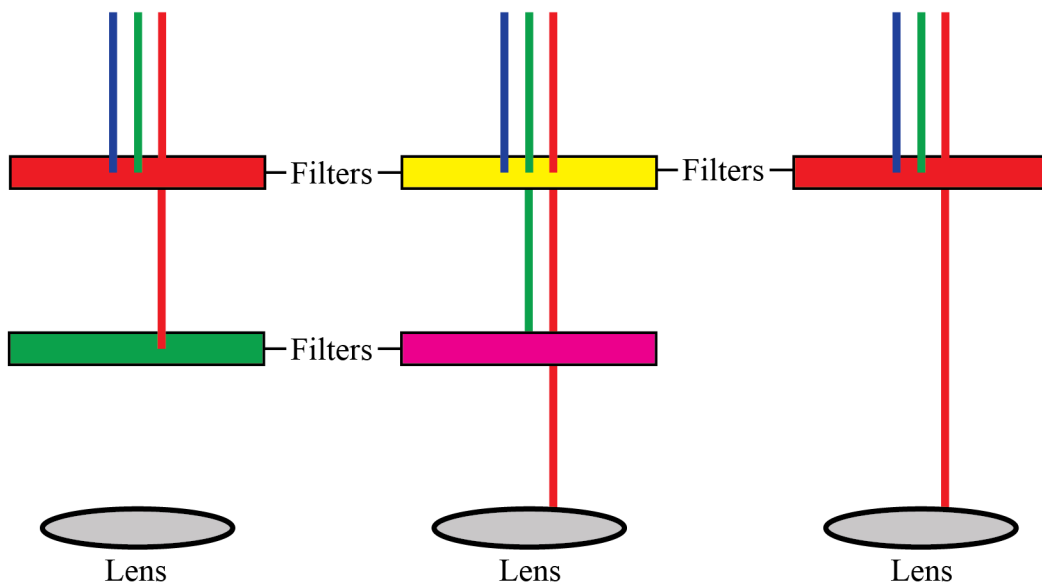
Figure 3.16: Effects of combined red and green filters (left), combined yellow and magenta filters (middle), and a red filter on light entering a camera (right).

The final filter on the visible spectrum is a visual pass filter, which transmits all wavelengths from 300-700nm (Schott 2017). These filters block only near-infrared light.

It does not absorb UV light, because unconverted cameras generally cannot detect UV light except in trace amounts and the extra treatment of the filter is therefore unnecessary. In a fully converted camera, however, a visual pass filter transmits wavelengths between 300-700nm, which includes the ultraviolet spectrum. To replicate human vision or to ensure only the visible range reaches the image sensor in a converted camera, we must pair a visual pass filter with a UV-block filter (Chapter 3.4).

Archaeological photographers have used visible-range filters since the invention of photography. Every manual for archaeological photography prior to the advent of digital cameras dedicated at least one chapter to the practice (Conlon 1973; Cookson 1954; Dorrell 1994). However, these manuals focus on using filters for landscape images or images of structures or rock art rather than objects. While each of the manuals provide detailed workflows for photographing objects, they rarely discuss the use of filters for doing so, even filters within the visible range.

Understanding the relationship between filters and object photography is paramount to understanding spectral imaging and the research contained in this thesis. Photographers generally view filtered images in greyscale, meaning the intensity of light through a filter becomes registered as lighter or darker for more or less intense light respectively. In other words, light that a filter allows to pass to the image sensor appears lighter, while light it blocks appears darker. If we photograph a turquoise object using a red filter, the object will look very dark in our image because there is no red light coming from the object to transmit to the image sensor. If an object reflects red light instead, it will appear lighter when photographed with a red filter because there is an abundance of red light for the sensor to register. If the object transmits red light, then it will look transparent to the sensor. The different reactions of light to each filter can provide valuable information about an object by differentially lightening or darkening certain

features (Chapter 4). The effects will vary depending on the degree to which the object reflects, absorbs, and transmits certain wavelengths of light. If an object absorbs the filtered light, then the object will appear both opaque and dark. If the object reflects the filtered light, then it will appear relatively opaque and light. If it transmits the filtered light, then the object will appear transparent. Simply put, colours that are the same as the filter and colours directly adjacent to it on the RGB model will appear lighter in the resulting image, while the opposite colour to the filter and colours directly adjacent to this opposing colour will appear darker.

Figure 3.17: Comparison between a standard colour image of a dark blue bead (left) and one with a digital blue filter applied to the image (right) (Replica bead, RO 002) (Appendix E).

Figure 3.18: Comparison between a standard colour image of the same bead (left) and one with a red filter applied to the image (right) (Replica bead, RO 002) (Appendix E).

These reactions provide valuable information about the object. For example, attempting to examine the interior of a translucent dark blue glass bead from a standard, visible-range image of the object is difficult, even when using a macro lens. When we apply a blue filter (i.e. the same colour as the glass), however, the interior matrix of the glass becomes clear, showing bubbles, inclusions, and even the perforation (Figure 3.17, Appendix E). Alternatively, a red filter (opposite on the RGB model) highlights surface detail, wear, and corrosion that would otherwise remain invisible in an unfiltered image (Figure 3.18, Appendix E). A filter that is the same colour as the object therefore allows for a closer inspection of the interior matrix of the object, while a filter opposite to the object's colour on the RGB spectrum allows for a closer inspection of surface features. This is the foundational principle at work in the analysis of bubble concentrations in glass beads found in Chapter 4, which serves as the first case study in this thesis.

3.4 NEAR-ULTRAVIOLET AND NEAR-INFRARED SPECTRAL PHOTOGRAPHY

The above section details the use and application of visible-range filters in archaeological photography, but the same principles also apply to photography using non-visible light (Jenkins et al. 1981, 459). While the results are largely invisible to the human eye, we can still photograph them using a converted dSLR and specialised near-ultraviolet and near-infrared filters.

Ultraviolet filters come in two varieties: UV-pass and UV-block filters. UV-pass filters transmit wavelengths from roughly 300-400nm and from roughly 700-1100nm or more, but absorb anything from 400-700nm (i.e. the visible range) (Hoya Optics 2017a). This means that all UV-pass filters also transmit some infrared light. Consequently, when using a UV-pass filters with a converted dSLR, we must pair it with a visual pass filter to

absorb all infrared light and ensure only UV light passes to the sensor (Figure 3.19). On the other hand, UV-block filters only transmit wavelengths over 400nm through to the sensor (Hoya Optics 2017b). Landscape photographers use these filters to negate the blueish haze that appears on the horizon, which results from near-ultraviolet light (395nm) in the ozone reaching the image sensor (Freeman 1985, 117).
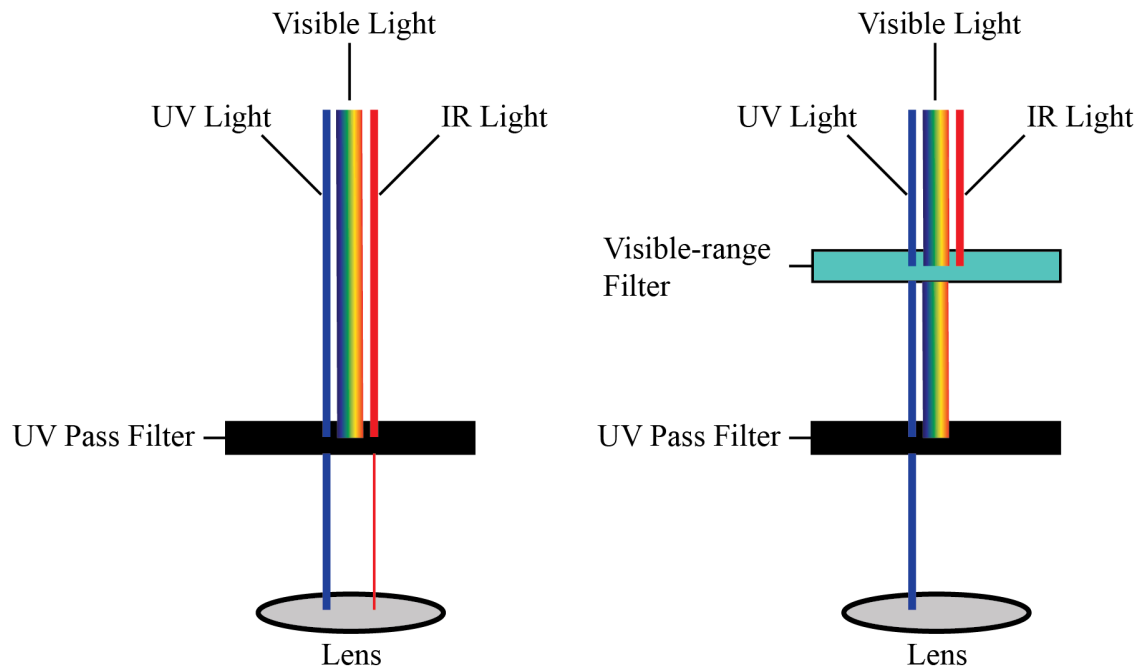
Figure 3.19: Effects of using only a UV-pass filter (left) vs. a UV-pass filter stacked with a visual pass filter (right).

Most infrared filters are band-pass filters, usually noted with a nanometre designation (e.g. 720, 760, 850, or 950). These filters transmit that wavelength of light and higher, though only that wavelength up to 1000nm will register on the image sensor (Neewer 2014a; Neewer 2014b; Neewer 2014c). Thus, a 720nm filter transmits from 720-1000nm, while a 950nm filter only transmits from 950-1000nm to the camera sensor.

Ultraviolet and infrared photography is important in archaeological photography because the degree to which an object absorbs, reflects, and/or transmits different wavelengths of light directly relates to the chemical composition of the object (Ditchburn 1991, 439; Jenkins et al. 1981, 458). In the visible range, differences in these reactions

correspond to the elements of the object that give it its colour. Outside the visible range, however, varying reactions stem from chemical components that may or may not provide any colour (Chapter 5). Often, objects which appear similar in the visible spectrum react very differently to ultraviolet or infrared light (Figure 3.20, Appendix E). Thus, analysing the reactions of various objects to these non-visible wavelengths of light can assist in identifying chemical similarities and differences through photography alone. This is perhaps the most important result of this thesis: the ability to analyse the chemical relationship between objects through photography alone (Chapter 5). This particular use of photography does not appear in the archaeological literature, likely because it requires deviating from the standard methods of archaeological photography described in Chapter 2.
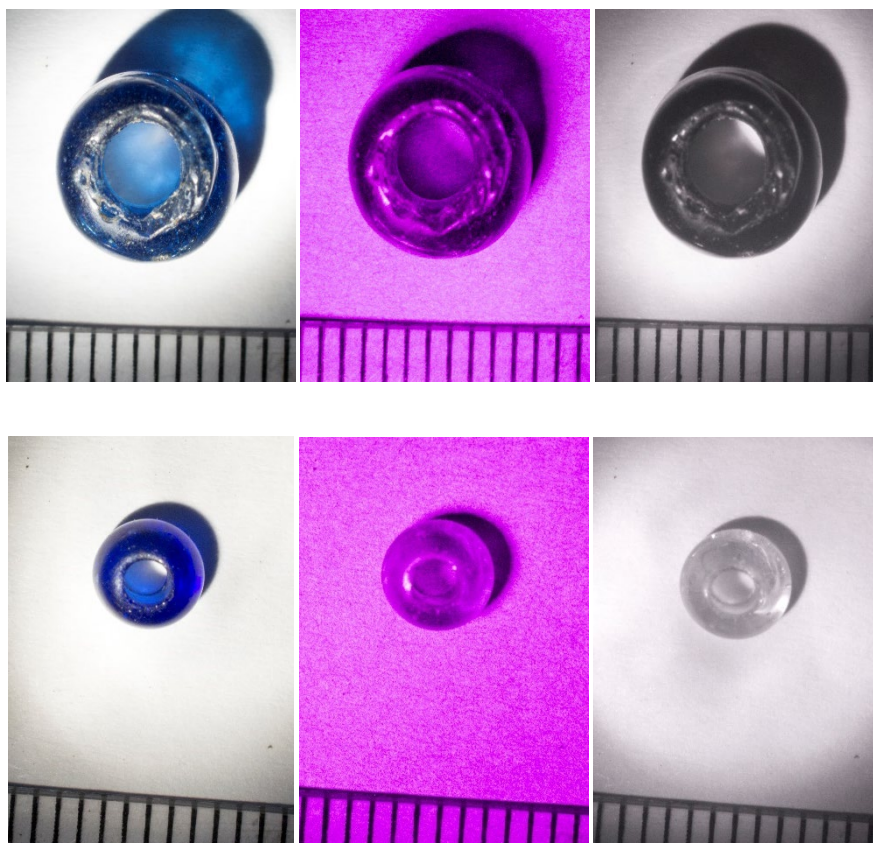
Figure 3.20: Comparison between two beads under visible (left), ultraviolet (middle) and infrared (right) light (Top: Rhynie, UG SF 15021; bottom: Clachbreck, UG CLB 1) (Appendix E).

3.5   SPECTRAL REFLECTANCE TRANSFORMATION IMAGING (RTI)

Spectral imaging does not end with photography. Reflectance transformation imaging (RTI) and photogrammetry are both photography-based digital visualisation techniques that benefit heavily from spectral imaging, particularly when applied to objects that do not lend themselves well to such imaging techniques (Chapter 2.1.2 – 2.1.3). This forms the basis for the third case study of this thesis (Chapter 6).

The RTI used in this thesis uses polynomial texture mapping, or PTM RTI. PTM RTI involves capturing 30-50 images of an object under varying angles of light (Diaz-Guardamino and Wheatley 2013, 191; Malzbender et al. 2001, 3). Within these 30-50 images, neither the object nor the camera changes position. Instead, the photographer moves a single light source around the object in a dome-like formation, capturing one image per lighting position (Malzbender et al. 2001, 3). They then process these photographs in software like RTIbuilder (Cultural Heritage Imaging 2018a) to calculate the surface normals of an object and create a 2.5-dimensional visualisation (Figure 3.21, Appendix E).

Figure 3.21: RTI of a polychrome glass bead (Loch Eriboll, UG F128) (Appendix E).

There are two primary advantages of PTM RTI. The first is the ability to manipulate light within this 2.5D representation of the object, especially in ways that are not physically possible in reality. This often emphasises surface and subsurface characteristics through naturally occurring lighting conditions that may be otherwise

difficult or impossible to see (Cultural Heritage Imaging 2010, 12; Diaz-Guardamino and Wheatley 2013, 192). The second advantage of RTI is the ability to emphasise certain surface characteristics beyond their natural state—most often the depths of grooves—to increase their visibility (Cultural Heritage Imaging 2010, 12; Diaz-Guardamino and Wheatley 2013, 192). Both applications are valuable for visualising wear on objects and, to a degree, subsurface features like bubbles or inclusions (Figure 3.22). However, many objects are highly reflective, like glass beads, or present problems of translucency or transparency that many would argue eliminates the possibility of RTI.
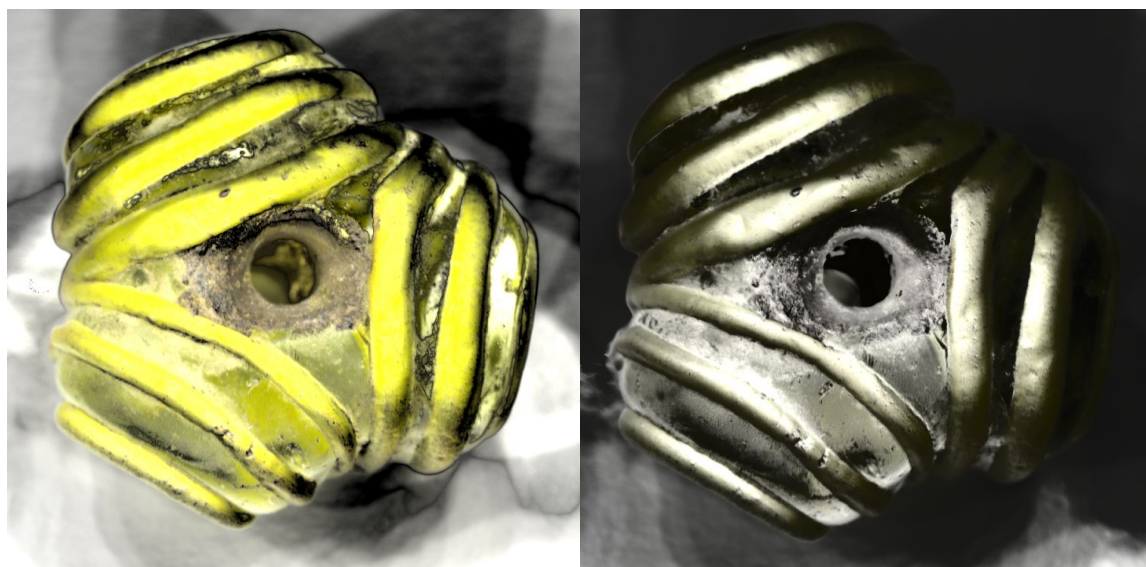
Figure 3.22: RTI of the above bead using diffuse gain (left) and specular enhancement (right) (Loch Eriboll, UG F128).

Spectral RTI combines spectral imaging and RTI by either placing a physical filter over the lens during image capture or by applying a simulated filter to images in post-processing (Figure 3.23). This method allows for the manipulation of light while only capturing specific spectra, negating many of the issues created by reflective or translucent objects. For example, using certain filters can eliminate overexposed patches captured under normal lighting conditions (Figure 3.23, Appendix E). Additionally, using filters allows for RTI image capture in many areas where the photographer cannot control ambient light sources. Spectral RTI can allow for viewing surface and subsurface features

that might otherwise remain invisible such as wear patterns or bubbles in the glass. Likewise, it can lead to further discovery of invisible features, thus enhancing our knowledge of the object. A full discussion of spectral RTI forms the first half of the third case study of this thesis (Chapter 6).
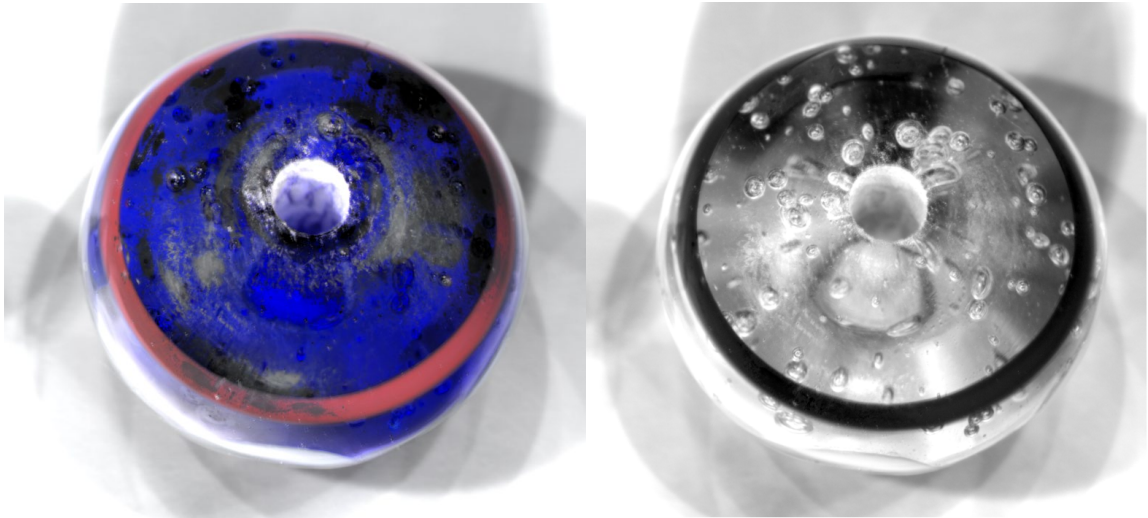
Figure 3.23: RTI using no filter (left) and a blue filter created in Adobe Lightroom (right) (RO 002) (Appendix E).

3.6   SPECTRAL PHOTOGRAMMETRY

Finally, we can combine spectral imaging with photogrammetric 3D models. Structure from Motion (SfM) photogrammetry involves capturing 40-60 overlapping images of an object from various angles (Doneus et al. 2011, 82; Westoby et al. 2012, 301). The photographer then imports the images into photogrammetric modelling software, aligns them through overlapping points, turns the resulting data into a point cloud and then creates a three-dimensional model by joining the points together (Figure 3.24, Appendix E) (Westoby et al. 2012, 301; Zhao and Li 2006, 70-71).
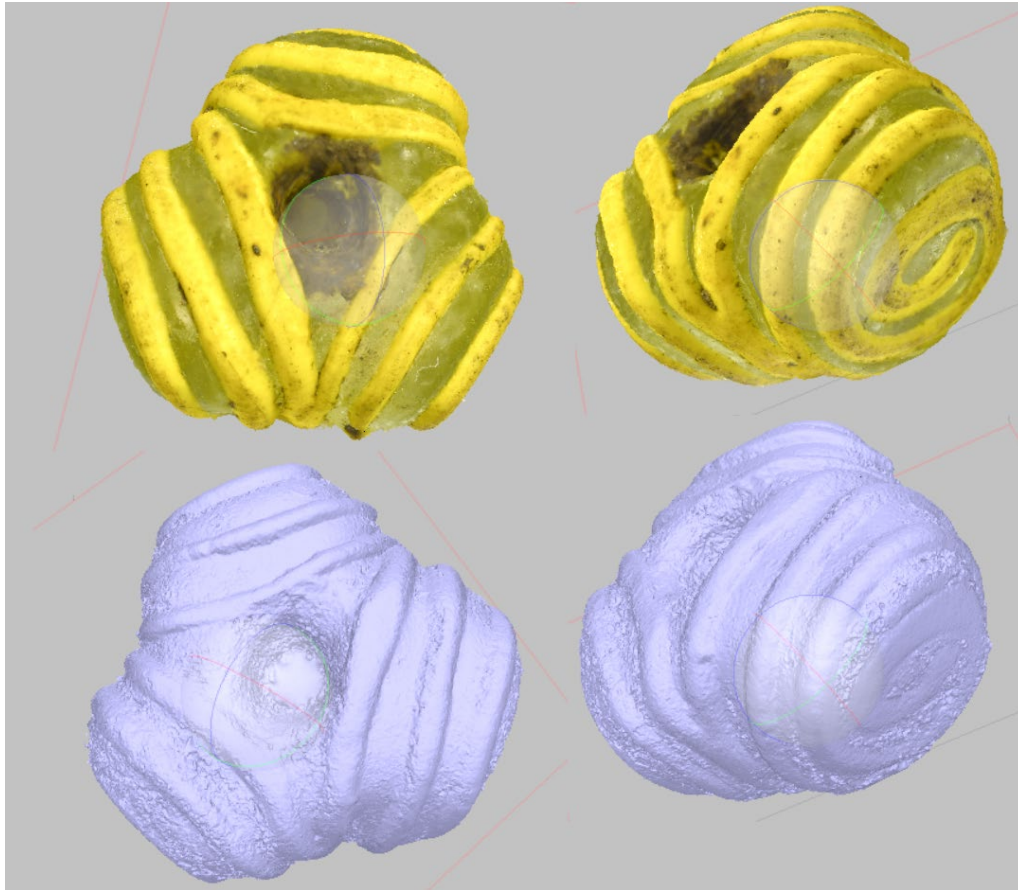
Figure 3.24: Snapshots of a photogrammetric model of a bead (Loch Eriboll, UG F128) (Appendix E).

However, SRT objects present similar problems for photogrammetry as they do for RTI and for photography in general. Photogrammetric software often cannot recognise that reflective patches are not part of the object or that inclusions and bubbles are not part of the object's surface. Consequently, the software cannot align the photographs properly (Figure 3.25, Appendix E). Just as spectral imaging can solve many of the issues of reflection and translucency for RTI, however, it can also solve them for photogrammetry. There will always be at least one filter that brightens or darkens the matrix of the object, allowing for the software to find overlapping points and eliminate confusion. The experimentation with and application of spectral photogrammetry forms the second half of the third case study in this thesis (Chapter 6.2).
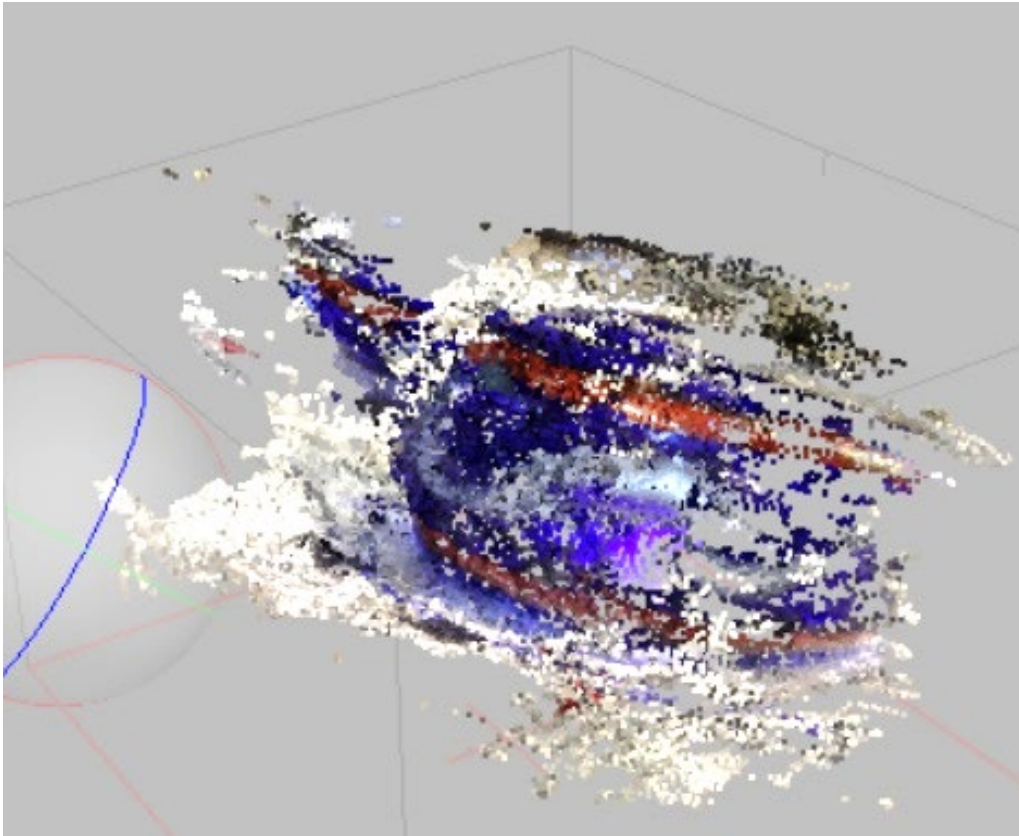
Figure 3.25: Snapshot of a failed photogrammetric point cloud of a bead due to high reflection (RO 002) (Appendix E).

3.7 ARCHIVING PRACTICES WITHIN THIS THESIS

Archiving practices are an integral part of any archaeological endeavour, including digital imaging research. It is important to archive any images captured, both raw and processed, and to archive any RTI or photogrammetric outputs resulting from the images. The Archaeology Data Service (ADS) in the UK has guidelines for archiving many types of digital data, including raster images, shapefiles, photographs, laser scans, and other digital data (Archaeology Data Service 2018a). They recommend archiving data after each major phase of the project (i.e. at preservation intervention points), such as after image or data capture, image or data processing in the field, image or data post-processing, and after the creation of outputs for publication (Archaeology Data Service 2018b). These files should have accompanying metadata associated with them, examples of which can be found in the ADS guidelines (Archaeology Data Service 2018a). They

can then be archived with ADS or other archive services, like Zenodo or The Digital

Archaeological Record (tDAR).

All images in this thesis have been retained in their raw format and as processed

files leading to any type of digital output, regardless of that output's perceived success.

All files associated with the final output images or 3D models were also retained

regardless of the success of the output. The retention of all files regardless of their

ultimate success stems from the argument that failed models and images still provide

valuable data in how and why they failed. Few published sources discuss failed attempts

at digital imaging and even fewer discuss why those failures may have occurred. We

cannot progress as rapidly in our understanding of these technologies if we do not share

our failures with the field as much as we share our successes, however, and engaging in a

published dialogue as to why we have failed is as valuable as the published conversations

about how we have succeeded. Given this, I have retained all files created during the

course of this thesis regardless of their success (e.g. Appendix E).

Metadata about the files provides valuable information as to how and when they

were captured and processed, and it is as vital to the archival process as the files

themselves. The metadata for files in this thesis has been compiled into a Microsoft

Access database for use in conjunction with the files themselves. It details when images

were captured with which equipment and how final models were processed (e.g.

Appendix D and Appendix E).

Most of the objects imaged in this thesis currently reside in museum collections.

Some of these museums have policies in place that allow the creator to maintain

copyright over the images or models, while others retain the copyright as property of the

museum. Consequently, I cannot currently archive all the data generated in this thesis in a

public archive. The data has been maintained, however, and it is hoped that a solution for long-term archiving will be found shortly.

3.8   CASE STUDIES

There are four case studies in this thesis, all of which experiment with photography and photography-based imaging to create and evaluate more effective and representative visual representations of archaeological subjects. The first applies visible-range spectral photography to Iron Age and Early Medieval glass beads in Scotland to evaluate differences in bubble concentration between objects. The identified differences provide valuable information about the long-distance trade and manufacture of beads in Scotland at this time, and this technique could provide similarly valuable information for other object categories. The second case study employs non-visible spectral imaging in near-ultraviolet (300 – 400nm) and near-infrared (950 – 1000nm) to determine chemical differences in otherwise typologically similar beads by measuring differences in the intensity of reflection for each light. This technique has also led to significant findings concerning long-distance trade of glass beads in Iron Age and Early Medieval Scotland and serves as a highly affordable, non-contact technique for determining chemical relationships between objects. The third case study investigates techniques for eliminating issues of size, reflection, and transparency in SfM photogrammetry and PTM RTI and demonstrates their use on glass beads. This research allows for the creation and analysis of PTM RTI and SfM photogrammetric outputs, which is currently challenging or impossible with standard techniques. The final case study applies the techniques developed in all three previous case studies to non-glass objects such as ceramics, lithics, metalwork, and site trenches. This final study demonstrates the applicability of these

techniques to other subjects within archaeology and implies the benefits of their use outside the discipline.

Each of these case studies challenges the standards of archaeological photography, particularly for small finds. They encourage the systematic manipulation of images to isolate data not seen by human eyes and analyse this data to arrive at new insights and conclusions about the objects themselves. They demonstrate the value of experimenting with archaeological imaging techniques and champion affordable means of object analysis and imaging, beginning with the analysis of bubble concentrations in Iron Age and Early Medieval glass beads.

4   CASE STUDY 1: VISIBLE-RANGE PHOTOGRAPHY AND BUBBLES IN GLASS BEADS

In the first of the four case studies presented in this thesis, I use digital visible-range filters (Chapter 3.3) to analyse the relative concentration of bubbles in glass beads recovered from Scottish contexts possibly dating to the Iron Age and Early Medieval period (800 BC – AD 800). Bubbles differ between beads in their shape, orientation, and relative concentrations. These differences provide information about the manufacture techniques used to create a bead: bubbles oriented parallel to the perforation denote a drawn bead, for example, while bubbles oriented perpendicular to the perforation denote a wound bead. Unfortunately, bubble variation in ancient glass is under-researched due to the difficulty of seeing them in person and the lack of published, detailed images of beads that would allow for such a comparison.

In pushing the boundaries of archaeological photographic techniques, however, I have been able to visualise, categorise and analyse the relative bubble concentrations of 352 glass beads from Iron Age and Early Medieval Scottish contexts. The results show significant regional variation between otherwise typologically similar beads, which would suggest differences in manufacture and long-distance trade routes between different areas of Scotland. For example, significant differences between the southeast and northeast of Scotland highlight the increased influence of the Romans versus the Picts. This case study therefore demonstrates the value of investigating alternative photographic techniques, particularly more affordable ones, for their use in uncovering new information about archaeological finds.

4.1   BUBBLES AND GLASS

All pre-modern glass has bubbles, or pockets of air trapped inside the glass. Producing glass without bubbles requires sterile equipment and melting under a vacuum (Shelby 2005, 40), neither of which were available in the Iron Age and Early Medieval periods. The concentration and cause(s) of bubbles in an object depends on a range of factors, intentional and unintentional, most of which correlate to the manufacturing process itself. To understand how bubbles form in glass beads, then, we must first understand how early craftspeople made both glass and glass beads.

4.1.1   GLASS AND BEAD MANUFACTURE

There were three general steps to glass manufacture between 800 BC and AD 800. First, glassmakers combined silica, an alkali (usually soda or potash) and a stabiliser (usually lime or alumina), in a furnace and heated the mixture for several days to allow the components to react to each other in a solid state (Biek and Bayley 1979, 1; Kanungo 2004, 1–2). This reaction produced a solid, dark mass called frit. They then ground the frit as finely as possible and melted it to form glass. Once the frit had melted, requiring temperatures between 900º and 1200º C, they could add any desired colourants, such as iron, copper, cobalt, or manganese (Biek and Bayley 1979, 3 – 5).

In Iron Age and Early Medieval Europe, glass making and glass working occurred at different sites, often called primary and secondary workshops respectively (Degryse et al. 2005, 289; Freestone et al. 2008, 31; Guido et al. 1999, 5; Messiga and Riccardi 2001, 58; Paynter 2006, 1047). Rehren has suggested three separate workshops: one for glass making, one for glass colouring, and a third for glass working (Rehren 1997, 366), though many – including Rehren – have questioned this theory (Smirniou et al. 2011, 53). The model of primary and secondary workshops largely originated in studies of Near Eastern

and Roman glass, and scholars have extrapolated the system to most of Europe for this period. Little evidence exists for glass making in Iron Age and Early Medieval Europe outside the Romans and the Merovingians, and so most manufacture was likely glass working rather than glass making. However, many objects from this period exhibit signs of recycling, in which the glassworker melted chunks of raw or broken glass together to create a workable material. Recycling required far less space to melt the glass, and there is significant evidence for recycling across Europe at this time (Aerts et al. 1999, 890; DeGryse 2005, 295; Freestone 2015; Messiga and Ricardi 2001, 68). Since no direct evidence exists for glassmaking in Scotland during the Iron Age and Early Medieval period and there is no evidence for alternative systems in Europe at this time, we can assume a similar system of glassmaking, trade, recycling and glassworking for glass beads in Scotland for this thesis.

Beadmakers used four primary techniques for making glass beads during this period, of which two predominate: winding and drawing (Figure 4.1). There are two primary techniques for making wound beads: melting a cane or piece of glass over a flame and winding it around an iron rod (lamp-winding) or dipping the iron rod into a crucible of melted glass, pulling it out and quickly twisting to form a bead (furnace winding) (Francis 2002, 11; Kanungo 2004, 95; van der Sleen 1973, 23). In modern times, lamp-winding predominates in Europe and South, East, and Southeast Asia, while furnace winding occurs in the eastern Mediterranean, the Middle East, and East, South, and Central Asia (Kanungo 2004, 95).

There is no archaeological evidence that allows us to deduce the exact procedure for drawn bead manufacture, which is the other most common technique for manufacturing glass beads in the ancient world. However, Peter Francis did identify a modern workshop at Papanaidupet, in Andhra Pradesh, India, which uses a technique that

produces identical waste material to that found at Arikamēḍu, a major glass beadmaking centre occupied between 200 BC and AD 1000 (Francis 1991; Francis 2002). At Papanaidupet, a craftsperson placed broken chunks of glass into a trough in a furnace. They heated the glass for about two hours, after which they transferred it onto a large tapered iron tube and rolled the glass into a large cone, so that it looked rather like a spear with a large glass point (Francis 2002, 22). Another worker pierced the tip of the cone of glass, creating an air pocket that became the bead's perforation. A master bead-maker then pierced a long-handled iron hook through the tip of the glass cone and pulled it towards himself to form perforated glass canes (Francis 2002, 22 – 24; van der Sleen 1973). The master continued to pull on the tube, breaking it every meter to form lengths of glass tubing. Workers then cut the tubes into beads and pack them into ash, which they place into a kiln to round off the edges before sorting and stringing the beads. Given the similarities between debris found at Arikamēḍu and that produced at Papanaidupet, we can infer a similar technique was in use between 800 BC and AD 800.

Both van der Sleen and Francis describe another method for making drawn beads, in which a worker manipulated a lump of glass on an iron rod such that it created an air pocket (Francis 1991, 29; van der Sleen 1973, 25). Another worker pierced the lump with another iron rod, then pulled the rod away to elongate the glass and create glass tubing (Figure 4.1). They broke the tubing into metre-long segments and then cut the tubes into beads. Finally, they rounded the edges off by tumbling the beads in sharp sand (van der Sleen 1973, 25). This technique was less industrial than that at Papanaidupet, but it produced similar waste material to its more industrial counterpart. Importantly, no evidence exists for drawn bead-making in Europe prior to the 14th century (Francis 2002, 171), meaning that any drawn bead found in Europe either was imported or dates to later periods.

The two other forms of glass beadmaking at this time were considerably less common than wound or drawn beads. Moulded beads were made by placing softened glass into a mould (Beck 1928, 62). Folded beads were made by folding glass around a wire so that the edges fused together to make a tube (Beck 1928, 60–61; Francis 2002, 11; Sleen 1973, 26). Of the roughly 1250 glass beads I have examined in Scottish collections, roughly half are wound, a third are drawn, and fewer than 25 are either folded or moulded. The remaining 14.5% are unidentifiable.
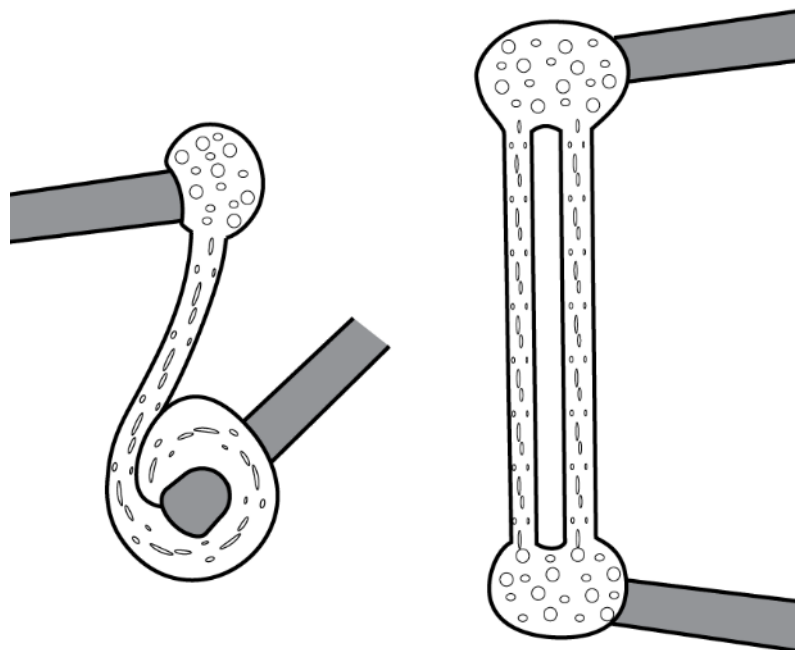
Figure 4.1: Differences in manufacture and bubble orientation between wound (left) and drawn glass beads (right).

The manufacture of a bead determines the orientation of its bubbles (van der Sleen 1973, 81 – 85). Wound and folded beads have elongated bubbles that are oriented perpendicular to the perforation, while drawn beads have elongated bubbles that are oriented parallel to the perforation (Figure 4.1). Moulded beads usually lack orientation or elongation in the bubbles. However, alterations such as decoration, further shaping, or additional heating can affect the orientation or elongation of the bubbles and even

eliminate them entirely. This often makes the manufacture of the object unclear and is one reason the manufacture for so many of the beads in this corpus is unidentifiable.

Elongation or orientation are the predominant factors of conversations about bubbles in archaeological glass studies. Specialists occasionally note the concentration of bubbles in a glass object if it is particularly unusual, but rarely provide detailed discussions or analyses of bubbles in glass objects (e.g. Bourke 1994; Campbell 2007; Whitehouse 2000). This is especially true for glass beads. Given their correlation to manufacture, however, investigating differences in bubble concentrations between geographical regions could allow us to trace the origins of different bead types worldwide, or to at least identify differences between otherwise typologically similar objects.

4.1.2   CAUSES OF BUBBLES IN GLASS

Glass bubbles form when air becomes trapped in a glass mixture (Shelby 2005, 40). This can happen through chemical reactions between the ingredients used to make the glass or when dust, sand, or other particles enter the mixture and form pockets of air (Shelby 2005, 40 – 41). The size of the bubble depends on the size of the sand or dust mixed into it; the finer the sand, the smaller the bubbles (Shelby 2005, 40). Bubbles also form when stirring glass, both because the stirring creates air pockets in the mixture and because the chemical makeup of the tools can cause certain ingredients in the glass to react by creating bubbles (Shelby 2005, 40).

The above bubble formation processes occur during the initial melting and manufacture of the glass. These bubbles therefore reflect the setting in which the glass was made and can provide information about glass manufacture (Shelby 2005, 40). Many of the processes described above also occur during glass working, however, and many modern beadmakers intentionally introduce bubbles into their work. For example, there

are well-known modern techniques for creating 'champagne beads' in which the bead-maker rolls the glass in dust, fine sand, or baking soda and immediately covers it with more glass to create dozens of tiny bubbles in a piece (Chrys Art Glass 2015a). There are even specialised metal pokers and spikes, used to create symmetrical holes that are covered with additional glass to create air bubbles (CheekyTorchGlass 2009; Chrys Art Glass 2015b; Williams 2015). All these techniques save for perhaps the baking soda were available in ancient times. Thus, bubbles always form as part of a manufacturing process, but can do so at any phase and may even be intentional. Following the model of primary and secondary workshops (Chapter 4.1.1), one workshop may cause or add some bubbles while another adds more. Similarly, bubbles created by the primary workshop can change or disappear based on the methods used by the secondary workshop.

4.1.3   REDUCING BUBBLES IN GLASS

In addition to producing bubbles, glass- and beadmakers can reduce bubbles in several ways. The first is simply allowing the bubbles to rise to the surface, which will eventually occur through continual heating due to the lower density of the bubbles compared to the glass mixture (Shelby 2005, 42). The smaller the bubble, however, the slower it will rise. Modern recommendations have found the rate of fining, or elimination, of small bubbles through allowing them to rise to the surface is inefficiently slow and requires further measures, like mechanically stirring the melt from below to form an upwards current and push the bubbles to the top (Shelby 2005, 43). There is no archaeological evidence for stirring from below prior to modern times, however, since the only containers able to withstand the high temperatures required for glass melting were ceramic crucibles (900º – 1200º C).

Craftspeople could also reduce bubbles chemically by adding fining agents to the glass. Fining agents introduce gasses into the mix that either release large bubbles that

amalgamate with smaller bubbles and float to the surface, or absorb oxygen from existing bubbles to make them smaller and less noticeable (Shelby 2005, 43). Arsenic and antimony oxides are the most efficient and best studied modern fining agents, both of which were available in the Iron Age and Early Medieval periods (Shelby 2005, 43). The most common practice for removing bubbles from glass beads is to continue heating the object, however, which allows bubbles to float to the surface or to merge to form larger bubbles, which then rise to the surface.

4.1.4 BUBBLES AND INTENTION

As discussed earlier, many of the factors or reactions that cause or eliminate bubbles in glass can be either intentional or unintentional on the part of the craftsperson, and the degree to which those in the past cared about the bubbles in their glass likely varied from group to group. Many bead-makers today do not worry about bubbles, while many others do. Similarly, most modern glassmakers do worry about bubbles, because societal and scientific demands for bubble-less glass are high. It is difficult to know the degree to which craftspeople in the past considered bubbles in the making of a single object, and if so, at what phase. Additionally, if glass making and glass working occur at separate sites, then the individual or workshop making the glass may have distinct ideas about bubbles from the person making the object itself and from those ultimately purchasing and using it. It could be challenging, also, to determine whether bubble concentrations in a single object resulted from cultural or individual preference. To increase the likelihood that observed difference correspond more to cultural preference, this study generally compares objects between geographical regions rather than between specific sites (Chapter 4.3.4).

Figure 4.2: Example of a glass bead with 'white' trail design (Rumbleton, HMAG B.1914.521/14).

There are many glass beads in Scotland for which bubbles seem intentional and important. Many, for example, are so saturated with bubbles that they appear more bubble than glass. Others have trails of what appears to be white glass, but upon further inspection could be a section of the base colour that has been saturated with bubbles (Figure 4.2). This would have required significant control and skill, and it was clearly intentional as part of the design. Conversely, early Scottish window glass has relatively few bubbles compared to glass beads because bubbles impair the view through the window. Creating glass with minimal to no bubbles was of a similar level of difficulty to creating glass with many bubbles, and it required a degree of skill and forethought (Shelby 2005, 40-42). Thus, early glass manufacturers must have considered bubbles, at least when creating certain objects. Since these bubbles reflect both the techniques used in manufacturing the object and the possible preferences of individuals using the beads, analysing these bubbles in some way provides valuable insight into both the manufacture and use of glass beads during the Iron Age and Early Medieval period in Scotland.

4.2   DEVELOPING THE TECHNIQUE
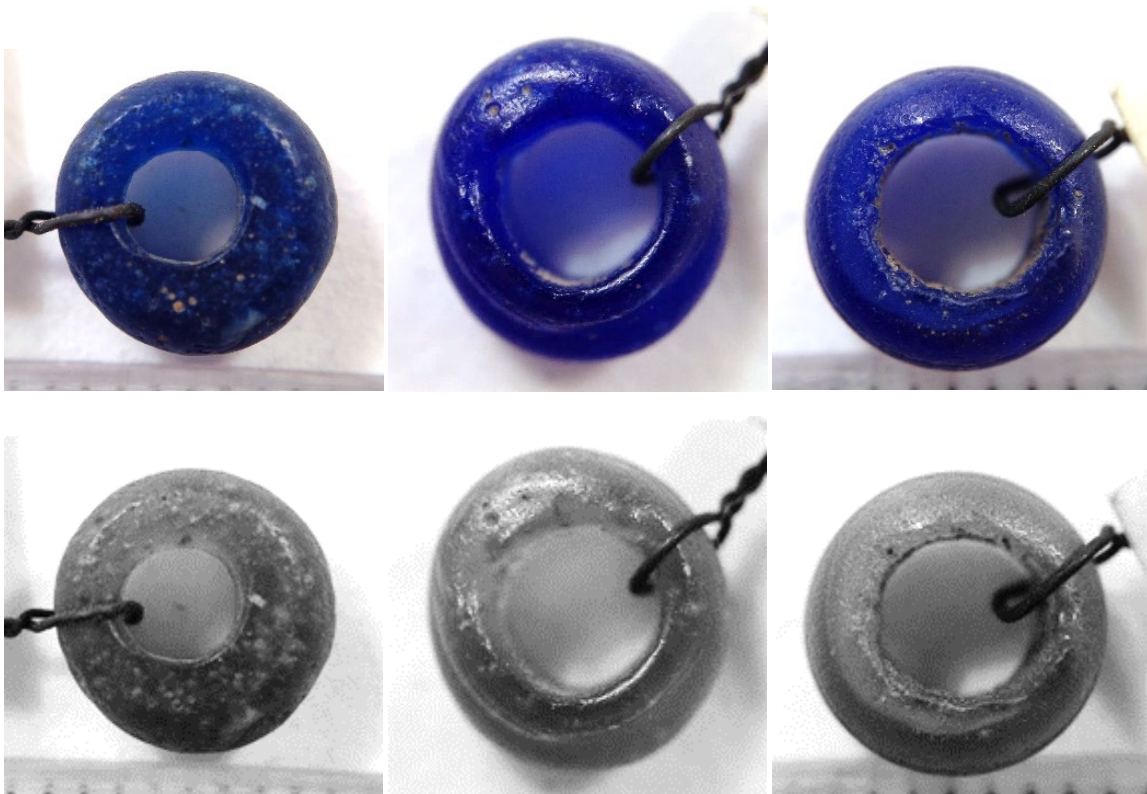
Figure 4.3: Initial comparison of bubbles in three cobalt-blue glass beads from Culbin Sands (NMS X.BIB 40 (left),

NMS X.BIB 41 (middle) and NMS X.BIB 42 (right) (Appendix E).

Having established that digital visible-range filters were no different in their results from using physical filters, I began applying them to a series of cobalt-blue glass beads from Culbin Sands on the Moray Coast of northern Scotland. A red filter completely opacified these dark blue beads, highlighting surface wear and corrosion, while a blue filter rendered the beads almost transparent, highlighting bubbles and the perforations. These images showed significant differences in bubble concentration between these otherwise typologically similar beads (Figure 4.3, Appendix E (PowerPoint Slide 6)).
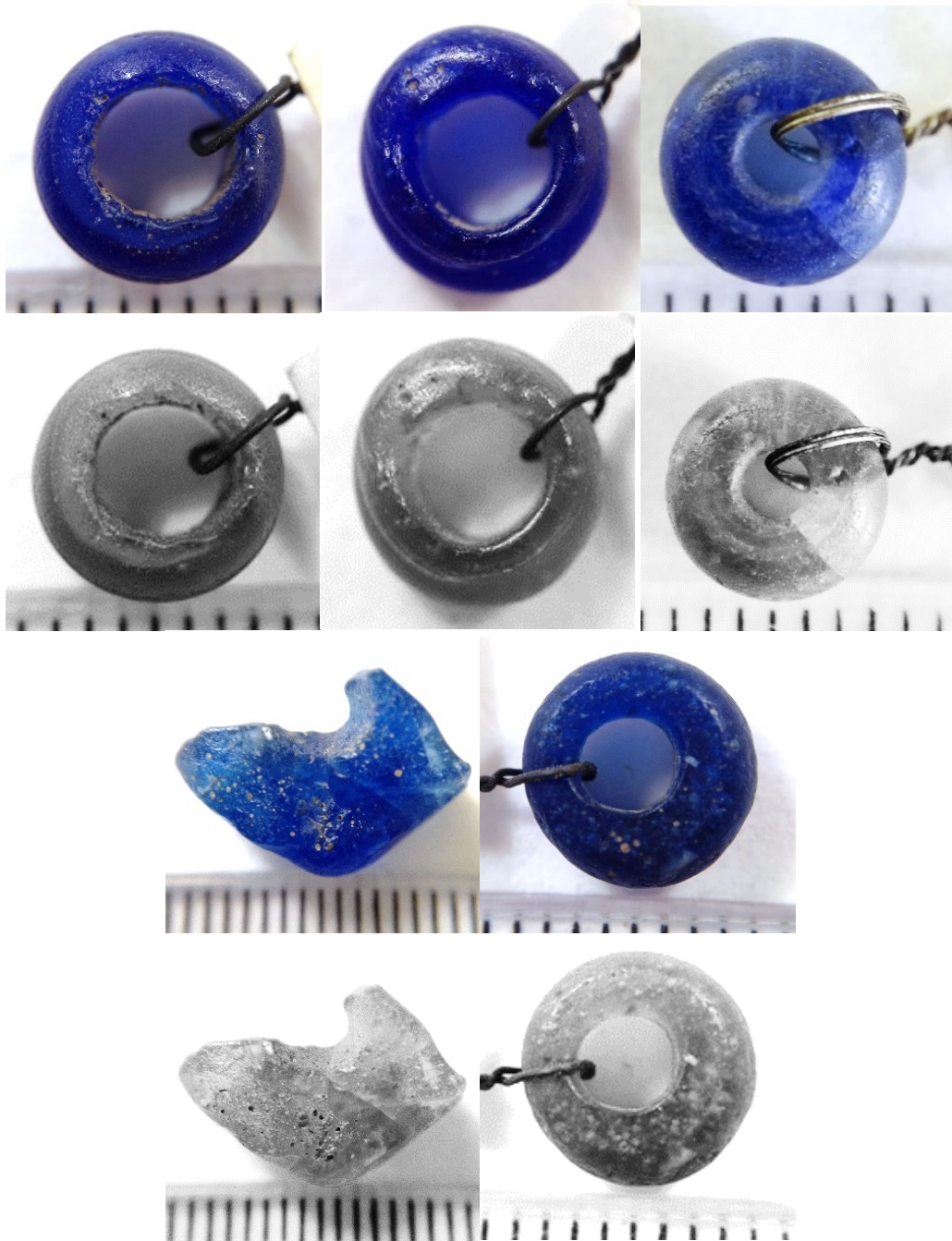
Figure 4.4: Examples of each category of bubble concentrations, before and after applying filters Top row: None (NMS X.BIB 42), Few (NMS X.BIB 41), and Moderate (NMS X.BHB 11). Bottom Row: Many (NMS X.BIB 70) and Superabundant (NMS X.BIB 40) (Appendix E).

Given the importance of bubbles in providing information about bead manufacture and the relative lack of studies concerning bubbles in glass beads, I began investigating whether filtered visible-range photography could help archaeologists identify differences in bubble concentrations between otherwise typologically similar beads. No current

method exists for the categorisation of bubble concentrations in archaeological glass objects, however, so determining an appropriate method was an experiment. Initially, spectral images of the objects were examined manually and bubble concentrations classified using a five-point system: None, Few, Moderate, Many, and Superabundant (Figure 4.4, Appendix E). 'None' signified virtually no bubbles while 'few' was any glass with bubbles covering less than half the object. 'Moderate' applied to glass that appeared to be roughly half bubbles and half glass, while 'Many' denoted any object that seemed more bubble than glass. 'Superabundant was reserved for glass that was saturated with bubbles.

While this system yielded interesting preliminary results that suggested value in documenting and analysing this characteristic of glass, it was too subjective to speak of statistical significance. What looks like many bubbles to one person may look like moderate amounts to another, and it is difficult to define the boundaries between concentration categories. Before continuing, then, I began examining quantitative methods for measuring bubble concentrations instead.

Geologists examine a thin section of a stone and determine the percentage of specific minerals present through point counting, or the process of determining the specific mineral for between 200-500 specific, randomly selected points on the thin section (Aziz 2013, 22-23; Garrison 2003, 129-130). Many use freeware to assist in the randomisation and selection of points, one of which (JMicroVision) was used in this study to test the effectiveness of such a method on identifying bubbles in glass beads (Figure 4.5). Classifications remained simple: glass or bubble. A survey area was traced around the bead, within which 200 points were categorised per object for 100 translucent dark blue and turquoise glass beads.
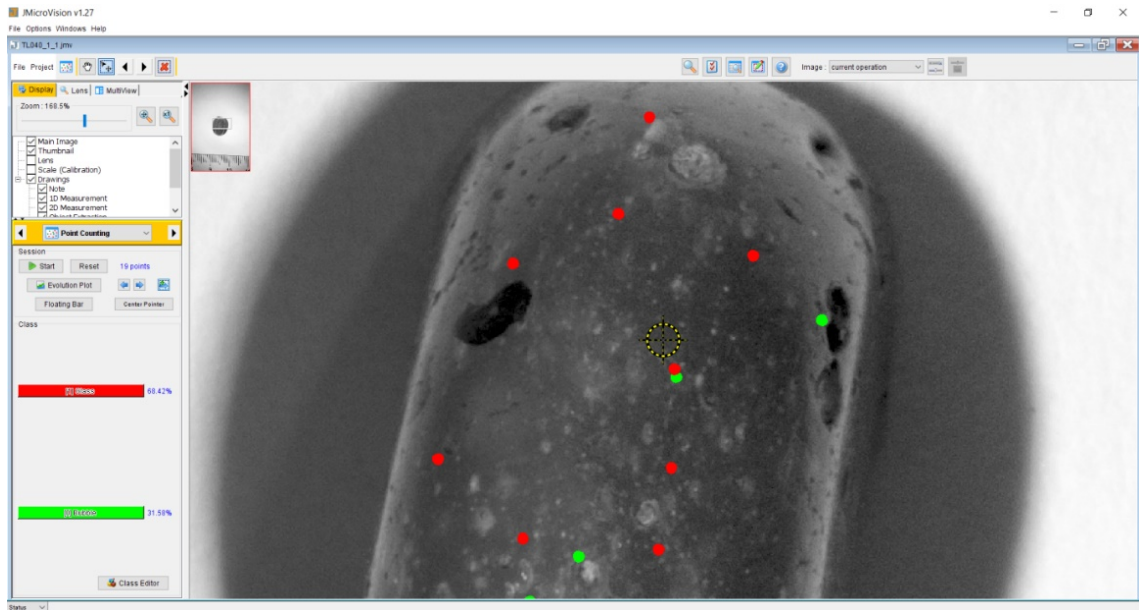
Figure 4.5: Example of bubble point counts using JMicroVision.

While this technique provided statistically significant results between different

sites and regions, there were significant problems with the accuracy of the data. First,

bubbles in glass are less distinct than specific minerals on a geological thin section

viewed through a microscope. Bubbles bend and scatter the light in different ways

depending on where they are, how large they are, where the light is coming from, and

where it is hitting the bubble. Glass is also highly reflective, and most images contain

patches of an object that are impossible to use for point counting. Glass objects also

generally suffer from corrosion, and not all corrosion relates to bubbles. This corrosion

can block the view of or masquerade as bubbles in a filtered image. Bubbles can be

similar size to either grain or pixilation in an image, making it difficult to differentiate

between them. Finally, the point counts used here look at the entire bead, because

acquiring thin sections is destructive and therefore not possible with most bead

collections. Because of this, the counts made for each object depend largely on the

diaphaneity of the object and the thickness of the wall of the bead between its outside

edge and its perforation, both of which often differ significantly between beads. Given the

large number of problems with this technique, it was deemed inappropriate for quantitatively categorising bubbles in glass.

Biologists estimate population counts of animals that travel in large groups (e.g. herds of water buffalo or schools of fish) by photographing several parts of the group and counting the individuals in each image (Elzinga et al. 2009, 42). They then estimate the area of the herd and extrapolate population counts from the counts in each image. This technique can be adapted for glass objects by scaling images of beads to each other, selecting 3-5 areas of a specific size (e.g. $0.5mm^2$) on each bead, counting the bubbles that appear in those areas, averaging the counts together and comparing them across objects. Unfortunately, the same problems arose as those for point counting, so the data was equally problematical. Additionally, three to five areas of $0.5mm^2$ covers different percentages of each bead, depending on how large it is. The size of the object therefore affected the average number of bubbles for each bead, reducing the ability to compare results in a standardised manner.

Given these difficulties, I concluded that an affordable, non-destructive, quantitative technique for assessing bubbles in glass was not possible, at least for the duration of this thesis. I therefore returned to the subjective method discussed above for determining relative bubble concentrations in an object but limited the categories to three instead of five. The distinctions between 'Few,' 'Moderate,' and 'Many' are relatively clear, much more so than the previous five-point system (Figure 4.6). Most significantly, the three-point system still yields statistically significant patterns. This system therefore yields more consistent results than the practical and affordable quantitative methods discussed above and became the established methodology for this case study.

Figure 4.6: Images showing the difference between few (NMS X.BIB 42), moderate (NMS X.BHB 11) and many bubbles

(NMS X.BIB 40).

4.3 METHODOLOGY

I examined total of 372 glass beads from Iron Age and Early Medieval contexts in
Scotland for relative bubble concentrations, leading to data for 427 individual colours
(Table 4.1). There are significant differences in the interior visibility of opaque,
translucent, and transparent beads, so I avoided cross-comparison where possible. Glass
beads of other colours, such a red, orange or purple, did not have more than a few
examples for comparison and therefore were omitted from this discussion. The distinction
between cobalt-blue and copper-blue is in the colourant used to create them, with cobalt-
blue beads being quite dark and copper-blue beads having a blue-green colour. Any beads
made of glass that does not appear to have colourants added to it falls under the term
'Natural'. Glass is not naturally clear, due to impurities in the sand colouring the glass a
light yellow, green, brown, or blue colour. Separating these here would lead to the

category not having enough samples for comparison, and so they have been combined to determine how the general category compares to other colours.

Colour	Diaphaneity	Number of Samples
Cobalt-blue	Translucent	120
Copper-blue	Translucent	61
Green	Translucent	23
Natural	Transparent	28
White	Opaque	29
Yellow	Opaque	166

Table 4.1: Number of bubble samples per colour.

Of the objects examined, 301 are currently housed at the National Museum of Scotland. One object is from the Iona Abbey Museum while seven are in the Kilmartin House Museum. The Marischal Museum in Aberdeen holds 25, a further 28 are housed in the Hunterian Museum and Art Gallery at the University of Glasgow and a final 11 are housed in the University of Glasgow Department of Archaeology.

4.3.1   IMAGE CAPTURE

Beads were photographed on a white sheet of computer paper with a clear plastic ruler beneath for scale. I used a 40mm macro lens with stacked visible pass and UV cut filters to limit the captured image to the visible spectrum (400-700nm). The camera was attached to a tripod for stability and lit using an LED torch and the ambient fluorescent lighting of the museum (Figure 4.7). Spaces with sunlight coming through a window, such as in the image below, warranted the use of a makeshift paper light studio. For specific exposure settings, ISO fell between 100 and 200 and aperture between f/18 and f/22. This consequently set the shutter speed at or near 1 second for proper exposure.

Focus was set automatically, then switched to manual prior to image capture to avoid

changes. Images were captured in raw format using a remote shutter.

Figure 4.7: Camera set-up for spectral photography at Kilmartin House Museum.

Some objects were too small to capture with a macro lens and therefore

necessitated a digital handheld microscope. Images were composed identically and

captured by mounting the microscope on a flexible tripod and positioning it directly over

the object (Figure 4.8). Magnification varied between objects to allow each to appear in

focus, since the microscope itself was fixed to the tripod. The object was lit using the

LED lights attached to the microscope itself. There are no ISO or aperture settings for the microscope. I captured images as .bmp files using the microscope's internal software, which can only capture .bmp (uncompressed) or .jpg (compressed) images.

Figure 4.8: General equipment set-up for micrography.

4.3.2   IMAGE PROCESSING

Images were white-balanced in Adobe Bridge. Visible-range filters of similar colour to the glass were applied in Adobe Lightroom to allow for clear examination of the bubbles (Chapter 3.3). In some instances, semi-contrasting filters resulted in clearer definition of the bubbles and were applied instead (e.g. green filters to blue beads or red filters to yellow beads). The digital filters in this study were modelled after Neewer colour filters (Appendix C). Filtered images were saved as .jpg files with 300 dpi because images of lower resolution presented difficulties in identifying whether a feature was a bubble versus grain or noise.

4.3.3   DATA RECORDING AND ANALYSIS

As described above, relative bubble concentrations were categorised using a three-category system of "Few," "Moderate," and "Many" bubbles (Chapter 4.2). While this

system was subjective, it proved the best possible method for this study. Several other glass characteristics were recorded for this analysis, including the object and site the sample came from, its diaphaneity and colour, its location on the bead, the bead's size, and the region of Scotland (Appendix D).

The object's site information comes from the associated museum records. Many beads lack contextual information, either because they are stray finds or because the data has since been lost. In these cases, I recorded the site as best as possible. For this study, 7 objects (13 samples) do not have associated site information while a further 3 objects (4 samples) have an associated site, but no information that would allow for the location of that site on a map or even within a broad region of Scotland. While this number may seem low, eight of the samples come from colours for which samples already number fewer than 30, rendering 10 – 15% of the samples of these colours ineligible for regional comparison. Additionally, over 90% of the samples, and indeed glass bead finds in Scotland, lack specific contextual information (Christie 2014, 30). Thus, while a comparison between bubble concentrations of glass beads found in different contexts may be informative, such a study is currently impossible for Iron Age and Early Medieval Scottish material.

The diaphaneity and colour of each sample are some of the most prominent typological characteristics of the object and could correlate to significant differences in bubble concentrations. Only opaque yellow, opaque white, translucent cobalt-blue, translucent copper-blue, translucent green, and transparent 'natural' glass beads were included in this study. Opaque objects block light from passing through, while translucent objects allow light through, but not images. Transparent objects allow enough light through to see objects beyond them.

Another recorded factor was whether a sample forms the core of the object or a part of the decoration, which would indicate whether the simple fusing of glass creates significantly more bubbles. If so, then yellow samples forming the designs of polychrome beads would skew the results if combined with yellow samples forming the core of monochrome beads, for example. For polychrome beads, I also recorded the type of design to see whether there were discernible differences in bubbles – and therefore manufacture or manufacture location – between beads with different decorations.

The length and diameter of each bead was recorded to determine whether size variation affected bubble concentrations. All size measurements were recorded to the nearest 0.25mm. Finer measurements would be difficult for the bead-maker to regulate, and likely went unnoticed by those using the objects. I also divided the diameter by the length of the object to determine whether the ratio affected bubble concentrations, even if length and diameter did not affect it individually.

Finally, I recorded the general region of Scotland an object came from, which was determined loosely (Figure 4.9). The northeast comprises sites from north of the Forth River into Perthshire and Aberdeenshire and up towards Inverness. The southeast includes the Scottish Borders, the Lothians, Falkirk and parts of North and South Lanarkshire. The west includes the western highlands and islands down to Dumfries and Galloway. The west and southwest are combined in this study due to low numbers of beads in both regions that were eligible for analysis – 9 from the west of Scotland, and 36 from the southwest. While there are enough objects from the southwest for it to serve as a single region, all 36 beads come from a single site: Glenluce Sands (or Luce Sands) in Wigtonshire. Combining the two regions as western Scotland allowed for the inclusion of objects from more than one site. The north includes the northern region of Caithness and

the isles of Orkney and Shetland, which are also combined in this study due to a lack of

Iron Age and Early Medieval examples available for this thesis.
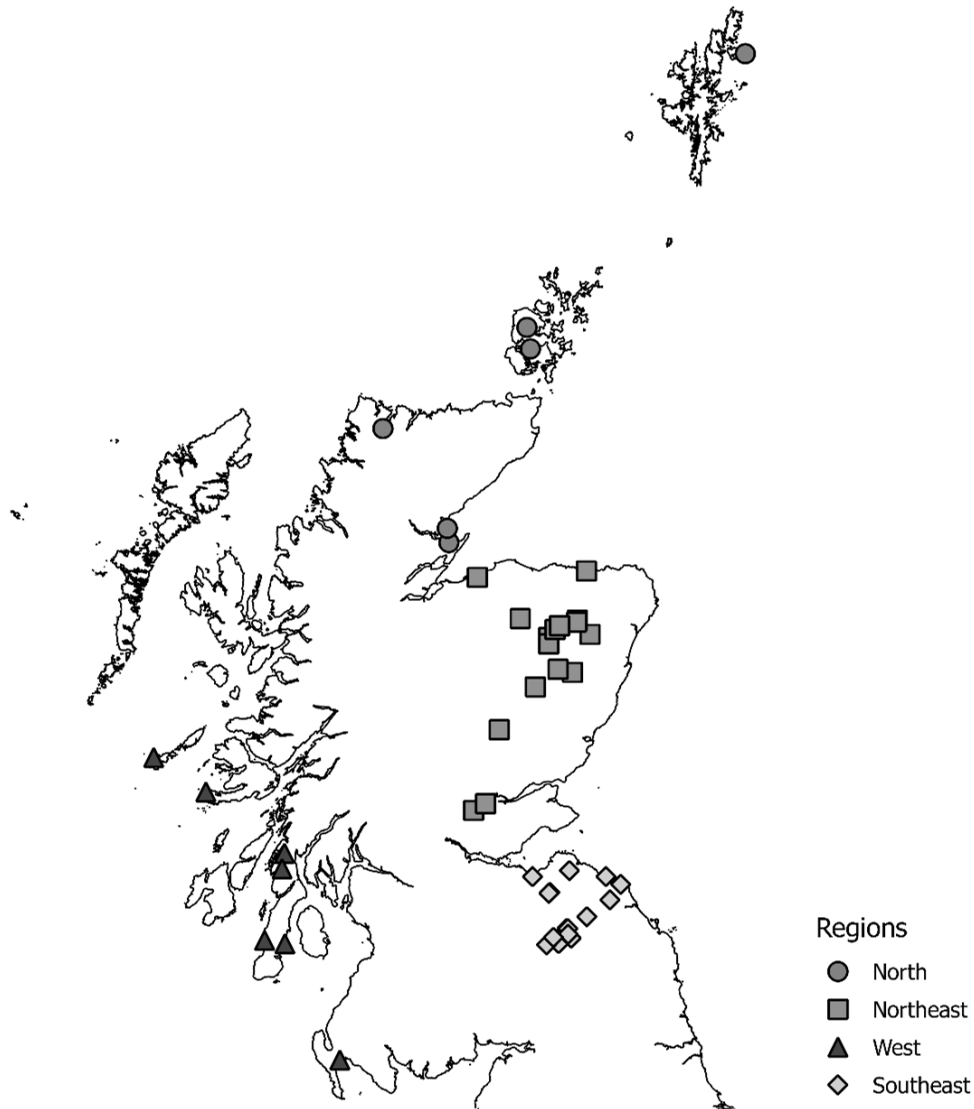
Figure 4.9: Regional division of Scotland used in this study.

The data was first analysed on a subjective level by examining percentages for

each category and judging whether the difference was large enough to indicate a pattern,

given the sample size. To clarify the likelihood that the perceived patterns were

significant, I then confirmed their possibility using Pearson's chi-square test of

independence using the standard statistical significance threshold of 0.05. Given the

fragmentary nature of archaeological data and the subjectivity of the classifications used,

any test scoring under 0.05 was treated as a significant pattern, while any test scoring under 0.1 was treated as being very likely.

4.4 RESULTS

Many significant patterns emerge from the data in relation to bubbles and what they reveal about Scotland between the Iron Age and Early Medieval periods. The results are presented here in sub-sections corresponding to broad categories of the factors listed above. The following section contains further discussion of the significance of these results.

4.4.1 DIFFERENCES IN REGIONAL AND SITE DISTRIBUTION

Visually, there appear to be regional differences in bubble concentrations on a broad level (Figure 4.10). Bead glass in the northeast (n=249) tends towards few to moderate concentrations of bubbles, while most bead glass in the southeast (n=79) and west (n=56) have fewer bubbles. Beads in the north (n=26) have an even spread between all three categories, but there are also fewer beads from this region included in this study. This difference is not statistically significant using these regional separations (p=0.126), but it still appears likely due to the nature of the data.

There are also significant differences in bubbles between the 36 sites represented. Only five of these sites have more than ten beads, but the results are still statistically significant (p = 0.0096) when limited to these five sites (Figure 4.11). Bead glass at Glenluce Sands on the southwest coast has few bubbles (60%), while that at Culbin Sands in the northeast has relatively equal numbers of few and moderately-bubbled glass beads (42% and 39% respectively). Traprain Law and Newstead, both in the southeast (roughly 40km apart as the crow flies), exhibit significantly different patterns of bubble concentrations in glass beads. Roughly half of the bead glass at Traprain Law has few

bubbles, while a further third has many. Alternatively, roughly half the bead glass at Newstead has moderate amounts of bubbles, while a further third has few bubbles. Finally, Knowe of Moan in Orkney has equal numbers of moderate to many-bubbled beads (43% each), with clear preference given to these over beads with fewer bubbles (14%).
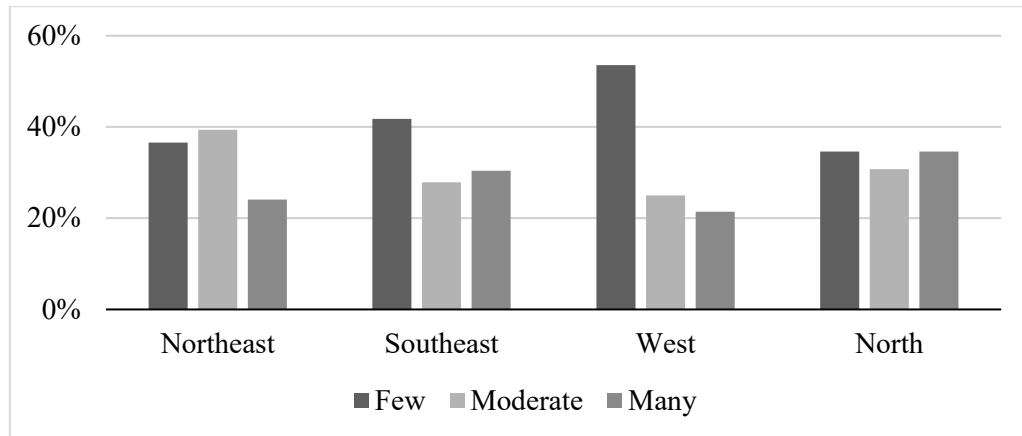
Figure 4.10: Regional bubble concentrations in glass beads from Iron Age and Early Medieval Scottish contexts.
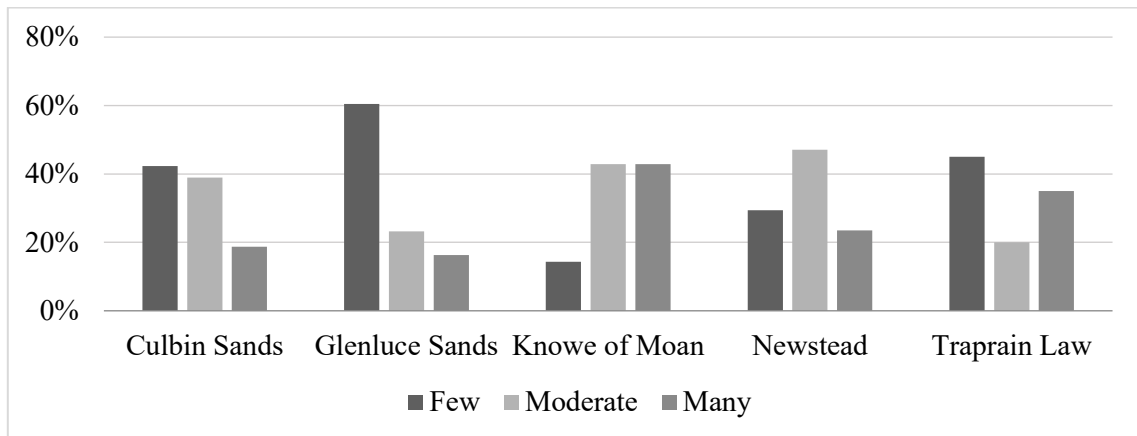
Figure 4.11: Comparison of bubble concentration between Culbin Sands, Glenluce Sands, Knowe of Moan, Newstead, and Traprain Law (p=0.039)

4.4.2 DIFFERENCES IN COLOUR AND DIAPHANEITY

Bubbles differ significantly between different colours and diaphaneities as well. In examining different diaphaneities without accounting for colour, opaque and transparent beads tend to exhibit fewer bubbles while translucent ones exhibit an even spread across

the three categories (Figure 4.12). Opaque beads do not allow us to see as far into the matrix of the glass as translucent material, which likely explains the bias towards fewer bubbles for that category. The transparent beads included in this study are all naturally coloured, which indicates fewer inclusions in the glass to form bubbles (Chapter 4.1.2). Naturally-coloured glass often served as window glass during the Early Medieval period, and it is possible broken window panes could be used to make glass beads. Since bubbles impair the view through a window, window glass necessarily had fewer bubbles. Finally, the even spread of concentrations between translucent beads is important because it suggests that any difference between translucent beads results from factors other than their diaphaneity, such as colour or manufacture.
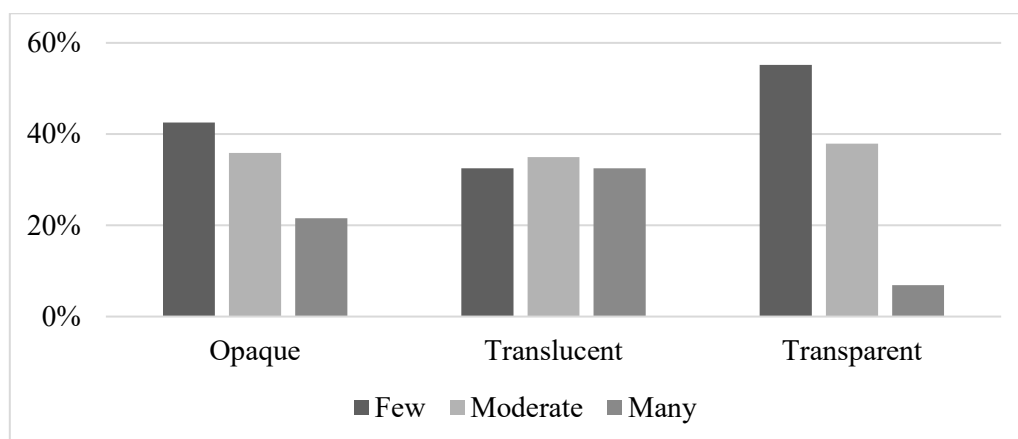
Figure 4.12: Differences in bubble concentrations between opaque, translucent, and transparent glass beads (p = 0.008).

In terms of general colours, white and copper-blue beads tend towards more bubbles. Natural and yellow beads have fewer, which may stem from the opacity of yellow beads and the reuse of window glass for natural beads (Figure 4.13). Cobalt-blue beads tend towards moderate to few bubbles, while greens exhibit predominantly moderate or many bubbles.
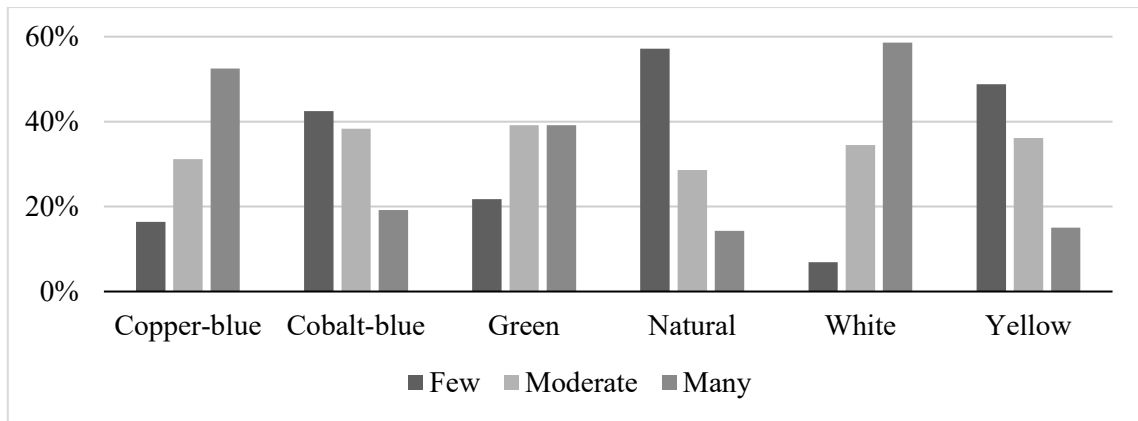
Figure 4.13: Comparison of bubble concentration between copper-blue, cobalt-blue, green, natural, white, and yellow glass beads (p=0.0000000000728).

Natural colours in beads (e.g. very light blues, greens, yellows, and browns) tend towards few bubbles (54%) with a further 31% falling into the moderate category. There are no statistically significant differences on a regional level for natural bead glasses (p = 0.118), though this may be due to the small sample size (n = 26) (Figure 4.14). The west appears to have relatively equal numbers of few, moderately-, and many-bubbled natural bead glass (38%, 25%, and 38% respectively), while the southeast clearly favours fewer bubbles (75%). The northeast has an even spread between natural bead glasses with fewer and those with moderate bubbles (50% each, n = 10).
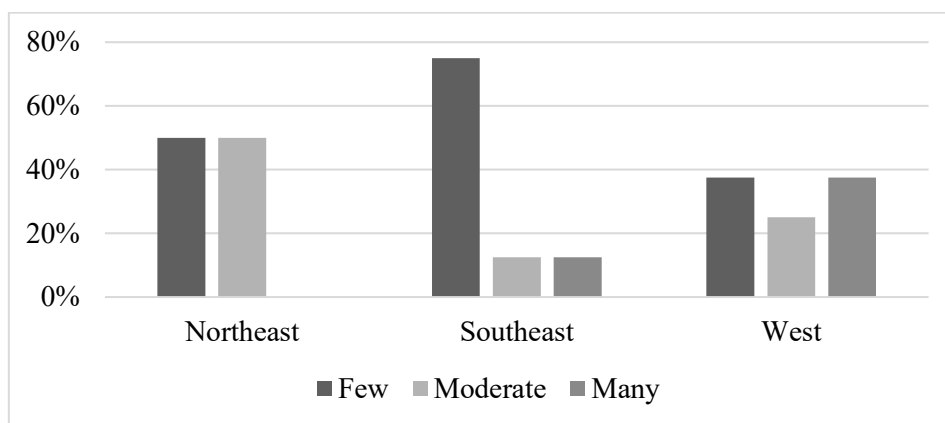
Figure 4.14: Regional bubble distributions of naturally-coloured bead glasses (p = 0.118).

Cobalt-blue glass exhibits predominantly few (43%) or moderate (38%) bubbles (n = 120). There are statistically significant differences in cobalt-blue beads between

regions (p = 0.012), particularly between the west and the northeast on the one hand and the southeast and the north on the other (Figure 4.15). These differences are accentuated when looking at only monochrome cobalt-blue beads (p = 0.010). Polychrome cobalt-blue beads likely differ between regions (p = 0.069).
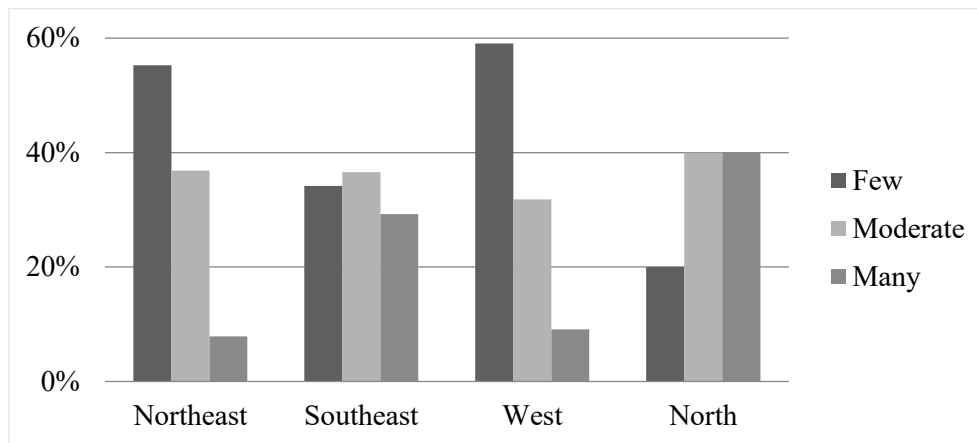
Figure 4.15: Regional bubble distributions of cobalt-blue bead glasses (p = 0.012).

Copper-blue bead glass has significantly more bubbles than the cobalt-blue glass in Scotland, with 54% of the overall copper-blue bead glasses having many bubbles (compared to 23% for cobalt-blues). There are also statistically significant regional differences in copper-blue bead glass (p = 0.000095) (Figure 4.16). The northeast has a number of many-bubbled copper-blue beads (60%) with a further third being moderately-bubbled. The southeast, on the other hand, has few copper-blue beads, most of which have few bubbles (75%). The west also has a higher percentage of sparsely bubbled beads (60%). Importantly, 61% of copper-blue samples come from Culbin Sands on the Moray coast. When we remove these objects from the data, however, the differences between regions become less statistically significant, but still likely even with a lower sample size (p = 0.0828; n = 19) (Figure 4.17).
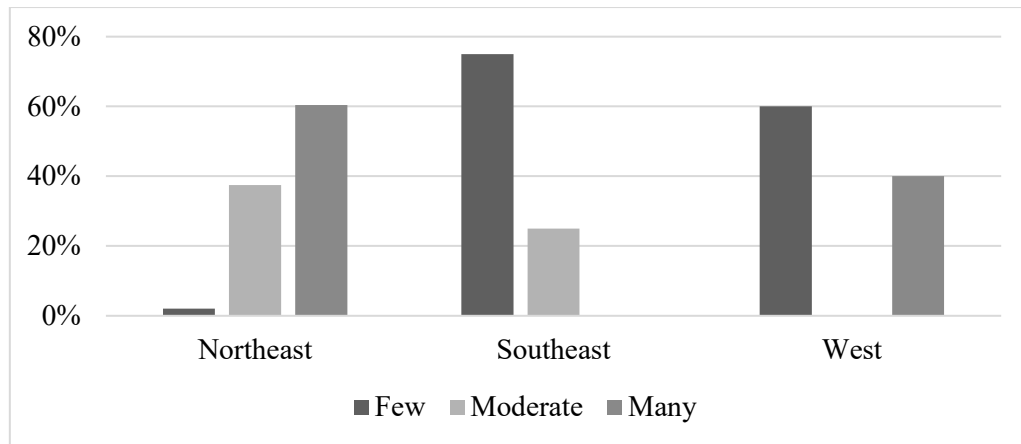
Figure 4.16: Regional bubble distributions of copper-blue bead glasses (p = 0.000095).
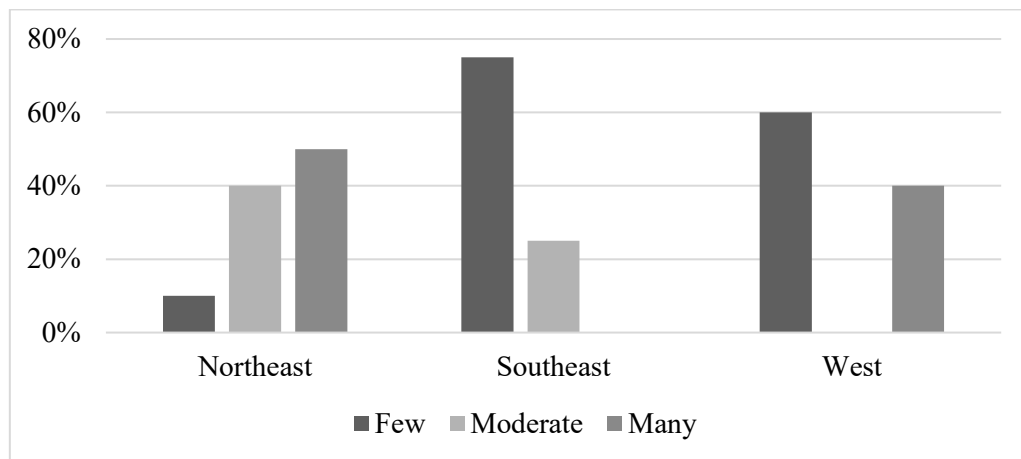
Figure 4.17: Regional bubble distribution of monochrome copper-blue bead glasses excluding 35 beads from Culbin Sands (p = 0.0828).

Only the northeast and southeast (n = 21) yielded green beads for use in this study, and both regions seem to differ in bubble concentrations (Figure 4.18). The northeast has more green beads with moderate bubble concentrations while the southeast has more many-bubbled beads. Green glass beads that are not a naturally-coloured green are relatively uncommon in Iron Age and Early Medieval Scottish beads, with the largest number coming from Culbin Sands in Moray (Christie 2014, 38 - 39). Unfortunately, most of the green beads from Culbin Sands could not be analysed for bubble concentration due to the heavily corroded nature of the objects.
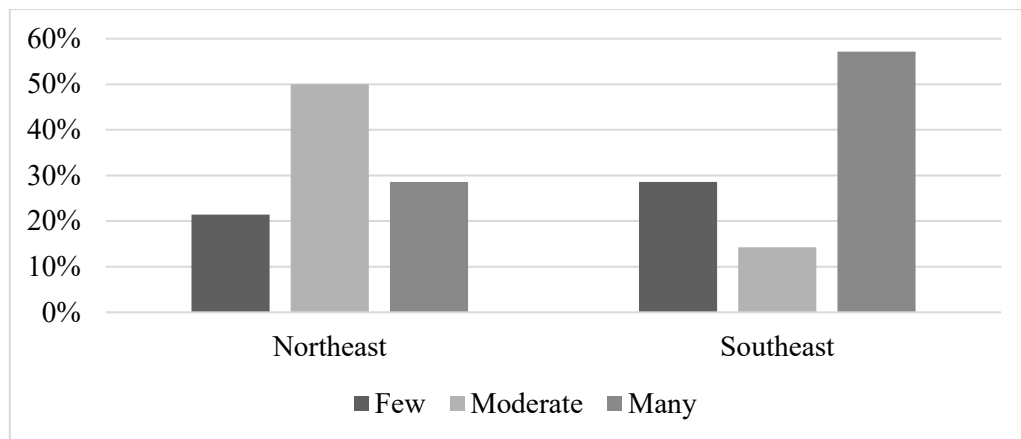
Figure 4.18: Regional bubble distribution of green bead glasses (p = 0.264)

White bead glasses in Scotland have large concentrations of bubbles overall, with 32% and 61% classified as having moderate and many bubbles respectively (n = 28; Figure 4.19). All but three samples come from design elements of polychrome beads. Interestingly, the southeast and west do not seem to have any few- or moderately-bubbled white beads despite clear trends towards those concentrations with other colours. They do have 10 many-bubbled white beads between them, however, and many of them form white trail or reticella designs.
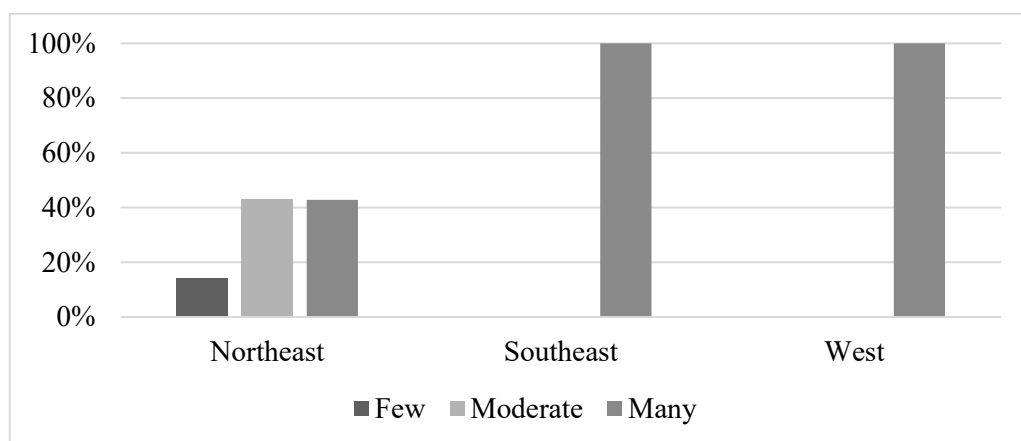
Figure 4.19: Bubble concentrations of white bead glasses (p = 0.073).

Yellow bead glasses tend towards fewer bubbles. While we can argue this is due to the opacity of yellow bead glass, all the white glass sampled is also opaque and they tend towards having many bubbles. There are no statistically significant differences

between regions (p = 0.579) and no discernible patterns between regions either (Figure 4.20). There are statistically significant differences between monochrome and polychrome uses of yellow glass, however, with polychrome yellow glass containing significantly more bubbles (p = 0.000044) (Figure 4.21).
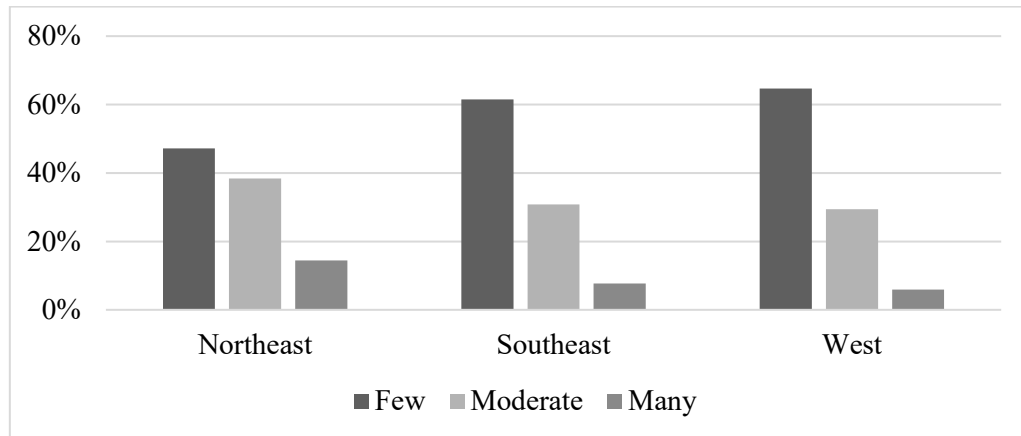
Figure 4.20: Regional bubble distribution of opaque yellow bead glasses (p = 0.579).
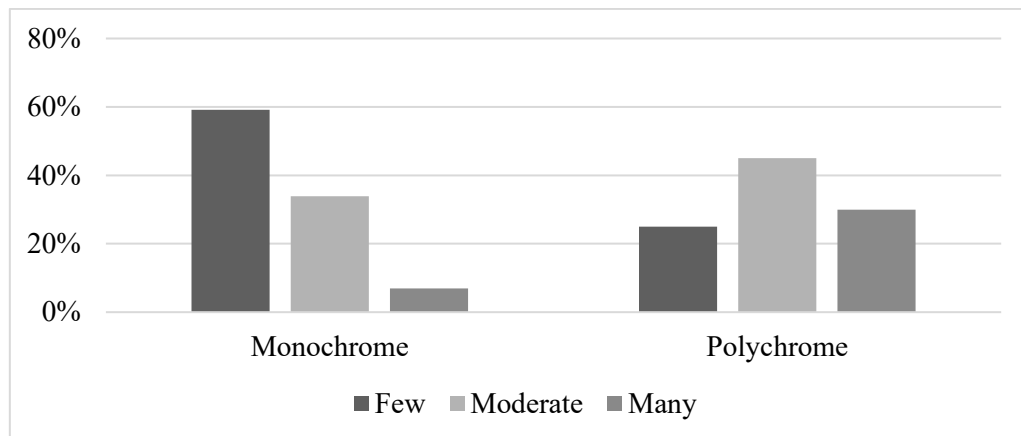
Figure 4.21: Monochrome and polychrome bubble variation in opaque yellow bead glasses (p = 0.000044).

4.4.3 DIFFERENCES IN LOCATION AND DESIGN OF GLASS ON THE OBJECT

In addition to differences in colour and diaphaneity, there are significant differences in bubble concentration depending on the location of the glass on polychrome objects (p = 0.019) (Figure 4.22). Glass used as the core of the bead tends towards moderate amounts of bubbles (50%), with some having few (33%). Glass used to create

the design of a bead, however, tends towards having moderate to many bubbles (40% and 31% respectively). Interestingly, there is no statistically significant difference between glass used in different polychrome designs (p = .217).
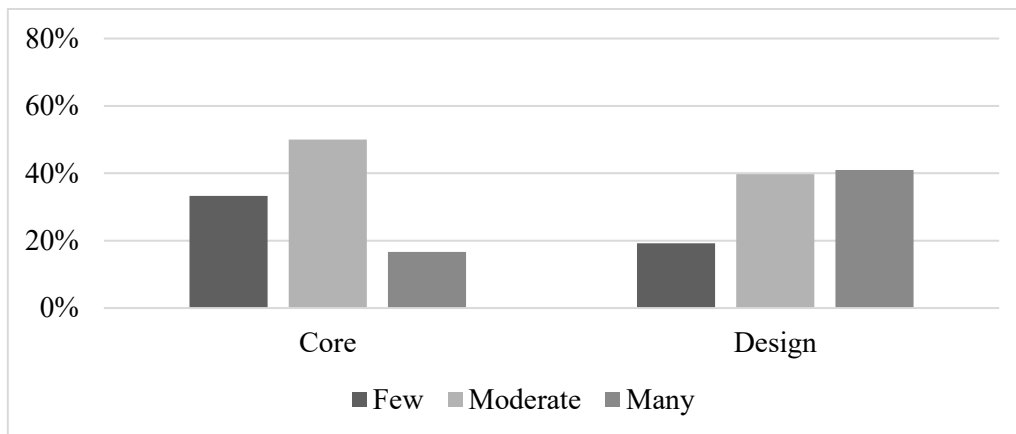
Figure 4.22: Bubble variation between core and decorative samples (p = 0.019).

4.4.4 DIFFERENCES IN MANUFACTURE

There are statistically significant differences between bubble concentrations in wound and drawn beads in Scottish Iron Age and Early Medieval contexts (p = 0.0000043) (Figure 4.23). Wound beads (n = 213) tend to have few (50%) to moderate (35%) bubbles while drawn beads (n = 71) tend to have moderate (35%) to many (41%) bubbles. In further subdividing the samples to translucent and opaque beads, the pattern continued for translucent material (p = 0.0003) (Figure 4.24).
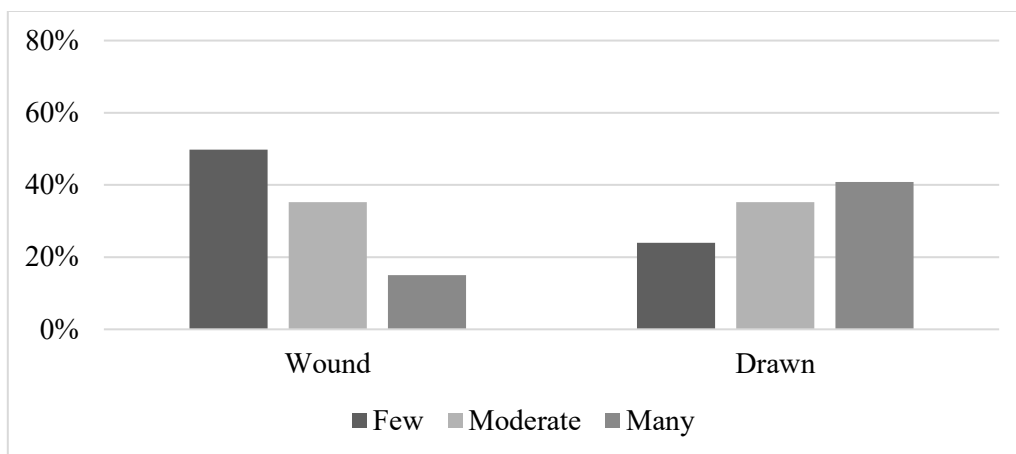
Figure 4.23: Bubble variations between wound and drawn glass beads (p = 0.0000043).
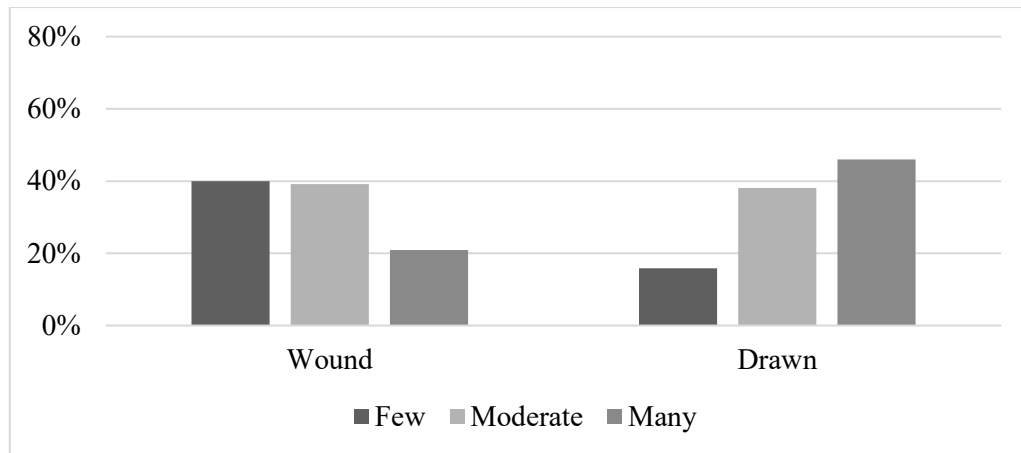
Figure 4.24: Bubble variations between translucent/transparent wound and drawn glass beads (p = 0.0003).

When divided by colour, only bubbles in copper-blue glass differ significantly between wound and drawn beads (p = 0.000027) (Figure 4.25). Drawn copper-blue beads had many bubbles (67%) while wound copper-blue beads had few (67%). Neither cobalt-blue nor yellow beads (the only other colours with significant sample sizes) differed significantly between wound and drawn beads.
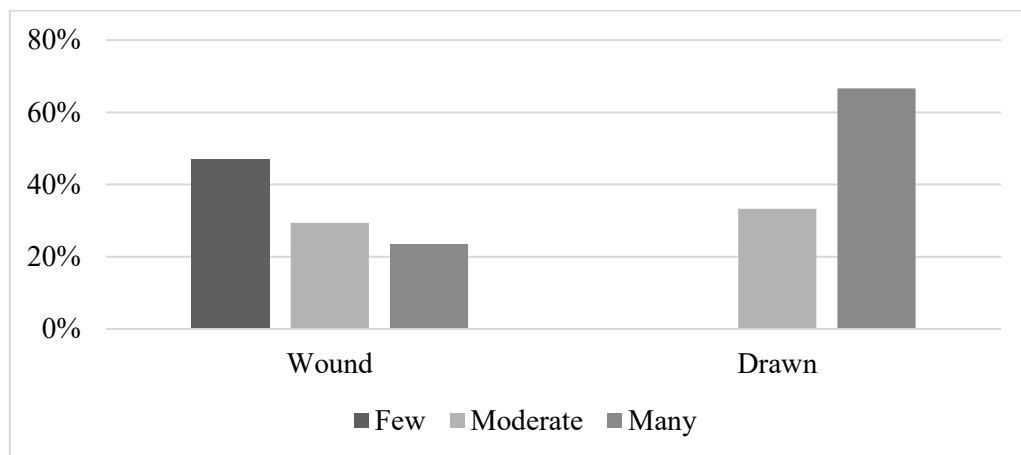
Figure 4.25: Bubble variation between wound and drawn copper-blue beads.

4.4.5   DIFFERENCES IN SIZE

There is no significant difference in bubble concentrations between beads of different lengths (p = 0.434), but there are significant differences between beads of different diameters (p = 0.00042) (Figure 4.26). Beads with larger diameters often have

fewer bubbles than smaller beads. Similarly, when looking at the relative thickness of the wall of the bead (i.e. the difference between the diameter of the object and the diameter of the bead's perforation), we also see a general decrease in bubble concentrations as the thickness of the bead wall increases. Since 70% of the beads in this study range from 0 – 10mm in diameter, however, this difference in bubble concentrations is unlikely to have significantly affected the above data.
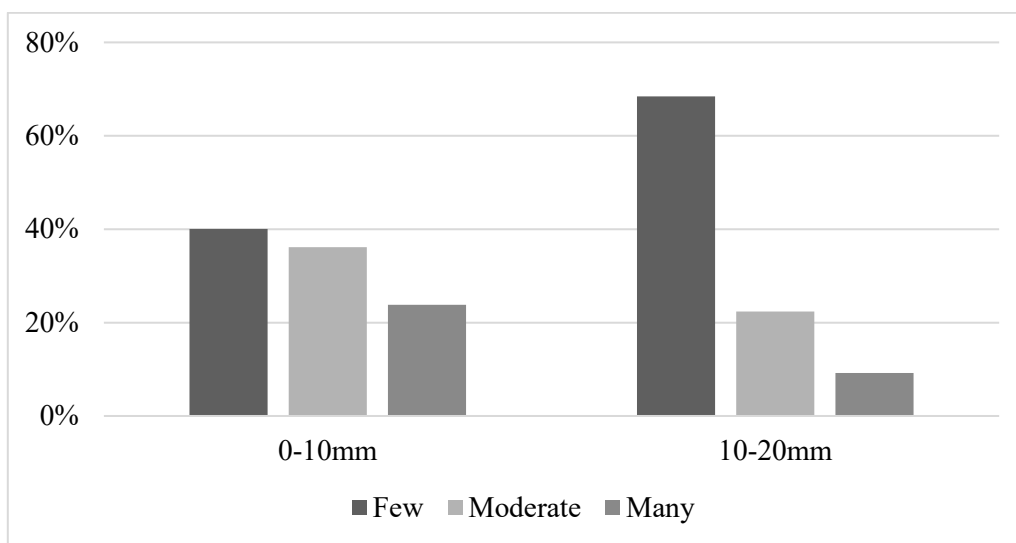
Figure 4.26: Bubble variation between objects of different diameters.

4.5   BUBBLES AND BEAD MANUFACTURE

There are several significant results to discuss in relation to bubbles in beads. First, there are significant differences between objects made with different manufacturing techniques. Wound beads overwhelmingly have fewer bubbles while drawn beads tend to have many (Figure 4.23). Given the myriad ways in which bubbles can form in glass, many of which are connected to manufacture, it is unsurprising there are significant differences between objects depending on manufacture. Winding beads is a relatively individual, hands-on technique in which the craftsperson forms each bead individually. They may make a batch of up to 10 wound beads on a single rod before removing them, but they would have difficulty making more at once. We might expect, then, that the

pattern of bubble concentration in wound beads might vary or favour concentrations that are more difficult to achieve due to individual agency in altering the bubbles in a single object. However, drawn beads are less individualised. The craftsperson draws long canes of glass that they cut, anneal, and string for sale. They cannot adjust bubble concentrations for each individual bead, and likely cannot necessarily do so even for the individual canes they draw. We could therefore expect drawn beads to have fewer beads with few or many bubble concentrations and more with moderate concentrations due to the difficulties associated with producing glass with few or many bubbles (Chapter 4.1).

Instead, drawn beads in Scottish contexts have significantly more bubbles than we would expect, and significantly more than wound beads. It is unlikely for this pattern to be a product of the manufacture technique, because the process does not allow for the control required to intentionally maintain such an abundance of bubbles. Additionally, while the annealing process requires the beads sit in a container of ash for an extended time, ash or dust only form bubbles in melted glass if additional glass covers it to seal the ash or dust inside. It is possible, then, that the differences seen here between wound and drawn beads relates more to the chemistry of the glass than its process of manufacture.

However, when dividing wound and drawn beads by colour in addition to manufacture technique, only the copper-blue beads showed significant differences between wound and drawn beads (Figure 4.25). The only other colours with significant sample sizes (cobalt-blue and yellow) showed nearly identical patterns of bubble concentrations between the two manufacture types. This again suggests that it is not necessarily the process of drawing versus winding a bead that produces more or fewer bubbles respectively; it is more likely a difference in glass chemistry. Given the difference between wound and drawn copper-blue beads in Scottish contexts, it is relatively safe to assume the difference in bubbles does not stem from a chemical

difference in colorants, but more likely alkalis (e.g. soda or potash) or secondary ingredients like stabilisers (e.g. lime or alumina). The drawn copper-blue beads in Scotland – or at least the glass used to make them – likely come from a different workshop than the wound copper-blue beads and may even indicate a chronological difference between objects. Additionally, these results suggest that while the drawn and wound cobalt-blue and yellow beads may come from different workshops due to differences in manufacturing technique, the glass may come from the same workshop or at least use similar recipes. In other words, it supports the idea of primary and secondary workshops in Europe during the Iron Age and Early Medieval periods.

4.6 THE INTENTIONAL MANIPULATION OF BUBBLES IN PRE-MODERN GLASS

Another significant result is the relative lack of bubbles in naturally-coloured glasses. Naturally-coloured glass does not have any colorants added in the manufacture process, instead taking its colour from natural impurities in the sand (usually varying combinations of iron and copper). The resulting glass is transparent brown or a transparent pale blue, green, or yellow. The difficulties of eliminating bubbles still apply to this colour group, but they overwhelmingly have few bubbles. Windows or glass vessels often used naturally coloured glass, which suggests a desire to make naturally-coloured glasses with few bubbles; the more bubbles in a windowpane, the more difficult it is to see out of. Naturally-coloured beads may have used recycled shards of broken windows or vessels, resulting in beads with few bubbles. Unfortunately, there are too few examples of naturally-coloured beads from Iron Age and Early Medieval Scotland to comment on this further.

White glass in beads also gives some insight into glass and bead manufacture for this period, both within Scotland and in Europe as a whole. Most white glass examined here was saturated with bubbles (59%). Most of these samples are decorations on polychrome beads, though some are monochrome. In many of these cases, it is difficult to discern whether the glass is white or whether it is simply either a natural glass (in the case of monochrome beads) or the base glass (in the case of polychrome beads) that has been packed full of bubbles in certain areas rather than white glass being added. Similar white designs appear on imported glass vessels from the Early Medieval period (Type C; Campbell 2007, 64), but the vessels are generally different colours than beads using the same design.

While these results may suggest a simple chemical difference between white glass and other glasses during this period, the two most common opacifiers used to create white glass were antimony oxide (Sb_2O_3) or tin oxide (SnO_2), which also serve as fining agents (Agua et al. 2017, 119; Dejneka and Gomez 2012, 3; Freestone et al. 2008, 41; Henderson 1985, 270; House et al. 2009, 5; Molina et al. 2014, 171; Shelby 2005, 43). Specialists often assume white glass contains either antimony or tin oxide because most white glass found in Europe from the Iron Age and Early Medieval periods contain these oxides, but these compounds should significantly *reduce* the concentration of bubbles. The apparent abundance of bubbles in white glasses therefore suggests either the use of a different chemical opacifier, if one was used at all, or the intentional introduction of bubbles to many white glass beads at the time. Chemically testing the trails on both vessels and beads to determine whether any antimony oxide or other decolourisers or opacifiers have been added and whether the two object types share chemical (and therefore manufacture) signatures would help answer the question, but this is outside the scope of this thesis.

These results show that there was significant, intentional control of bubbles both within and between beads. While manufacturers may not have worried about bubbles constantly, they clearly manipulated and controlled them to achieve specific types or designs, such as a clearer natural glass or a more highly bubbled white glass. The difficulty of controlling bubbles in glass, particularly without the use of a vacuum, suggests a sophistication and knowledge of the craft that often does not enter the current discussion of glass working for this region.

4.7   THE PROBLEMS WITH CULBIN SANDS

One possible caveat to the data is that each region differs significantly in the number of objects included in this study, which may alter the results. The northeast has 235 samples, while the southeast and west have 72 and 56 respectively. Northern Scotland has only 26 samples included in this study. The primary culprit of such disparate numbers in the northeast is a group of several hundred beads said to be from Culbin Sands, on the Moray coast. This site has the largest number of reported beads in total for the entirety of Scotland - over 700 compared to the site average of five or six for all other sites with beads in Scotland during the Iron Age and Early Medieval period. All the beads recovered from Culbin Sands are stray finds, with no associated contextual information.

There are two large problems with the beads from Culbin Sands. The first is that it is perhaps the best-known site in Scotland for glass beads in the Iron Age or Early Medieval periods. As such, it is entirely possible that individuals donating or accessioning beads to museum collections had been told the objects were from Culbin Sands without confirming they had originated from that site. There is no specific research into whether this phenomenon has occurred in the United Kingdom, but it plagues many bead sites in Asia, particularly Ban Chiang, in northern Thailand. Scholars and tourists alike have

found thousands of tiny glass seed beads at Ban Chiang, so much so that vendors often refer to beads of this type as Ban Chiang beads. Now, when individuals donate strings of beads to museums or speak to archaeologists about their beads, they say the beads came from Ban Chiang because that is what vendors told them. Instead, these beads often come from dozens of other sites in Thailand or are modern replicas. It is not unlikely for such a phenomenon to have occurred with Culbin Sands. The Society of Antiquaries published widely on the site several times around when most of the glass beads from Culbin Sands were donated to the National Museum of Antiquaries (Black 1891; Callander 1911; Linton 1876; Matthewson 1877). Since many of the beads from Culbin Sands were stray finds, it would not be surprising for some to be misattributed to the site.

The second issue with Culbin Sands is the lack of contextual information for the beads. Most were recovered in the 1800s and donated to the National Museum of Antiquaries shortly afterwards. The museum strung many of the monochrome beads together, organising strings by colour rather than by objects that may have been found together. We therefore have one string of cobalt-blue beads, one of copper-blue beads, one of green, two of yellow, one of black or deep purple, three of clear glass of which two sets have what appears to be seaweed clung to it, and one of a milky-white colour. Of these strings, the three clear and one milky-white string are likely post-medieval objects, given the quality and colouring of the glass. It would not be surprising to find certain other strings were also either post-medieval or modern, but the other colours are more difficult to eliminate based on the glass alone. Given the differences in bubble concentrations of the copper-blue beads from Culbin Sands, this 'string' may post-date the early medieval period.

4.8   BUBBLES AS EVIDENCE OF LONG-DISTANCE TRADE

If the drawn beads discussed in this chapter date to the Iron Age or Early Medieval period, particularly those from Culbin Sands, then they would provide clear evidence of long-distance trade. Little, if any, evidence for glass bead manufacture exists in Scotland for the Iron Age or Early Medieval period. There is also no current evidence for European manufacture of drawn beads prior to the 14th century, meaning that any drawn beads in Scotland either postdate the 14th century or came from outside Europe (Francis 2002, 171). Major centres of drawn bead manufacture between 800 BC and AD 800 are concentrated in the Near East, southern India, Sri Lanka, and Thailand (Francis 2002). Claims of manufacture have been made for roughly 30 sites in South and Southeast Asia, though fewer than 10 provide significant evidence for it. Thirty-five of the 36 drawn beads in this study are the small, monochrome copper-blue drawn beads found at Culbin Sands on the Moray Coast. Of these, the majority have many bubbles while some have moderate amounts. Comparable beads in terms of size, colour, and bubble patterns occur in Thailand, with significant numbers of many-bubbled copper-blue drawn beads occurring at Tham Chhaeng in Phetchaburi province on the northeast coast of the Thai peninsula (Figure 4.27). It is unlikely that the drawn turquoise beads from the Culbin Sands came from Thailand. If the turquoise beads from Culbin Sands date between 800BC and 1000 AD, however, then they likely were made at a site outside Europe, possibly one in Asia. Otherwise, these beads likely post-date the early medieval period.

Figure 4.27: Small drawn monochrome copper-blue beads from Culbin Sands (NMS X.BIB 57) (left) and Tham Chhaeng (right).

Regional differences in bubble concentrations more generally also indicate differences in trade routes between different regions of Scotland. First, there is a probable difference between the northern regions of Scotland versus the southeast and west (Figure 4.10). This difference could result from the increased Roman presence or influence in the south, but it is impossible to know without further contextual information for the beads. However, the picture changes as we separate out individual colours. The west and northeast of Scotland have similar bubble concentrations in their cobalt-blue beads, for example, despite differing in bubble concentrations in their glass beads in general. The copper-blue beads in the northeast differ greatly from those elsewhere in Scotland, even if we remove the string of small copper-blue beads from Culbin Sands. Despite these contrasts, there is no significant regional difference in bubble concentration between yellow glass beads across Scotland. These regional differences between colours suggest that each region had its own import routes for glass beads, and possibly its own manufacture technique(s) if objects were made within the region itself. Import routes may have overlapped when multiple regions acquired glass either from the same trade partner or from each other. Without contextual information for the objects in question, however, the specifics of these routes are difficult to comment on further.

Finally, there are the possible connections between beads with highly bubbled white decorations and imported vessel glass exhibiting similar techniques (Figure 4.28). These are Campbell's Group C vessels, or glass vessels in the Atlantic tradition with highly bubbled white trail designs (2007, 64). These tend to be either naturally light green or light yellow, though some are amber or deep green in colour (Campbell 2007, 55). None of the vessels in Campbell's corpus are dark blue, however, which is the predominant colour for glass beads with highly bubbled white trails. The technique does not appear in bead literature, nor is it used in neighbouring regions. It is possible that different colours and colour combinations were reserved for different object types. It is also possible that the vessels and the beads come from different workshops and one has been designed to mimic the other. Full comparison between beads and vessels could establish a connection, but this is currently outside the scope of this study.
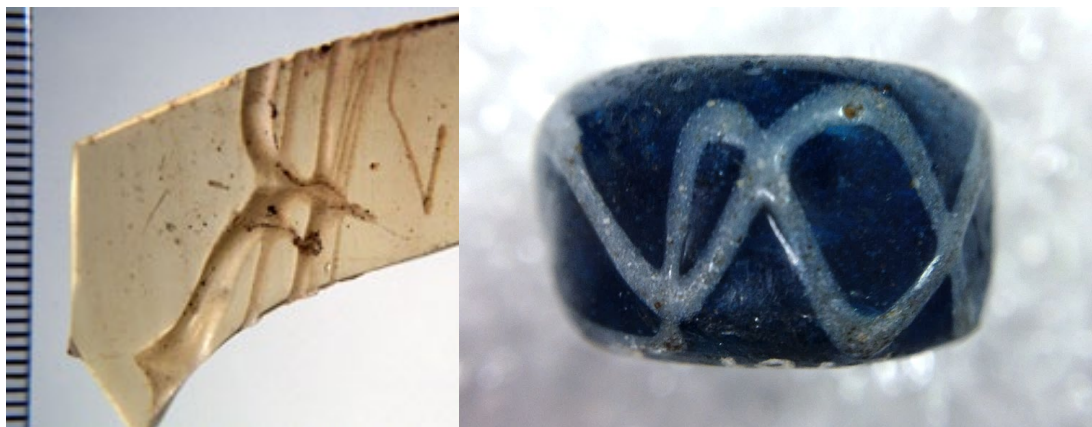
Figure 4.28: Examples of 'white' bubbled trails in vessel and bead glass (Rumbleton, HMAG B.1914.521/14). Vessel image courtesy of Ewan Campbell.

4.9   CHRONOLOGICAL INSIGHT FROM BUBBLES

The regional differences seen here may have more to do with chronology or ethnic group than trade, or they are at least affected by a combination of the three. Traprain Law and Newstead, for example, are in the same region (southeast Scotland, roughly 40km apart) but have significantly different patterns of bubble concentrations. Beads at Traprain

Law have few or many of bubbles, while Newstead favours moderately-bubbled beads (Figure 4.29). This data only includes beads of colours present at both sites to avoid confusing the results.
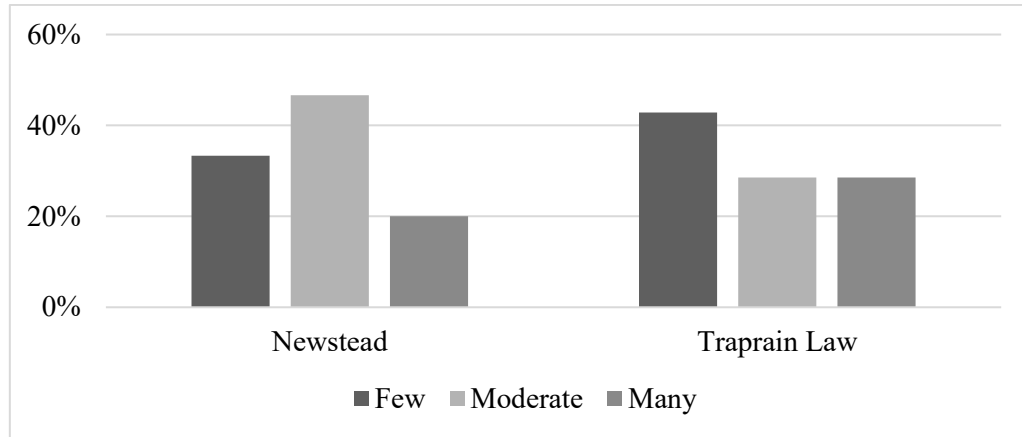
Figure 4.29: Comparison of bubble concentrations between Traprain Law and Newstead (P = 0.026).

Newstead was a Roman fort largely occupied between the late 2nd and early 3rd centuries AD (Richmond 1950, 1), while Traprain Law was a Late Iron Age hillfort occupied in the first couple centuries AD and then again between the 3rd and 5th centuries AD (Hunter 2013, 6). Newstead therefore exhibits a large amount of culturally Roman glass while Traprain Law exhibits largely non-Roman Iron Age and Early Medieval beads. The differences in their glass likely reflects the different chronological periods between each site, the different cultural preferences between groups at each site, or both.

Figure 4.30: Faience and glass melon beads from Newstead (NMS X.FRA 890 (left) and NMS X.FRA 862 (right)).

Some of this bubble data also indicates the possibility of modern beads being falsely attributed to the Iron Age or Early Medieval period. The difference in bubble concentrations in the drawn copper-blue beads from Culbin Sands suggests they are either coming from outside Europe or they may be post-medieval or even modern beads instead. Comparing bubble density to other glass bead collections in Europe and between the early medieval period and the present would provide further insight.

4.10 The Benefits of Visible-Range Spectral Photography for Archaeological Finds

The preliminary results discussed above indicate that visible-range spectral photography produces insight into the glass bead assemblage for Iron Age and Early Medieval Scotland that previously was not possible without technologically advanced equipment. This insight would have been impossible without challenging the standards of archaeological imaging and experimenting with current affordable technologies. The application of visible-range filters to archaeological photography is not a new technique (Chapter 3.3). The analysis of objects through imaging has been reserved instead for more scientific imaging techniques, however, such as microscopy or multispectral and hyperspectral imaging, 3D modelling, or RTI. These techniques are helpful for archaeological research, but often require expensive equipment and software that many projects cannot afford (Chapter 8).

Using digital filters does not require new images, either, just the original digital image files. Even scans of a slide made from the original image will work, though an original digital image is ideal. Only photographs of the original image are unlikely to provide useful results, as the colours will change between the original image and a photograph of said image. Many of the images in this study were captured in 2014

without any knowledge of this imaging technique and were still able to be included in this study.

Visible-range spectral photography can be applied to a wide range of materials, too. Some filters highlight corrosion or surface wear, while others emphasise paint or staining. Digital software can apply filters to any digital image to emphasise certain features over others, such as surface wear on lithics or ceramics, carvings or surface wear on stone sculpture, wear and corrosion on metalwork, cropmarks in the landscape or differences in stone or mortar in buildings. The possible applications are varied, and the equipment affordable. Nor is this technique limited to archaeology. Filters work the same no matter the subject of the image. Spectral photography can highlight wear or weathering on anything from rocky outcrops or gemstones to mechanical elements or other metalwork in vehicles or machines. It can forensically identify markings on bone or weapons. If something is worth imaging for analytical purposes, it is worth examining through filters to emphasise or discover new information.

The case study provided here uses filters to examine a single characteristic of a single, specific set of archaeological objects: bubble concentrations in Iron Age and Early Medieval glass beads found in Scottish contexts. Even limited in this way, the technique provides significant conclusions about glass beads, which have led to an advancement in possible conclusions concerning trade and manufacture of these objects within Scotland during this time. Additional data will certainly help further this discussion, but the conclusions resulting from this brief case study provide more information than has previously been available relating to glass beads. If such experiments can gain significant insight for objects with as little contextual information as glass beads, it stands to reason that we would only reap even more benefits from objects associated with specific archaeological contexts.

5 CASE STUDY 2: NON-VISIBLE-RANGE PHOTOGRAPHY AND OBJECT CHEMISTRY

Having demonstrated the benefits of visible-range filters in archaeological photography in the previous chapter, this chapter will now turn to filters in the non-visible range. Objects react to light based on their chemical composition, regardless of whether human eyes can see it (Chapter 3.2.1). Consequently, we can determine the chemical composition of an object by examining and measuring its reactions to light (i.e. spectroscopy). This principle has allowed the scientific community to chemically test objects for nearly a century. Chemical differences in glass indicate differences in manufacture and trade, and their analysis can determine possible connections between specific objects and the workshop in which they were made. For example, chemical studies of ancient glass have led to the identification of glass objects made at Roman versus pre- or post-Roman workshops due to differences in available resources (Henderson et al. 2004, 466; Rehren 2000, 1225; Silvestri et al. 2005, 798). Spectroscopy and other techniques for acquiring chemical data usually requires expensive equipment, however, and the techniques available for chemically analysing glass are all at least partially destructive.

This chapter uses non-visible-range spectral photography as a non-destructive, non-contact technique for identifying chemical relationships between objects using a dSLR converted for full spectrum imaging. The results from this study lead to important conclusions about these objects without requiring expensive equipment or permissions. In bead studies, archaeologists chemically test relatively few objects, particularly those made of glass, due to the associated costs and the potential destructive nature of the technique. For example, only 55 objects have been chemically tested from Arikamēḍu despite the site yielding over 9,000 glass beads (Dussubieux et al. 2008, 801; Francis

2002, 213). The ability to identify chemical differences and possible similarities using only a converted dSLR and photo editing software allows us to generate far more information about these objects than is otherwise currently feasible in a non-destructive manner, and it significantly reduces the effects of the two largest barriers to object chemical studies: cost and destructiveness.

To demonstrate the application of this technique, I focus again on glass from Iron Age and Early Medieval Scottish contexts. Glass chemists rarely test Scottish material, with few sources publishing object-specific chemical data (e.g. Bertini et al. 2011; Campbell and Lane 1993). Given the relatively unique nature of each glass bead in Scotland, acquiring permission and funding to chemically test these objects is difficult. This collection is therefore ideal for investigating the possible benefits of this non-destructive, non-contact technique. I have compared the Scottish material to contemporary Roman and Anglo-Saxon glass to determine the chemical relationship of Scottish material to these assemblages. I also have compared these assemblages to New Kingdom Egyptian, medieval English and modern glass to examine possible chronological differences between them. The results demonstrate clear differences between each of these assemblages and provide new information concerning the manufacture and trade of glass beads found in Iron Age and Early Medieval Scotland.

5.1 IRON AGE AND EARLY MEDIEVAL GLASS CHEMISTRY

There are six general categories of chemical components in glass: formers, alkalis, stabilisers, colorants, opacifiers, and trace elements (Francis 2002, 211; Ramli et al. 2009, 586 – 587). Each occur to varying degrees, with formers comprising the largest portion of the object and trace elements the least. Each affects the chemical composition, and therefore the spectral reactions, of a glass object.

Glass formers comprise most of the glass, often ranging between 55 and 75% of the total weight (Francis 2002, 211; Ramli et al. 2009, 586). The most common glass former is silica (SiO_2), which comes from the sand or quartz pebbles used to make the glass (Ramli et al. 2009, 586). Lead (Pb) also occurs as a glass former and can account for up to 90% of the total weight due to its high specific gravity (Ramli et al. 2009, 586). Heavily lead-based glasses are often found in ancient Chinese contexts, while glasses with smaller proportions of lead often occur in Iron Age and Medieval European contexts (Biek and Bayley 1979, 11 – 17; Francis 2002, 73).

Silica melts at too high a temperature for ancient ovens to achieve (~1700ºC), so glassmakers added an alkali (or flux) to lower the melting point (Francis 2002, 211; Kanungo 2004, 1). Two dominant alkalis occur in glass-making: soda (Na_2O) and potassium oxide (K_2O). Lead (Pb) can function as an alkali, but is less common (Francis 2002, 211; Ramli et al. 2009, 586).   Most alkalis were a mixture of sodium and potassium, especially if derived from plant ash. Alkalis often compose 15 to 20% of the total weight of the ingredients (Francis 1988, 4).

When an alkali mixes with silica at such high temperatures, the melt becomes chemically unstable. To avoid explosion and cracking, a stabiliser was added to strengthen the glass and its chemical bonds, usually lime (CaO) or alumina (Al_2O_3) (Francis 2002, 211; Ramli et al. 2009, 587). Most ancient glass in Europe used lime, while large portions of Asian material used alumina. Some recipes use both in relatively equal amounts.

Colorants are any component that gives colour to the glass. Glassmakers can add these to the melt during the manufacture process or they can occur as impurities in the sand (Francis 2002, 211). The two most common colorants are iron oxide (Fe_2O_3) and cupric oxide (CuO). These two components, added in varying amounts at different times

in the process, can form any colour save dark blues, purples, or colourless/clear glasses (Francis 2002, 211; Kanungo 2004, 2; Ramli et al. 2009, 587). Cobaltous oxide (CoO) creates deep blues while manganese oxide (MnO) produces deep purple or clear glass, depending on how much is added and when (Kanungo 2004, 2; Ramli et al. 2009, 587). Iron and copper often occur naturally in sand and give glass a natural colouring depending on how much of each is in the sand used to make the glass (Ramli et al. 2009, 587). These natural colours range from brown to very light green, blue, or yellow.

Opacifiers are additions to the glass to make it opaque. In ancient glass, many of these components appear to be impurities in the sand, but there is significant evidence for the intentional use of opacifiers (Francis 2002, 211; Ramli et al. 2009, 587). Antimonates are the most common opacifier and serve as a fining agent to reduce the bubbles in glass (Shelby 2005, 43). Lead-antimonate ($Pb_2Sb_2O_7$), arsenic oxide (As_2O_3), calcium-antimonate ($Ca_2Sb_2O_7$ or $Ca_2Sb_2O_6$), and lead-tin ($PbSnO_3$) or tin oxide (SnO_2) also occur as opacifiers in ancient glass (Biek and Bayley 1979, 9; Francis 2002, 211; Ramli et al. 2009, 587). The use of certain opacifiers will impart certain colours, such as lead-antimonate or lead-tin for yellow and tin-oxide or calcium-antimonate for white. Bone, salt, sand, and bubbles can opacify glass if added in the right quantities.

Trace elements are any element that is not intentionally added, and generally make up less than 1% of the object's weight (Francis 2002, 211; Ramli et al. 2009, 587). One exception to this is magnesia (MgO), which can compose more than 2.5% of the object's weight. Magnesia often occurs in plants and can therefore indicate a plant-based source of soda rather than a mineral one (Biek and Bayley 1979, 5; Lankton and Dussubieux 2006, 135; Robertshaw et al. 2010, 5). Other trace elements include barium (BaO), titanium (TiO_2), gold (Au), silver (Ag), vanadium (V_2O_3), strontium (SrO), uranium (U), and zirconium (Zr).

Silica-soda-lime glass has been the primary glass type in Europe since glassmaking began, so much so that many papers written about ancient European glass assume a silica-soda-lime composition (Rehren 2000, 1225; Silvestri et al. 2005, 797). It consists of a silica former, soda alkali, and lime stabiliser, but can contain a variety of colourants, opacifiers, and other chemical components. There are two main varieties: one using a mineral (m-Na-Ca, after Dussubieux and Gratuze 2002, 139) and the other using a vegetal or plant-ash (v-Na-Ca) source of soda, though the plant ash source often contained elements of potassium as well. Egyptian and Middle Eastern glasses used a plant-ash source of soda (v-Na-Ca) prior to the Roman period. The rise of the Roman Empire prompted a shift to a mineral source of soda (m-Na-Ca) because they were able to collect resources from modern day Italy, Egypt, and Jordan to do so (Rehren 2000, 1225; Silvestri et al. 2005, 798). After the collapse of the infrastructure associated with the Roman Empire, glassmakers in most of Europe and the Middle East had difficulty acquiring the requisite materials for m-Na-Ca glass and instead experimented with local ingredients to create a type of v-Na-Ca glass in the 8th and 9th centuries AD. The site of al-Raqqa in Syria shows experimentation with recipes, which suggests the shift was not the remembrance but rather the rediscovery or reinvention of an old technique (Henderson et al., 2004, 466). By the thirteenth century, glass in Europe shifted again to a potash glass (K_2O), using wood ash as the alkali. This ash contained high levels of potassium oxide rather than soda and the glass develops a characteristic iridescent sheen upon corroding.

While it was (and still is) the primary glass type found in Europe, silica-soda-lime glass was not the only glass type in circulation in the ancient world. Silica-soda-alumina glasses predominate in Asia, particularly South and Southeast Asian contexts from the 4th century BC to the 10th century AD (Robertshaw et al. 2010, 5). They are also found in

Africa, particularly in Sub-Saharan and East African contexts from the 9th to 19th centuries AD (Dussubieux et al. 2010, 5). These glasses generally use a mineral source of soda (m-Na-Al) and trace element analysis of samples in Africa, South Asia, and Southeast Asia has determined five separate types depending on levels of barium, uranium, strontium, and zirconium (Dussubieux et al. 2010).

A plant-ash soda-lime glass with high-alumina (v-Na-Ca-Al) has been found in Pakistan and Northern India, but currently has very few examples (Dussubieux and Gratuze 2002, 142; Lankton and Dussubieux 2006, 135). There are also mineral-potash glasses found in Thailand and Vietnam in the last few centuries BC (m-K-Ca), in Vietnam, China, Korea, and Japan in the first few centuries AD (m-K-Al), and South and Southeast Asia (m-K-Ca-Al; no date range given) (Lankton and Dussubieux 2006, 130 – 136). Finally, mixed-alkali glasses use roughly equal amounts of soda and potash, but these appear limited to India and Sri Lanka (Lankton and Dussubieux 2006, 138).

While there were many glass recipes available worldwide during the Scottish Iron Age and Early Medieval periods (800 BC – AD 800), few specialists have chemically tested Scottish glass, particularly that from the Iron Age or Early Medieval periods. Most studies test between one and ten objects from a single site to compare to Roman or Anglo-Saxon glass, which have been examined more thoroughly. Few publish the full chemical results, instead averaging the samples together or opting to omit the concrete data from the publication. Given the lack of chemical testing of Scottish objects, it is possible some objects use a different recipe than that so often assumed for European assemblages. Comparisons between Scottish objects are difficult, however, because chemical testing of Scottish glass is rare and publication of chemical data for individual objects is rarer still.

5.2 CURRENT TECHNIQUES FOR TESTING GLASS CHEMISTRY

The primary reason few glass beads in Scotland have been chemically tested is the logistics required for doing so. Several methods exist for acquiring precise chemical compositions for glass objects, but the only techniques to provide complete chemical information are all at least partially destructive. Acquiring permission to destroy objects as relatively rare, unique, and small as glass beads is difficult at best. Non-destructive techniques generally do not provide complete information, and current destructive and non-destructive techniques are often expensive for many projects. This section details the most common techniques in archaeological chemistry and the benefits and pitfalls of each.

5.2.1 LASER-ABLATION INDUCTIVELY-COUPLED-PLASMA MASS-SPECTROMETRY (LA-ICP-MS)

One of the most popular techniques for chemically testing glass is laser-ablation inductively-coupled-plasma mass-spectrometry (LA-ICP-MS). A laser samples a minute portion of the object, after which the sample is dissociated, atomised, and ionised (Dussubieux and Gratuze 2002, 137). The ions move into a vacuum chamber where a quadrupole mass filter separates the ions based on their mass-charge ratio (Dussubieux and Gratuze 2002, 137). This method can detect between 20 and 50 elements in a sample with minimal destruction to the object. LA-ICP-MS provides accurate measurements for a wide range of elements, including trace elements, and it is the only minimally-destructive technique to measure sodium content in glass accurately. It also requires very small samples, such that the point at which the laser has carved into the object is often undetectable; you must be looking for it to find it.

However, while LA-ICP is minimally destructive, it is still destructive and acquiring permission to perform such analysis on museum collections is difficult. Additionally, while the average price of LA-ICP-MS for a single glass sample is roughly £30 (e.g. The Field Museum 2018; University of South Florida 2018), this would amount to over £3000 for 100 samples. This amount also does not include the cost of shipping or travel, nor does it include the difficulties associated with acquiring permission from museums for such study. Given the cost and the destructive nature of the technique, LA-ICP-MS is not feasible for most projects working on glass objects, particularly those with lower budgets.

5.2.2   FAST NEUTRON ACTIVATION ANALYSIS (FNAA)

Another technique for determining chemical composition is fast neutron activation analysis (FNAA), in which a fast neutron beam irradiates the object and measures elemental composition through direct gamma-ray spectroscopy (Dussubieux and Gratuze 2002, 136). The object is irradiated again several days later. Finally, specialists take three radioactive measurements after three, five, and sixty days cooling to determine the weight percentages of 31 elements (Dussubieux and Gratuze 2002, 137). This method determines all major elements in glass save for oxygen, which can be calculated assuming all elements are in an oxidised form.

One clear difficulty with this method is the time required for measuring. Upwards of sixty days is lengthy for analysis of limited samples, and it is difficult to obtain permission from collection owners to remove objects from storage for so long. It is even more difficult to acquire permission to remove objects from storage and irradiate them twice over 60 days. Standard rates average £100 per sample and require a minimum of 8 – 15 samples, which is too expensive for many archaeological project budgets (e.g. Delft University of Technology 2018; University of Missouri Research Reactor 2018). The

extended time frame, high cost, and irradiation of the object make FNAA a difficult option for chemically testing ancient glass.

5.2.3 RAMAN SPECTROSCOPY

Raman spectroscopy uses the principle of objects reacting differently to light to measure its chemical composition through the inelastic (Raman) scattering of light after illuminating an object with an ultraviolet, visible, or infrared laser beam (Renishaw 2018). A detector then collects and measures the electromagnetic radiation from the illuminated spot to generate results. Raman spectroscopy is non-destructive, only requiring a clean surface to measure. It also provides specific measurements for many major and trace elements. Raman spectroscopy seldom provides measurements of certain elements important to glass chemistry, however, such as sodium or magnesium. It also requires a sizable, clean surface for testing, which is not possible for many glass beads. Finally, while this technique is generally accurate and provides good results, it is expensive. Miniature Raman spectrometers cost a minimum of £2,500, while larger models cost about £10,000 (StellarNet 2018). Raman spectroscopy therefore falls outside the budget for many projects, including this one.

5.2.4 X-RAY FLUORESCENCE (XRF)

Perhaps the most popular chemical analysis technique is x-ray fluorescence, due to the versatility and portability of the machines. X-ray fluorescence works in much the same manner as fluorescence described in Chapter 3. The machine fires x-rays at an object, which then reacts with and either absorbs, reflects, or transmits the x-rays (Shackley 2011, 28). Some of these rays will be of a higher wavelength than those used in the original x-ray beam (Shackley 2011, 16). The nature and degree of these fluoresced

rays depends on the chemistry of the object. Thus, XRF can determine a wide range of elements through non-destructive means for most materials.

While XRF is non-destructive, it generally does not provide reliable data for one of the largest components of glass: sodium. Sodium is too light for the sensors to acquire a proper reading. Additionally, acquiring permissions and funds to use XRF equipment can be difficult, particularly if the collection is in a museum. XRF requires a sizable, clean surface for testing, and many glass beads are too small or too corroded or dirty to fulfil this requirement. Finally, XRF is far from affordable for many archaeological projects. A portable machine suitable for glass analysis currently costs between £20,000-25,000 at base level (NitonUK 2018), while repairs can cost between £3000-5000 (Bruker 2017). Individual samples cost between £80 – 100 (Instituto Nazionale di Fisica Nucleare 2018). This technique is not ideal for glass, then, and it is unaffordable for many projects.

5.2.5 PROTON INDUCED X-RAY EMISSION (PIXE)

Finally, proton induced x-ray emission (PIXE) is a non-destructive chemical testing technique in which the machine fires an ion beam at an object, which emits X-rays as a result. The energies of these x-rays directly correspond to the elements which emitted them, thus allowing for the measurement of these elements in the object. This is similar to XRF, only differing in the beam fired at the object and in its ability to accurately measure lighter elements than XRF. PIXE is more accurate than XRF, but comes with similar limitations in sample size, cost, and elements analysed (Instituto Nazionale di Fisica Nucleare 2018; Janssens et al. 1996, 691; Weber et al. 2002, 357).

5.3　CHEMICAL ANALYSIS THROUGH SPECTRAL PHOTOGRAPHY

All the techniques described above, along with any other chemical testing techniques that we may apply to ancient glass, encounter similar problems in their

execution. They are often destructive, require permissions that may be difficult to obtain, and require expensive and often non-portable equipment. Yet, objects react differently to various wavelengths of light based on their chemistry, some of which dSLR cameras can capture through photography. This chapter discusses the capture and analysis of chemical data for glass objects using non-visible-range spectral photography. This technique cannot capture precise measurements of individual elements in an object's chemical composition (Chapter 5.2), but it does determine chemical relationships between objects using an affordable, portable, non-destructive, non-contact technique. This allows for a general comparison between objects prior to investing in more precise and expensive chemical testing, leading to a more targeted approach. It also allows for general chemical testing of a larger collection of material than often is feasible through the above methods due to cost and logistics.
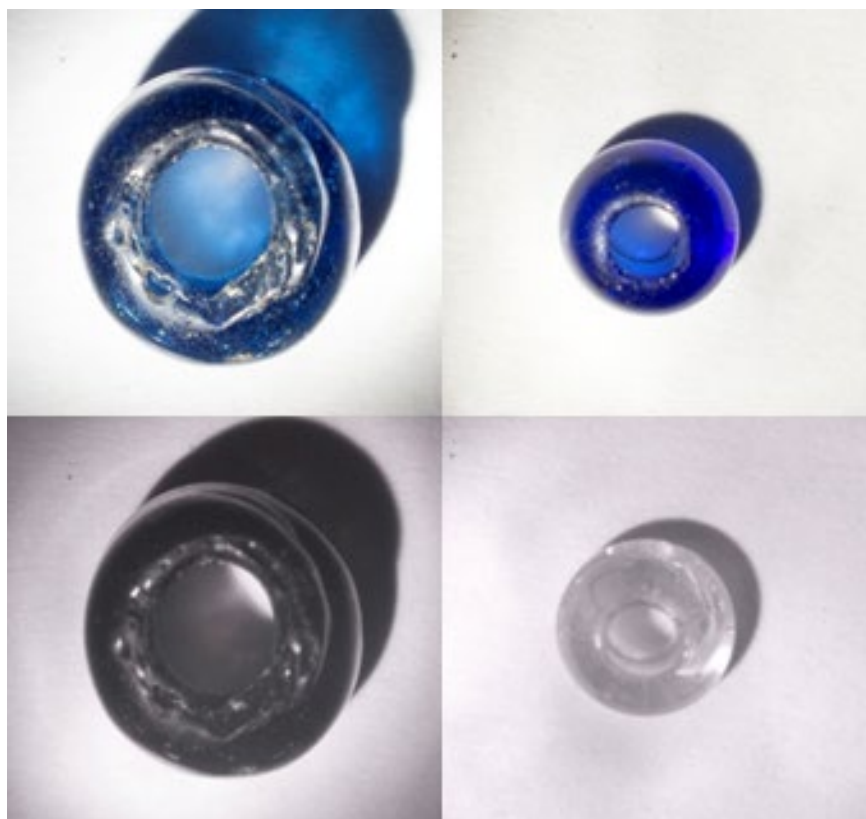
Figure 5.1: Difference between visible-range (top) and near-infrared (bottom) of cobalt-blue beads from Rhynie (UG SF 15021, left) and Clachbreck (UG CLB 1, right) (Appendix E).

This technique developed after noticing a significant difference in spectral reactions to non-visible light between two otherwise typologically similar cobalt-blue glass beads (Figure 5.1, Appendix E (PowerPoint Slide 11)). The bead from Clachbreck is both smaller and more vibrantly dark blue than that from Rhynie, but most specialists would consider these objects typologically and likely chemically similar if following current practices (e.g. Brugmann 2004; Guido 1978; Guido 1999; Mannion 2015). The bead from Rhynie absorbs near-infrared light while that from Clachbreck transmitted it, however, indicating significant chemical differences between the two.

Multispectral imaging in art conservation has produced a general flow chart of reactions that leads to pigment identification (Cosentino 2014; 7 – 8). Further experimentation with glass objects negated this as an option, however, when glass objects yielded a spectrum of reactions rather clear differences between 'absorption,' 'transmission,' or 'reflection,' (Chapter 3.2.2). The dilemma then became how to measure the reaction to light from digital photographs alone.

Cameras and computer screens only display red, green, and blue pixels to create a wide variety of colours on the screen (Chapter 3.3). They do this in a similar way to human eyes, by combining red, green, and blue in various intensities to create the perception of other colours. In digital image manipulation software like Adobe Photoshop or Gimp, artists define and create colours using 'colour values' for red, green, and blue. These colour values denote the intensity or amount of red, green, or blue in a single colour, and often range from 1 to 255 (i.e. the range a single 8-bit byte can provide). In digital photography, this colour value directly corresponds to the reflectance, transmission, or absorption of red, green, or blue light by the subject.

Isolating these colour channels in Photoshop results in a greyscale image like those produced using digital filters in the previous chapter. Photoshop will render any

image copied into any of these three channels as if it were the data for that colour channel. Switching the images represented by red, green, or blue to other light spectra provides measurements for those wavelengths. One common application of this is false colour imaging, which switches the colour channels of an image such that no colour in the image represents that same colour in reality (Chapter 2.1.1). False colour images work predominantly with both visible and non-visible spectra, such that infrared light appears red in the final image, red elements appear green, and green elements appear blue (Figure 5.2, Appendix E).
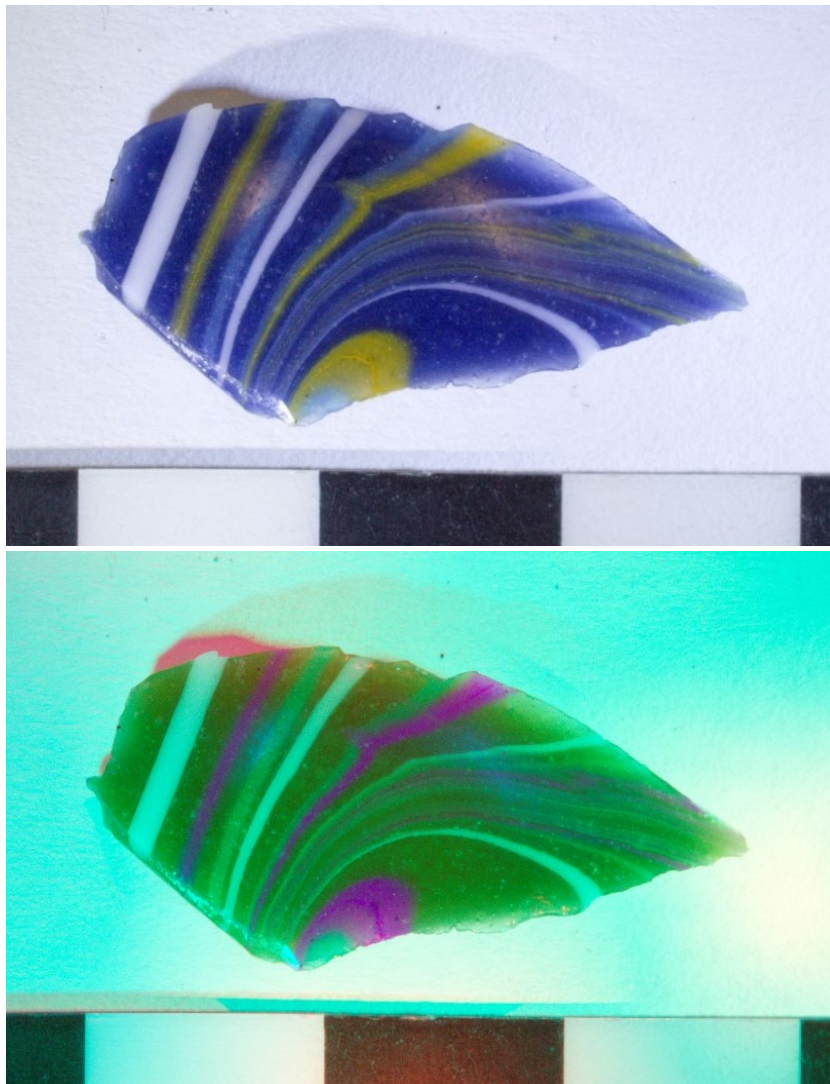
Figure 5.2: Example of a visible-range photograph showing an Egyptian glass vessel sherd (Amarna? BM 5615-29775 Z) (top) and a false colour image in which reds represent infrared light, greens represent blue light, and blue represents red light (bottom) (Appendix E).

False colour images need not be limited to the infrared and visible ranges. Copying the ultraviolet image into the blue channel, the entire visible spectrum image of an object into the green channel, and the infrared image into the red channel creates a false colour image in which blue represents ultraviolet reactions (300 – 400nm), green represents the visible spectrum (400 – 700nm), and red represents infrared reactions (950 – 1000nm) (Figure 5.3, Appendix E). Any colour that is a mixture of the primary RGB colours (e.g. yellow, magenta, purple) indicates reflection from two or more of the spectra represented by the channels. In the figure below, yellow elements indicate the reflection of both infrared (represented by red) and visible light (represented by green), while magenta elements indicate reflection of both infrared (represented by red) and ultraviolet light (represented by blue).

Figure 5.3: A false colour image in which reds represent infrared, greens represent visible, and blues represent ultraviolet light (BM 5615-29775 Z) (Appendix E).

These false colour images provide quantitative data for each spectral range it incorporates by recording the colour values of the pixels representing the object (Figure

5.4). In this case, the red value corresponds to infrared absorbance or reflection, the green value corresponds to the visible range, and the blue value corresponds to ultraviolet reactions. Recording and comparing these readings therefore allow for the quantitative analysis of chemical differences between objects.
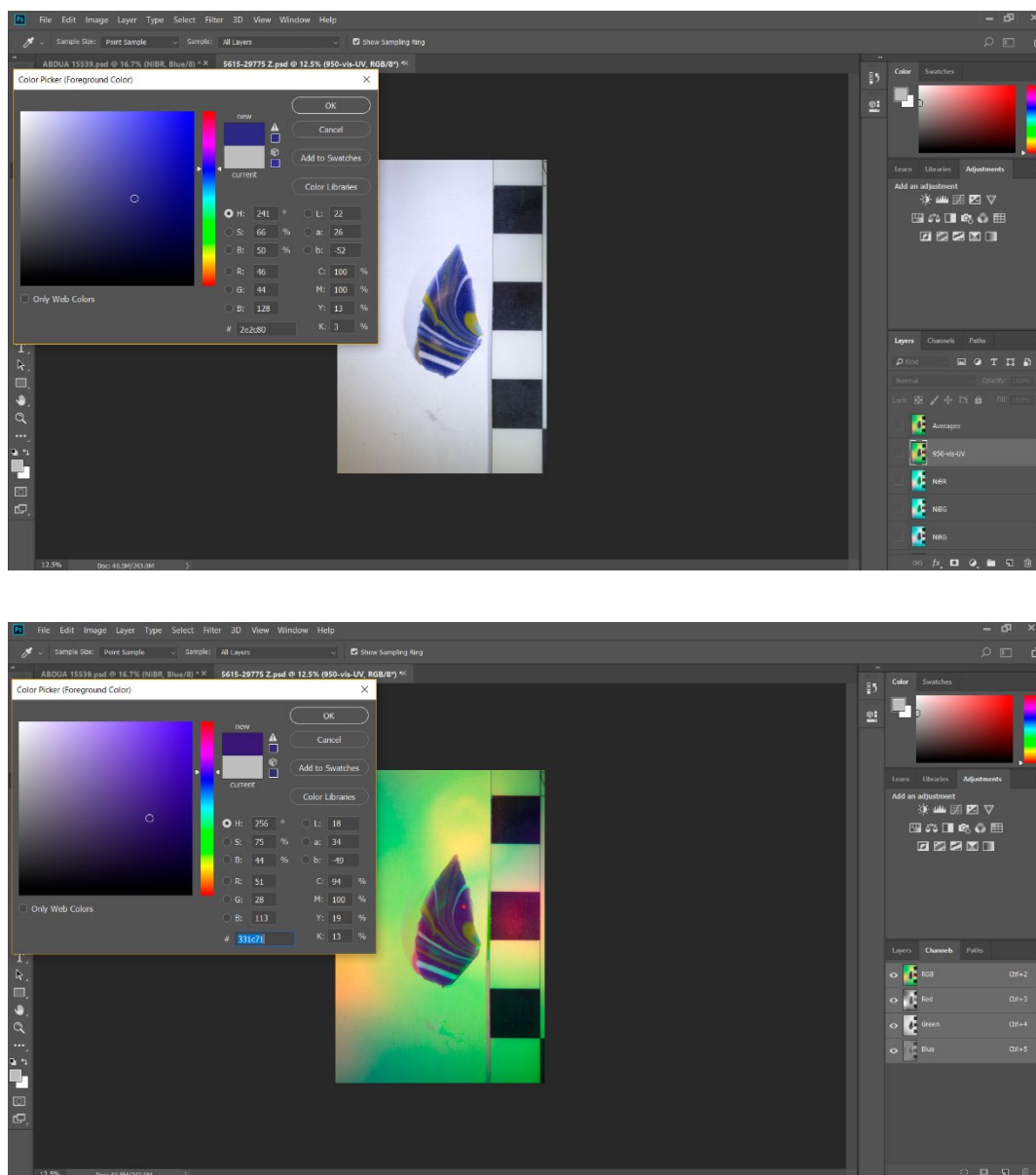
Figure 5.4: Using the eyedropper tool to acquire spectral data from a visible-range photograph (top) and a false-colour image (bottom).

However, these measurements depend greatly on the exposure of the image copied into each channel. Differences in image exposure will produce different measurements for

the same object, for example, negating the comparability of the data. To ensure comparable results from each false-colour image, the original images must be exposed as similarly as possible to all other images for all other samples in the study. The specific standard for exposure is relatively arbitrary, since the data indicates relational similarities and differences between objects; the relationships will remain identical whether exposure is set at -1.0, +0.0, or +1.0, so long as all objects follow the same standard. Additionally, the intensity of the light source affects the quality and rigour of this data more than standard exposure. In other words, images of the same object exposed similarly but using different intensities of light will result in different measurements. It is more important, then, to use the same light sources for each image and adjust the exposure in post-processing to acquire the same intensity readings from something common to all images. Photographs of glass objects in this thesis all contain a sheet of white computer paper as a background, which was used to standardise white balancing and exposure across all images.
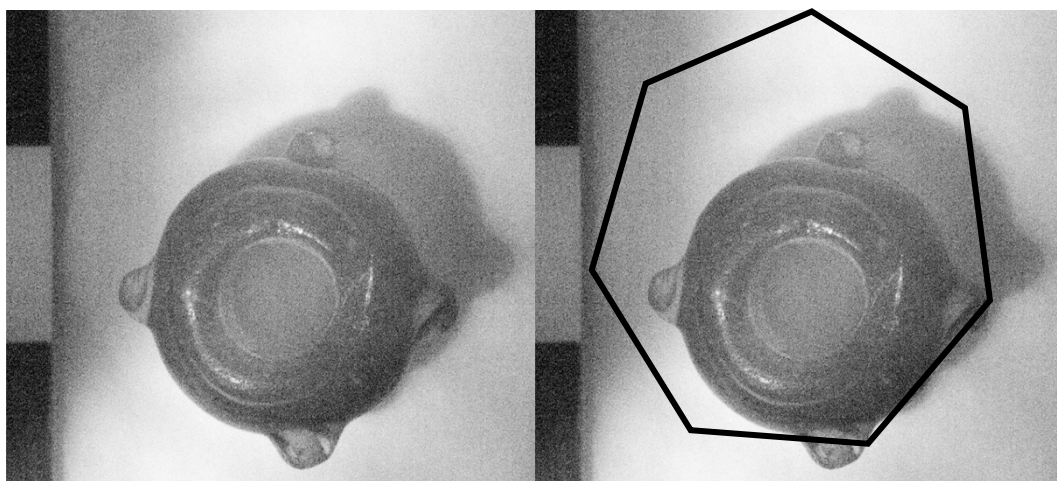
Figure 5.5: Example of a hotspot in infrared imaging (Ugadale Point, KHM Captm 0221.01). The images are the same, with the hotspot outlined on the right (Appendix E).

One final factor to consider in standardising object exposure is the tendency for hotspots to occur in infrared images. Hot spots are regions of an image, often in the shape

of the aperture, that register more light or register the light more intensely than the rest of the image (Melentijevic 2018). They manifest when a variety of lens and light intensity factors cause severe reflection of light, which concentrates near the centre of the image sensor (Melentijevic 2018). This results in an image with an area that appears over-exposed (Figure 5.5, Appendix E). It generally occurs in infrared images, and the difference between intensity values within and outside this area differ significantly. To combat this, images can be taken at such a magnification as to locate the object of interest entirely within the hotspot zone. It will therefore affect all infrared measurements equally and still results in consistent relational data between objects. In the event of capturing an image before recognising the presence of hotspots, such as the one above, one can either acquire new images or limit measurements to only that area of the object situated within the hotspot range.

Once reactions to specific light spectra are captured, they must be compiled and analysed. I investigated several techniques for doing so, the first of which involved collecting and averaging together 30 readings for ultraviolet and infrared reactions from a sample of individual pixels on the object. The sample was chosen to cover as much of the surface as possible while avoiding areas of corrosion and overexposure. Corroded glass reacts differently to light due to differing chemically from the glass itself, and differences in the type or manner of corrosion produce different reactions to light. Ultimately, data acquired for corroded areas likely gave more data for the corroding agent than the original glass. Similarly, over-exposed regions lack data, and therefore cannot provide accurate measurements for the object. Thus, both areas of corrosion and areas of overexposure should be omitted from studies investigating the chemical relationships of an object.

However, this method only collects data from 30 pixels. As described in Chapter 4, geologists use no fewer than 200 points when counting minerals in rock samples, and

one could argue that 30 pixels is too few to acquire an average reading. Point choice was also subjective, further questioning whether the sample is truly representative of the object. A single pixel is not a standard measurement that can be controlled between objects, either; the space it covers on an object will depend on the size of the object in the camera's frame. Additionally, this technique would require 19,200 readings to cover the 640 samples in this study, which is a large amount of work for only 640 data points.

Given these issues, I decided to collect samples from 30 fixed 0.25mm squares for which the data had been averaged using Photoshop's Blur: Average filter, which averages the readings in a selection together (Figure 5.6). This technique collected data for roughly $2mm^2$ per object, measured using the scale included in the frame of each image. While this standardised the area of each object averaged for a reading, $2mm^2$ as a fixed area still constitutes different percentages of differently-sized objects. Readings for a smaller bead therefore cover a higher percentage of the object than readings for a larger bead. Thus, while it appears to standardise the area of measurement, it does not account for objects of different sizes. This technique therefore differed little from that collecting readings from individual pixels.
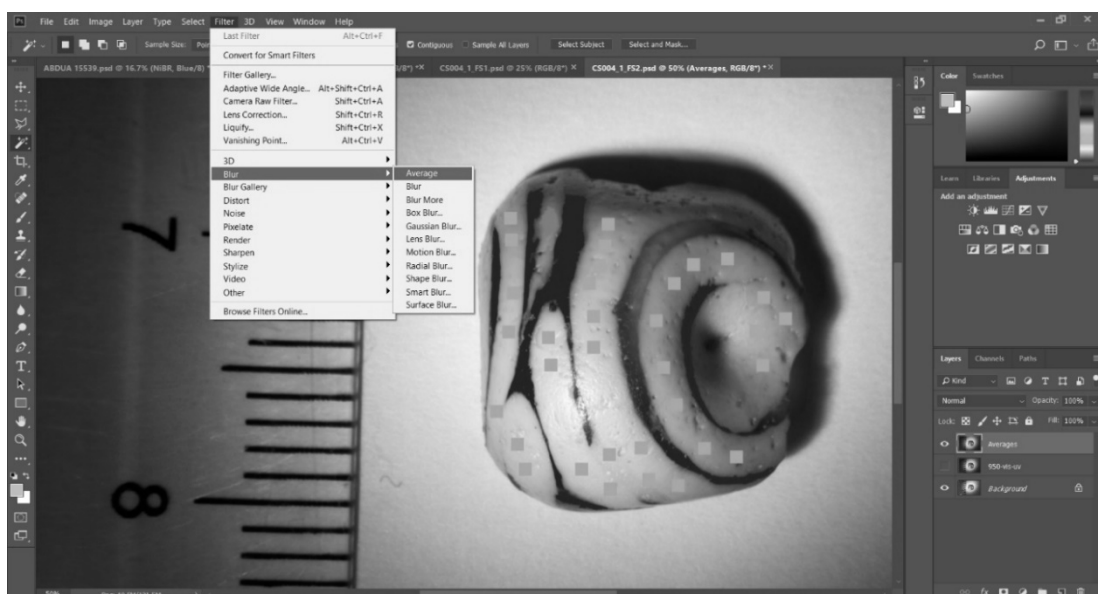
Figure 5.6: Example of data collection through averaging 30 0.25mm squares per sample.
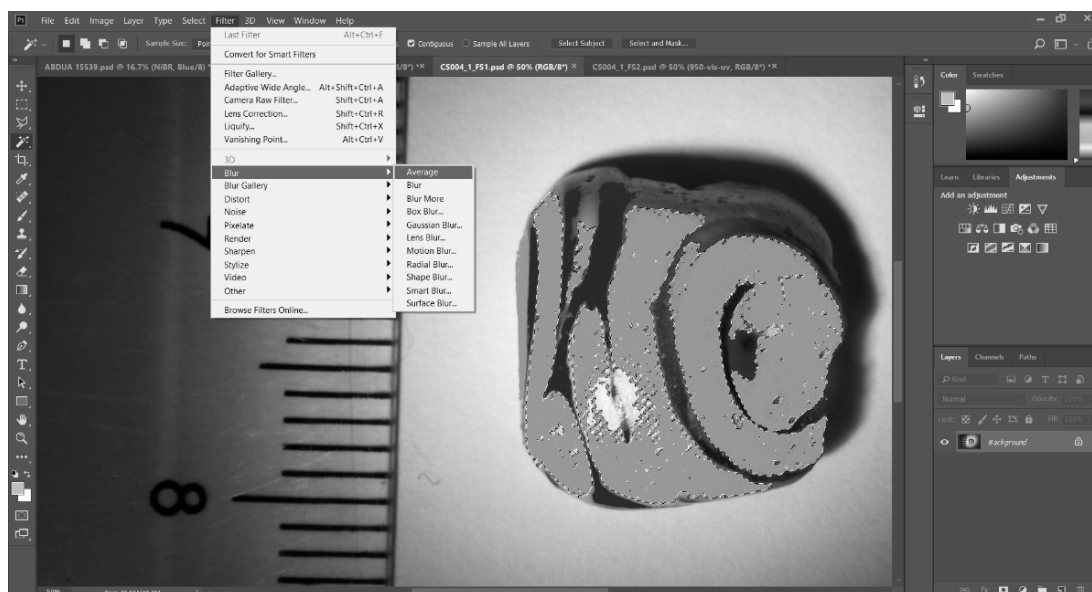
Figure 5.7: Final spectral measurement technique, selecting and averaging the entire surface of a sample except for areas of corrosion and over-exposure (Culbin Sands, NMS X.BIB 10) (Appendix E).

Instead, the data in this case study derives from selecting as much of the object or area of interest as possible and averaging the colour for the area to produce a single reading for infrared (red), visible (green), and ultraviolet (blue) light for the entire sample (Figure 5.7, Appendix E). While this still resulted in different percentages of each sample being represented in the data due to differences in corrosion or exposure, each measurement captures as much of the object's available data as possible. For polychrome objects, I limited each average reading to specific colours in specific areas of the object. For example, separate readings exist for the cobalt-blue glass used in the core of the object and the cobalt-blue used in a reticella line across the bead. This final technique seemed the most standardised and controlled that a study of this nature could achieve.

5.4　MATERIALS

For this study, I photographed 370 objects in the near-ultraviolet (300 – 400nm), visible (400 – 700nm), and near-infrared (950 – 1000nm) ranges. Of these objects, 25 come from the Marischal Museum in Aberdeen, three are at the University of Glasgow,

seven at Kilmartin House Museum, six at the Iona Abbey Museum, and 180 at the National Museum of Scotland. I imaged a further 14 pieces currently housed at the University College London Department of Archaeology and 135 objects from the Anglo-Saxon, Roman, and Reference collections at the British Museum for comparison. When accounting for polychrome objects, this provides multispectral data for 461 samples of glass (Table 5.1).

Origin	Objects	Samples
Anglo-Saxon	10	10
Egyptian (New Kingdom)	43	95
English (Late Medieval)	10	10
Roman	30	36
Scottish	221	254
Modern	56	56
Total	370	461

Table 5.1: Total number of objects and samples from each region imaged for this study.

I collected the 254 Scottish samples from 221 objects housed at museums across the nation. Yellow Scottish glass yields higher infrared readings than ultraviolet and tends to cluster towards the right side of the chart (Figure 5.8). Copper-blue glass tend to yield higher ultraviolet than infrared readings, while both white and cobalt-blue glasses vary widely. Unfortunately, there are insufficient samples of other colours in Scottish glass to allow for comparison between colours.
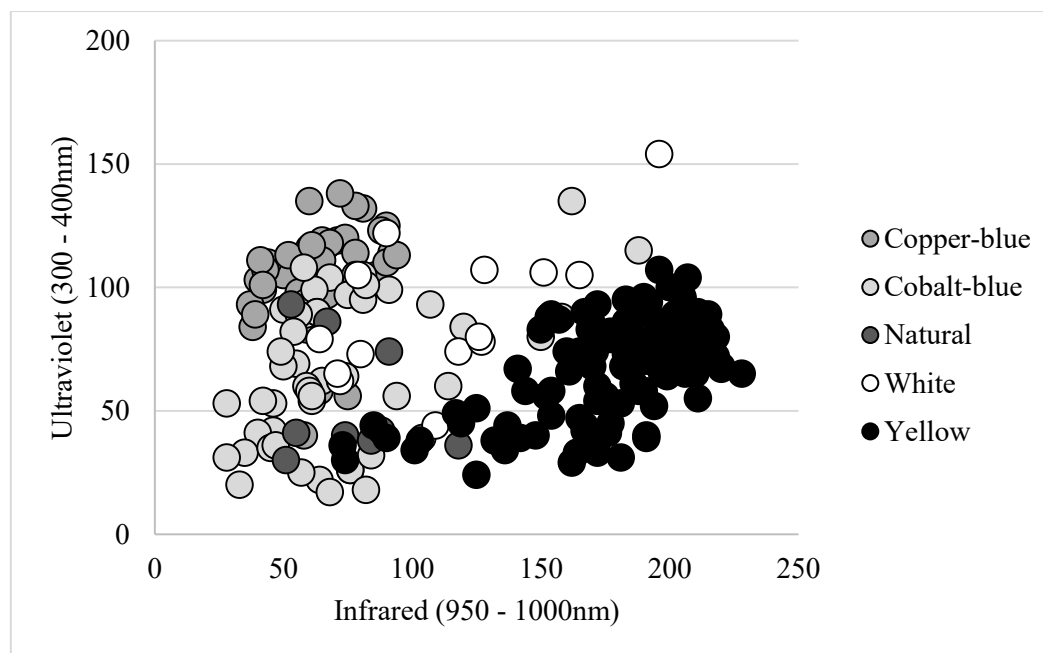
Figure 5.8: Scatter plot of near-infrared and near-ultraviolet spectral data of Scottish glass beads, grouped by colour.

Roman samples came from three mosaic glass vessel sherds and 27 glass tesserae (Figure 5.9). While there are many samples of Roman glass, there are relatively few of each colour, making comparison to samples from other regions difficult. Another possible caveat is the tendency for Roman tesserae to show evidence of recycling. However, much of the glass in circulation in Europe during the Iron Age and Early Medieval periods was recycled, particularly that in regions with no evidence for glass manufacture (Chapter 4.1.1).
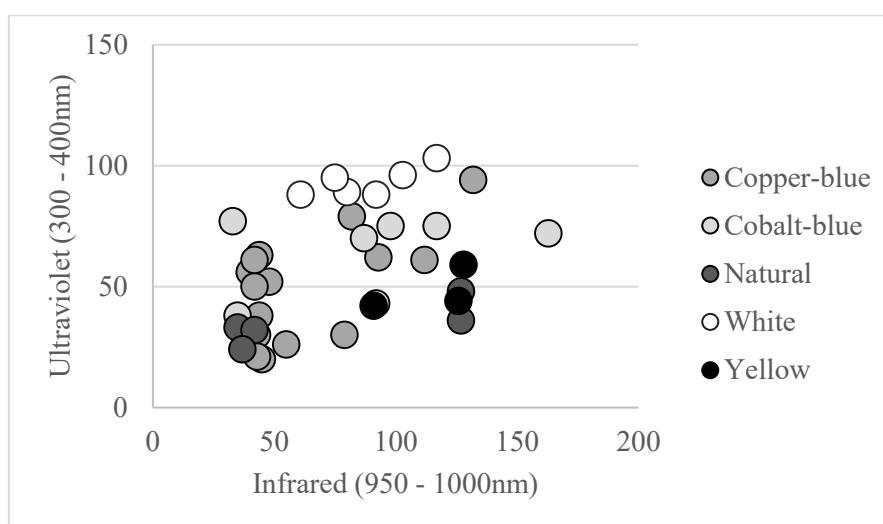
Figure 5.9: Spectral data for Roman tesserae and vessel glass.

Anglo-Saxon objects form the smallest sample group, with results from 10 monochrome glass vessel sherds across 8 sites. Most objects were naturally-coloured and many were claw beakers. All Anglo-Saxon glass gave very low readings for both infrared and ultraviolet light, which appears to be common for many naturally-coloured glasses (Figure 5.10).
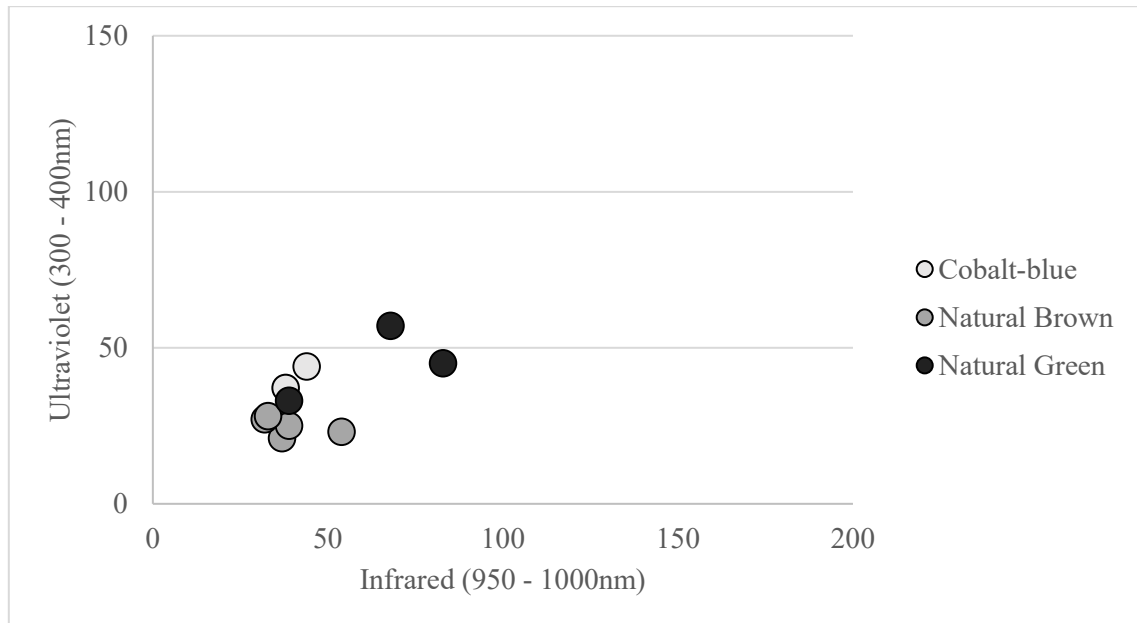
Figure 5.10: Spectral data for Anglo-Saxon vessel glass.
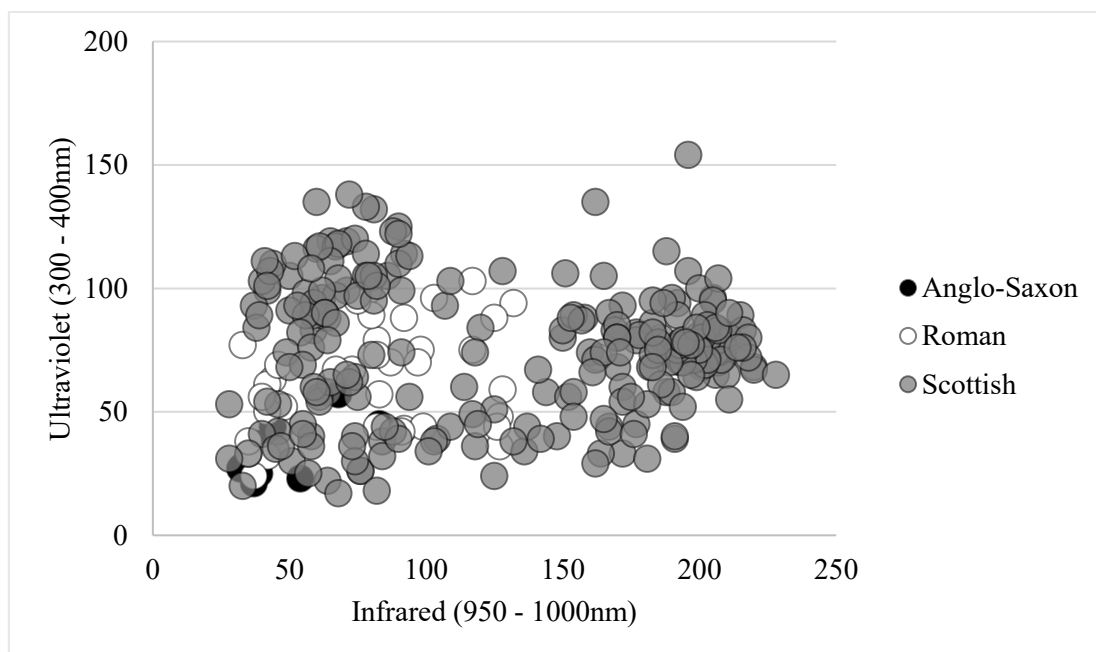
Figure 5.11: Spectral data for Scottish, Roman and Anglo-Saxon glass.

Compared to the Scottish material, the Roman and Anglo-Saxon glass clusters towards the middle of the chart. Some of the Scottish material overlaps with the glass from these regions, but much of the Scottish glass does not (Figure 5.11). This suggests that certain glass objects in Iron Age and Early Medieval Scotland were made using different recipes of glass, were made using recycled glass or are from a different chronological period than previously assumed.

Egyptian samples for chronological comparison came from 43 glass vessel sherds, most of which were polychrome (Figure 5.12). These sherds date to 18th Dynasty New Kingdom Egypt (1550 – 1292 BC). While this predates the Scottish Iron Age and Early Medieval periods by at least 500 years, it still provides a valuable comparative assemblage both in verifying the effectiveness of this technique and in examining the possibility of recycled Egyptian glass appearing in the Scottish Iron Age or later periods. The primary colours represented were cobalt-blue, yellow, and white, with some examples of black and copper-blue. These samples could be compared relatively easily to the Scottish material, given the many samples of each colour.
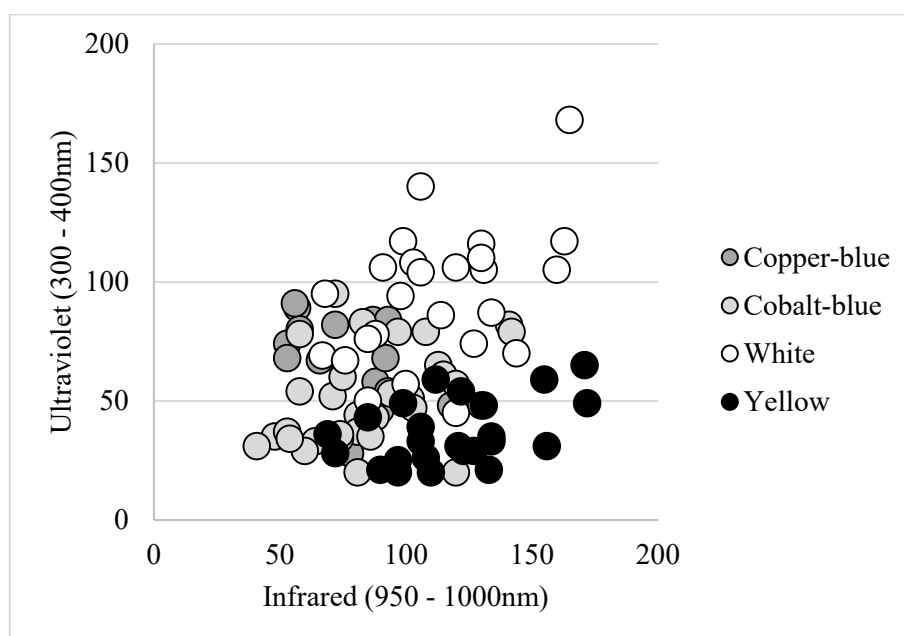
Figure 5.12: Spectral data for Egyptian vessel glass.

I also compared the Scottish samples to medieval potash window glass from Wells Cathedral in Somerset and 56 modern Venetian tesserae to determine whether it was possible to see a difference between the soda and potash glasses discussed earlier in this chapter. Interestingly, there is a visible difference in spectral data between modern tesserae and the stained window glass from Wells Cathedral (Figure 5.13), indicating that the difference in glass recipe is at least visible between medieval and modern samples.
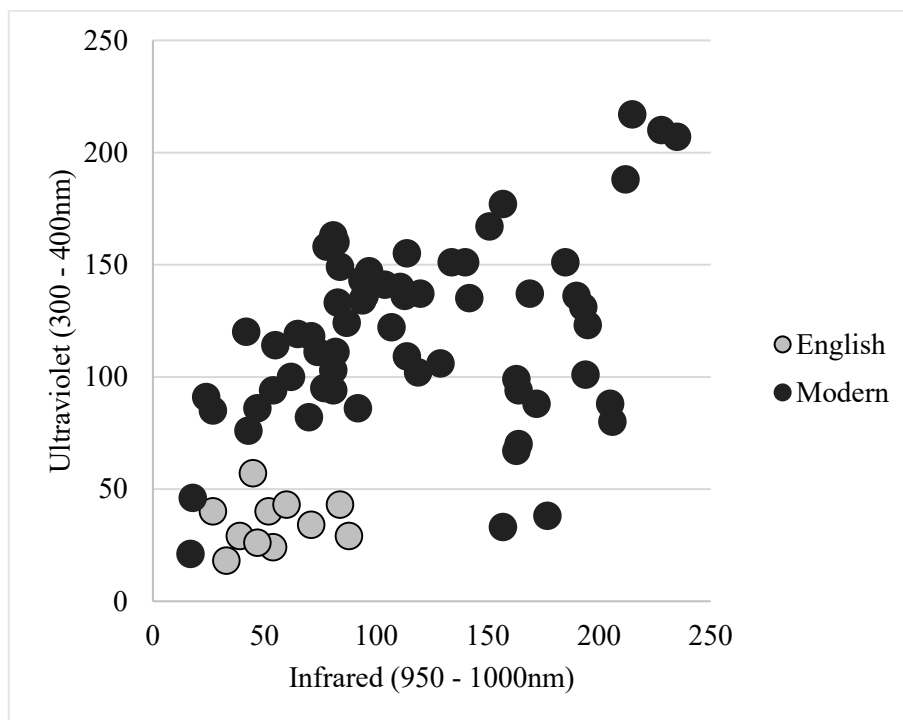
Figure 5.13: Spectral data comparing medieval English window glass to modern tesserae.

5.5   METHODS

To ensure accurate comparisons between spectral images, all objects were photographed using the same equipment and procedure (Chapter 5.3). This also help when combining the photographs to create a false colour image, because changes in the angle or focus between images require alterations in post-processing to ensure the images line up properly. Images were captured using a converted dSLR (Chapter 3.2.1). Objects were placed on a white sheet of computer paper with a clear plastic ruler within the frame

for scale. Smaller objects sometimes required the use of a macro lens, which did not affect the data. The camera was secured to a tripod and a remote shutter used to capture images of each object from as close to the same angle as possible (Figure 5.14). For a full list of equipment used in this thesis, see Appendix B.

Figure 5.14: Camera set-up for visible and non-visible spectral photography.

Each object was photographed using five combinations of filters and lighting (Table 5.2). Zoom was set automatically, then switched to manual for image capture and switched back to automatic before changing filters to ensure identical focus between

images. The camera inevitably moves when changing filters, but maintaining as much similarity as possible between photographs of the same object reduces the amount of correction required in compiling the false colour images.

Image	Filter(s)	Wavelengths	Lighting
Ultraviolet Reflectance	Schott S8612 Hoya 360	300 – 400nm	LE UV torch
Ultraviolet Fluorescence	Schott S8612 Hoya HMC UV cut	400 – 700nm	LE UV torch
Visible Reflectance	Schott S8612 Hoya HMC UV cut	400 – 700nm	LED torch
Infrared Fluorescence	Neewer 950nm Infrared	950 – 1000nm	LED torch
Infrared Reflectance	Neewer 950nm Infrared	950 – 1000nm	Maglite Solitaire Xenon torch

Table 5.2: Filter and lighting combinations for each photograph taken per object.

All locations used to photograph objects in this study had standard fluorescent lighting, which was not captured in infrared or ultraviolet images when tested on-site. Some locations had windows that cast sunlight onto the workspace and therefore altered the intensity of light on the object, particularly ultraviolet and infrared. To combat this difference in lighting, objects were photographed in a portable light studio to block the light from the window (Figure 5.15). All objects therefore have as similar lighting as possible to each other despite being photographed in widely different locations. To ensure even lighting across the object despite using a single light source, I took multiple photographs with light from various angles for each combination of filters and lighting. I captured images in raw format to allow for greater processing capabilities.

Figure 5.15: Camera set-up in locations with ambient infrared and ultraviolet light.

Photographs were imported into Adobe Bridge to adjust exposure and white balance to the white sheet of computer paper used as a background, then saved as .tiff files and imported into Adobe Photoshop. Here, photographs for each wavelength were combined in stacked layers with the blending set to 'Lighten,' (Figure 5.16, Appendix E). This sets all pixels to the lightest reading registered across all layers. Practically speaking, it creates an evenly lit image with no shadows, even when using a single light source to capture the original image. The layers were merged into a single, composite image. These

I exposed manually in Adobe Photoshop so the readings of either red (in infrared images) or blue (in ultraviolet images) for the white sheet of paper used as a background ranged between 235 and 255 all around the object (Figure 5.17, Appendix E). The final composite image was saved in .tiff format for further processing.
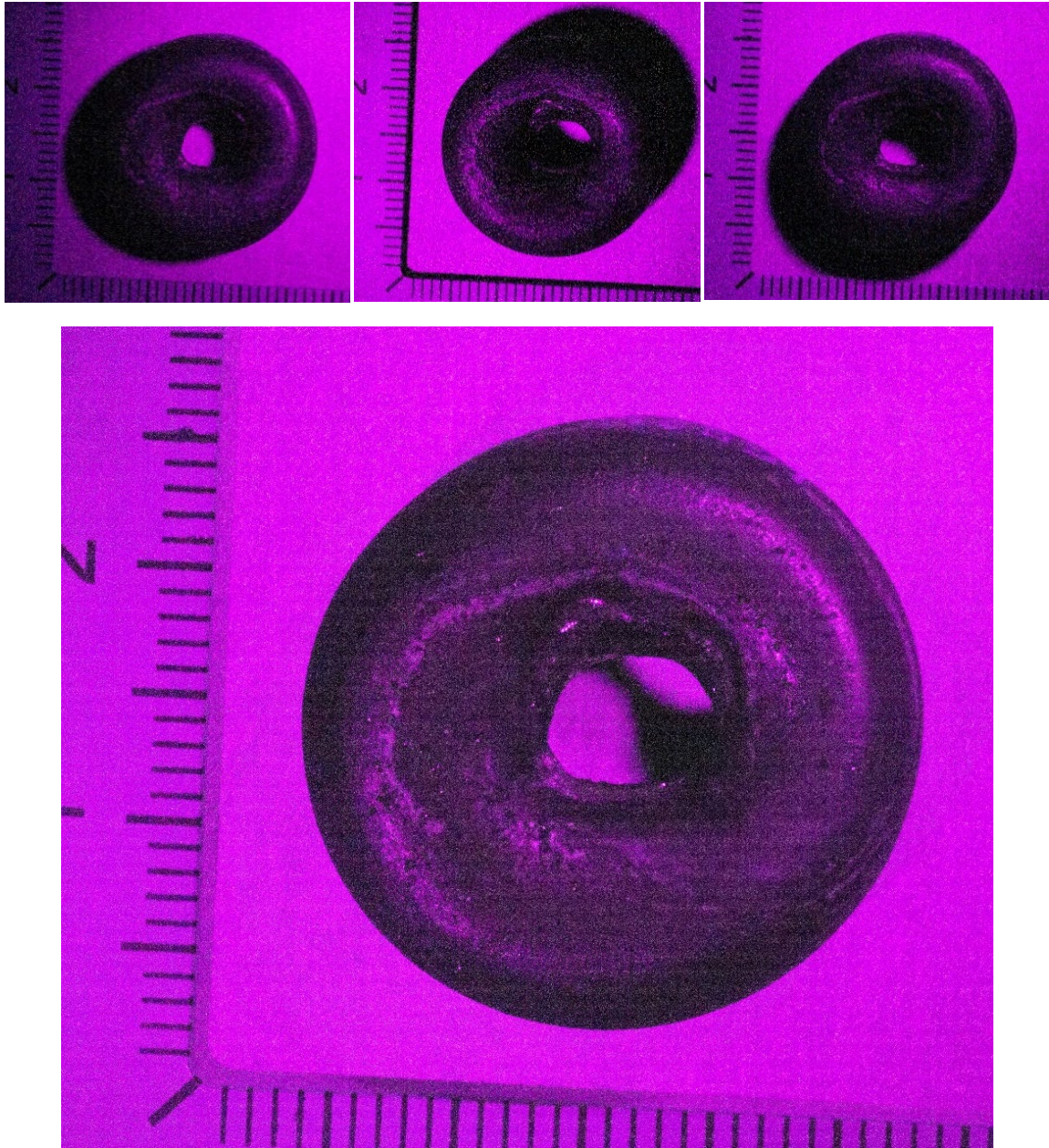
Figure 5.16: Top row: Processed original ultraviolet images of a polychrome Guido Class 14 bead from Banff (MM ABDUA 15526; Guido 1978, 87) with light from varying angles; Bottom: Final processed image combining the originals into a single, composite image (Appendix E).
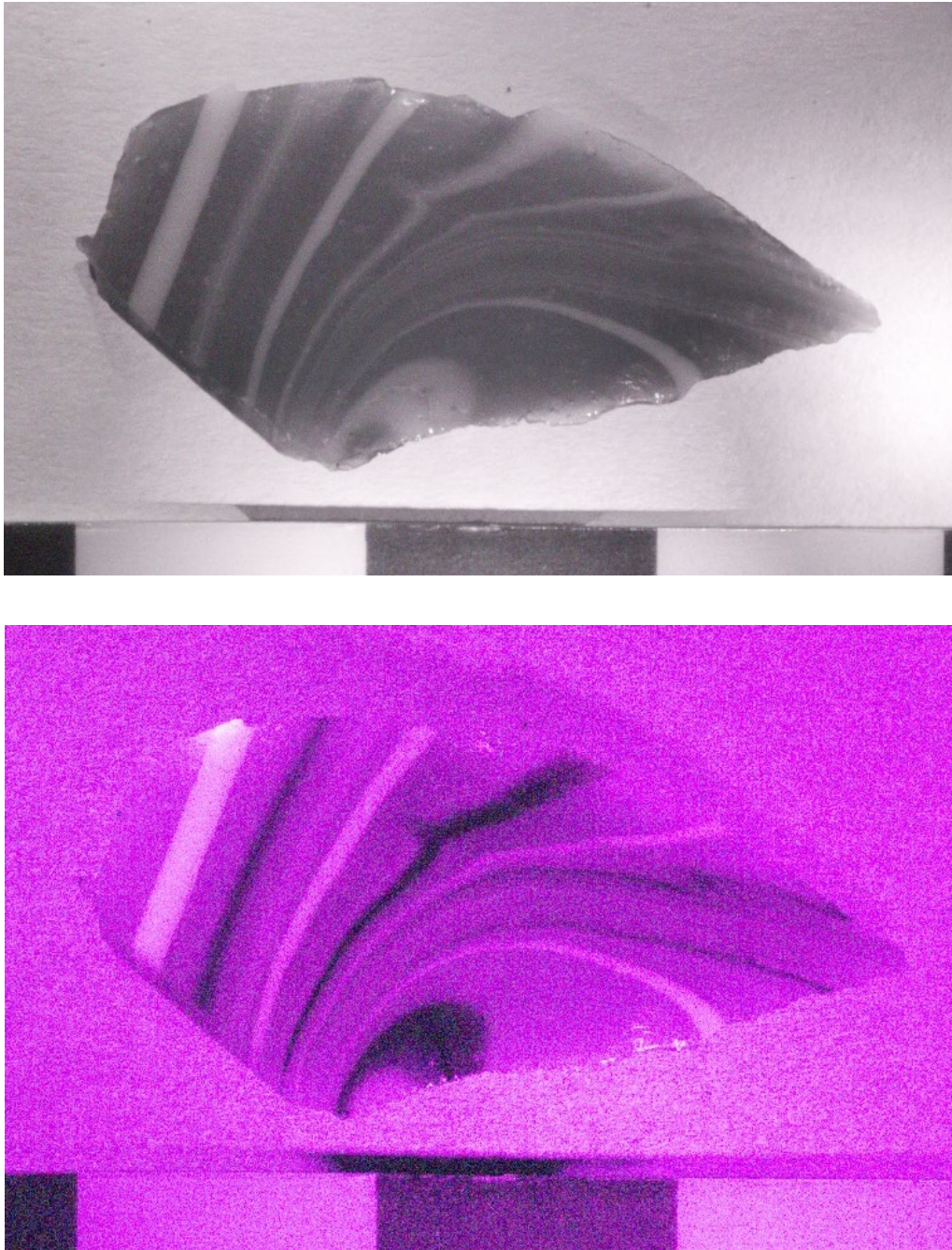
Figure 5.17: Example of an infrared (top) and ultraviolet (bottom) image with acceptable exposure readings (Amarna?

BM 5615-29775 Z) (Appendix E).

5.5.1 SPECTRAL MEASUREMENT AND ANALYSIS

The composite near-infrared (950 – 1000nm), visible (400 – 700nm) and near-ultraviolet (300 – 400nm) images were copied into Photoshop's red, green, and blue channels to create false colour images. I manually aligned the images to each other to

ensure readings corresponded to the same areas of the object. I then duplicated the image, generated readings for each element of the object as discussed above (Chapter 5.3) and recorded the readings for infrared and ultraviolet light for each sample.

The readings were then compiled into scatterplots (Figure 5.18). These plots omit the data for the visible range, instead opting to compare samples of similar colour to each other rather than print 3D scatter plots in two dimensions. I compared these readings for differences in region, colour, size, manufacture, and bubble concentration within the Scottish collections. I then compared this material to samples from contemporary Roman and Anglo-Saxon objects to determine chemical similarities or differences between each group. All interregional comparisons omit analysis of factors specific to beads, such as method of manufacture, because most comparative glass samples come from vessel sherds rather than beads. Finally, I compared these samples to New Kingdom Egyptian glass vessels, medieval window glass from Wells Cathedral and modern Venetian tesserae to determine whether known chemical differences between glass of differing chronological periods appeared in the data.
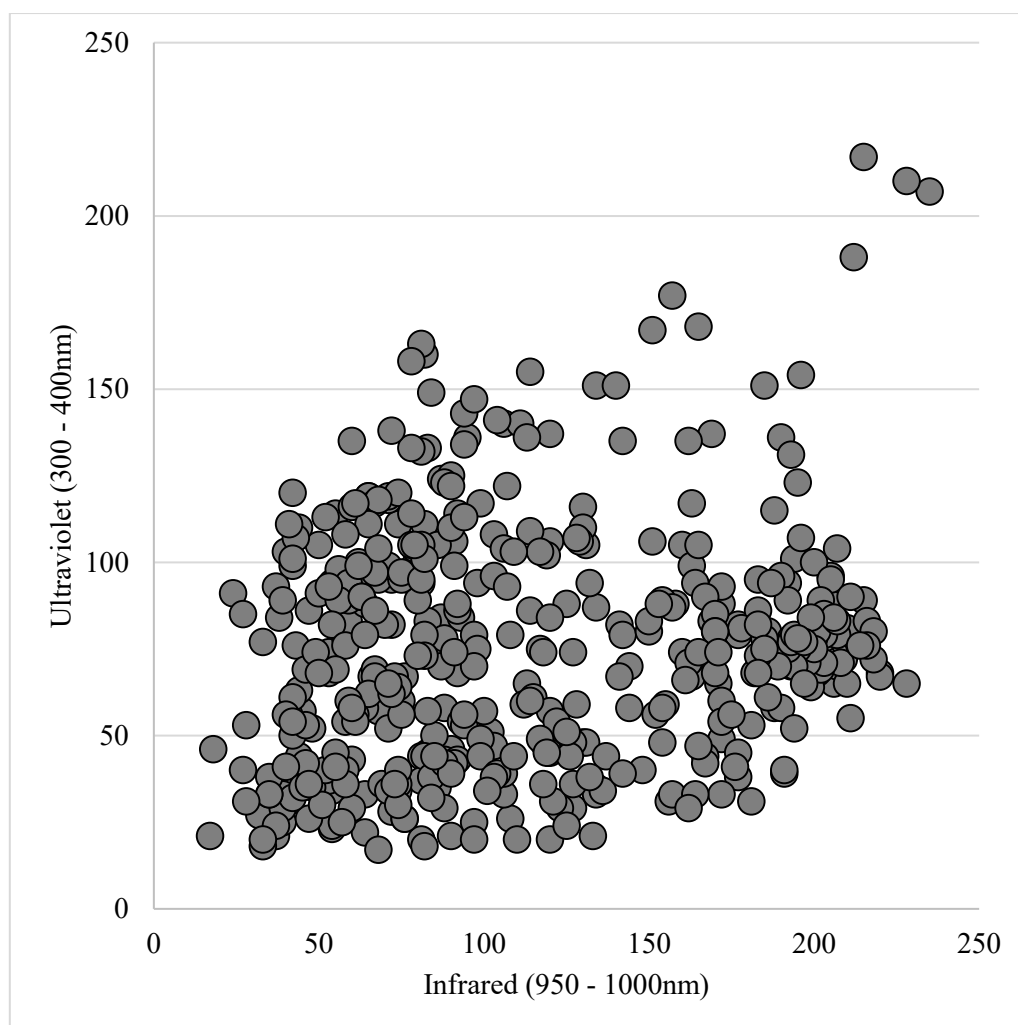
Figure 5.18: Scatterplot of spectral data for all glass samples included in this study.

5.5.2   CAVEATS TO THE DATA

There are several possible caveats with the data presented in this study, which should be kept in mind while considering the possible conclusions we can draw from it. First, while this method can show clear differences in chemistry, it does not show all of them. Different combinations of ingredients may reflect near-ultraviolet and near-infrared light in similar ways. A dSLR cannot capture the entire spectrum of light, after all, and certain objects may only differ in their reactions to light outside of the range a dSLR can capture. Two objects with different chemistry could appear adjacent to each other on a scatter plot despite their chemical difference. This method therefore shows patterns of

chemical differences between objects, but it does not necessarily show all possible differences. Similarly, clustering may not indicate chemical similarity between objects. However, it still provides more information than otherwise currently available using affordable, non-destructive methods.

Additionally, there are limitations as to the number of objects imaged for each region and time period and the degree to which those match objects from other regions and periods. For example, I initially imaged 60 Roman objects, but only 30 contained similar colours to Scottish samples and were therefore eligible for comparison. Comparing spectral data for an opaque red bead to that of a translucent cobalt-blue bead does not work well, because it is difficult to determine the degree to which observed spectral differences are a result of different colourants or other chemical components. Additionally, I could not image similar numbers of the same type of glass from each region. There are 135 samples of opaque yellow glass from Scottish contexts, for example, but only three from Roman contexts. Despite this, the data still provide significant insight into relational chemical data for Scottish glass beads when compared to the other groups discussed above.

Finally, this study also does not distinguish between possible recycled glass and visibly 'pure' glass. Recycling can drastically change the chemistry of an object, particularly if multiple batches of varying origins are melted together to form a new batch of glass (Freestone 2015). Spectral data for these objects would reflect the chemistry of the newly melted batch rather than the original glass and may not match spectral data for any other known glass sample. Accounting for recycling is beyond the scope of this study, but it remains a caveat to the data and the possible conclusions drawn from it.

None of these caveats are particularly problematic, or at least no more so than they might be for any other study of archaeological glass. Recycling is a common caveat

in archaeological glass studies, one which chemical specialists are working to alleviate (Freestone 2015). The lack of samples for certain colours in certain regions largely results from both cultural preference at the time and from the inherent bias of what survives in the archaeological record. Additionally, the purpose of this case study is to demonstrate the value of challenging the current paradigms in archaeological imaging; fully investigating chemical differences in Iron Age and Early Medieval glass through false colour imaging is a possibility for future work, but it is not within the scope of this thesis.

Finally, the inability to detect all chemical differences using a camera is negligible. While it would be ideal for the clusters in these scatter plots to indicate chemical similarity and the separations to indicate difference, it is unsurprising that not all chemical differences manifest as different reactions to light within the 300 – 1000nm spectrum. Still, the information gleaned from this study and described throughout the rest of this chapter is far more information than we might otherwise have about these objects. This technique is not meant to replace current methods testing chemical composition. Rather, it is meant to compliment them, to provide information that allows for a more targeted approach and to provide significant information to projects unable to access or afford more precise techniques. Additionally, this thesis did not focus on creating the best method for chemically testing objects through spectral photography. Further research would likely provide more insight into such a technique and the possible differences we could determine from it.

5.6   RESULTS AND DISCUSSION

Despite the caveats, the results of this study provide significant new information about bead and glass manufacture and trade in Iron Age and Early Medieval Scotland. Much of the Scottish material does not overlap with Roman or Anglo-Saxon material,

which becomes particularly apparent when comparing similar colours. There are also some preliminary chronological conclusions we can draw from the comparison between Iron Age and Early Medieval Scottish material, New Kingdom Egyptian glass vessels, Medieval stained glass and modern tesserae. This section will discuss the results and their significance for bead studies, while the next section will focus on the significance of this study for archaeological photography and spectral imaging.

5.6.1 CORRELATION BETWEEN BUBBLES AND SPECTRAL DATA

Given the possible indication in the last chapter that bubbles may correspond to object chemistry, comparing the spectral data to that for the bubbles within Scottish Iron Age and Early Medieval samples seemed beneficial. Interestingly, there was no significant difference between samples when grouped by the bubble concentration categories discussed in Chapter 4 (Figure 5.19). There were also no significant patterns when examining regional or colour variation for each bubble concentration. This does not mean there are no bubble or spectral differences between objects of the same colour or from the same region; the previous chapter clearly demonstrates such differences. Instead, it suggests that the differences seen through bubble concentrations in the previous chapter are providing different information than the spectral information acquired here. Most likely, the bubble concentrations provide more indication of manufacture techniques while spectral data give more indication of chemical composition.
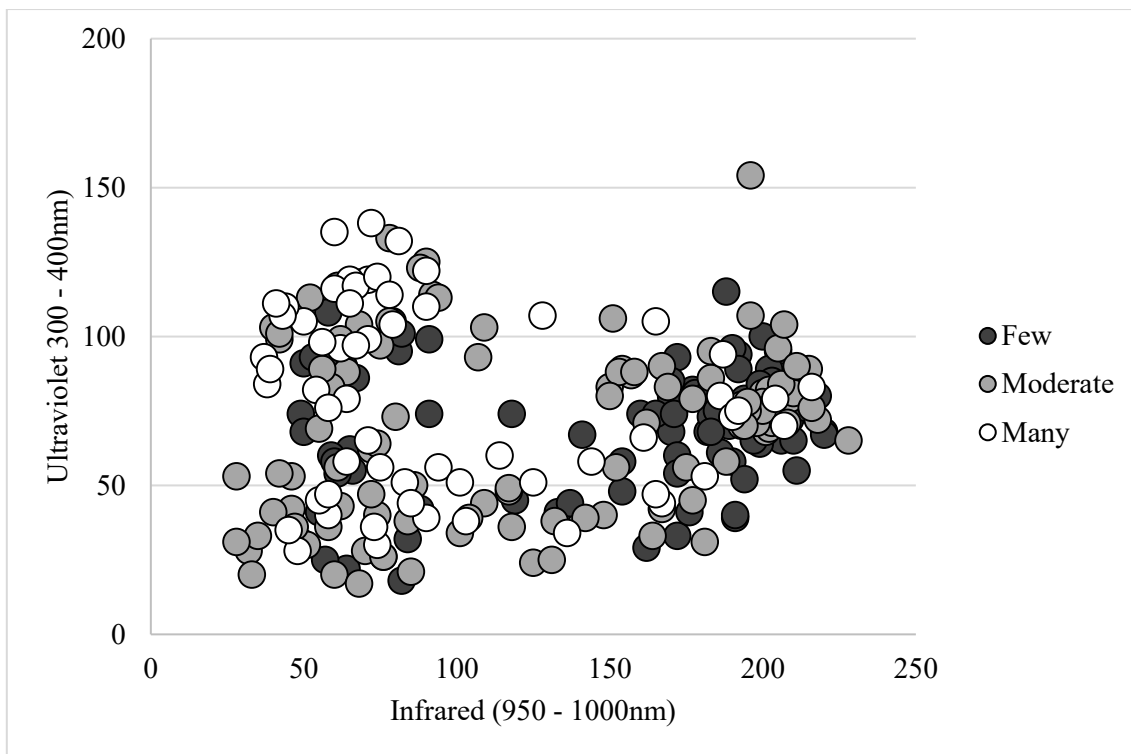
Figure 5.19: Spectral data for Scottish glass separated by bubble concentrations.

5.6.2   DRAWN BEADS IN SCOTTISH CONTEXTS

Separating the samples by the method of manufacture used to create the object shows a clear distinction between wound and drawn beads in Scottish contexts (Figure 5.20). The chart below only includes data for glass serving as the core material of the object, because that is the material affected by these manufacturing techniques. This indicates a chemical difference between wound and drawn beads, but it is unlikely to relate specifically to the method of manufacture.
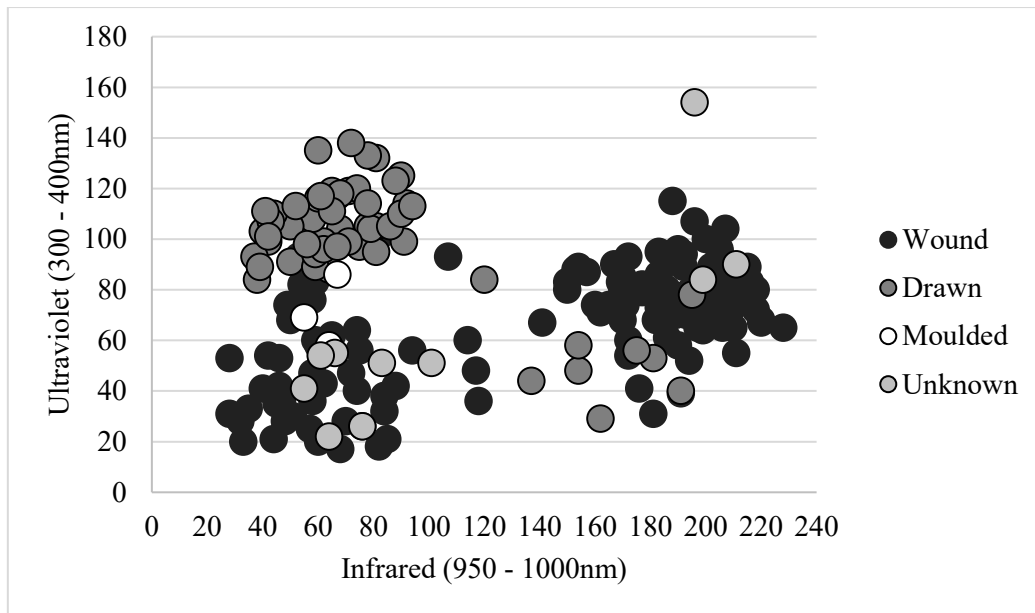
Figure 5.20: Spectral data for Scottish glass beads, separated by method of manufacture.

There are currently 56 drawn glass beads from Scottish contexts included in this study, 48 of which come from the beach at Culbin Sands (Chapter 4.7). Drawn beads were not made in Europe prior to the 14th century, and therefore must either come from the Near East at the closest or date to a later chronological period (Francis 2002, 171). Only three colours of drawn beads appear in Scotland: copper-blue, cobalt-blue, and yellow. All the copper-blue and cobalt-blue drawn beads in this study come from Culbin Sands, while all but one of the drawn yellow beads were found at Glenluce Sands in the southwest. The final drawn yellow bead comes from Traprain Law in the southeast.

The drawn copper-blue beads form a distinct cluster in the data, with infrared values less than 100 and ultraviolet values greater than 80. These blue beads also cluster separately from other objects of similar colour, both from Scotland and from Roman contexts (Figure 5.21). It is therefore unlikely that they are made with Roman glass, given the differences in spectral reactions. Similarly, it is unlikely that the glass used in the drawn copper-blue beads at Culbin Sands was made using a similar recipe to that found in other copper-blue beads in Scotland from this period.
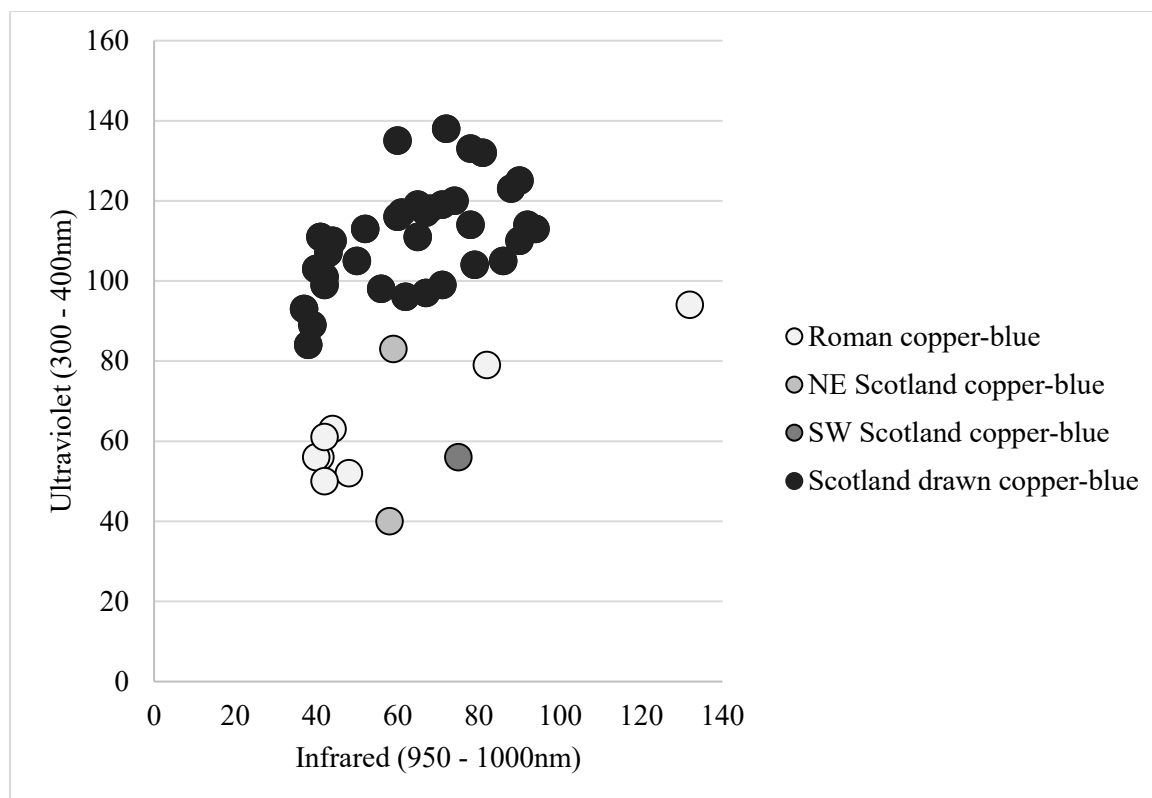
Figure 5.21: Spectral data comparing Scottish and Roman copper-blue glass.

Some of the modern copper-blue samples do overlap with the drawn copper-blue beads from Culbin Sands, however, suggesting these objects may be more modern than originally thought (Figure 5.22). In fact, when we eliminate the copper-blue beads from Culbin Sands, the modern samples do not overlap with any other samples. While overlap in these plots does not inherently signal chemical similarity, these beads do differ significantly from all other copper-blue samples in the study and, significantly, differ from Egyptian and Roman samples. Other beads from Culbin Sands date to later periods (Chapter 4.7), and none of the objects have secure contextual information. There are no other tiny drawn copper-blue beads in Scottish contexts from this period, and no parallels in nearby contemporary European contexts. When we consider both the spectral data provided here and the differences in bubbles discussed earlier (Chapter 4.8), it is likely that the copper-blue drawn beads from Culbin Sands are, in fact, modern beads.
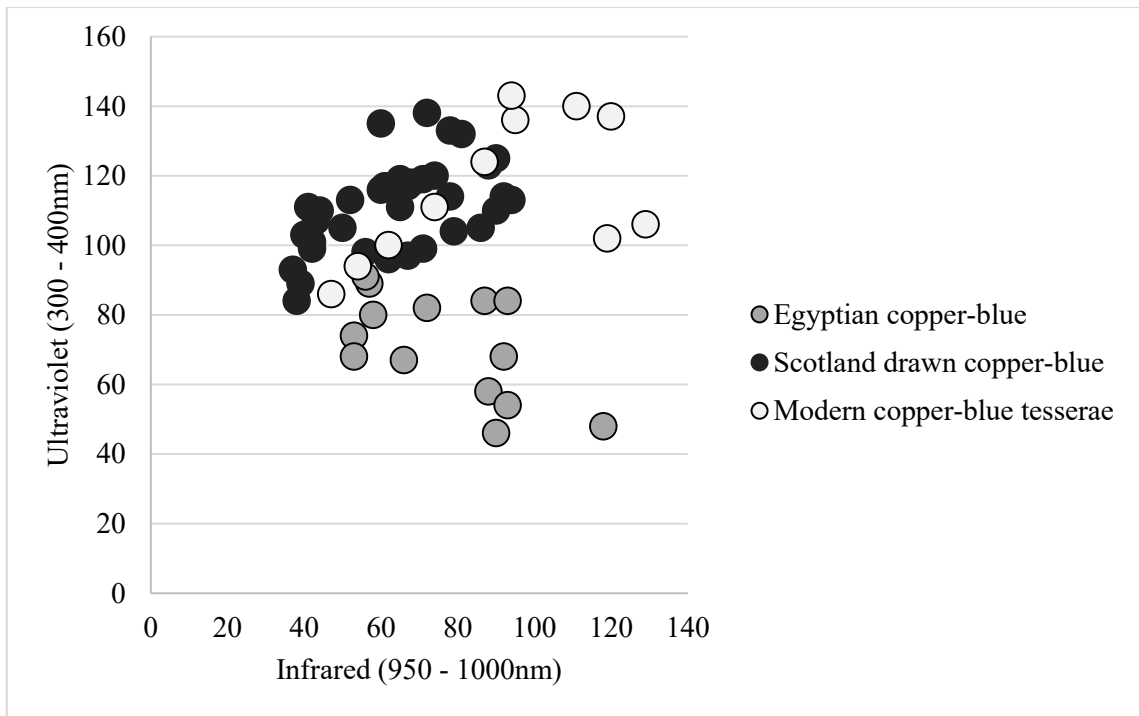
Figure 5.22: Spectral data comparing drawn copper-blue samples from Culbin Sands to New Kingdom Egyptian glass and modern tesserae.
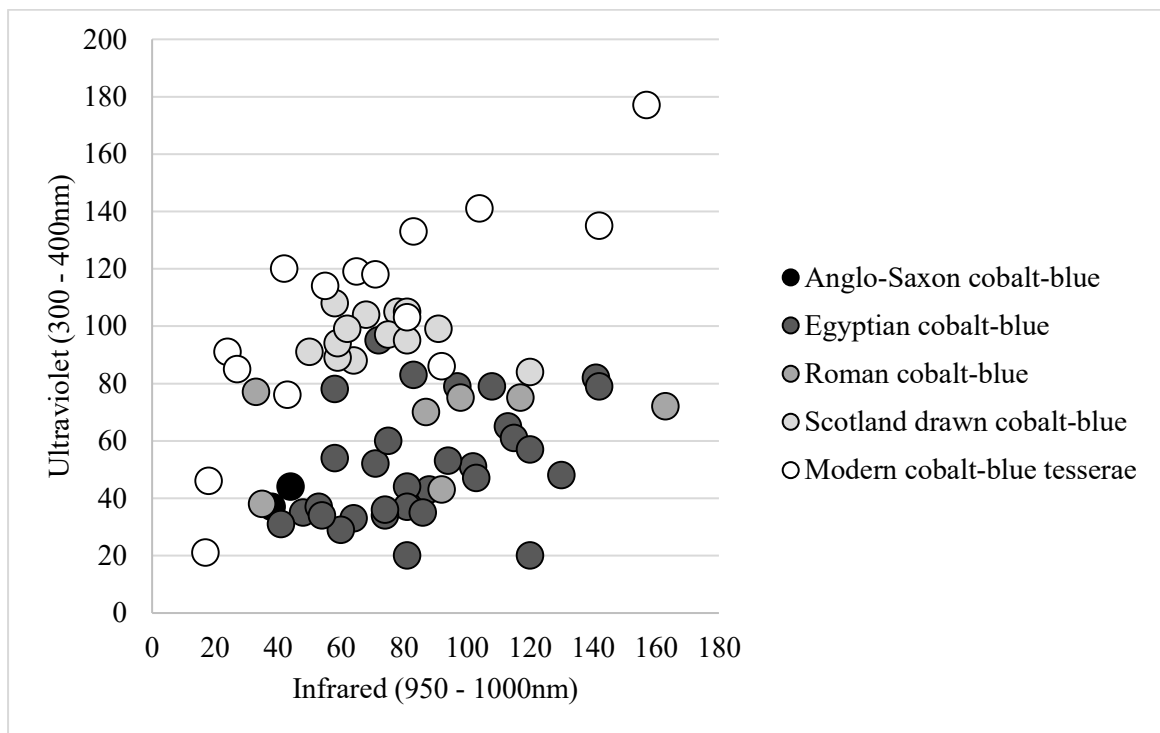
Figure 5.23: Comparison of spectral data for drawn cobalt-blue Scottish samples to Anglo-Saxon, Egyptian, Roman, and modern cobalt-blue glass.

The drawn cobalt-blue beads do not separate themselves from Roman or Egyptian glass as nicely as the copper-blue beads do, but they also do not overlap with them (Figure 5.23). Scottish cobalt-blue samples do not overlap with Anglo-Saxon material either. Interestingly, the drawn cobalt-blue samples again correlate more closely with the modern tesserae. This could indicate that these beads, also largely from Culbin Sands, are likely modern as well. Alternatively, they could be from other regions not included in this study, like Scandinavia or the Near East. While many drawn cobalt-blue beads occur at Norse sites across Scotland, however, these are of a different shape and size to those at Culbin Sands. It therefore appears more likely that these beads postdate the 8th century AD, but more samples are needed given the scattered nature of the spectral results for cobalt-blue glass in this study.
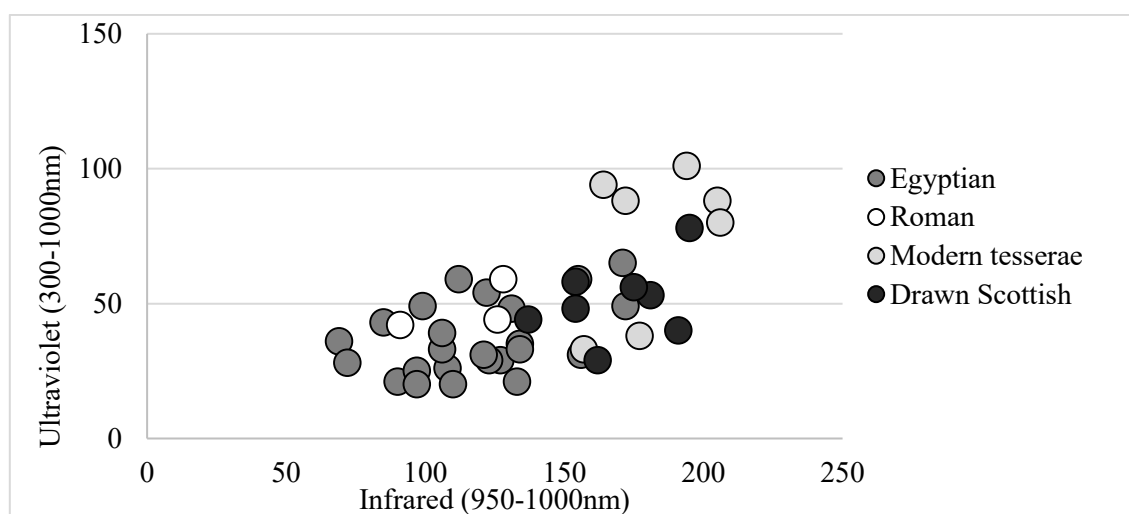
Figure 5.24: Comparison of drawn yellow Scottish samples to Egyptian, Roman, and modern yellow glass.

Perhaps most interesting is the lack of drawn yellow beads in northern Scotland, coupled with the lack of drawn blue beads outside Culbin Sands for the Iron Age and Early Medieval periods. While drawn, these yellow beads do overlap with Egyptian and Roman yellow glass (Figure 5.24). In fact, the one drawn yellow bead from Traprain Law is the only yellow bead from the southeast to overlap with Egyptian and Roman material. Since these are still drawn beads, they cannot be coming from Europe in the Iron Age or

Early Medieval period. Their possible similarity to New Kingdom Egyptian material suggests they could be coming from the Near East.

5.6.3   Opaque Yellow Glass in Scottish Wound Beads

Opaque yellow glass, particularly that from wound beads in Scotland, is generally quite reflective of infrared and moderately reflective of ultraviolet light. There are not enough samples for regional comparison within Scotland, but there is a distinct difference between Scottish, Roman and Egyptian opaque yellows (Figure 5.25 top). There is Scottish material that overlaps with the Roman and Egyptian readings, but most yellow Scottish glass does not. However, most yellow data for Scotland comes from roughly 200 monochrome wound yellow beads from Culbin Sands. Given the overlap between these and modern yellow samples as well as possibility of the copper-blue and cobalt-blue beads coming from post-medieval contexts, this group of beads could have similar problems. In fact, when we eliminate these beads from the data, the separation between Scottish and Roman and Egyptian samples almost disappears (Figure 5.25 bottom).

While these results are compelling, other factors are affecting the data. When the Scottish data is isolated and grouped by samples coming from monochrome objects (for which the glass forms the core of the bead) versus polychrome objects (for which the glass forms a design element of the bead), a distinction between the two becomes clear (Figure 5.26). This suggests that the samples overlapping with Roman and Egyptian material may not indicate similarities between these collections. Instead, they could indicate chemical mixing between yellow glasses and the glass forming the core material of the bead they decorate, usually cobalt-blue, deep green or natural colours. Additionally, all Egyptian samples come from polychrome designs and could indicate similar mixing. Experimental archaeology would allow for further insight into this possibility.
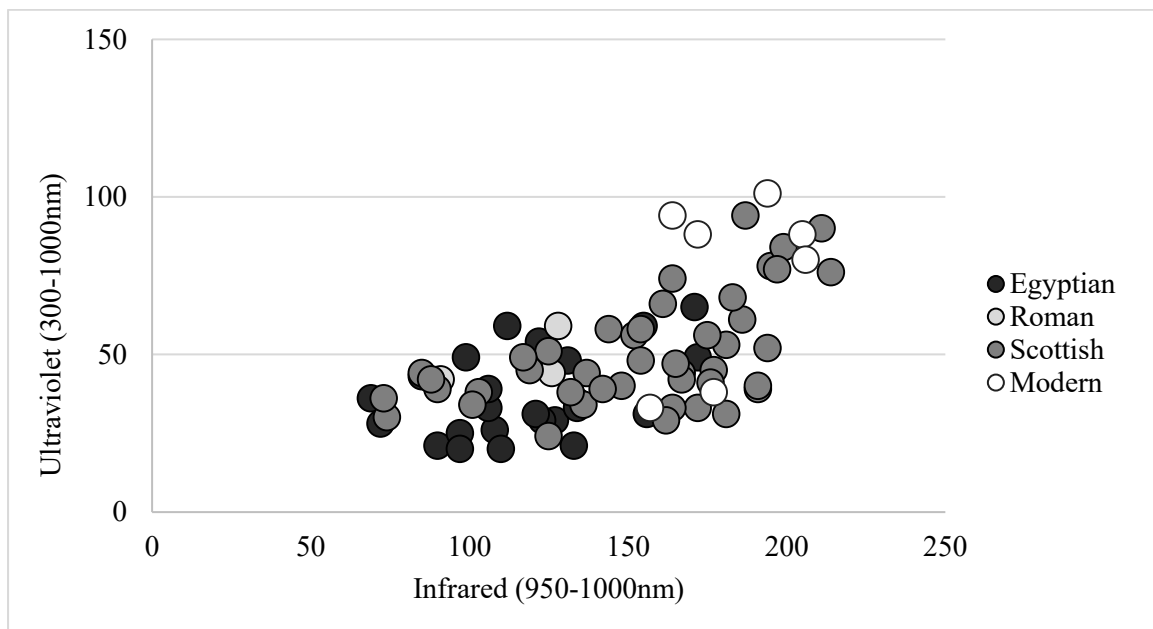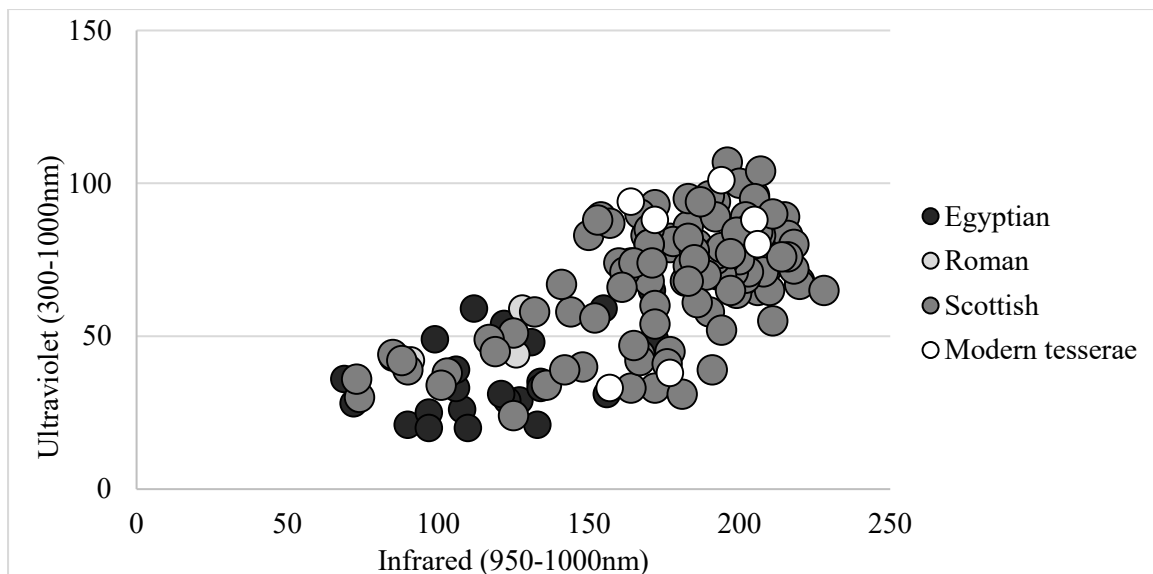
Figure 5.25: Spectral data for Scottish, Roman, Egyptian and modern yellow glass including (top) and excluding

(bottom) strings from Culbin Sands.
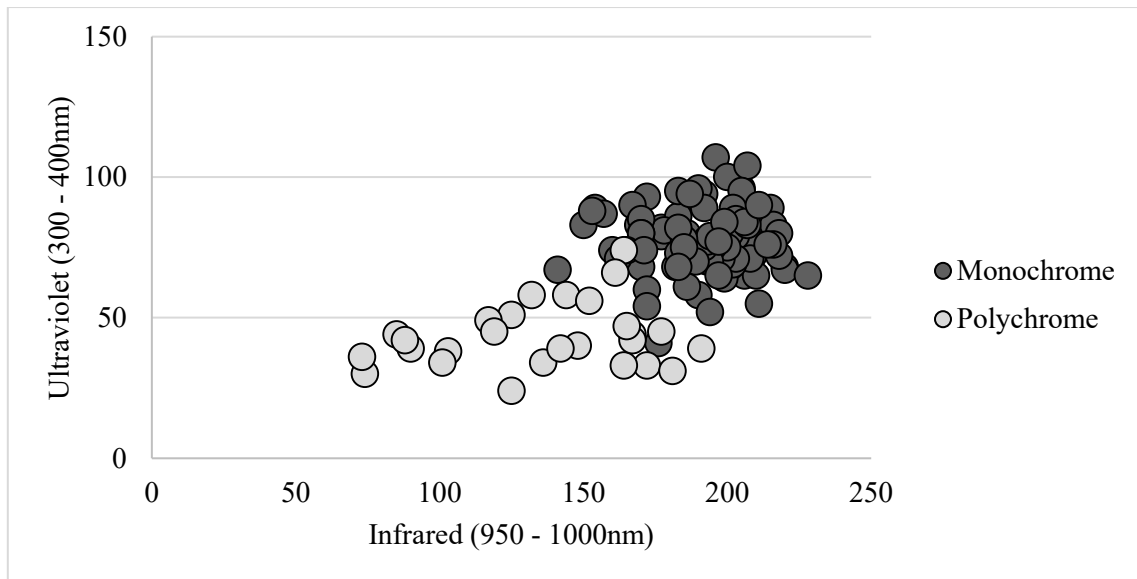
Figure 5.26: Comparison of Scottish monochrome and polychrome yellow glass samples.

Finally, we cannot discuss possible chemical differences in yellow glass without examining differences in colourants. There are two primary colourants used to create opaque yellow glass: lead-antimonate and lead-tin. Importantly, lead-antimonate is the preferred (if not the only) colourant for Roman and Egyptian yellow glass, while the Merovingians used lead-tin (Heck et al. 2003, 43; Molina et al. 2014, 171; Nicholson and Henderson 2000, 208; Sayre and Smith 1973, 6; Shortland 2002, 518; Tite et al. 2008, 67). It is possible, then, that the observed differences result from a difference in colourant between yellow beads.

Some of the samples of yellow glass imaged in this study have been chemically tested, but only three of them are lead-tin yellows while the other 13 are lead-antimonate (Bertini et al. 2011; Bertini 2012; Freestone 2018). When plotting these samples using their infrared and ultraviolet reactions, there is no clear difference between those using lead-antimonate and those using lead-tin (Figure 5.27). It is possible that these objects are using larger percentages of lead in their recipes, particularly because lead is a prominent ingredient in yellow glasses and because similar increases in reflection are observed among cobalt-blue samples with high lead content (Chapter 5.6.4). Given the issue of

polychrome versus monochrome samples and the fact that all chemically tested samples of yellow glass in this thesis are polychrome designs, however, differences between lead-antimonate and lead-tin may be overpowered by intermixing with other glass types in polychrome samples.
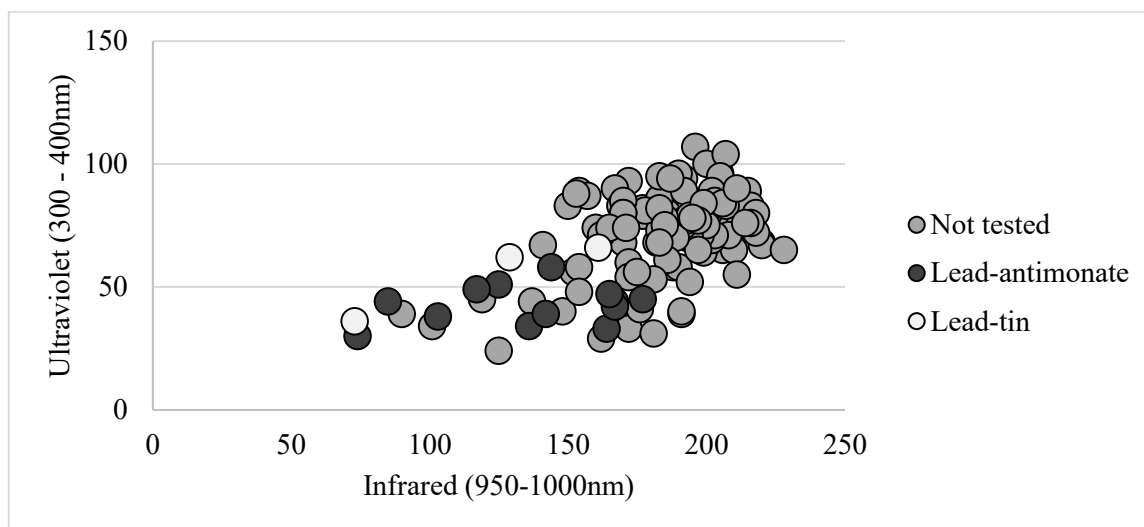
Figure 5.27: Comparison of yellow samples grouped by known colourant.

5.6.4 COBALT-BLUE GLASS IN SCOTTISH WOUND BEADS

The most confusing of the colour categories is the wound cobalt-blue beads. These beads range from 28 to 188 on the infrared scale and 17 to 135 in ultraviolet (Figure 5.28). When separating them by region in Scotland, there is no clear pattern of separation or clustering between these ranges. Comparing the data to Roman, Egyptian, and Anglo-Saxon cobalt-blue glass only adds to the confusion (Figure 5.29). This could be an indication that cobalt-blue glass in Scotland is chemically similar to that from Anglo-Saxon, Roman, or Egyptian contexts, but the difference between the extremes of the spectrum are too significant to suggest all samples form a single cluster. It was only after seeing the different reactions of cobalt-blue beads to infrared light that I developed this study, after all (Figure 5.1).
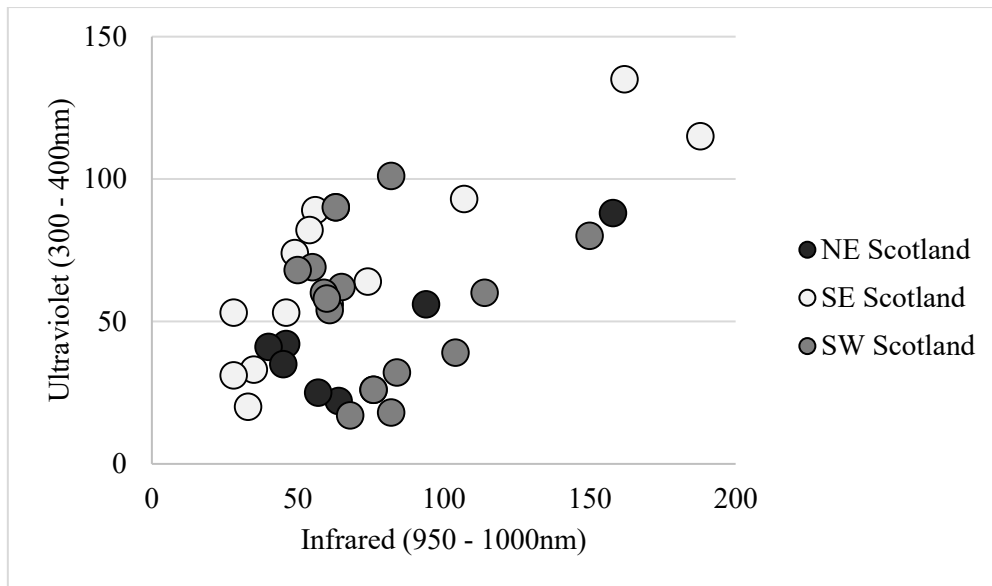
Figure 5.28: Spectral data for cobalt-blue glass in Scotland, separated by region.

Modern cobalt-blue tesserae do appear to respect the outer edge of the Scottish

samples (Figure 5.29). They generally do not overlap with Scottish, Egyptian, Roman, or

Anglo-Saxon glass, but neither do they cluster together particularly strongly by

themselves. Modern cobalt-blue samples do show similarly wide variations to ancient

samples: they continue to include samples that are absorptive of ultraviolet and infrared

light as well as samples that are highly reflective of both.
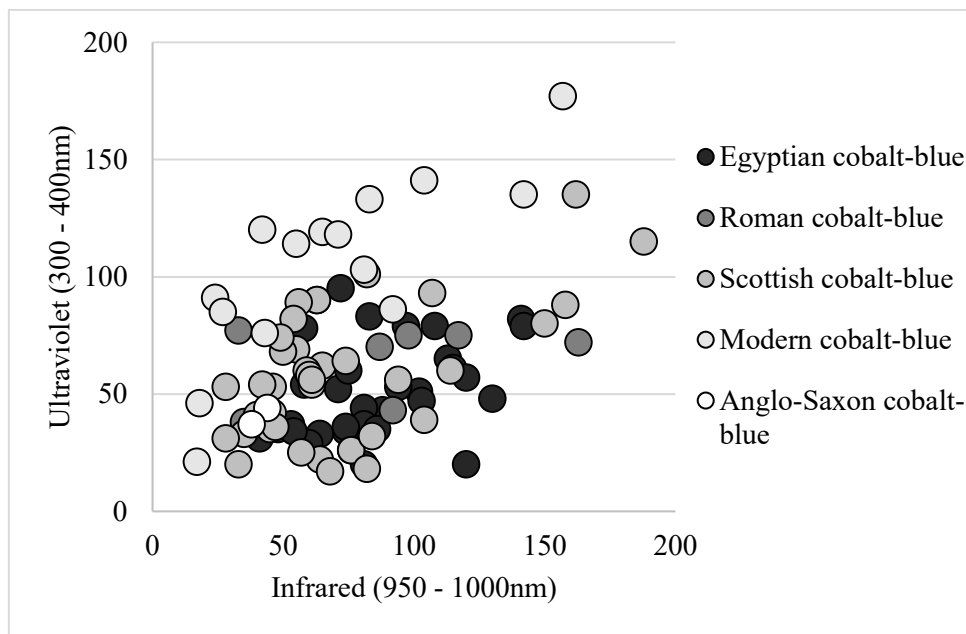
Figure 5.29: Spectral data comparing wound cobalt-blue Iron Age and Early Medieval Scottish glass beads to Anglo-Saxon, Roman, Egyptian and modern samples.

The wide variation in readings likely is due both to different recipes used for making cobalt-blue glass and to the frequency with which it was recycled. The varied measurements from 18th Dynasty Egyptian samples to Iron Age and Early Medieval Scottish samples and even modern tesserae indicate that people have been recycling cobalt-blue glass for millennia. Despite the continuous range of readings, however, there is a clear difference between certain extremes (Figure 5.30, Appendix E). Interestingly, one of the highly reflective samples has been chemically examined through pXRF and found to have a significantly higher lead content (33.5%) than one of the highly absorptive samples tested at the same time (0.07%). This lead makes the blue more vibrant and may render the glass highly reflective in infrared and ultraviolet light. Additionally, chemically tested Roman samples showed similar patterns: samples with higher lead concentrations produced higher infrared readings than those without. There are samples with high lead percentages that do not produce high spectral readings, but these also appear to have higher percentages of cobalt, which may be negating the effects of the lead. More precise, quantitative chemical testing is needed to determine the nature of this relationship, but it appears that the more lead a cobalt-blue object has, the more reflective it becomes in non-visible spectra.

Regardless of which chemical compound has caused the differences observed in cobalt-blue beads, one important outcome of this study is that we can see a difference between these objects. Cobalt-blue glass and glass objects often appear typologically similar, particularly in monochrome objects. Coupled with the frequency with which this glass was recycled in pre-modern glass-working, it is often difficult to identify difference at all. While this method has not produced specific clusters of cobalt-blue glass that could serve as typological categories, it does indicate a significant chemical difference between objects for which typological classification is otherwise difficult.
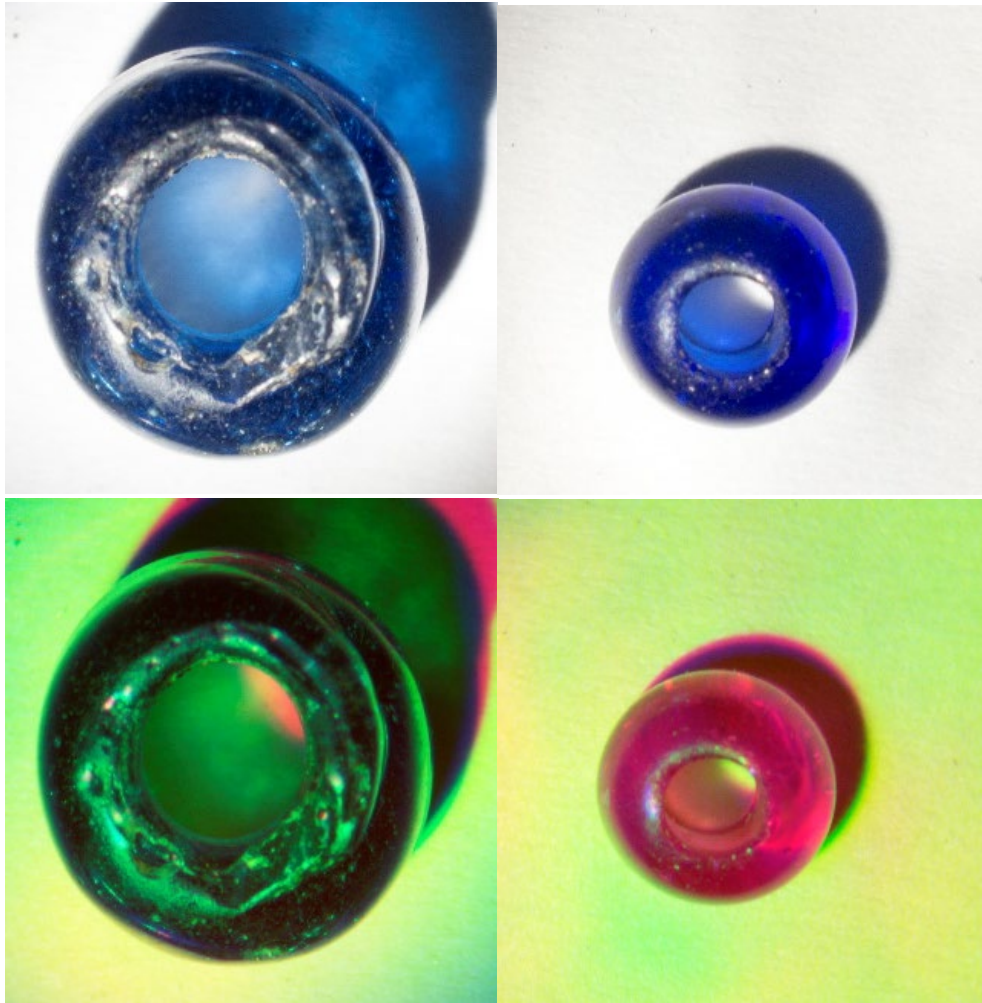
Figure 5.30: Visible-range and false-colour images of a highly absorptive cobalt-blue bead from Rhynie (left) (UG SF 15021) and a highly reflective cobalt-blue bead from Clachbreck (right) (UG CLB 1) images (Appendix E).

5.6.5   OPAQUE WHITE GLASS IN SCOTTISH WOUND BEADS

Some opaque white samples come from Scottish objects in which the white appears as an accidental inclusion in an otherwise yellow design (Figure 5.31, Appendix E). Invariably, these white samples give ultraviolet readings below 100 and infrared readings over 100 (Figure 5.32). Overheating lead-tin, a common colourant of opaque yellow glass (Chapter 5.5.3), will create tin-oxide and turn the glass white beginning around 1000º C (Biek and Bayley 1979, 16). This could indicate that those white glasses with infrared and ultraviolet readings above and below 100 respectively were made using tin-oxide. However, overheating lead-antimonate, the other common colourant of opaque

yellow glass (Chapter 5.5.3), creates calcium antimonate and turns the glass white beginning around 1000º C as well (Molina et al. 2014, 178 – 179), leading to a lack of clear identification for the possible chemistry of this cluster. Another cluster of white glass invariably produces readings over 100 for both ultraviolet and infrared, which may indicate the use of either tin-oxide or calcium-antimonate, but without further testing we cannot be sure. However, this group does have higher concentrations of bubbles. These may be coming from bone ash or other sources of calcium used to create calcium-antimonate white glass, which would react with the glass to form large numbers of bubbles. There is also a third group with readings below 100 for both infrared and ultraviolet wavelengths, which also has high concentrations of bubbles. This could indicate that these 'whites' are instead areas of the core glass colour that have been saturated with bubbles to appear white (Chapter 4.1.4).
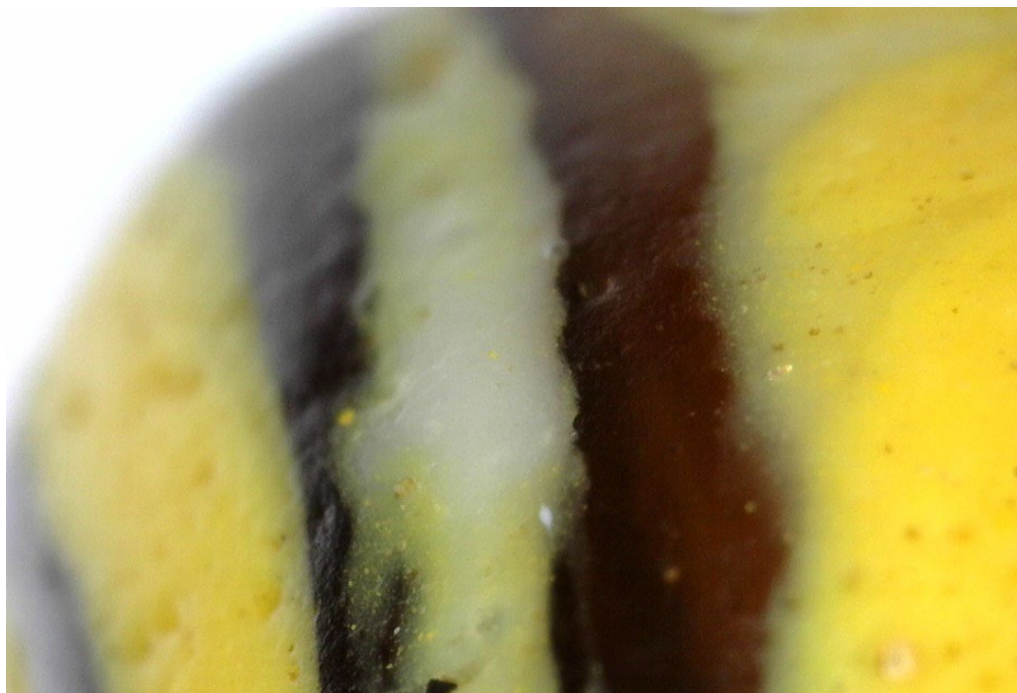
Figure 5.31: Example of possible overheating of either lead-tin or lead-antimonate yellow to create white glass (Culbin Sands, NMS X.BIB 10) (Appendix E).
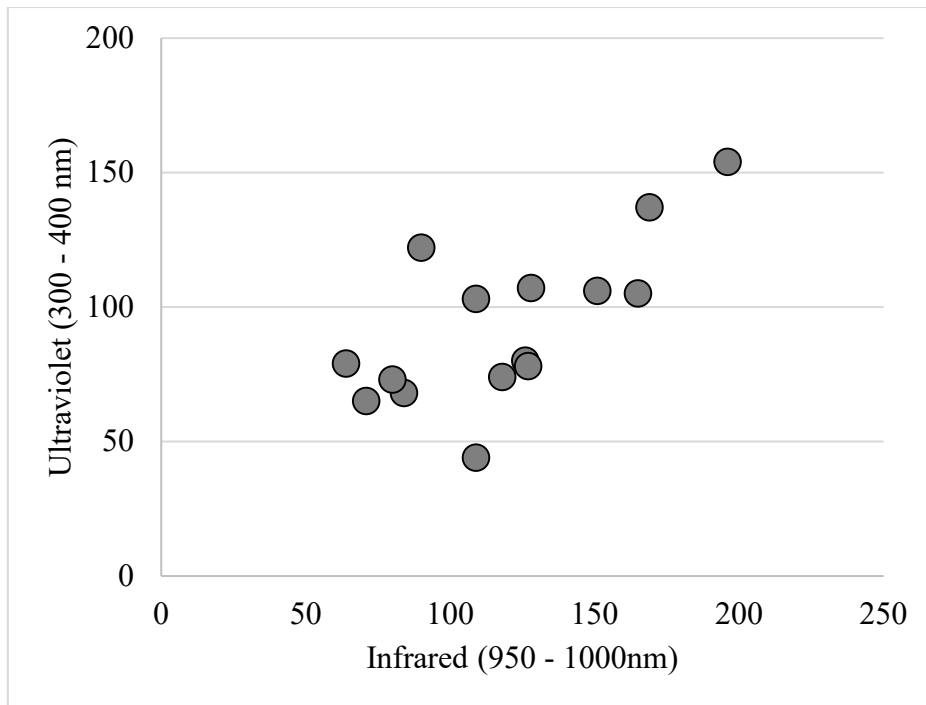
Figure 5.32: Spectral data for Scottish samples of white glass.

Available chemical data for Scottish samples shows two calcium-antimonate glasses with both readings above 100 and two calcium-antimonate glasses with both readings below 100. There is not enough evidence to determine what is causing such a difference in readings, particularly because one of the glasses with higher readings has larger amounts of silver and manganese than the other samples, including the one with similarly high readings. There is also chemical evidence for another sample with low ultraviolet and infrared readings that indicates it is not coloured white, but rather is a colourless glass that has been saturated with bubbles, as stated above. It appears, then, that both white glasses coloured with calcium-antimonate and colourless glasses saturated with bubbles may give similarly low readings while having starkly different chemical compositions. Further chemical testing of these samples would allow for confirmation and clarification of these patterns, particularly because none of the published data for the samples included in this study include a lead-tin white glass.

White glass in Scotland does overlap strongly with that used in New Kingdom Egyptian objects (Figure 5.33). Scottish glass seems to separate into clusters, but this may be due to a relative lack of samples. Roman white glass clusters together, while Egyptian white glass presents more of a spread. Scottish glass does not seem to overlap with the Roman material per se, but this could be due to the relative lack of samples from Roman contexts.
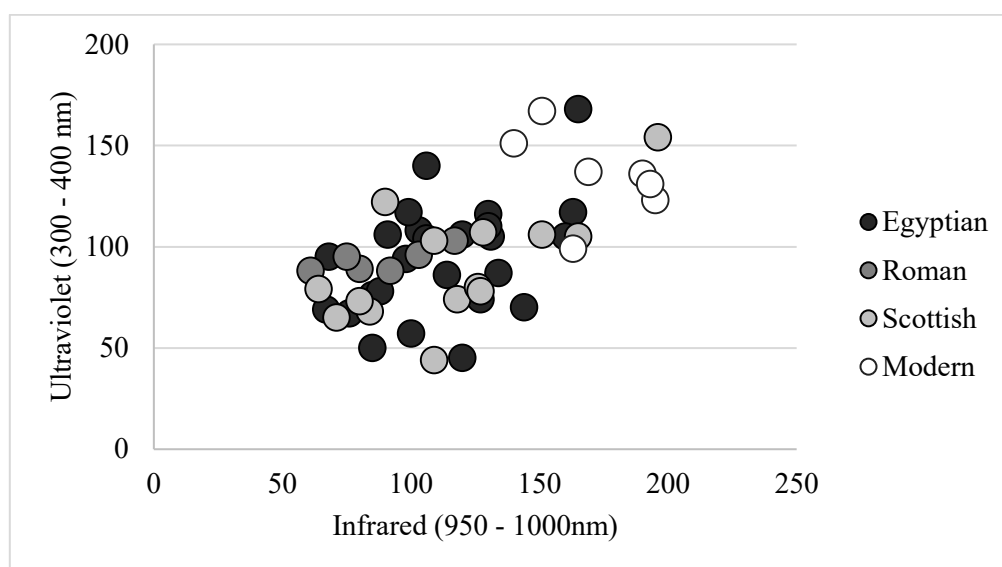
Figure 5.33: Spectral data comparing Scottish, Roman and Egyptian white glasses to modern white tesserae.

Modern white glass forms a highly reflective cluster that is somewhat separate from the ancient samples (Figure 5.33). It is quite distinct from the Roman white glasses included in this study, and barely overlaps with the outer edges of Scottish and Egyptian samples. One sample of chemically tested modern white glass shows elevated levels of both lead and manganese, which may indicate why these samples are highly reflective (5.4.4). This sample does not have detectable levels of tin or antimony, if any, suggesting it is neither lead-tin or calcium-antimonate. Still, it is not clear whether all modern samples are chemically separate from the Scottish and Egyptian samples or whether a relative lack of samples coupled with a lack of chemical testing is affecting the current data.

5.6.6   NATURALLY-COLOURED GLASS IN SCOTLAND

There are clear differences between naturally green and naturally brown glass within the Scottish assemblage (Figure 5.34). This suggests that larger differences in base chemistry or trace elements may be affecting these results, since colourants have not been added to these samples. We cannot know which elements are affecting the change without chemical testing, but it likely is due to the impurities in the sand used to make the glass.
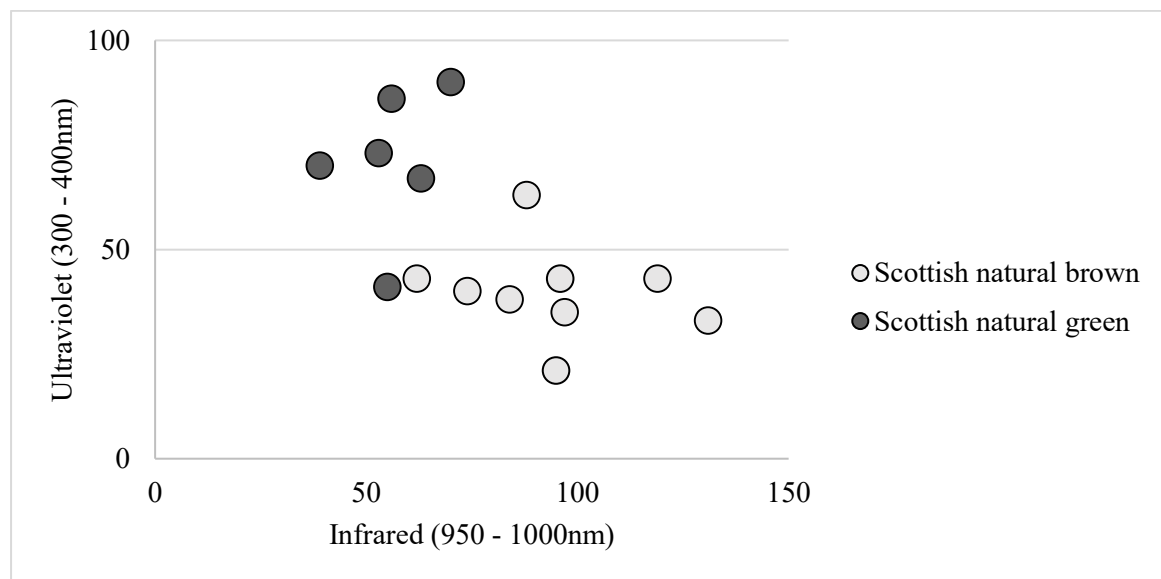
Figure 5.34: Spectral data for Scottish naturally-coloured glass samples.

Naturally-coloured Scottish glass does not generally overlap with Roman or Anglo-Saxon samples either, particularly when separated by colour (Figure 5.35). Naturally brown glasses form two clusters, one with infrared readings under 60 and ultraviolet under 35, and the other with infrared over 70 and ultraviolet over 40. All Roman and Anglo-Saxon samples cluster in the first group, while all but one of the Scottish samples cluster in the second. This separation between Scottish and Roman samples is unexpected, because many of the Scottish samples come from window glass often said to be Roman in origin. Chemical data suggests the Anglo-Saxon material has

higher concentrations of manganese than some of the Scottish samples, but this is speculation without other chemical data for comparison.
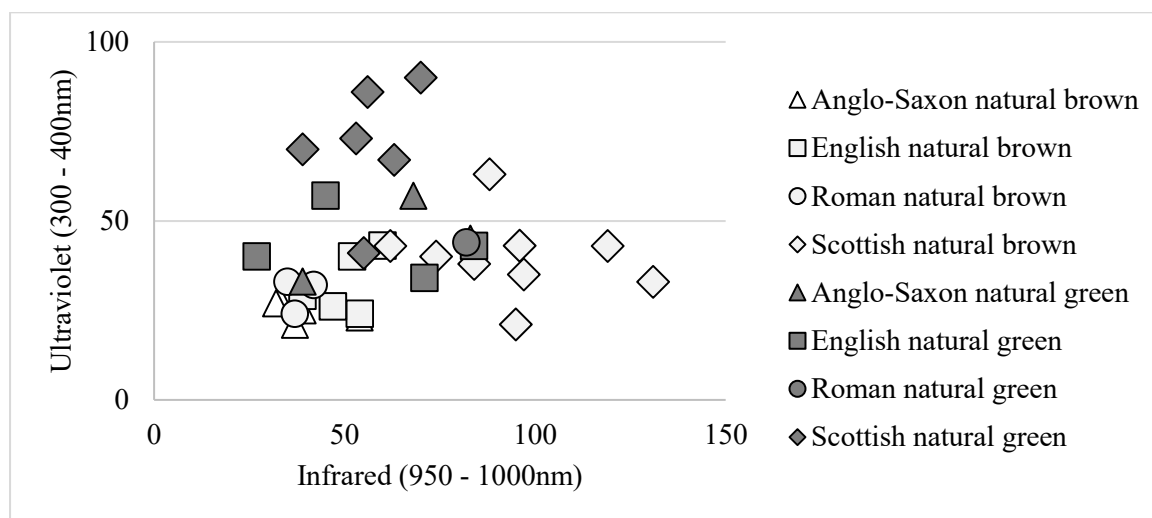
Figure 5.35: Spectral data for Scottish, Roman, Anglo-Saxon and medieval English naturally-coloured green glasses and naturally brown glasses.

Most of the naturally-coloured glass from Wells Cathedral does not overlap with the Scottish samples (Figure 5.35). Interestingly, some of the naturally-coloured browns from Wells Cathedral do overlap well with Roman and Anglo-Saxon natural brown samples. This could indicate some medieval window glass at Wells Cathedral is remelted or reused Roman or Anglo-Saxon glass. As stated earlier, however, we cannot equate overlap in these scatter plots with chemical similarity.

5.6.7   NEWSTEAD AND TRAPRAIN LAW

Samples from Newstead and Traprain Law do cluster separately in the data, suggesting a chemical difference between the glass at each site (Figure 5.36). Relatively few samples from both sites are eligible for comparison, because I could only image five objects from Newstead for this study. All five are cobalt-blue glass melon beads, which are highly distinctive in the archaeological record in Scotland. When comparing only cobalt-blue beads from Traprain Law and Newstead, we see differences in the glass that

mirror the conclusions drawn in the last chapter using bubble data (Chapter 4.9). Only one object from Newstead has an infrared reading over 40, compared to all cobalt-blue objects from Traprain Law. These results suggest a significant difference between the beads at Newstead and those at Traprain Law, particularly when combined with the differences in bubble concentrations discussed in the previous chapter (Chapter 4.9). This is relatively unsurprising, however, since all samples from Newstead are cobalt-blue melon beads while none of the samples from Traprain Law are. Melon beads are a distinctly Roman style in southeast Scotland. However, difference in the glass used to make the beads between Newstead's melon beads and the other cobalt-blue beads at Traprain Law indicates differences in cultural preference between the Roman-occupied Newstead and the local population at Traprain Law.
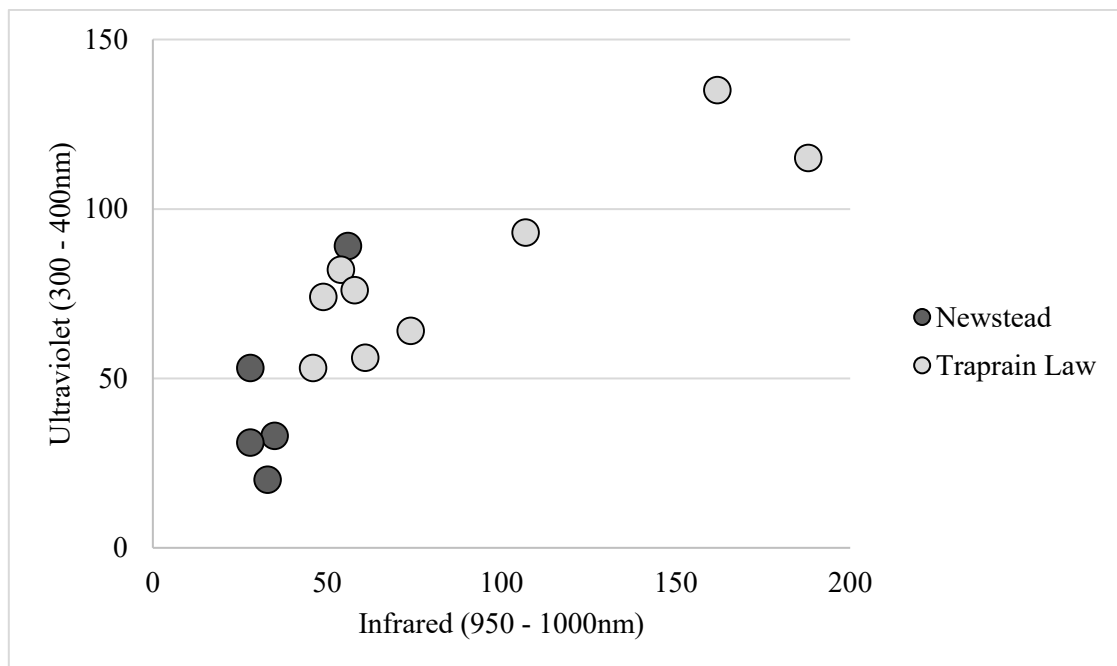
Figure 5.36: Scatterplot showing cobalt-blue samples from Traprain Law and Newstead.

5.7   NON-VISIBLE-RANGE SPECTRAL PHOTOGRAPHY AS CHEMICAL TESTING

Compared to the techniques discussed at the beginning of this chapter, there are many benefits to spectrally photographing archaeological finds. First, there is a much lower minimum size requirement, if one exists at all. So long as the camera can see the object, it can spectrally photograph it. This is important for beads, since most archaeological beads from Iron Age and Early Medieval contexts worldwide are less than 6mm in diameter. Objects that are too small for XRF, Raman Spectroscopy, or other techniques with minimum size requirements can still be spectrally photographed. Second, the technique is non-destructive for most archaeological materials. Art historians often use it to identify pigments, suggesting the types of infrared and ultraviolet light used are safe for more sensitive objects. Photography is entirely non-contact, allowing for imaging of fragile or delicate objects, and does not require a sample for testing.

Spectral photography as described here is also affordable. The largest expense is a camera and its conversion to full spectrum imaging, totalling roughly £600 for a standard dSLR. In total, then, the equipment required for visible and non-visible spectral photography will cost a project roughly £1200 – 2300 if starting from scratch (Chapter 8.4). While this is still out of reach for certain project budgets, it is significantly more affordable than any of the techniques mentioned earlier in this chapter.

The equipment is portable, allowing for travel to museums and other locations. This enables specialists to image objects that may not be able to move to a lab, such as sensitive or fragile collections or larger monuments such as buildings or standing stones. The kit can fit into a backpack or camera bag and can be transported to any desired site so long as proper precautions are taken to weather-proof the bag. Additionally, anything can be spectrally photographed, from the landscape to buildings and monuments to small

finds (Chapter 7). The principles apply to everything in existence, so there is no limit to the type or number of things one can spectrally image. Few if any techniques for chemical analysis currently exist that are affordable, portable, non-destructive, and can be applied to any archaeological material.

Non-visible spectral photography of archaeological objects is a non-destructive, affordable, portable technique that archaeologists can use to gather general chemical information about an assemblage or collection of objects. While there is currently a significant need to chemically test certain groups of objects to confirm the patterns seen here, the mere existence of patterns is data not previously acquired for many of these samples, particularly the Scottish ones. These results provide significant data that can lead to both new conclusions about the objects and a more targeted approach to further, more precise chemical testing, should a project desire. The technique does not replace more precise methods like XRF, PIXE, or LA-ICP-MS, nor was it ever intended to do so. Rather, it provides quick, relative chemical data in an affordable, non-destructive manner that can then be confirmed or expanded upon using a more precise technique if needed. There is the possibility that this methodology could provide further data on chemical relationships between objects, but this would require additional chemical testing to confirm the patterns seen above.

Our obsession with the latest new technology in archaeology has led to the general assumption that a project must either spend significant amounts of their budget on determining the precise chemical composition of a series of objects or that they simply do without. Projects with lower budgets must choose their samples carefully to acquire the desired data. This approach directly correlates to our assumption that the latest new technology is more objective and provides the best results, our subsequent tendency to

invest less in existing affordable technologies and our hesitance in challenging the current standardised techniques in archaeological photography.

Chemical testing is not an all-or-nothing endeavour. There is no fault or shame in forgoing precise chemical measurements in favour of a more affordable technique. There is also no reason archaeology as a field should not be striving to create such techniques, particularly because most archaeological projects have relatively low budgets. This chapter presents a technique that can provide a degree of relational chemical data for any object or assemblage using three torches, a camera, some filters, and photo-editing software. While the process for developing this technique was complex, it was less complex than inventing XRF or LA-ICP-MS. Questioning the boundaries of archaeological imaging techniques is therefore an accessible, relatively affordable endeavour that yields highly informative results, particularly for object categories that the field has historically struggled to represent well.

6   CASE STUDY 3: SPECTRAL RTI AND PHOTOGRAMMETRY

Archaeology need not limit its use of spectral imaging to photography alone; it can also benefit any visualisation technique that uses photography as its core principle, like reflectance transformation imaging and structure from motion photogrammetry. Glass beads are notoriously difficult to photograph due to issues of size, reflectance, and translucency or transparency (Chapter 1.2.3). The problems encountered in photographing these objects naturally transfers to creating 2.5- and 3D visualisations that use photography as their dataset. For example, the algorithm used to predict the location of an image relative to the object in SfM photogrammetry appears to treat reflective patches as a surface design feature, thereby thinking it has correctly aligned the images to produce a model of the bead when instead it has aligned the reflective patches. In this chapter, I apply spectral imaging techniques to PTM RTI and SfM photogrammetry of Iron Age and Early Medieval glass beads from Scotland to demonstrate their success where standard methods typically fail.

The difficulties associated with imaging SRT materials has encouraged many specialists to avoid imaging these objects altogether. During this PhD, several archaeological imaging specialists voiced that it was impossible to successfully 3D model such objects without expensive equipment like a CT scanner. In a sense, they are correct: it is difficult, if not impossible, to create 2.5- and 3D visualisations of SRT objects like glass beads using the standard methods for RTI and SfM photogrammetry. By experimenting with and applying non-standard archaeological photography techniques to the base images used in PTM RTI and SfM photogrammetry, however, I have successfully imaged objects for which such visualisations are supposedly impossible.

6.1   REFLECTANCE TRANSFORMATION IMAGING

Reflectance transformation imaging creates a 2.5-dimensional visualisation by calculating the surface normals of an object from a single perspective, normally using 30 – 50 images with varying lighting angles (Diaz-Guardamino and Wheatley 2013, 191; Malzbender et al. 2001, 3). The result is a visualisation of the object from a single viewpoint that has the appearance of being three dimensional. Specialists can create polynomial texture maps (PTM) within RTI to manipulate the surface through varying texture adjustments and measurement alterations, allowing them to deepen grooves or to apply certain settings that allow for easier identification of surface features such as carvings, surface wear, or tool marks (Cultural Heritage Imaging 2010, 12; Diaz-Guardamino and Wheatley 2013, 192).

6.1.1   CURRENT IMAGE CAPTURE TECHNIQUES FOR PTM RTI OF OBJECTS

The current procedure for generating PTM RTI of an object is as follows. Place the object on a neutral background with a reflective RTI sphere next to it. These spheres come in a range of sizes and all are either black or red. Certain objects require two spheres, but these spheres also block light in some images. For this reason, one sphere is preferable to two. Place the sphere so that it will always show a highlight reflection regardless of where the light source is, but also casts minimal shadow on the object (Figure 6.1).

Figure 6.1: Ideal positioning of the RTI sphere such that it can capture reflections from all angles, but casts minimal shadow on the object itself.

Next, attach the camera to a tripod at an angle that captures both the object and the sphere straight on. Set the field of view such that both the object and the sphere lie within the frame at their maximum level of detail. Set the focus to automatic to avoid accidentally adjusting the field of view while adjusting other settings. Next, attach a remote shutter to ensure the camera remains still during image capture. Touching the camera or even shifting your weight during image capture often results in micro-movements of the camera or object. Images captured when the camera or object has moved therefore show the object at a different angle or in a different position than the rest of the images. Consequently, the compression of these images into a single RTI will be blurry because the object is in different locations in each image.

Set the camera to manual exposure, turn off all other light sources that may interfere with the process and turn on the single light source used for RTI image capture (e.g. a torch). Aim the torch at a roughly 60-degree angle to the object, then set the aperture. Set ISO around 100-200 for the largest sensitivity to light (Figure 6.2). Aperture will range between F11 and F30, but ideally would fall at or above F18. The aperture and ISO determine the necessary shutter speed for even exposure, which usually falls around

1 second. Next, move the torch to the level of the table to ensure the camera can still capture an image at the lowest level of light. This image will be darker but should still register on the camera's sensor. Finally, move the torch to the same angle as the lens and ensure the camera can capture an image without areas of overexposure on the object. This image will be lighter but should still contain the necessary data for RTI.
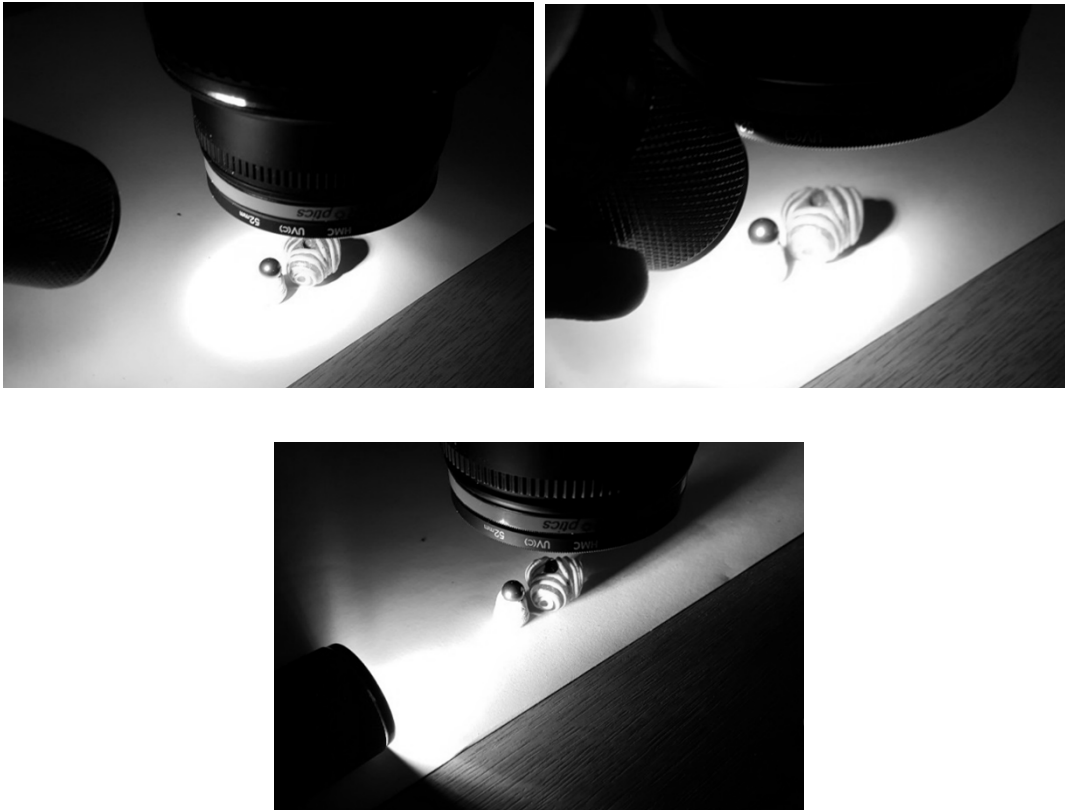
Figure 6.2: Setting focus and exposure using various angles of light.

With the torch next to the lens, set the focus of the camera automatically. Take a test image and examine it to ensure it has captured the desired detail. Continue setting the focus automatically and taking test images until you are satisfied with the result. Immediately set the focus to manual to avoid the autofocus changing between images. Do not touch the lens until you are finished with image capture to avoid moving the camera.

Using the remote shutter, begin taking images while placing the torch at different angles to the object. Follow a dome pattern between the camera and the object, taking

care not to touch the camera or the object (Figure 6.3, Appendix E). Remain as stationary as possible while moving the torch, as many floors are flexible and may bounce when you take a step. Capture between 30-50 images. More will help the process up to a point, while fewer will jeopardise the possible success of the resulting visualisation. Take care in placing the torch near the tripod, since any movement will jeopardise the results. Always capture images in the camera's raw format to ensure the most detail.
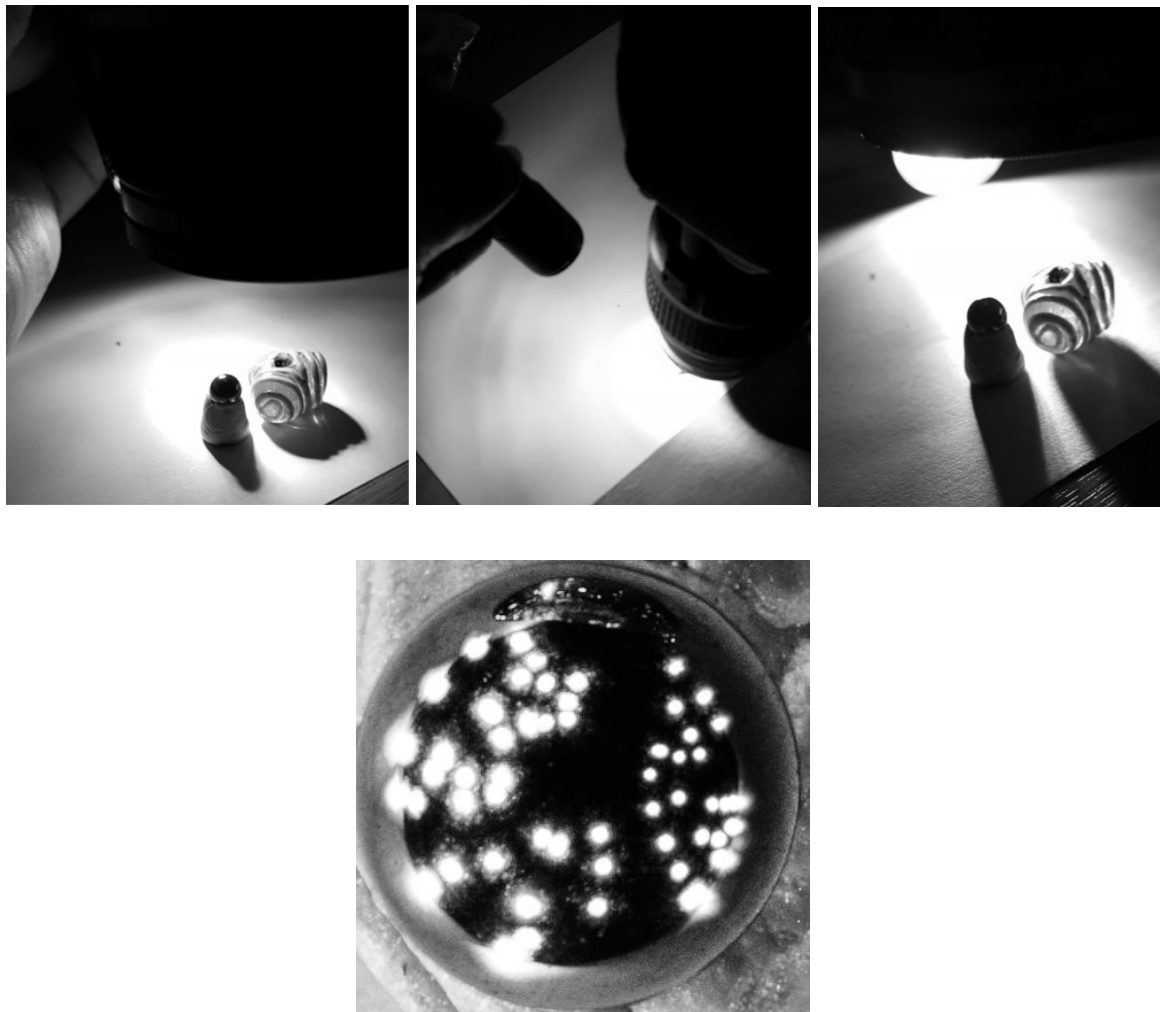
Figure 6.3: Example of the dome pattern of light (top) and the resulting composite image of all reflections captured by the RTI sphere indicating coverage (bottom) (Appendix E).

It is possible to automate light angles using a dome of various automated light sources (Cultural Heritage Imaging 2018c). One light flashes per image taken, standardising both the number of images and the angle of each light source. Domes

ensure full coverage of an object and are slightly faster in capturing images than changing the light by hand, but they are also expensive. Domes often contain between 40 and 100 individual lights as well as the separate mechanisms for running each of them, which quickly becomes too expensive for many projects. The primary supplier for RTI domes has stopped selling them and making a 12" dome from scratch costs roughly £800 (Cultural Heritage Imaging 2018c; Pawlowicz 2015). A good torch costs between £10 - £50, and manually moving or holding the torch while capturing images is not difficult.

Import the images into the photo-editing software of your choice and white balance to the neutral background behind the object. Process images as a batch to ensure they maintain the same settings relative to each other. Do not make any adjustments other than white balancing or adjusting exposure by an identical interval for each image. Other alterations such as sharpening the images, reducing noise, or altering images individually can destroy data vital to RTI processing. Import the images into RTIbuilder using the settings for polynomial texture mapping (PTM) and follow the steps for processing (Cultural Heritage Imaging, 2010). In the completed file, examine the surface normals to ensure proper coverage.

If the RTI is fuzzy or out of focus, it is likely that the camera or the object moved during image capture. If so, there are three primary methods to fix the blurriness. The first option is to reset the object and camera and acquire a new set of photos. This negates the previous image set in favour of a new one and requires equal amounts of work. The second technique is to eliminate the images that are in a different position from the RTI process. This eliminates certain exposure angles from the RTI, but it is a quick solution if there are a small number of offending images. The final option is to edit the misplaced images by shifting them to the correct relative location. This requires access to photo-manipulation software and can take significant amounts of time, but it is worthwhile if

either only a few images are out of alignment or if the object is not available for further imaging.

6.1.2 RTI OF SRT OBJECTS USING CURRENT PRACTICES

The above technique for RTI works quite well for objects measuring between 0.05 - 1m in length, width, or diameter and made from an opaque, non-reflective material. I have found it problematic for any object outside this description, particularly SRT objects. The results vary considerably and often contain large patches of missing or poorly represented data due to issues of transparency or translucency (Figure 6.4, Appendix E).
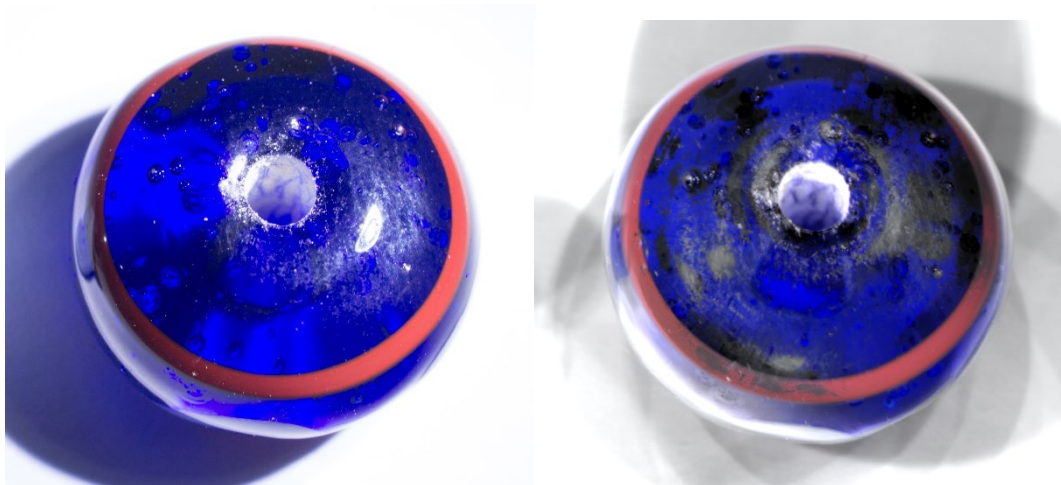
Figure 6.4: Photograph (left) and standard RTI output (right) of a highly reflective bead, resulting in grey patches (Appendix E).

Small objects run the risk of not being captured by the camera. A standard zoom lens cannot capture objects smaller than a few centimetres in enough detail to produce informative results. Additionally, most surface features of small objects are smaller and shallower than those on larger objects and may not register on the sensor if using a standard lens. Reflective objects result in overexposed patches in the images that produce grey areas on the final output (Figure 6.4). These areas contain little to no surface data.

The more patches of overexposure there are of an object, particularly when moving the light source around, the less information the final reflectance transformation image will contain. Finally, images (and therefore RTI) of translucent or transparent objects capture elements that are beneath rather than a part of the surface. These could include bubbles, inclusions, striations, or anything behind the object such as a background, table, or even the opposite surface of the object. The resulting visualisation will provide information about the perceived surface of the object, which will include its interior or the objects behind in addition to the surface itself.

Each of these factors often result in failed RTI, particularly if an object has two or more offending characteristics. Unfortunately, many archaeological small finds are SRT objects (e.g. glazed ceramics, lithics, glass vessel sherds, amber pendants, faience beads, bangles, semi-precious stone ornaments, or any type of metalwork). Specialists recommend covering a reflective, translucent, or transparent object in talc or other powders to create a matte surface, a recommendation that appears in earlier texts concerning the photography of reflective surfaces (e.g. Ives 1941, 264). This is often unhelpful for archaeological objects, however, since many materials react poorly to powders and acquiring permission to use them on archaeological objects may be difficult. Additionally, many surface features of these objects are shallow or faint enough that the powder fills them in, thereby defeating the purpose of the RTI. Standard techniques and troubleshooting for PTM RTI of SRT objects often fail, rendering RTI difficult if not pointless for these objects.

6.1.3 Photomacrographic and Photomicrographic RTI

To solve the issues of poor RTI outputs, we must solve the issues encountered in photographing SRT objects. First, we must solve the issue of size; RTI software cannot create RTI of an object if it cannot 'see' it. I originally began experimenting with a 40mm

macro lens to capture photomacrographic RTI, or RTI with a macro lens (Figure 6.5, Appendix E). Macro lenses work well for bead photography, and this does not change the standard RTI procedure significantly. Macro lenses require care in setting the focus and aperture due to differences in depth of field to a standard lens (Chapter 3.1.3), but otherwise follow the same steps as standard RTI.

Figure 6.5: Example of successful photomacrographic RTI (Loch Eriboll, UG F128) (Appendix E).

Because the macro lens focuses an object so that the ratio of the object's size to the space it covers on the sensor is at least 1:1, images taken with a macro lens appear to have a shallower depth of field (i.e. more of the image appears out of focus). Rather than setting the focus automatically to the surface of the object, then, set the focus to just beyond the object's surface instead. The range of acceptable focus as perceived by human eyes falls on either side of the specific focal length of the macro lens. Setting the focus to the surface of the object only uses half of the range of acceptable focus and results in more of the image appearing blurry (Figure 6.6). Setting the focus to just beyond the surface of the object captures the surface in the front half of this range and the rest of the

object in the back, thus maximising the amount of the object that appears focused. All

other processing is the same as the standard method described above.

Plane of Focus

Object

Camera

Range of acceptible focus

Plane of Focus

Object

Camera

Range of acceptible focus
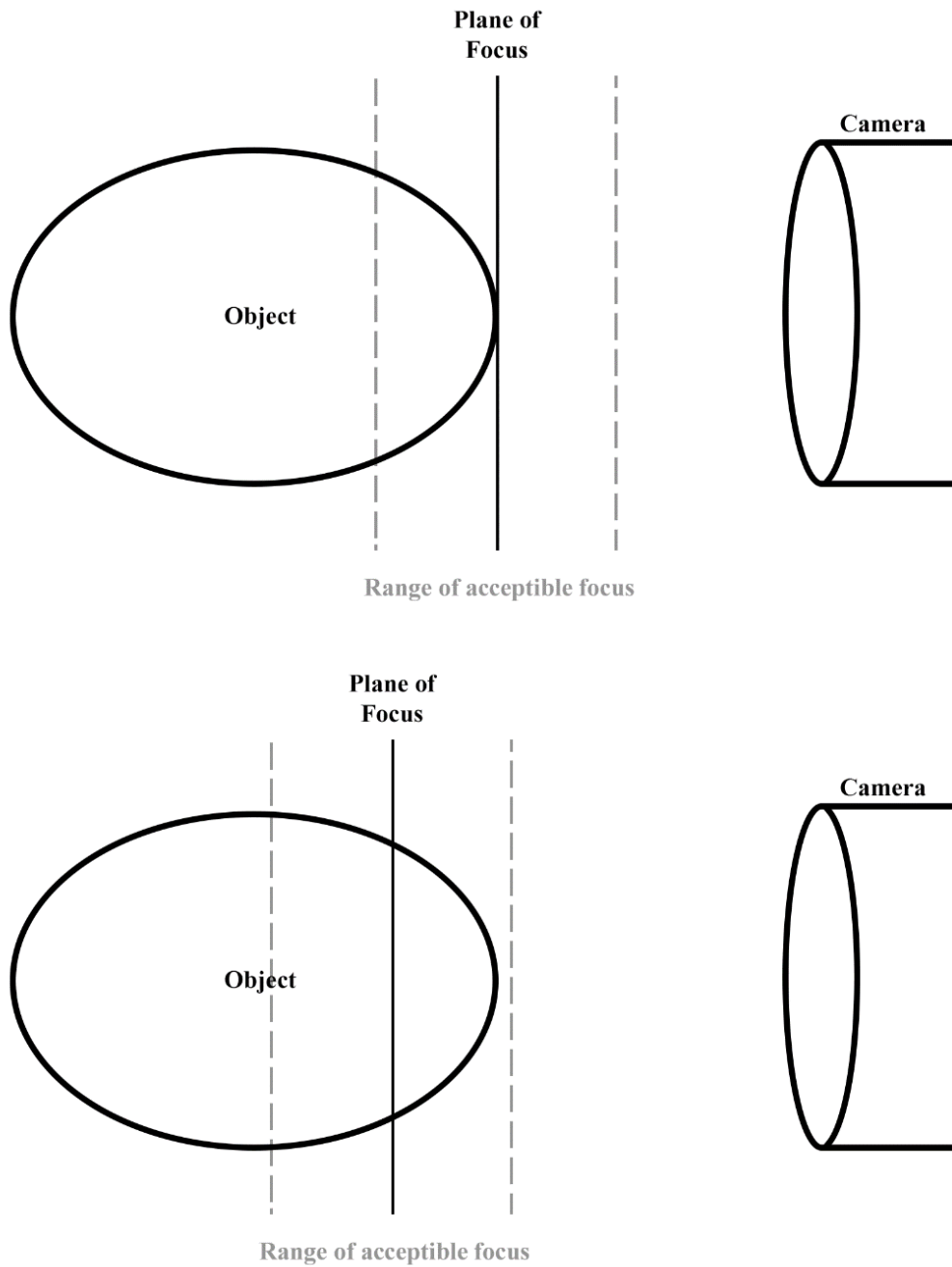
Figure 6.6: The range of acceptable focus when the plane of focus lies at the surface of the object (top) versus just beyond the surface of the object (bottom).

Despite the benefits of photomacrographic RTI, there were still many beads that

failed due to their size. Having worked with a digital handheld microscope in the field for

several years, photomicrographic RTI seemed a logical option (Figure 6.8, Appendix E (PowerPoint Slide 10)). For this, I used a DinoLite AM4113ZT Pro Digital Microscope, but many other models should also work. These microscopes require a tripod and cannot use the same tripod as the camera due to their size. DinoLite and various other providers do sell tripods for their microscopes, but a Gorillapod Original tripod, a bicycle light mount and some blu-tack work well enough (Figure 6.7). This kept the microscope stationary enough for image capture and cost £25, whereas the cheapest tripod from the microscope suppliers costs £80 – 100 (GT Vision 2018b).

Figure 6.7: Set-up for RTI using a microscope (Appendix E).

Figure 6.8: Example of successful photomicrographic RTI (Glenshee, NH no known number) (Appendix E).

For photomicrographic RTI, I fixed the tripod so that the microscope was directly over the object, then affixed a small RTI sphere on the table next to the object. A handheld LED torch is recommended as a light source; the microscope has built-in LED lights, but these do not help in RTI because they never change position. Otherwise, photomicrographic RTI proceeds similarly to photomacrographic RTI, with the focus set to just beyond the surface of the object to maximise depth of field and ensuring automatic exposure settings for the microscope have been turned off. Images were saved as .bmp files and processed the using RTIBuilder 2.0.2 using the standard PTM methods described in section 6.1.1 (Cultural Heritage Imaging 2018a). I have not encountered any

problems relating to size that could not be solved through photomacrographic or photomicrographic RTI.

6.1.4 SPECTRAL RTI

Solving the issue of size helps, but it does not eliminate all difficulties encountered when imaging glass beads or other SRT objects; they are still reflective and often translucent or transparent (Figure 6.9, Appendix E (PowerPoint Slide 7)). Most advice for reducing reflection in photographing and object centres around diffusers or light tents, which spread light out from its source to soften its effect on the subject. Alternatively, photographers can use a polarising filter, which only allows light in a certain orientation to pass through and thereby eliminates reflective patches. Unfortunately, diffusers, light tents, and polarising filters also block or eliminate the reflection of light on the RTI sphere, which RTI software requires for calculating surface normals.
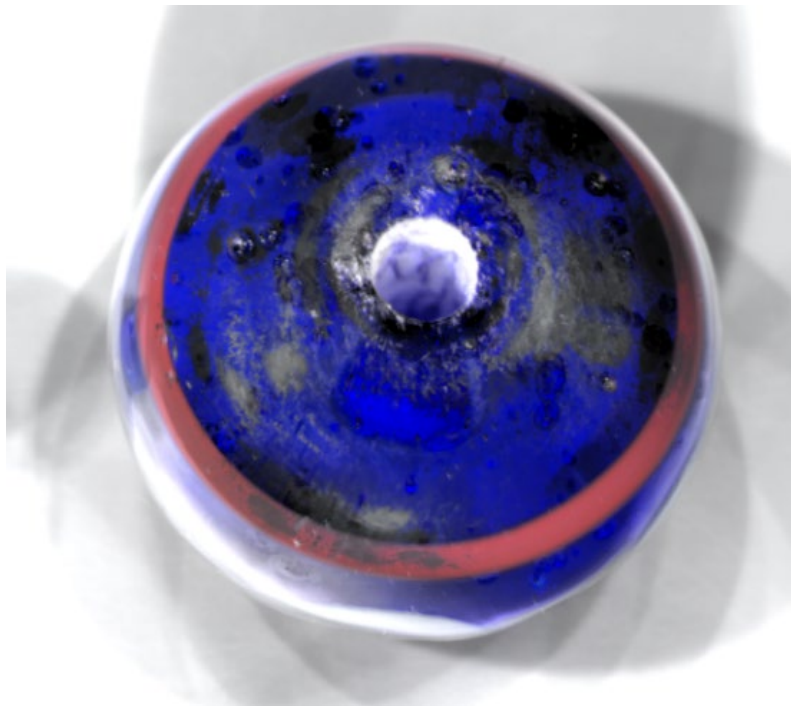
Figure 6.9: RTI result of a replica Norse bead using conventional techniques, resulting in grey patches across the surface of the bead (RO 002) (Appendix E).

Spectral photography provides a solution. Certain filters make translucent or transparent objects appear opaque while others make them appear transparent (Chapter 3.3). Applying these filters to RTI images produces significantly better results than visible-range images (Figure 6.10, Appendix E (PowerPoint Slide 7)). Additionally, both outputs allow for analysis of how surface wear (in the case of opacifying filters) or bubbles (in the case of clarifying filters) react to light at varying angles, something that rarely has been examined in archaeological glass studies. Interestingly, I have never encountered problems with translucent or transparent objects in RTI after solving the issue of reflection. Either the object is opaque in the image, thus negating the issue of translucency, or it is entirely transparent. Perhaps, then, translucency or transparency is not as problematic as previously thought.

Figure 6.10: The same Norse replica bead after applying a digital red filter (left) and a digital blue filter (right) to the images (RO 002) (Appendix E).

Shortly after discovering this technique and beginning my experiments with non-visible-range spectral imaging, I travelled to Kilmartin House Museum to photograph eight glass beads and toggles using spectral photography, RTI, and photogrammetry. I could to turn off the light for image capture, but there was a large window with no drapes or blinds to block the light from outside. I was not capturing any ambient light through

the window with a UV filter, however, and could use ultraviolet-RTI to eliminate the window problem. This is because ultraviolet light fixtures are rare in a public setting, especially in museums, and because modern window glass blocks ultraviolet light. Capturing RTI images in the ultraviolet range rather than the visible in spaces for which one cannot control ambient light produces results similar to capturing visible-range RTI images in a space in which one can (Figure 6.11, Appendix E (PowerPoint Slide 12)).

Figure 6.11: Example set-up of ultraviolet RTI in an open office with ambient fluorescent light (above) and its results (below) (Newstead, NMS X.FRA 890) (Appendix E).

The ability to capture RTI images without worrying about ambient lighting from windows or fluorescent lighting is a significant benefit to archaeological imaging. While photography in a light-controlled room is possible in museums, it often requires further scheduling in larger institutions and may be impossible in smaller ones. There may be other people in the workspace unless reserving specific photographic areas, making it inconvenient if not impossible to turn off overhead lights. The lack of ultraviolet ambient lighting indoors allows specialists to capture ultraviolet RTI image sets in an indoor space lit with natural, incandescent or fluorescent lighting without either compromising the results or inconveniencing others in the room (Figure 6.11, Appendix E).
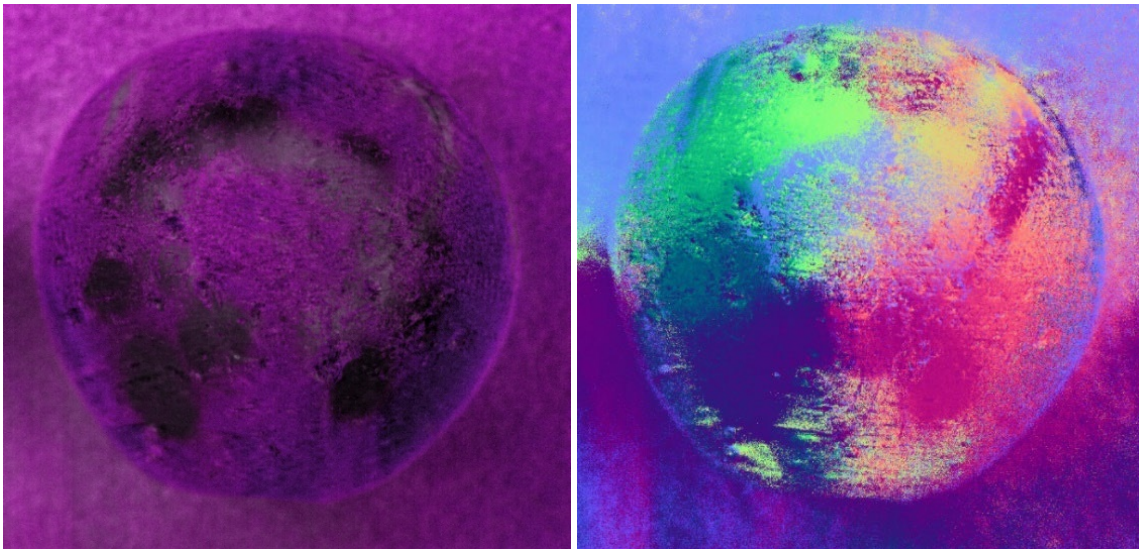
Figure 6.12: Example of an unsuccessful UV-RTI with dark patches and poor surface normals (Balure Dun, KHM SF 56) (Appendix E).

Not all UV-RTI outputs were successful; many produced the same grey or black patches of lost data and the calculated normals only provided minimal information, if any (Figure 6.12, Appendix E). Applying visible-range digital filters eliminated all reflection problems and resulted in successful RTI of even the most highly reflective glass beads (Figure 6.13, Appendix E). Thus, using UV-RTI when in indoor spaces without light control and applying visible-range filters to any image set that produces artefacts in the RTI, including non-visible-range RTI, solves any issue of reflection.
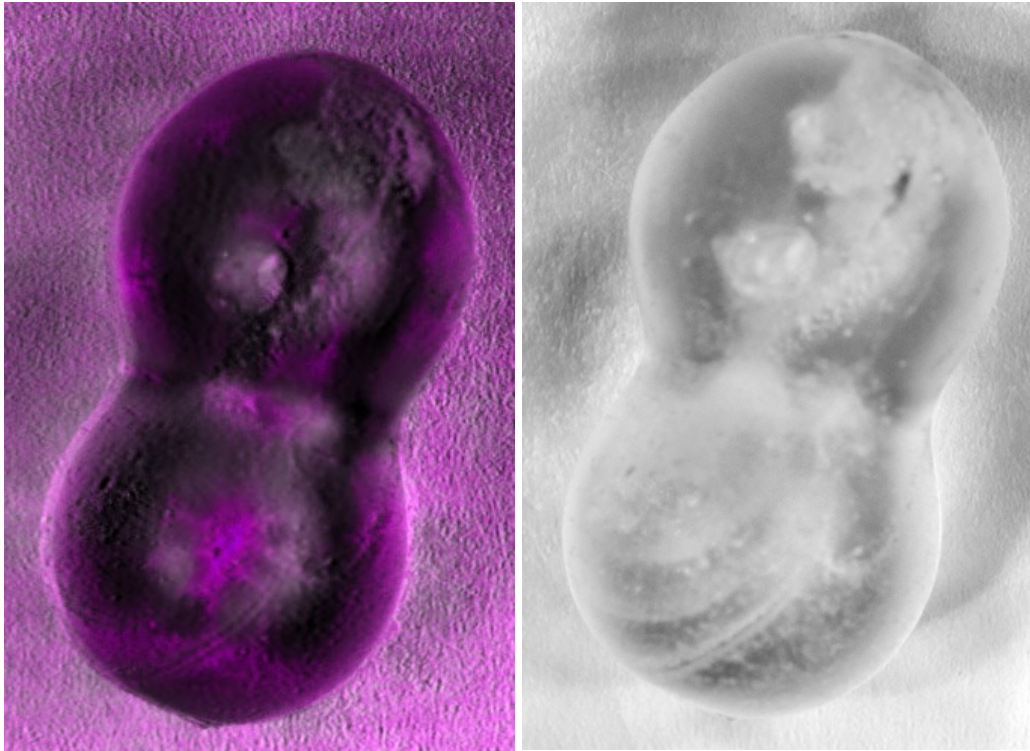
Figure 6.13: Example of an unsuccessful UV-RTI and successful filtered UV-RTI (Balure Dun, KHM SF 57) (Appendix E).

6.2 PHOTOGRAMMETRY

Similar issues of size, reflectiveness, and translucency or transparency also plague standard photogrammetric 3D modelling processes. Structure from Motion (SfM) photogrammetry is the creation of 3D models by digitally aligning multiple overlapping images of an object taken from various angles (Doneus et al. 2011, 82; Westoby et al. 2012, 301). It builds on the principles of stereoscopic imaging to calculate three-dimensional data for individual points found in overlapping images taken at different angles (Campana 1977, 345 – 346; Doneus et al. 2011, 82; Eder 1948, 402; Westoby et al. 2012, 301). Yet, these standard methods often produce worse results for SRT objects than those created using alternative techniques.

6.2.1   CURRENT PHOTOGRAMMETRIC TECHNIQUES

There are two current styles of SfM photogrammetric image capture: one in which the object remains stationary as the camera moves around it and one in which the camera remains stationary as the object rotates on a turntable. This thesis focuses on the technique in which the camera moves, because experience has shown that the software currently has more difficulty aligning images captured using a turntable than those captured by moving the camera for SRT objects. I also focus on rendering images in Agisoft Photoscan, because that was the most affordable software available for photogrammetric 3D modelling during the research phase of this PhD. The methods for image capture and rendering prior to importing them into 3D modelling software will be similar if not the same for other 3D modelling software.

According to current, standard methods, place the object on a neutral background. Light the object evenly. Set camera settings to auto focus and auto exposure and attach the camera to a tripod at the desired angle. Setting the camera settings manually may result in failed models if images are unfocused or poorly exposed. Either manually or using a remote shutter, take an image in the camera's raw format. Move the camera to the next desired angle around the object, but do not change the lighting or background. Repeat the process until you have acquired a minimum of 40 images from as many angles as possible. When assembled, the images should capture numerous angles of the object with significant of overlap between them. There is no required number of images for photogrammetric 3D modelling, but the minimum recommended number is around 40. Most projects should take closer to 60 – 100 images to ensure full coverage with enough overlap between images. Capture images in the raw format and process them into .tiff or .png files for modelling. While photogrammetry software can process .jpg files into a

model, most .jpg files have eliminated certain amounts of data in favour of smaller file size (Chapter 3.1.5).

To minimise error for difficult objects, current methods suggest using a diffuser, light tent or polarising lens to minimise glare or overexposed patches. For symmetrical objects, current methods also suggest placing targets it at certain intervals which the software can identify and align instead of the object itself. For glass or SRT objects, however, current techniques suggest it is best to not attempt making a 3D photogrammetric model due to near-certain failure.

6.2.2   PHOTOGRAMMETRIC RESULTS FOR GLASS BEADS USING CURRENT TECHNIQUES

To begin experimenting with non-standard methods, we must first understand why these standard methods fail to produce a successful model. How does each model fail, and can we create a technique that minimises the factors responsible for such failure? For example, some image sets create photogrammetric models of the background and its targets but leave a gaping hole where the object should be. Others align all the images, but do so incorrectly, such that they align in a single position with all their points stretching from there infinity (Figure 6.14, Appendix E). Still others merely render the points of a single image into a flat, two-dimensional set of points forming a single image, despite registering other cameras as having aligned (Figure 6.14, Appendix E). All these issues occur regularly in object photogrammetry.
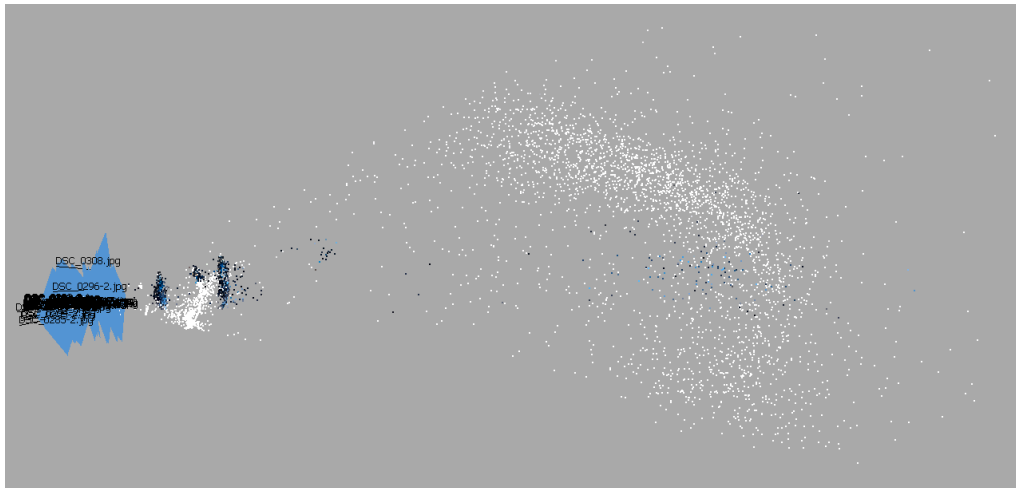
Figure 6.14: Examples of a failed model (UG SF 15021) with a long string of points and with certain point cloud rendering as a two-dimensional series of points (Appendix E).

More problems arise when following the standard proposed solutions for working around these issues. Agisoft (2017, 51) often recommends using targets or some sort of background design for objects that are having difficulty aligning. Targets are specific patterns, usually printed on cards or paper, which specialists can place around the object during image capture. These targets remain in the same position relative to the object throughout image capture. Upon importing images into photogrammetric software, certain options inform the software to align images based on the targets rather than other elements in the photographs. This theoretically aligns images which otherwise may not do so, because the software can always align the targets. Unfortunately, targets or decorated backgrounds not only do not help the situation for most difficult objects or materials, but often produce worse results (Figure 6.15, Appendix E (PowerPoint Slide 4)). While the targets do align, the calculation of specific points on an object are difficult if not impossible for the software to calculate in relation to the targets, likely due to the object's reflective and translucent properties. Each image still captures the way light behaves on an object, which still differs significantly for highly reflective or translucent materials. The algorithm appears unable to account for this difference in behaviour due to extreme

variability between objects, and so it cannot calculate accurate points to create a model of the object. This is uncertain due to the lack of published information about the algorithm itself, but I suggest it here based on the numerous failed models employing targets throughout this research.
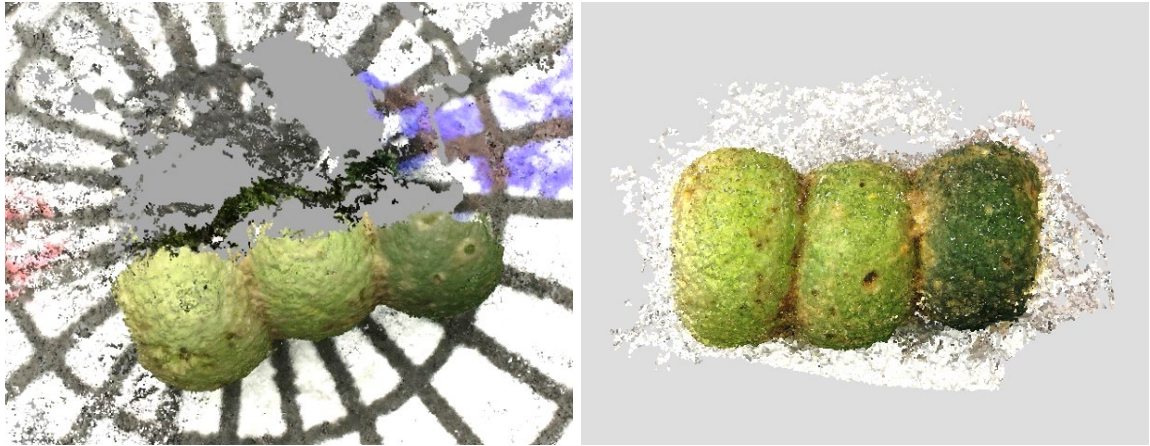
Figure 6.15: Examples of models using a decorated background (left) versus an undecorated background (right), assuming all other factors are identical (Glenshee, NH Unknown #) (Appendix E).

Agisoft also recommends the use of markers, which pinpoint identical locations on each photograph in which an element appears (2017, 41). Markers work along a similar principle to targets, save that the user is physically telling the software which points of the image are identical. Markers can occur on an object or on the background or other elements in the photograph. Unfortunately, the same problem arises with markers as with targets: the markers may align, but the other points forming the object often align incorrectly, because the algorithm for calculating their location does not appear to account for variable reactions of light due to differing degrees of reflection or translucency. Consequently, markers often produce worse models for SRT objects (Figure 6.16, Appendix E (PowerPoint Slide 5)).
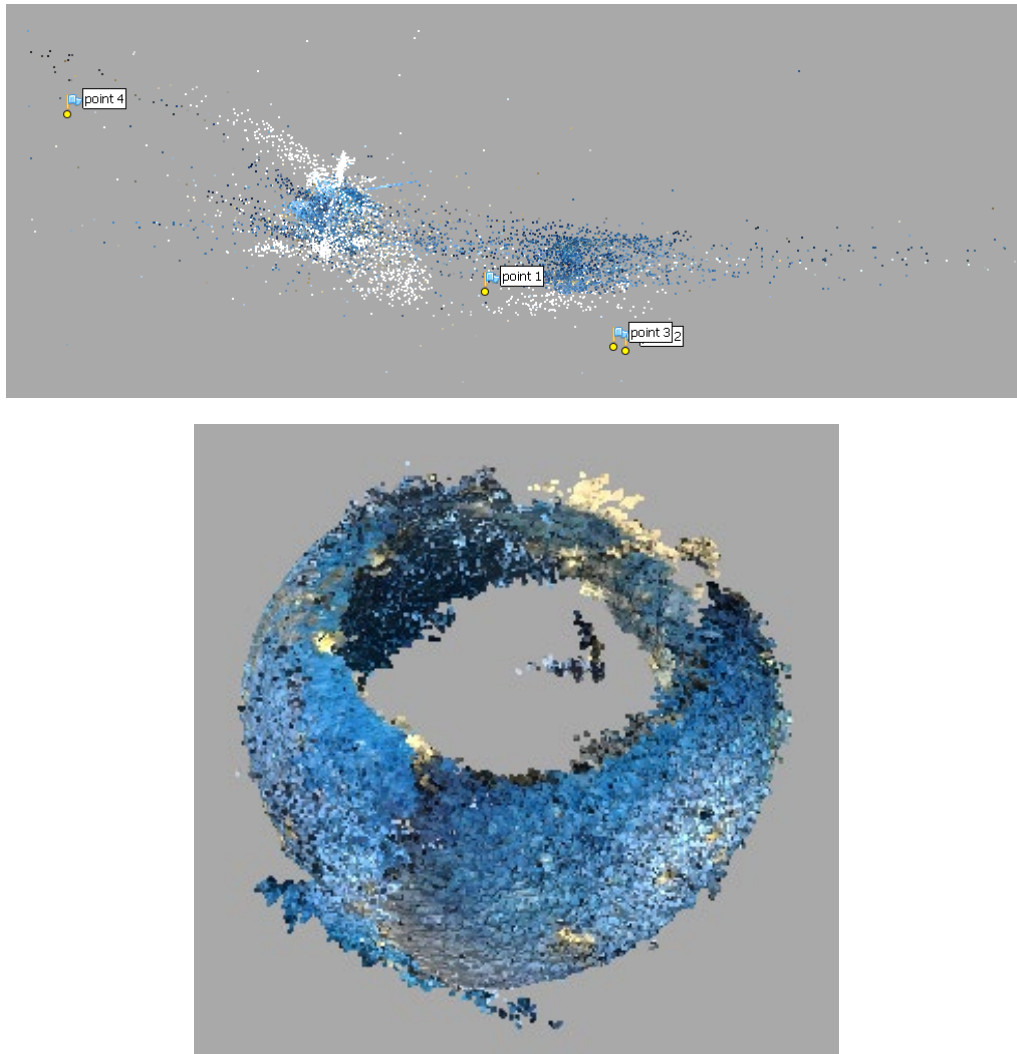
Figure 6.16: Example of a model using markers (top) and one not using markers (bottom), assuming all other factors are identical (Culbin Sands, NMS X.BIB 37) (Appendix E).

One recommendation for reducing reflective patches is to use a polarising filter. Polarising filters only allow light aligned on a single plane through to the sensor, so rotating the filter changes the angle of light allowed through (Dorrell 1994, 48). Polarising filters generally eliminate glare or reflection on an object, because the filter blocks the light from the angle causing the glare. While this is a viable solution for certain highly reflective materials in photogrammetry, however, many highly reflective archaeological objects are rounded in such a way that light from even a single source creates multiple spots of overexposure or glare that refract in different ways (Dorrell

1994, 48). This means that even a polarising filter cannot eliminate all reflective patches on an object (Figure 6.17, Appendix E), and it is not a viable solution for most highly reflective archaeological objects.

Figure 6.17: Image of a bead captured with a polarising filter (Loch Eriboll, UG F128) (Appendix E).
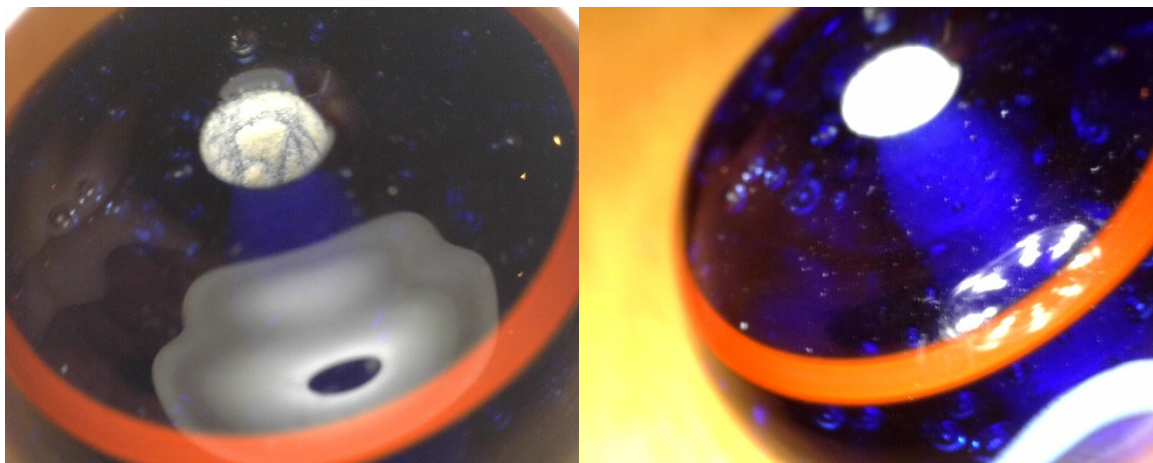
Figure 6.18: Image of a bead with (left) and without (right) a diffuser (RO 002) (Appendix E).

Another recommendation is to use a diffuser, which is either a piece of milky or textured clear plastic placed over the flash of a camera or a piece of white cloth placed

between the light and the subject being photographed (Dorrell 1994, 219). Diffusers reduce patches of overexposure in an image by spreading the light from its source, and therefore should eliminate the problem of reflection in photogrammetry. While a diffuser does eliminate specific patches of glare, however, many objects still reflect the diffuser itself, particularly objects made of glass or similar materials. Rather than a small patch of overexposure, a photographed reflective object now has a large patch of white reflected on its surface from the diffuser (Figure 6.18, Appendix E). This creates similar problems to the reflective patches it tries to solve and generally does not produce better models. The same issue arises when using a light tent or cloth diffuser.

A final suggestion for reflective materials is to place light sources at angles that minimise reflection, such as behind the object at an angle (Dorrell 1994, 218 – 219). This can work well for standard photography, since only one image is captured from any given angle and lighting need not remain the same between shots. In photogrammetry, however, changing the lighting to remain similar in each image rather than to remain in a similar position relative to the object will result in multiple images from starkly different angles with similar shadow patterns. The software often registers these shadows as areas to use for alignment, leading to a model that aligns the shadows rather than the object.

Masking is an oft-suggested solution for instances in which the software uses undesirable elements to align images, such as shadows (Agisoft 2017, 60). Masks are areas of each image that the specialist selectively deletes or omits from the process to eliminate bias from those elements. Unfortunately, masking does not solve most of the issues above. Images using the same lighting and creating the same shadows will continue to cause problems even after masking the shadows in the background, because these shadows still appear on the object itself. At times, differential masking of specific areas does create a more successful model than that produced without masks (Chapter 7.3). In

many cases, however, eliminating the images' backgrounds creates more confusion in aligning the images, not less (Figure 6.19, Appendix E (PowerPoint Slide 3)).
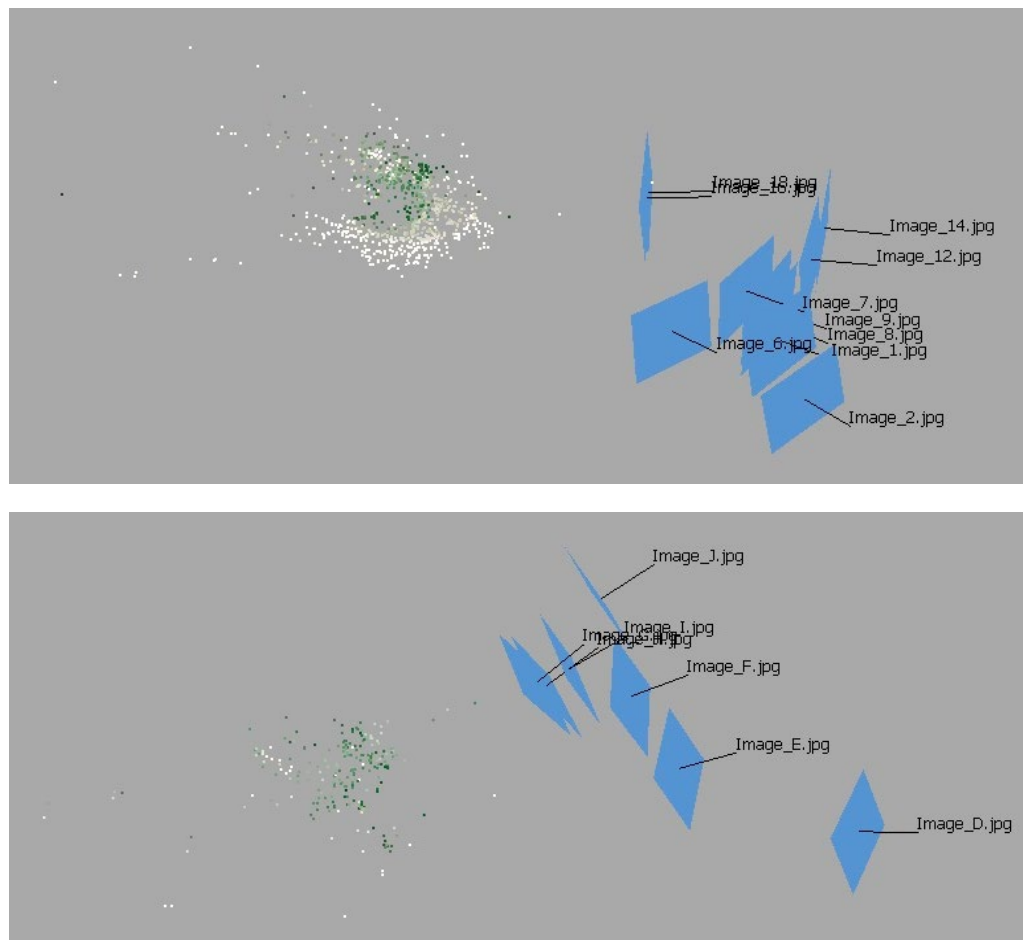
Figure 6.19: A model of a glass bead before (top) and after (bottom) masking (Appendix E).

Current techniques for making photogrammetric models of SRT objects fail, then, because neither they nor the suggested methods for fixing the issues take these factors into account. Targets, markers, and masks do not reduce reflection or translucency, nor do they account for size. A polarising filter often does not eliminate all reflective patches in a series of images and diffusers often create even larger reflective patches than the lights they are diffusing. To create viable models of SRT objects, then, we must work to reduce the effects of these issues in the images used to create the model.

6.2.3   ACCOUNTING FOR SIZE: PHOTOMACROGRAMMETRY

Many objects fail to render as viable 3D models because they take up too little space in the image for the software to process. There are two solutions to this problem, both of which have appeared in this chapter already: macro lenses and digital handheld microscopes (Chapter 6.1.3). In photogrammetry, macro lenses with shorter focal lengths work better because they reduce the required space between the object and the camera lens. I use an AF-S Nikkor 40mm Micro lens, but others also work.

For photomacrogrammetry, place the object on a blank, neutral background (preferably a white sheet of computer paper). It is surprisingly common to fail to capture images of small objects with enough overlap between them. To combat this, I have created a background with a range of equally-spaced markers surrounding a blank central area with a dot in the centre (Figure 6.20). The number of equally-spaced lines corresponds to the number of overlapping images desired per set camera angle; I use more rays for more intricately shaped SRT objects to ensure enough overlap. To make a reusable version, line the edges and corners with sellotape before affixing it to a table using tape or blu-tack. Objects were placed on the central dot to keep it centred and therefore equidistant from the camera as it moved around the template. All models I have attempted have benefitted from the use of these backgrounds.
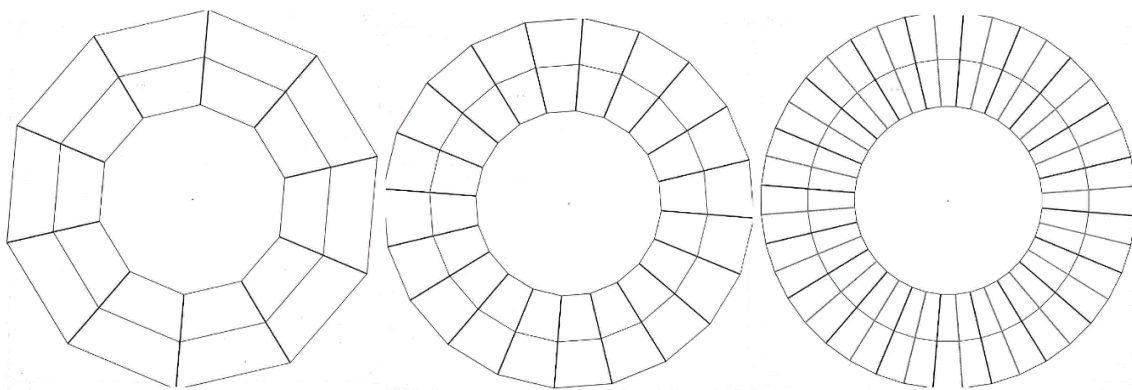
Figure 6.20: Possible backgrounds using 10, 20, and 40 rays.

The camera was affixed to a Gorillapod Hybrid flexible tripod (Joby 2018b), which allowed for stability and adjustments to the vertical angle while still fitting on a small table (Figure 6.21). Full size tripods generally keep the camera too far away from the object to produce high quality images of smaller objects. While a platform could be fashioned to raise the object to the desired level, the increased depth and complexity of the background of the image becomes more attractive for the software to align than the object, which results in failure similar to the models using targets or markers. Additionally, many platforms are not stable or contained enough to allow for unimpeded movement around the entire object without significant chance of collapse. Alternatively, freehand image capture (i.e. without a tripod) usually results either in fewer images taken than necessary or in large areas being omitted unintentionally. Flexible tripods provide stability and result in enough overlapping images for SfM photogrammetry, if following the pattern on the background above. They also allow for a wider range of adjustments in size and configuration than a standing tripod and are the most effective affordable option currently available.

Objects were lit with ambient lighting and an LED torch in most models. In experimenting with light placement, I found leaving the torch in the same location relative to the camera works well if placed directly next to the camera lens and facing the object straight on (Figure 6.22). If placed in an alternate location for the duration of the photoshoot, the changing shadows lead to the issues described earlier: the software appears to align the shadows before aligning the object, leading to problematic models. Interestingly, keeping the light source next to the camera does not produce similar issues of shadow alignment.
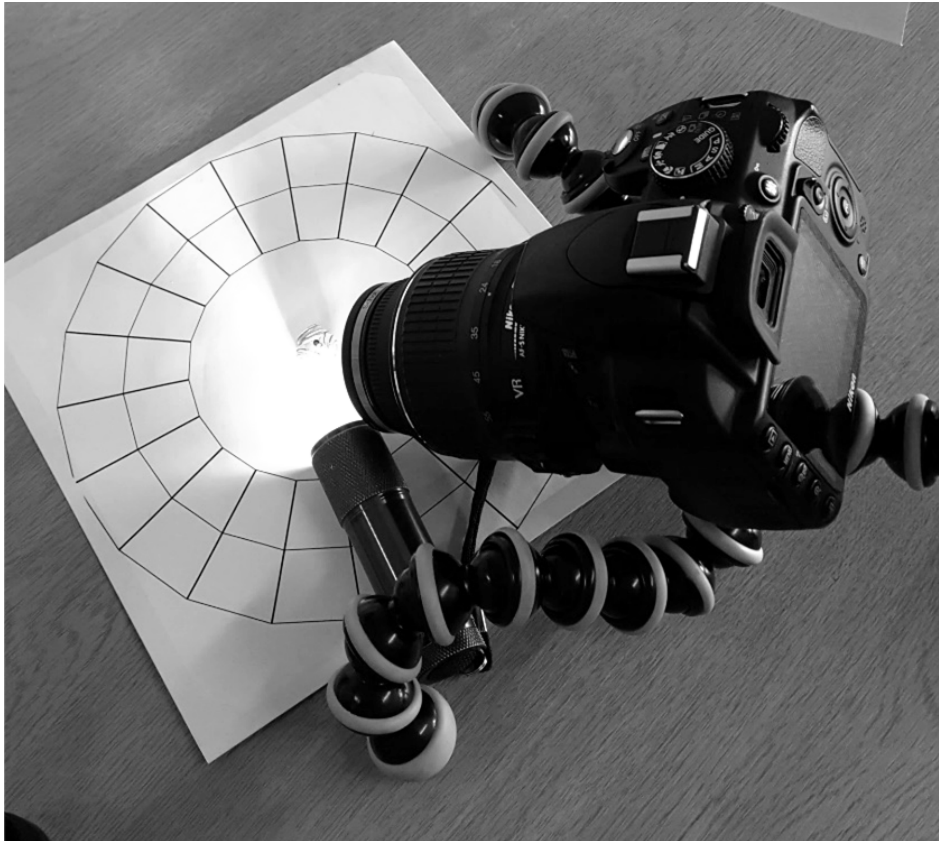
Figure 6.21: Set-up for photogrammetric imaging using a dSLR and a Gorillapod Hybrid tripod.

Figure 6.22: Placement of a focused light source during image capture.

I then placed the camera so that the bottom of the lens fell between two of the rayed lines forming the background (Figure 6.23). While lighting the object, ISO was set to 100 or 200 and aperture as high as possible while maintaining a shutter speed of 1 second or less to minimise capture time (i.e. between F16 and F30). Camera focus was set to automatic. While manual focus could help with certain objects, it rarely results in better images than those captured using automatic focus. If automatic focus did not provide the desired results, particularly given the issues with depth of field for macro lenses, I manually set the focus to just beyond the object's surface as described for photomacrographic RTI (Figure 6.6). A remote shutter was used to ensure the camera remained stationary during image capture. Any movement of the camera or object during the longer exposure times results in blurry images that do not work well for photogrammetry. All images were captured in raw format to allow for maximum data retention. I then repeated the process for each camera position on the template.

Figure 6.23: Placement of the camera lens in relation to the background.

After collecting 20 – 40 images for the first camera angle, the height of the camera was adjusted to be either taller or shorter and the circuit repeated until there were roughly

80 – 100 images for a single side of the object. This may seem like more images than needed, but a number of these images are always too unfocused for the software to process due to micromovements in the room. Taking 80 – 100 images per side of an object ensures there will be 60 – 80 images per side that the software could process. I finished capturing each side of the object by taking several freehand images, moving up and over the object from one side of the table to the other several times. This provided key areas of overlap that greatly assisted the alignment process.

I processed the captured images in Adobe Bridge, auto-adjusting the exposure and tone and setting white balance to the white area of the template background. Many programmes automatically set sharpness, grain, and noise above zero, which often negatively affects the 3D model. Reset these to the minimum amount (zero if possible) and save all images as .tiff or .png files. I then imported images into Agisoft Photoscan and estimated the image quality for each image, or the measurement of the focus of an image (Agisoft 2017, 15 – 16). Any images with an estimated quality less than 0.60 were disabled. Some graphics cards or hard drives do not have enough memory or RAM for processing models at the highest settings allowed by Agisoft Photoscan. I therefore aligned images using the highest settings my computer could handle, but I sometimes found lower quality settings produced a more complete model.

Once aligned, the point cloud was examined for accuracy and any non-relevant points were deleted, particularly those associated with the background. I then created a dense point cloud, again using settings as high quality as possible. Any non-relevant points were deleted either manually or through colour selection, then a mesh and texture created. If the alignment or quality of the model was unsatisfactory at any point in the process, I repeated the previous step using lower quality settings. This resulted in at least a section of the object that was well-aligned and formed a partial 3D model, if not a

complete one. It always resulted in a better model than that produced using standard methods.

6.2.4   ACCOUNTING FOR SIZE: PHOTOMICROGRAMMETRY

Some objects are too small to create viable 3D models using a macro lens. Many archaeological glass beads are less than 3mm in diameter, for example, and are too small to successfully model using a dSLR and macro lens. Having used microscopes for imaging beads in other ways, it was logical to try the technique to create photomicrogrammetric 3D models. There are a range of handheld microscopes on the market, but perhaps the most prominent are models sold by DinoLite. Each microscope is roughly 10cm long and works with a range of tripods. Most digital microscopes can capture digital images of an object between 10 and 220x magnification using visible light, though some use non-visible light or have increased magnifications.

I attached the microscope to a mount for a bicycle light and attached that to the foot of a Gorillapod Original tripod using blu-tack (Figure 6.24). The microscope plugs into the computer using a USB port and can view and capture images using the DinoCapture software. Focus was set manually by moving closer to or farther from the object, taking care to locate the point of focus just beyond the surface of the object (Chapter 6.1.3).
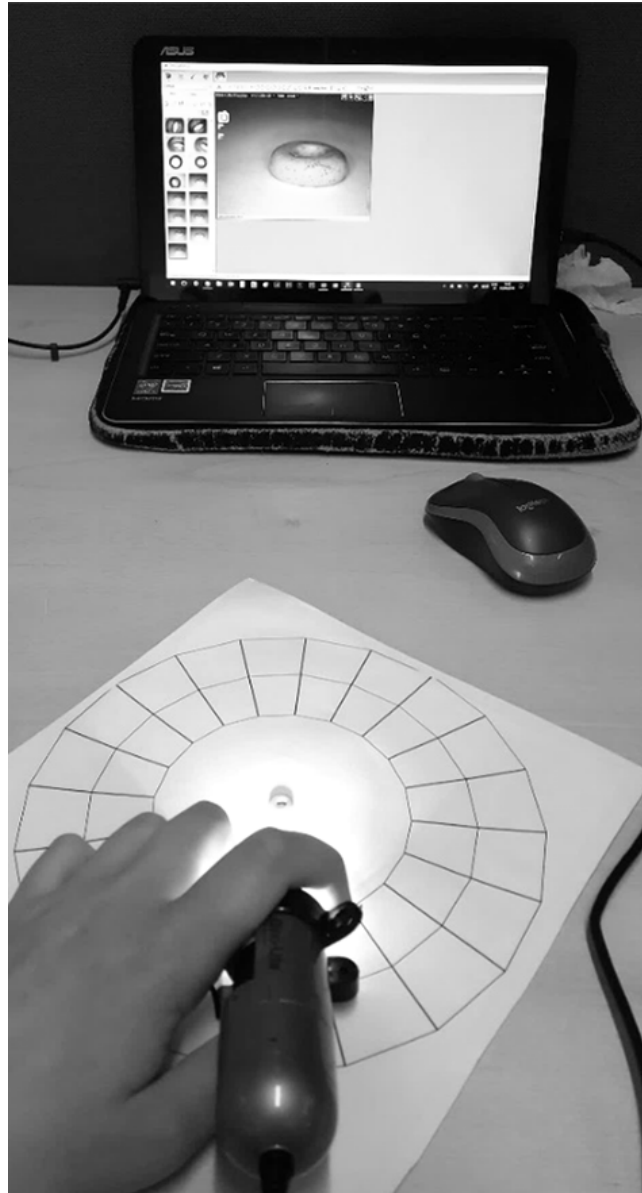
Figure 6.24: Set-up for photomicrogrammetry used in this study.

Image capture for photomicrogrammetry was similar to photomacrogrammetry and standard photogrammetry. Roughly 40 images were taken per circuit around the object, capturing as many overlapping angles as possible. Images were processed identically to photomacrogrammetry (Chapter 6.2.3). I have also found that combining images taken with the microscope and those taken with either standard or macro lenses often enhances the quality of the model. The images from the microscope provide detail to the general outlines in the macro images, thereby giving the software more data to use

when calculating camera and point locations. For some beads, such as a small early medieval triple bead from Glenshee, photomicrogrammetry was the only technique that created a functional model (Figure 6.25, Appendix E (PowerPoint Slide 9)).

Figure 6.25: Example of a photomicrographic 3D model of a small glass bead (3mm x 10mm) (Glenshee, NH Unknown #) (Appendix E).

6.2.5   ACCOUNTING FOR REFLECTION: LIGHT TENTS

For reflective objects, most patches of over-exposure can be eliminated by holding a sheet of paper between the object and the light source. Hold the paper far enough away that light can continue to reach the object; the paper merely serves as a large diffuser (Figure 6.26, top). If ambient lighting creates too many reflective patches or there are not enough hands available to hold the remote shutter, camera and piece of paper, a small light tent can be made out of computer paper and some tape (Figure 6.26, bottom). These tents can use black or grey paper to direct light in the desired manner as well. A portable light tent serves the same purpose but can be difficult to manoeuvre to adjust either the camera or the object to capture different angles.
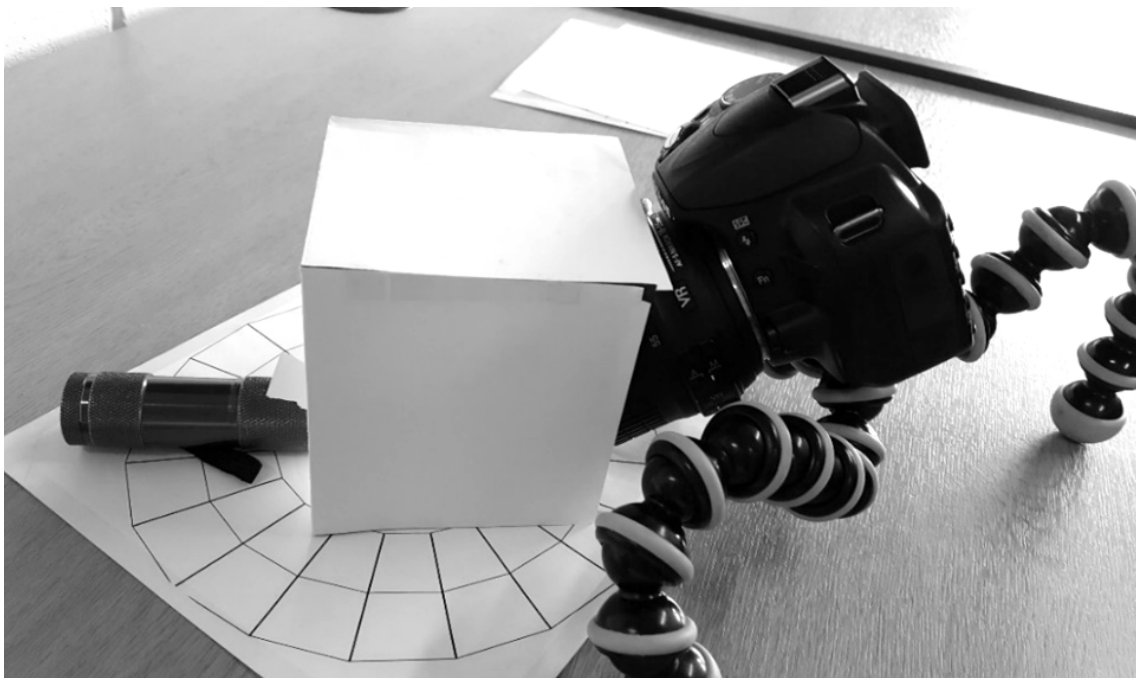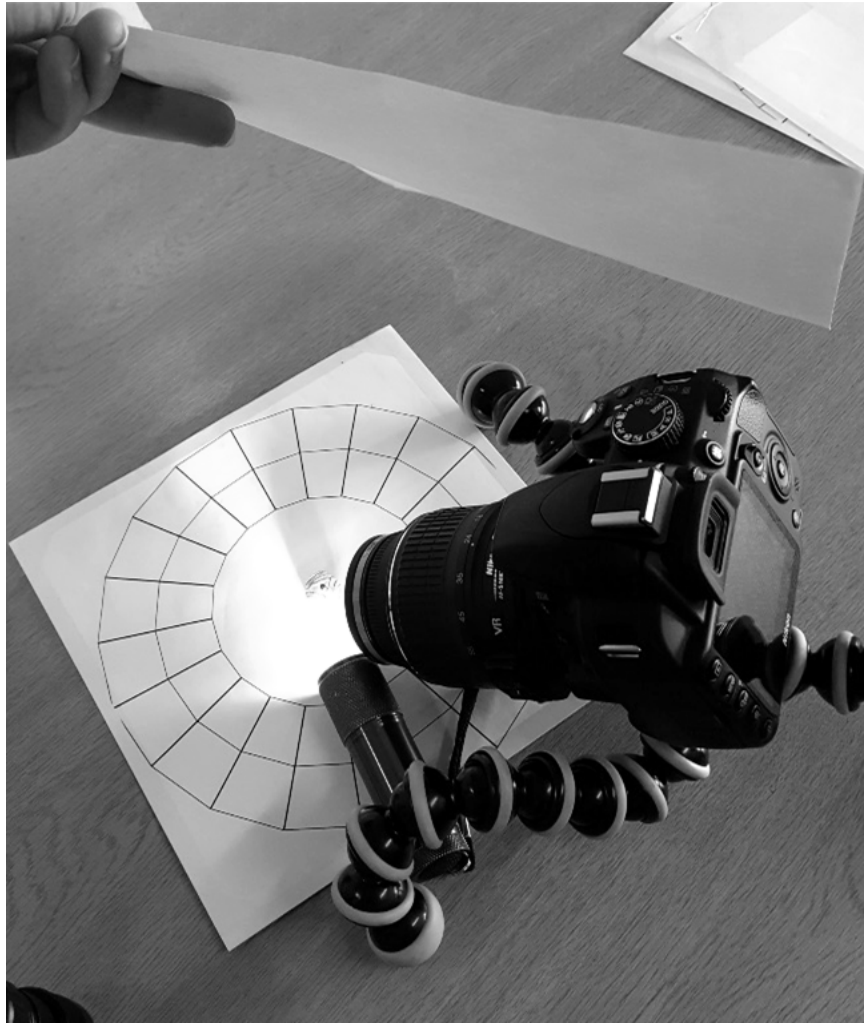
Figure 6.26: Using a sheet of paper (top) or a small paper 'tent' (bottom) to block reflections from ambient light.

When using these light tents, I rotated the tent with the camera as it moved around the object. Additionally, using white paper for at least the back of the tent ensured a neutral background for the software to analyse and minimised the contrast between the paper used as a base and the paper used as the back of the tent. A high contrast between the base and the light tent often led to confusion in the photogrammetric software.

6.2.6   ACCOUNTING FOR TRANSLUCENCY AND TRANSPARENCY: SPECTRAL PHOTOGRAMMETRY

Transparent or translucent objects are difficult to 3D model, because the software mistakenly assumes any element it can see within the bounds of the object is part of the object's surface. Translucent and transparent objects transmit at least some light, such that inclusions, bubbles, perforations and even other objects appear part of the object's surface. Because these elements do not behave like surface elements, the software cannot use them to accurately predict the locations of the cameras for each image and therefore cannot align a model of the object. Spectral photography can eliminate the transparency issue for many objects (Chapter 3.3 and 6.1.4). Spectral photogrammetry, then, is the creation of a 3D model using images filtered to specific wavelengths of visible or non-visible light.

There are several ways to create a spectral photogrammetric model, which largely depend on the desired wavelength of the images. Models using visible light (e.g. between 400 and 700nm) require images either captured or processed using visible-range filters. Capture the images as per the descriptions above (Chapter 6.2.3), and import them into Adobe Bridge, Lightroom, or other photo-editing software. I processed my images identically to the above sections, then applied the digital visible-range filter of my choice (Chapter 3.3). Save images as .png or .tiff and follow the same procedure for creating a model as described above (Chapter 6.2.3) (Figure 6.27, Appendix E).
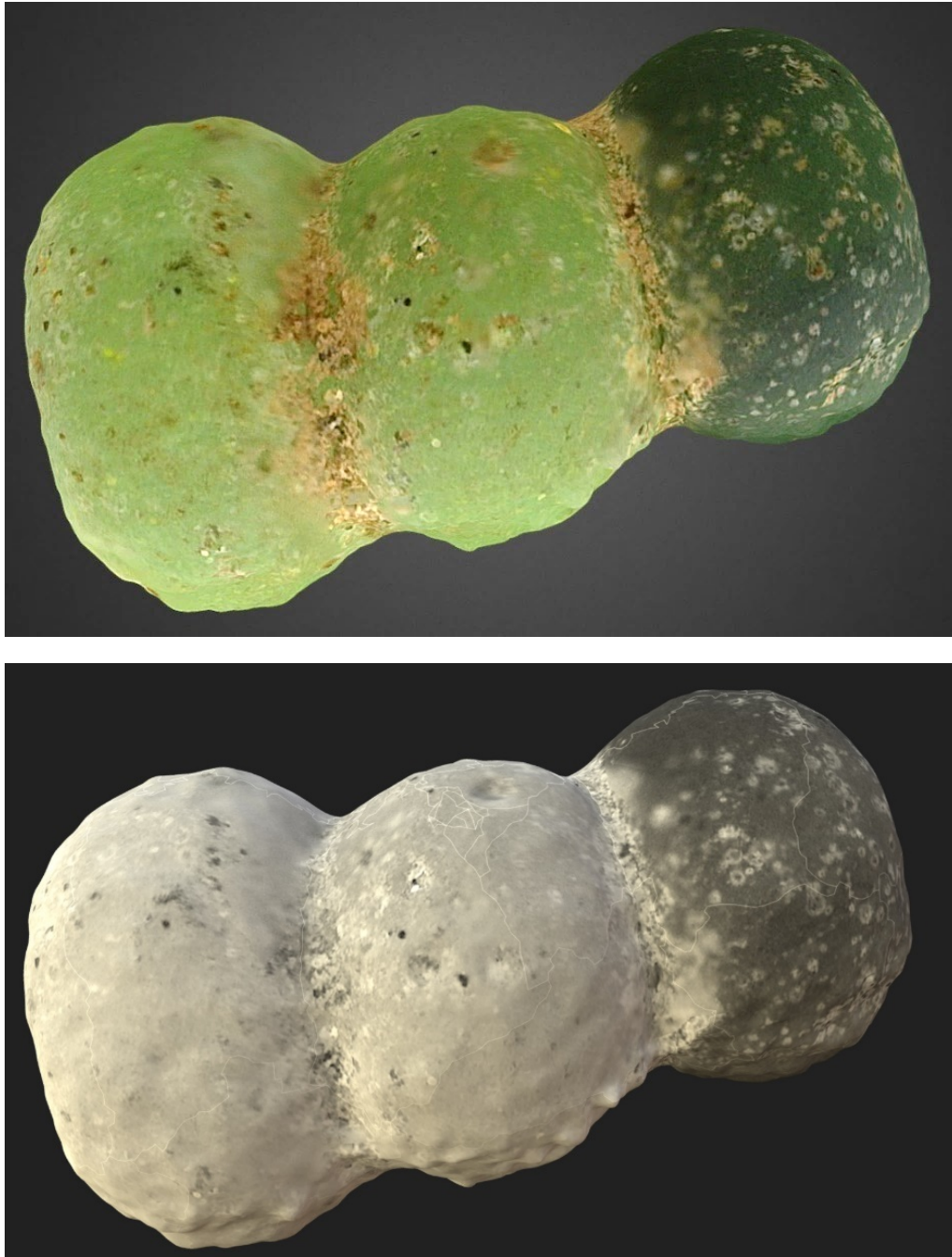
Figure 6.27: Results for standard (top) and visible-range spectral photogrammetry (bottom) of the same object
(Glenshee, NH no known number) (Appendix E).

It is possible to use non-visible light to create either a near-ultraviolet or a near-infrared photogrammetric 3D model. Infrared light has longer wavelengths and therefore penetrates further into the object, so any 3D model made with infrared images will render a model of the immediate sub-surface of the object rather than the surface itself (Figure

6.28, Appendix E (PowerPoint Slide 8)). Ultraviolet light has shorter wavelengths, however, and 3D models made with ultraviolet images capture the direct surface of the object. I therefore recommend ultraviolet photogrammetry, but not necessarily infrared. To create ultraviolet photogrammetric 3D models, I attached the appropriate filters to a fully converted camera. I used a UV-LED torch as a light source and captured and processed the images in a similar manner to standard images discussed in the above sections (Chapter 6.1.1 and 6.1.3).
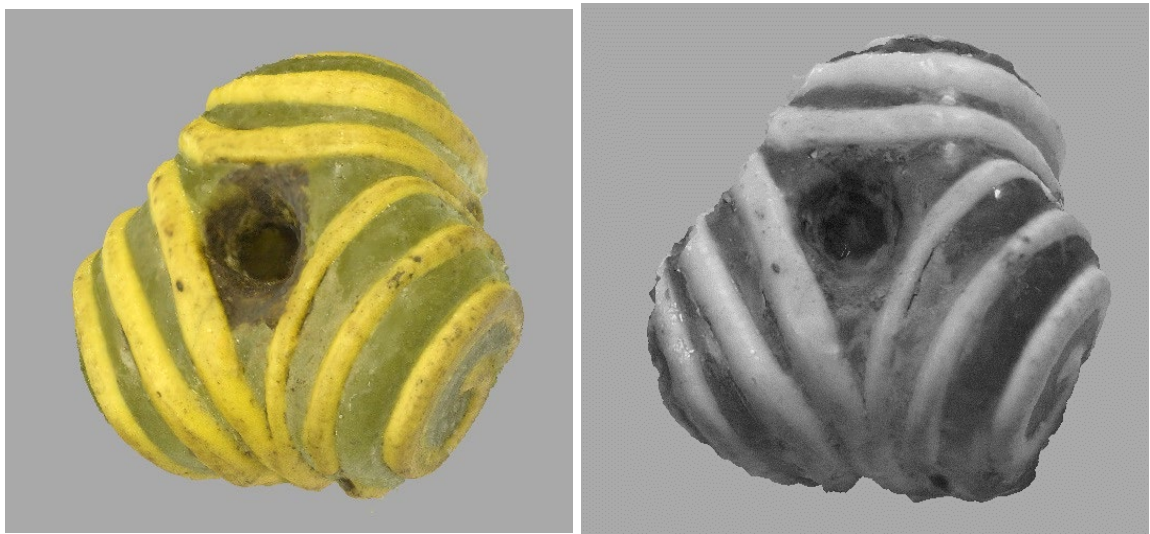
Figure 6.28: Results for standard (left) and infrared photogrammetry (right) of the same object (Loch Eriboll, UG F128) (Appendix E).

Note that this technique generally does not work for photomicrogrammetry unless using a specific microscope with ultraviolet or infrared lights and filters. My own had a transparent front cap that could not be removed. Placing a physical filter in front of the cap does not block all visible or infrared light from reaching the image sensor due to the space created by the cap. Even models with removable caps can be problematic, as they require holding the filter flush against the microscope lens to capture the ultraviolet image. This will likely either scratch the lens or let non-ultraviolet light through. Additionally, most microscopes are not built to capture non-visible light. I therefore

recommend avoiding ultraviolet or infrared photomicrogrammetry unless using a microscope that is built to capture non-visible light and either has or allows for the attachment of filters specific to that task.

Spectral photogrammetry allows for modelling of SRT objects that otherwise fail to produce viable models, like glass beads, precious and semi-precious stone or metal objects like coins or brooches. It also allows for the modelling of object elements that may not be visible to the naked eye, such as surface wear or inclusions. It allows for 3D modelling objects using false-colour images (Pilarska 2016), but this requires taking multiple individual images from the same angle and significantly increasing processing time for similar amounts of information to that given in a photograph. At the very least, however spectral photogrammetry allows us to create functional 3D models of objects that otherwise resist such efforts.

6.2.7   MODELLING ALL SIDES OF AN OBJECT

One problem that results not from reflective or translucent materials, but from modelling objects like beads is that specialists, myself included, would like to capture all sides of the object in a continuous model. This is unusual for many archaeological 3D models. A building sits on the ground, as do standing stones. The general landscape *is* the ground. Even models of excavated trenches only capture the side facing the excavator, not anything behind or below it. There is often at least one side that we omit from the model, giving the model a 'back' or 'bottom.' Objects often do not have an undesirable side. Some have a distinct 'bottom', but there are often markings or other important elements on the bottom of these objects. One difficulty in modelling objects, then, is to capture all possible sides of it to create a single, continuous 3D model.
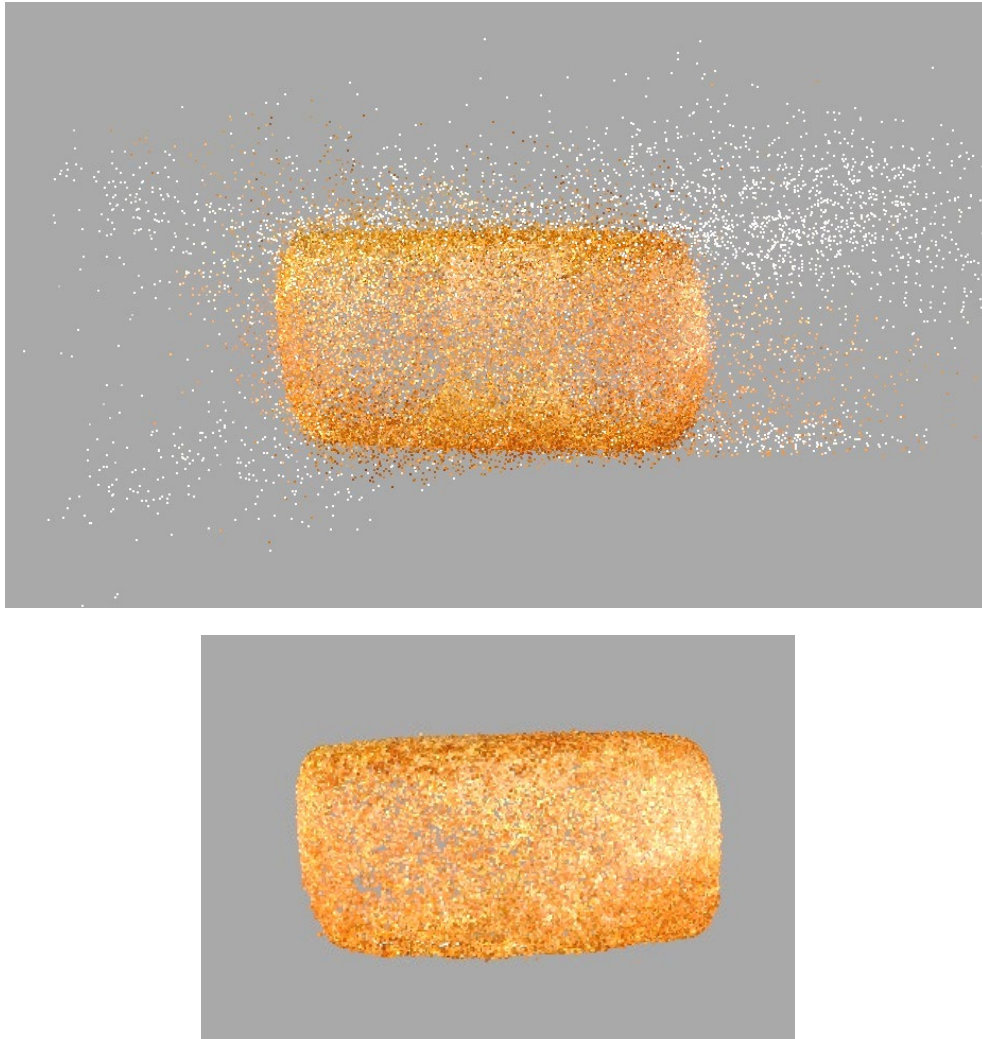
Figure 6.29: A point cloud showing two sheets of paper before (top) and after processing (bottom) (Culbin Sands, NMS X.BIB 27) (Appendix E).

In trying to create a model of a full bead capturing all sides of the object, I first attempted the simplest technique I could: flipping the object over and repeating the process. Contrary to current photogrammetric wisdom, this technique works. So long as enough images capture the overlap between one side and the next and so long as the specialist has photographed the object on a non-decorated, non-descript neutral background, the software appears to favour aligning the object over the background. The resulting point cloud will contain traces of two sheets of white paper in it – one on the 'top' and another on the 'bottom' – which can be deleted through colour selection before

processing the model further (Figure 6.29, Appendix E). This results in a complete three-dimensional model without holes.

6.2.8   FAILED PHOTOGRAMMETRIC MODELS
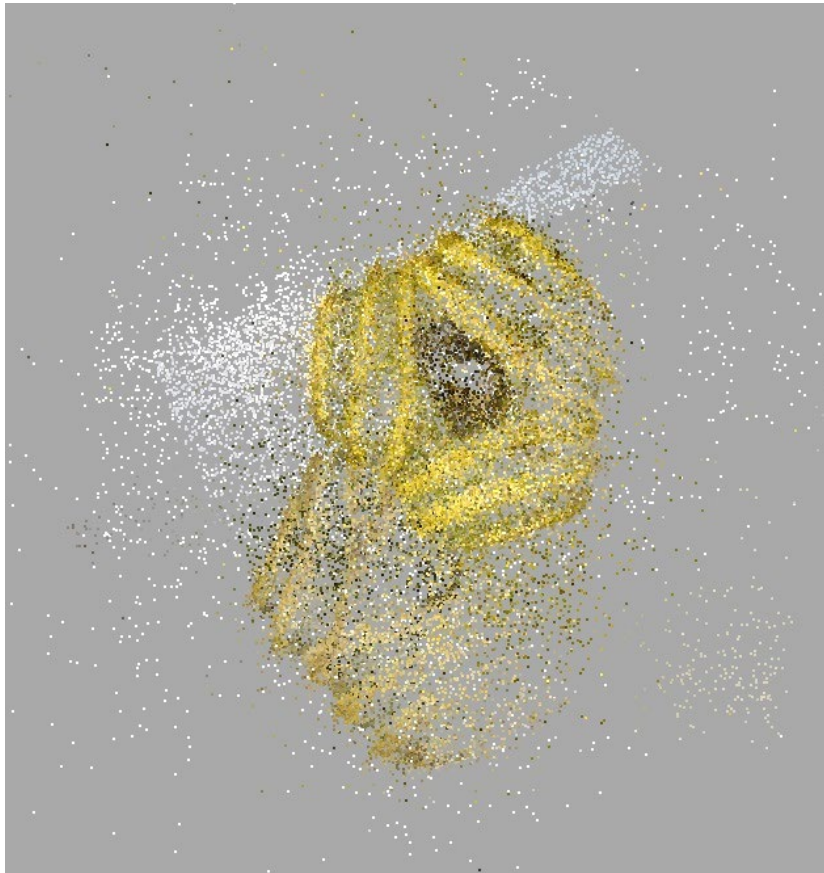
Figure 6.30: Example of a failed model in which two of the same object appear (Loch Eriboll UG F128) (Appendix E).

There are some standard ways in which these models fail, most of which we can fix through troubleshooting. First, a point cloud of aligned images shows what appears to be two of the same object, usually close together and possibly connected (Figure 6.30, Appendix E). This results from a misalignment between sides of the object due to a lack of overlapping images between the sides. To remedy it, I process each side as separate chunks in Photoscan, then align and merge them together. If this fails, there are not enough overlapping images between the sides for the software to join the two. In this case, either take more images of the areas common to both sides or bring both meshes

into another modelling software (such as Blender or MeshLab) and align them manually (Chapter 7.3). Depending on the software and technique used to manually align and merge the chunks, creating a photorealistic texture for them may not be possible afterwards. It is better to take more photographs of the problem areas, if possible, than to manually align and merge chunks.

Another common failed model is one in which the cameras all align in a single location rather than a dome, and the points stretch from the cameras to the far reaches of the workspace, usually in a linear fashion (Figure 6.31, Appendix E). This often occurs when only a few images can align or when the object has moved between images, rather than the camera. In either case, there is not enough overlap between both horizontal and vertical camera angles to align anything. We can solve this either by taking more images to cover the entire object or by taking entirely new images using a less discernible background. I have found that a blank sheet of computer paper works well; even most white tables have a texture that the software finds more interesting and align-able than many objects.
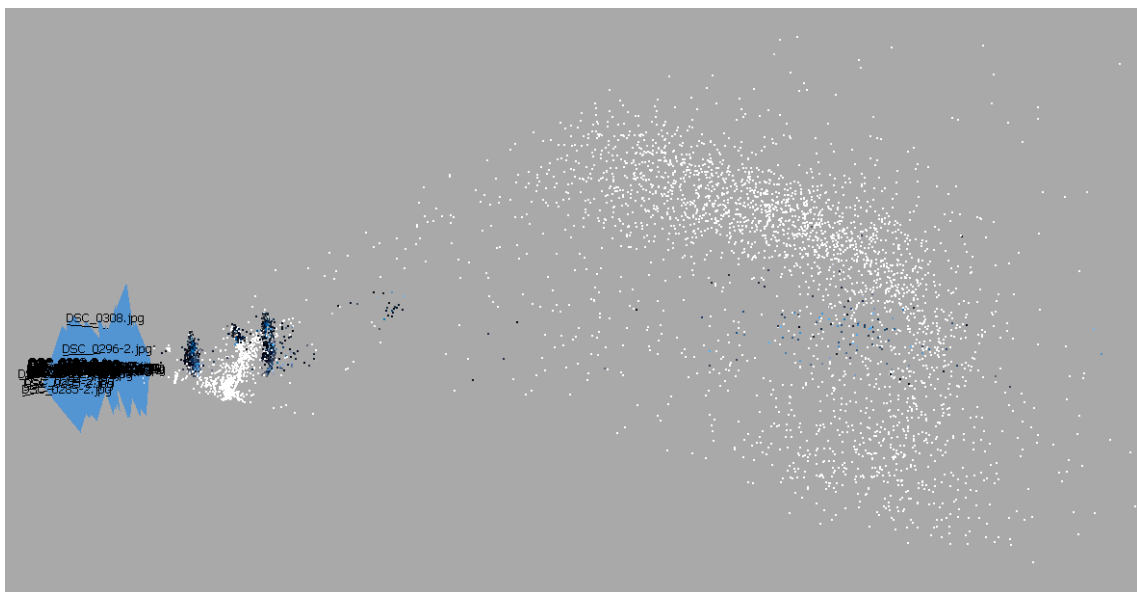
Figure 6.31: Example of failed model (UG SF 15021) in which cameras align in the same location and points stretch from there outwards (Appendix E).

Some models align the cameras properly and create what appears to be a useful point cloud, but do not include any points for the object itself. Instead, there is a large, gaping hole where the object should be (Figure 6.32, Appendix E). In this case, the object occupies too small an area within the image for the software to find useful details, the background may be too discernible to the software for the object to register, or both factors may be at play. To solve this, either zoom in closer to the object or use a different lens (Chapters 6.2.3 and 6.2.4) and place the object on a non-descript background.
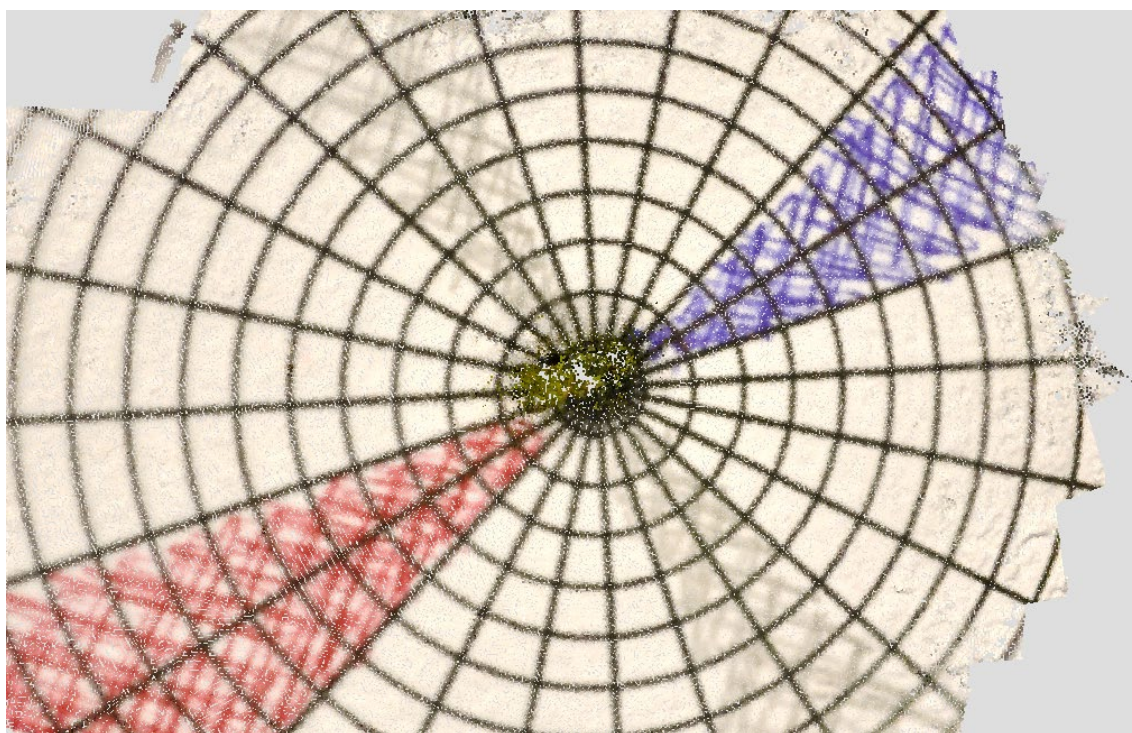
Figure 6.32: Example of an early attempt at coloured targets for modelling glass beads in which the cameras modelled everything but the desired object (Glenshee, NH no known number) (Appendix E).

Unfortunately, there are objects for which none of these techniques will work, and which continue to elude effective visual representation in the archaeological record (Figure 6.33, Appendix E (PowerPoint Slide 14)). It may be possible to create 3D models of these objects using more sophisticated equipment, such as better cameras or lenses, a higher quality microscope, or by altering the algorithm used by photogrammetric software. CT scanning or confocal laser scanning microscopy would create viable 3D

models of these objects or, but these techniques are prohibitively expensive for many projects (Chapter 8). Scientific x-ray computed tomography also requires different machinery to medical x-ray computed tomography, thus pushing both the monetary and logistical cost even higher. However, the techniques described in this chapter vastly improve upon any 3D modelling results for the objects and generally result in highly successful models of objects for which the industry often labels 3D modelling as impossible. Additionally, even failed models lead to the creation of 60 – 80 high quality images taken from as many overlapping angles as possible. This still yields 60 – 80 more images than currently exist for these objects, thereby often creating and vastly improving the existing visual record of these finds.

Figure 6.33: Example of a model that currently fails regardless of the adjustments made to the images or the process (Glenluce Sands, NMS X.BHB 20.4) (Appendix E).

6.3   THE USEFULNESS OF RTI ON ARCHAEOLOGICAL FINDS

This chapter has discussed several methods for creating viable SfM photogrammetric 3D models and PTM RTI of SRT objects, with a focus on glass beads. Yet, our ability to create these visualisations does not make them automatically useful for analysis (Chapter 2.2). Most archaeological finds research has never exploited reflectance transformation imaging, in large part because it is a relatively new technology and because many small finds are notoriously difficult to photograph in general, let alone for RTI purposes. When successful, RTI can provide a range of useful information for archaeological finds, particularly regarding surface wear. Studies of surface wear are rare for objects made from reflective or translucent materials largely due to the difficulty of visually analysing wear on such materials. For example, most publications for surface wear on ancient glass centre predominantly around use-wear on knapped glass implements in 19th century African American, Argentinian and Aboriginal Australian contexts which, while valuable, is linked more closely to the extensive studies of use wear on lithics than to that of more common glass objects (Clemente Conte and Goméz Romero 2008; Harrison 2000; Ulm et al. 2009; Wilkie 1996). Further examination of the varied applications of spectral RTI likely would lead to significantly more information for glass or other objects made of translucent or transparent materials, such as amber, semiprecious stones, or bone.

Many low-budget projects or research groups do not have access to scanning electron microscopes or other more technical tools that help significantly with surface wear analysis. Yet, spectral RTI eliminates issues surrounding reflectance and translucency or transparency and allows for the manipulation of both light and surface features to emphasise any surface wear that may exist. Spectral RTI would serve as a

highly affordable and practical technique for gathering large quantities of data for surface wear on any material, particularly those found and examined by low-budget projects.

6.4 THE USEFULNESS OF PHOTOGRAMMETRY FOR ARCHAEOLOGICAL FINDS

The usefulness of photogrammetric models for small finds is less clear, in part because of the difficult nature of the materials these objects are made of and in part because the possible uses of photogrammetry vary widely. One large benefit is the ability to create models for objects that are otherwise inaccessible, such as those in remote collections or locations or those which have since deteriorated or been misplaced (e.g. Rekrei 2018). Large numbers of archaeological finds are housed in remote locations and cannot leave their country of origin. Many of these objects are small, reflective, translucent or transparent. Photogrammetric models provide a visual representation of these objects which allow scholars to examine them virtually from afar.

However, making models simply to document an object in 3D is the same as the documentary photography we already limit ourselves to in archaeology. Such documentary imaging is not without purpose in archaeology, but it is not the totality of what can be achieved with 3D modelling. We can use these models to examine surface features of an object in more detail, for example, or to engage with the general public. We cannot incorporate accurate models of individual SRT objects into virtual or augmented reality if we cannot model them. The techniques described here allow us to create models of specific finds that we can incorporate into various VR and AR engagement tools and that we can 3D print. This allows the objects to serve as the best representation of themselves, rather than a model created by hand or using a template.

Unfortunately, photogrammetric models of SRT objects can be difficult to produce even with the techniques described above. Images do not align, the texture fails, there are holes in the mesh or there is less detail than desired. Creating a single model requires time to capture upwards of 100 images at low shutter speeds and the software often fails to create an accurate model on the first attempt. There is usually some troubleshooting involved, and what works for one object does not necessarily work for another. While I listed several possible problems and their solutions above, many models suffer from more than one, and it is difficult to know which method will fix them. There are also many objects for which none of the available troubleshooting methods work. Similarly, there are many objects for which the model, while successful, provides similar information to that provided by a few good photographs. Given the time and effort needed to create a 3D model, especially one that often either does not provide any more information than a few photographs or one which does not work at all, photogrammetric 3D modelling of archaeological SRT objects may not be worth the effort without specific research questions or outreach ideas in mind.

This does not mean that photogrammetric 3D modelling of archaeological objects is never useful or worthwhile. Rather, it means the benefits of and uses for the output must be worth the time, effort, and funds expended to create it. Many of the current difficulties encountered in accessing information about the objects discussed above, like glass beads, stems from a general lack of informative images of these objects, which in turn results from the difficulties associated with imaging SRT objects. Once we solve the issues surrounding the photography of these objects, these photographs tend to provide similar amounts of information to photogrammetric 3D models of glass beads. Thus, photogrammetric models of archaeological finds can be of great use, but we should always consider whether we can acquire the same information using more efficient

methods like photography. Otherwise, we begin to fall into the fetishism of the new, or the use of new technology for the sake of using new technology.

6.5   SPECTRAL RTI AND PHOTOGRAMMETRY IN ARCHAEOLOGY

According to conventional methods, RTI and photogrammetry of many SRT objects will result in problematic models at best, with the recommendation of most specialists limited to a single word: "Don't." However, this chapter demonstrates that it is possible to create informative, successful photogrammetric 3D models and viable RTI polynomial texture maps of SRT objects. While there are still objects that elude successful photogrammetric modelling, these methods significantly improve the chances of creating informative visualisations. Additionally, I have not found a single object for which the RTI techniques discussed in this chapter fail to produce a viable and informative polynomial texture map.

These techniques were successful because this research does not follow the standard techniques in archaeological imaging. However, there are thousands of archaeological finds in Scotland are small or reflective or translucent that we would omit from the visual record if we continue to use current techniques. This lack of imagery reduces the role of these objects in or even eliminates them from our understanding of the past.

Inevitably, when this point is voiced to colleagues, some insist I could acquire detailed results either by using their personal equipment of choice or by developing my own software. When the issue of expense is raised, they often suggest that if I know the right people, I can access these high-cost services at a more affordable rate. However, most projects cannot afford highly technical solutions or hiring someone to create project-specific software, and we cannot class 'knowing the right people' as a sustainable or

effective plan for research development. Our reluctance to question the standards of digital and archaeological imaging and our emphasis on new technologies either assumes all projects have the budgets to afford such things or reflects a field which is unconcerned about the loss of information resulting from a lack of funds for such analysis. The notion that knowing the correct people makes a technique affordable and our failure to develop or experiment with affordable means of creating informative visualisations of archaeological subjects ignores the reality of most archaeological projects worldwide.

In this chapter, I have proposed new RTI and photogrammetry methodologies that allow for a marked increase in the success of these techniques on SRT objects. The alterations proposed for RTI have not produced any failed attempts, while those proposed for photogrammetry have yielded significant improvements. There are many applications for which even partially successful RTI or photogrammetric models of SRT objects are essential, including studies of surface wear, the ability to 3D print objects for use in classrooms and communities worldwide, and the inclusion of specific object models in VR and AR experiences. These results therefore improve the applicability and results of these techniques in archaeological imaging significantly, particularly that of archaeological small finds.

None of the techniques developed here are unusual. They stem from examining the problem of photographing glass beads and mitigating those problems while maintaining the information required for RTI and photogrammetry. The primary difference between this and conventional troubleshooting techniques is that I ignored the conventionally understood limits of what these technologies could do and how we could exploit them to get at the desired result or information. The true innovation of this research therefore lies in changing our approach to digital imaging, in understanding the

technologies we use to their fullest extent and manipulating the boundaries of those

technologies to uncover new methods and information.

7   CASE STUDY 4: WIDER APPLICATIONS OF ARCHAEOLOGICAL SPECTRAL IMAGING

The previous chapters focused heavily on the uses of spectral imaging for glass objects, particularly glass beads. These are not the only objects that benefit from these techniques, however, and they result in equally informative visual representations of faience, amber, copper-alloy, gold, silver, glazed and unglazed ceramic, and lithic finds as well as stone sculpture, landscapes, archaeological trenches, and stratigraphic sections. These techniques also succeed in imaging a variety of archaeological finds, including beads, brooches, figurines, moulds, potsherds, vessel sherds, and flint debris. Some techniques work better for certain subjects and materials than others, but they all provide new information and valuable visual records of the subjects. This chapter demonstrates the value of spectral imaging for subjects other than archaeological glass beads.

7.1   STRATIGRAPHIC IDENTIFICATION

Spectral imaging of the north-facing section of Trench A (HY17A) at Cnoc nan Càrnan, Iona (Figure 7.1) has helped to identify differences between certain stratigraphic layers that were not visible in section, not recorded through drawings nor seen in images using the full visible range (Figure 7.2, top, Appendix E (PowerPoint Slide 13)). Cnoc nan Càrnan is a rocky knoll to the west of Iona Abbey, St. Columba's famous monastery founded in AD 563 (Campbell and MacIver 2017, 11). It forms part of the vallum, or enclosing banks and ditches of the monastery, and was excavated by Thomas in 1956 and again by Campbell and MacIver in 2017 (2017, 11). While digging in 2017, Campbell and MacIver suspected there was a palisade posthole at the eastern end of the north-facing section due to perceived texture differences in the soil, but they could not see a visible difference in section (Campbell 2018b). Having observed the benefits of spectral

photography for archaeological objects, we decided to apply it to the trench section. After imaging the section using near-infrared, visible, and near-ultraviolet light, the area suspected of being a palisade posthole appeared visibly different from the surrounding soil (Figure 7.2, bottom, Appendix E (PowerPoint Slide 13)).
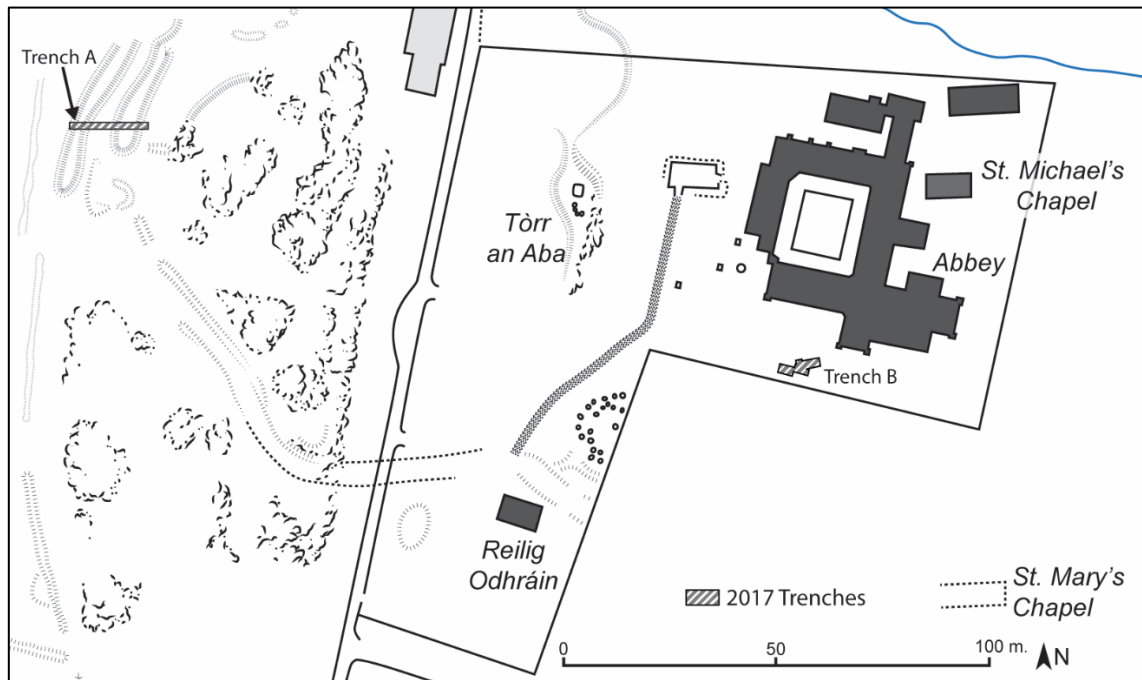
Figure 7.1: Location of trenches A and B, Iona excavations 2017 (base map derived from RCAHMS 1982).

Another outcome of spectral imaging at Iona was the classification of specific dark layers within the stratigraphy. The south-facing section of Trench B from the 2017 excavations (HY17B) contained a darker layer (208) rich with secondary deposits of charcoal, slag, and iron-working waste (Campbell and MacIver 2017, 31). This layer was deposited against the edge of a stone structure and dates to the 7th – 8th centuries AD (Campbell 2018b). When imaged with non-visible-range filters, (208) reflected significantly more ultraviolet light than the surrounding layers, rendering as a deep blue band in the resulting false colour image (Figure 7.3, right; Appendix E (PowerPoint Slide 13)). In Trench A the darker soils (105, 109, 116) contained organic material instead (Campbell and MacIver 2017, 19). These layers reflected more infrared light, which resulted in red bands when rendered as a false colour image (Figure 7.2, bottom;

Appendix E (PowerPoint Slide 13)). The difference in the contents of these darker layers

is clear in these trenches because both contained clear evidence of either ironworking

debris or organic material, but these results indicate the potential for using spectral

imaging to identify the presence or absence of characteristics like metalworking debris or

organic material in contexts where their survival is less certain.

Figure 7.2: Comparison of a visible-range image (top) and a false-colour image using near-infrared, visible, and near-ultraviolet light (bottom) of the north-facing section of Trench A, Cnoc nan Càrnan, Iona (Appendix E). Arrow indicates possible palisade posthole.
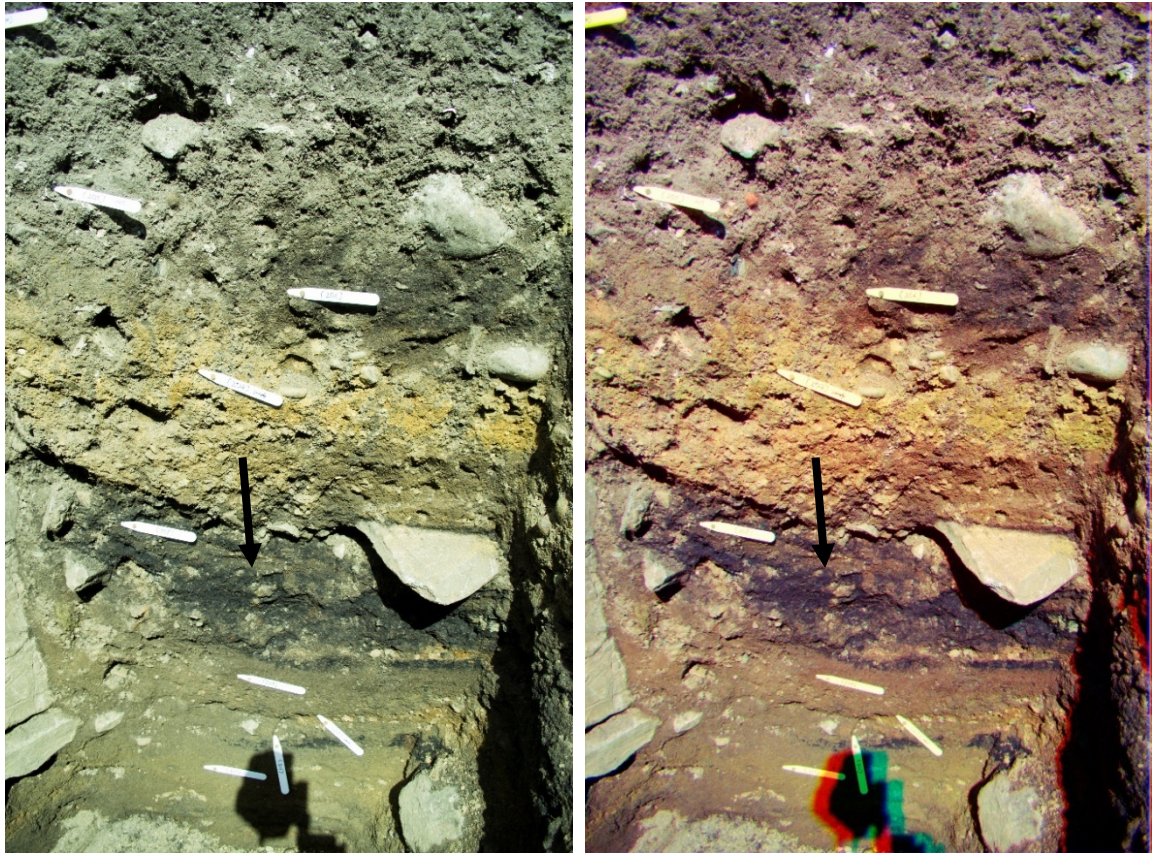
Figure 7.3: Visible-range (left) and false-colour images using near-infrared, visible, and near-ultraviolet light (right) of the south-facing section of Trench B, Iona Abbey (Appendix E). Arrows indicate layer with metalworking debris (208).

Additionally, the high reflectance of infrared light from buried organic material in Trench A suggests potential for understanding the relationship between vegetal decay and its reaction to light. Vegetation is highly reflective of infrared light when living, and the degree to which different plants reflect the light helps ecologists determine both the type and general health of the subjects. However, I have been unable to find significant literature on buried organic material and its spectral reactions. Much of the organic material from Trench A formed the basal layers of the original deposit in the vallum, which dates to the late 6th to early 7th centuries AD (Campbell and MacIver 2017, 18 – 21). For it to continue having a clear spectral reaction after many centuries underground is important both for being able to identify organic material in archaeological contexts and for understanding the relationship between near-infrared reflectance and plant decay.
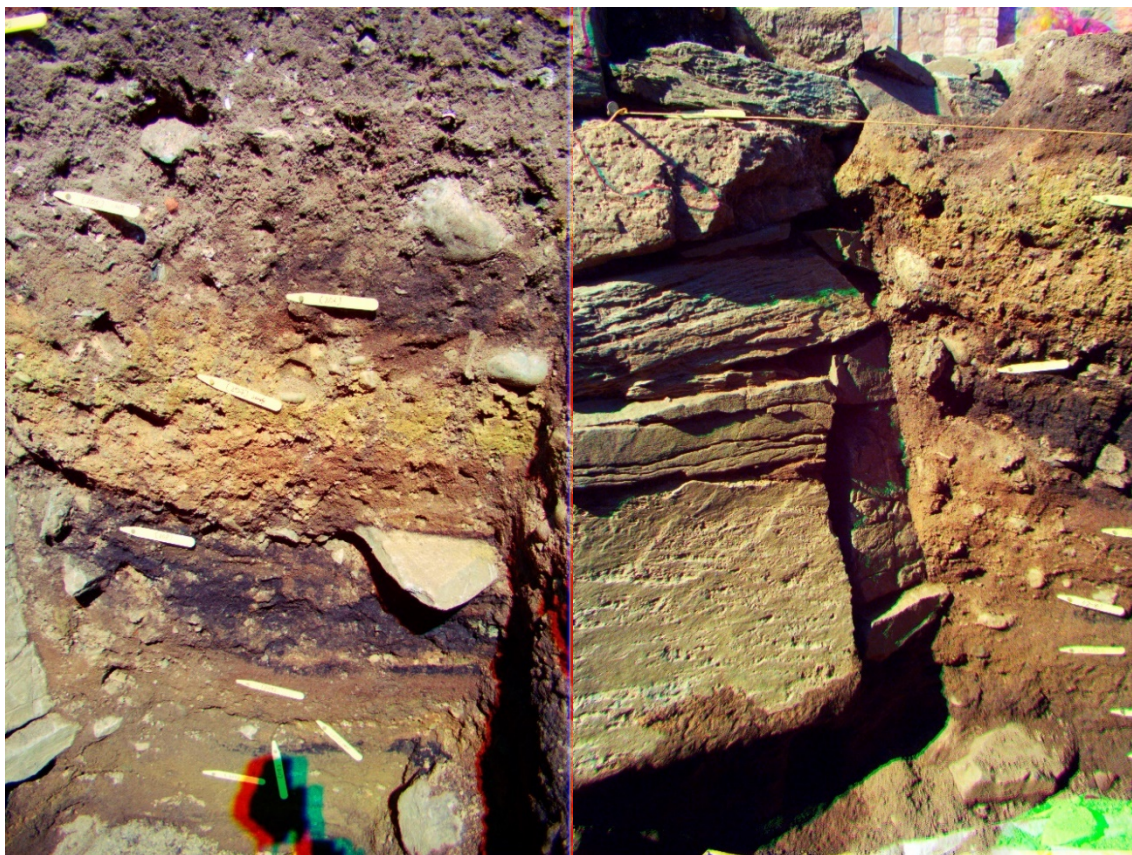
Figure 7.4: False colour images from 2017 (left) and 2018 (right) of the south-facing section of Trench B, Iona Abbey (Appendix E).

A final insight resulting from the spectral imaging of trench sections arose after returning to Iona for a second season of excavation and spectrally imaging the stratigraphic section near the wall again. Despite employing the same capture and processing techniques, the resulting images were not quite the same (Figure 7.4, Appendix E). While these images capture the section at two different angles, the images taken in 2018 have more visible and less ultraviolet light in them than the images taken in 2017. The only differences are the angle of the camera and the time of day during capture. The first set of images was captured around 14:00 on 18 May 2017 and the second around 16:30 on 12 May 2018. The weather on these days was relatively similar: sunny, mild spring days with a slight breeze. The earth's atmosphere blocks much of the sun's UV rays, however, and they are strongest between the hours of 10:00 and 16:00. Since I was

using sunlight for a light source, waiting to capture the second images until after 16:00 likely led to the observed difference between the images. I therefore recommend that any images captured outside use similar weather conditions at similar times of the year and similar time of day to minimise the differences caused by natural forces.

Thus, spectral photography need not be limited to objects; it can work equally well for landscape or site photography. Spectral photography and false colour imaging allow for the identification of soil types and for the potential to identify or confirm the presence of features that are invisible to the human eye. More research into the reactions of soil inclusions to light, such as metalworking debris or organic material, would provide valuable insight into the further applications of this technique and make it a valuable tool in field archaeology.

7.2 CHEMICAL DIFFERENCES IN COPPER-ALLOY, GLAZED, AND CERAMIC OBJECTS

In addition to trench sections, I also spectrally imaged two copper-alloy pieces from Iona: a small lion mount (SF 0997; Figure 7.5, top; Appendix E) and an even smaller human head (SF 0962, Figure 7.5, bottom; Appendix E), possibly from a reliquary shrine (Campbell and Maldonado 2016, 86 – 87). Both objects are currently on display at the Iona Abbey Museum. The lion mount was found in a pit to the north of the Reilig Odhráin in 1959 (Campbell and Maldonado 2016, 77). It has possible parallels to lions in the *Book of Kells* and to an 8th – 9th century hanging bowl mount found in Gausel, Norway (Campbell and Maldonado 2016, 86). The head was uncovered to the west of the Street of the Dead and shows possible similarities to 12th century Norse-influenced metalwork like St. Manchan's Shrine (Campbell and Maldonado 2016, 87).

Figure 7.5: Visible range and false-colour images of the Iona lion (top) and head (bottom) copper-alloy pieces (IAM, SF 0997 and SF 0962 respectively) (Appendix E).

Both objects were spectrally imaged in near-ultraviolet, visible, and near-infrared light and analysed as per the technique used for glass objects in Chapter 5 (Figure 7.5, Appendix E). Previous chemical testing indicates the lion is 23% copper, 45% tin, and 17% lead, while the head is 65% copper, 24% tin, and only 2% lead (Campbell 2018a). Spectrally, the lion and head have nearly identical results for infrared (118 and 117 respectively), but they differ in their reflectance of ultraviolet light (lion: 67; head: 82). It is unlikely that this difference is due to photographic factors, since both objects were imaged at the same time in the same location with identical techniques and conditions. Metals often are highly reflective of infrared light, but they can differ significantly in their reflectance of ultraviolet (Paquin 1995, 35.28 – 35.41). The higher reflectance of ultraviolet by the head figurine likely results from the difference in the percentage of

copper, tin, and lead within the metal. The difference in ultraviolet reflectance may be more a product of higher copper concentrations in the head than the lion. Referring to the glass data in Chapter 5, we also see that the beads most reflective of ultraviolet light tend to be those colours traditionally associated with copper, but the lack of chemical testing for these objects prevents further insight into this possibility.

In addition to the copper-alloy pieces, I spectrally imaged 31 glazed and unglazed ceramics recovered during the 2018 excavations at Iona Abbey. These represented a range of ceramics, but most samples were medieval green glazed white gritty wear coming from Trench B mentioned above (Figure 7.1) and Trench D, located in the field directly to the south of the Abbey. The ceramic data form two distinct clusters when charting their near-infrared and near-ultraviolet metrics in a scatter plot (Figure 7.6). The first cluster consists of samples with infrared measurements less than 130 and ultraviolet measurements less than 60, while the second has infrared measurements higher than 150 and ultraviolet measurements between 35 and 110. Interestingly, these clusters do not correspond to the general colour of the ceramic (Figure 7.7). Instead, they likely show a separate chemical difference in the samples that would become clear upon further testing.
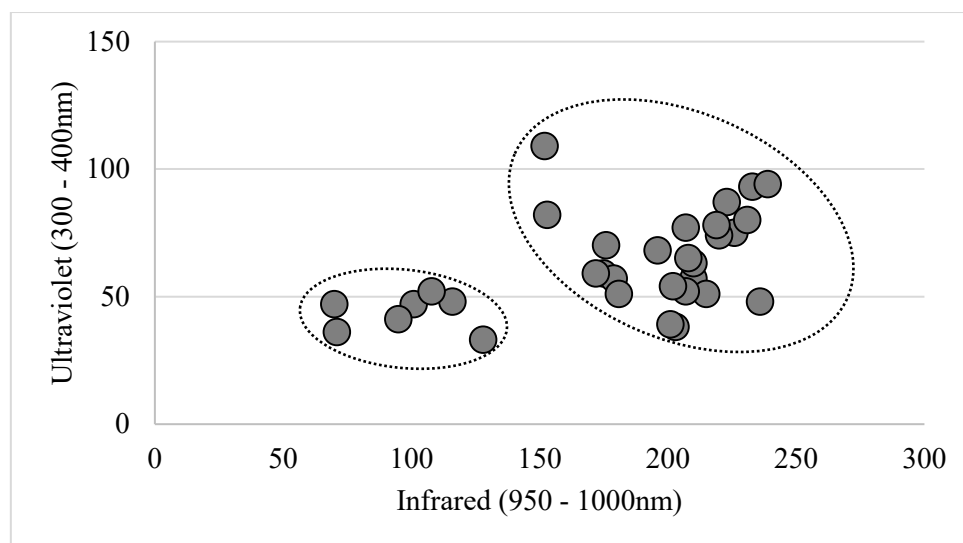
Figure 7.6: Near-ultraviolet and near-infrared reflectance data for medieval ceramic samples from the 2018 excavations on Iona with Cluster 1 (left) and Cluster 2 (right) highlighted.
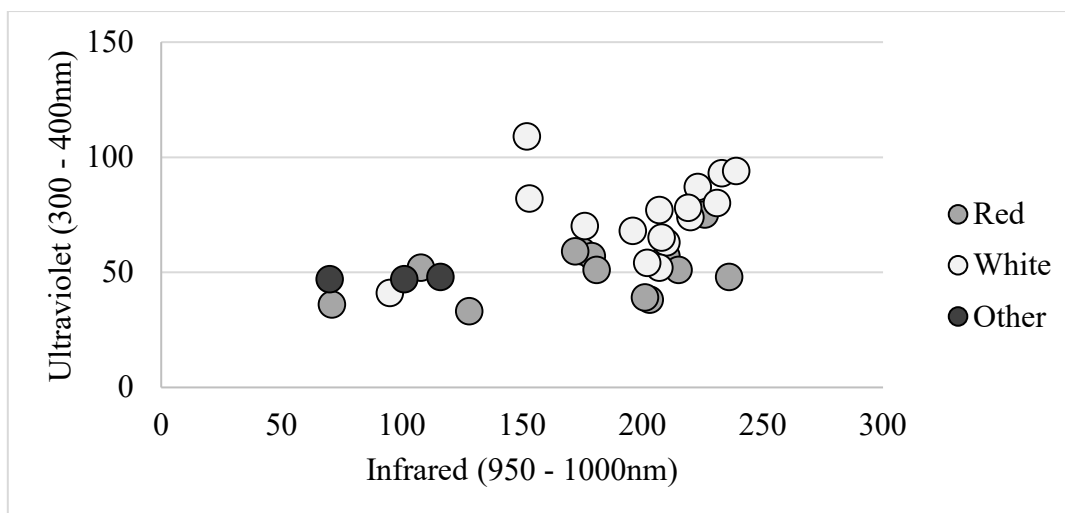
Figure 7.7: Iona samples separated by colour of the base ceramic.
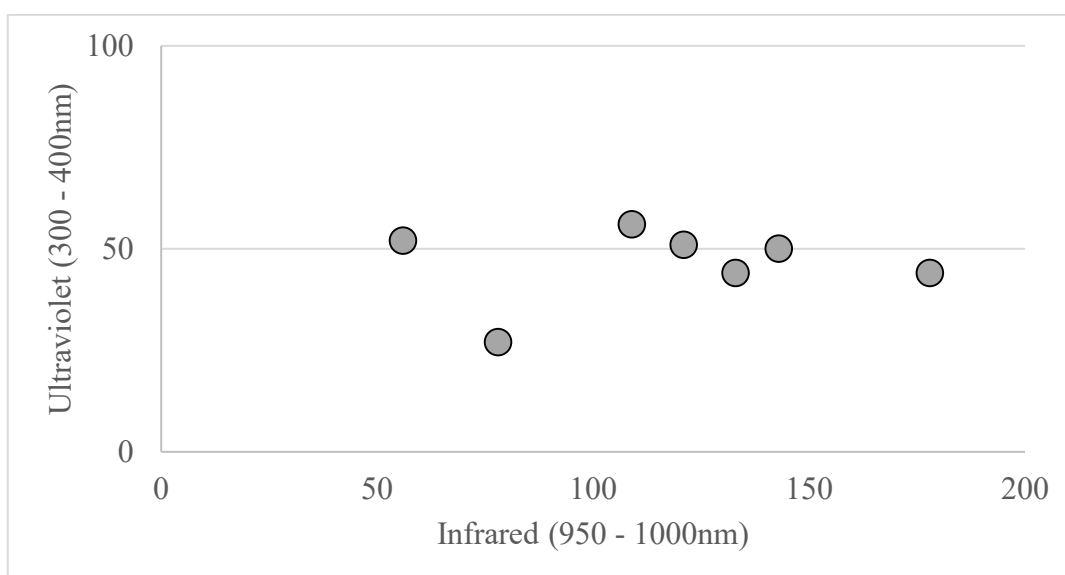
Figure 7.8: Scatter plot showing near-infrared and near-ultraviolet reflectance data for glaze samples from ceramics recovered during the Iona Abbey 2018 excavations.

The glazes show less clear evidence of clustering, likely because there are only seven samples (Figure 7.8). Still, two of the glaze samples do not cluster with the rest of the glazes from Iona (SF 510 and SF 523). The ceramic of one of these samples (SF 510) forms part of Cluster 1 while the other (SF 523) forms part of Cluster 2. This suggests that while these ceramics may have chemical similarities to others found nearby, the glaze on the samples has either come from elsewhere or has chemically reacted to something in

such a way that it now remains chemically distinct from contemporary vessels found on site.
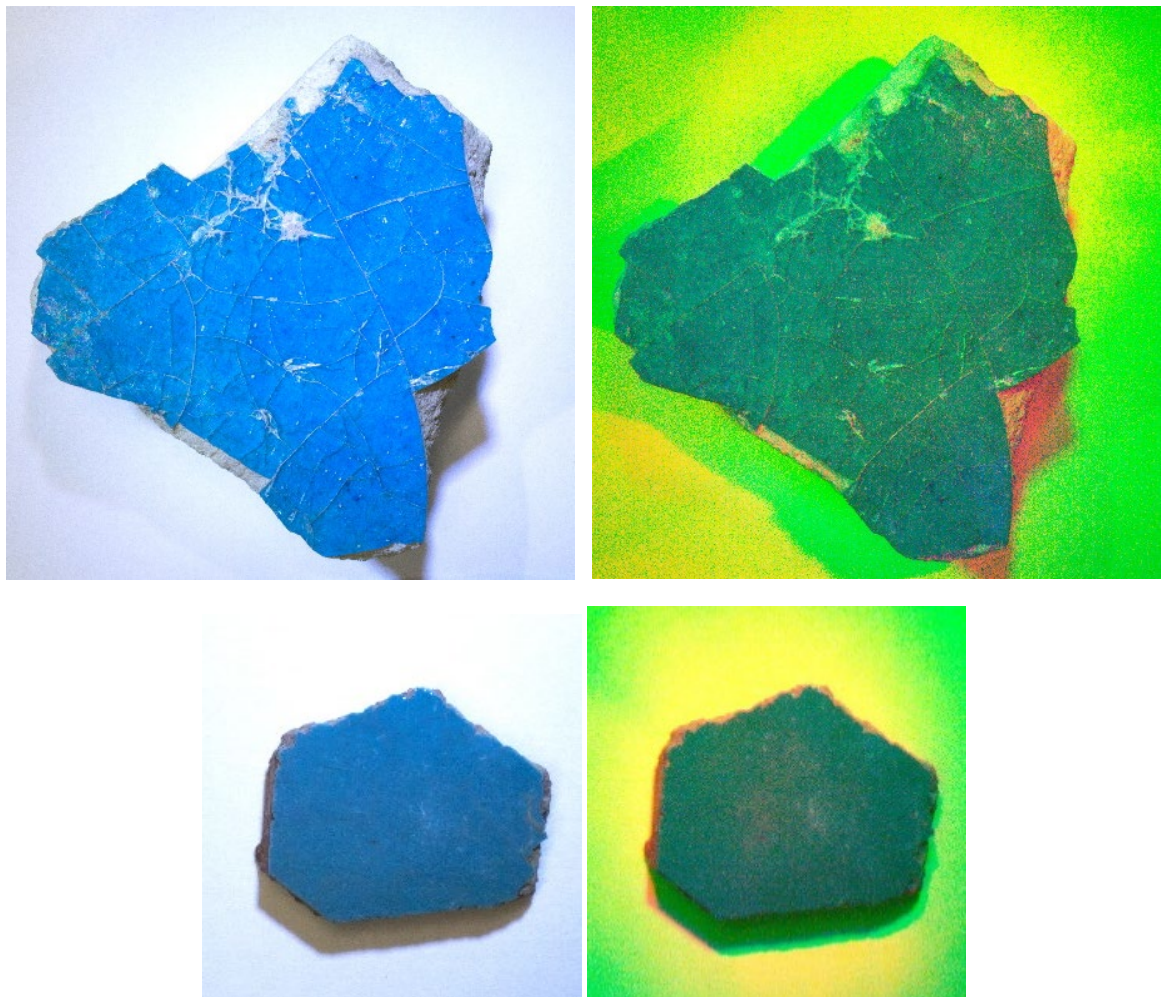
Figure 7.9: Visible-range and false-colour images of glazed ceramic sherds from Kubad Âbâd, Turkey (Kubad Âbâd 1, top (UCL Girişteki Hamam 4); Kubad Âbâd 2, bottom (UCL 35LL 2EngKU)) (Appendix E).

I also sampled two turquoise-blue glazed ceramic sherds from the Seljuk Palace of Kubad Âbâd, Lake Beyşehir, Turkey (Figure 7.9, Appendix E) using identical techniques for comparison with the ceramics from Iona. The palace was built in the 13th century AD and the tiles are likely from a similar period (Freestone et al. 2009, 3). Since the Turkish ceramics differed from the Iona samples in their glazing, fabric and where they were manufactured, we could expect to see a significant difference between the two groups in their reactions to non-visible light. Both Turkish pieces are monochrome turquoise-glazed ceramic tiles. The near-ultraviolet and near-infrared measurements for the glaze appear

very similar to each other (Kubad Âbâd 1 infrared: 60, ultraviolet: 105; Kubad Âbâd 2 infrared: 66, ultraviolet: 93). The ceramics beneath the glaze do differ in their reflectance of both infrared and ultraviolet, however, with that from Kubad Âbâd 1 (infrared: 169, ultraviolet: 195) producing significantly higher values than the ceramic from Kubad Âbâd 2 (infrared: 146; ultraviolet: 77). Interestingly, when plotted together with the ceramic material from Iona, Kubad Âbâd 2 falls into the previously identified Cluster 2, while Kubad Âbâd 1 is a clear outlier (Figure 7.10). However, the glaze on both ceramics from Turkey differs significantly from those used on Iona (Figure 7.11), suggesting that perhaps Kubad Âbâd 2 was manufactured with a similar recipe to the ceramics on Iona but glazed similarly to Kubad Âbâd 1. We should remember that this technique does not necessarily indicate chemical similarity, but one of the Turkish ceramics clustering so closely with material from Iona is certainly interesting.
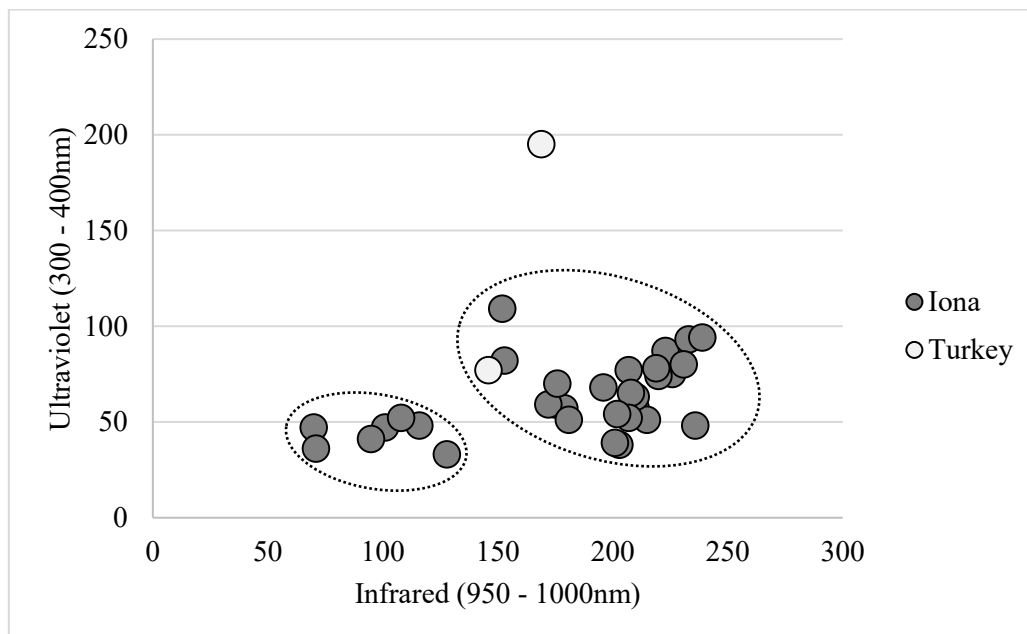
Figure 7.10: Scatter plot of near-ultraviolet and near-infrared reflectance data of ceramics from Iona and Turkey.
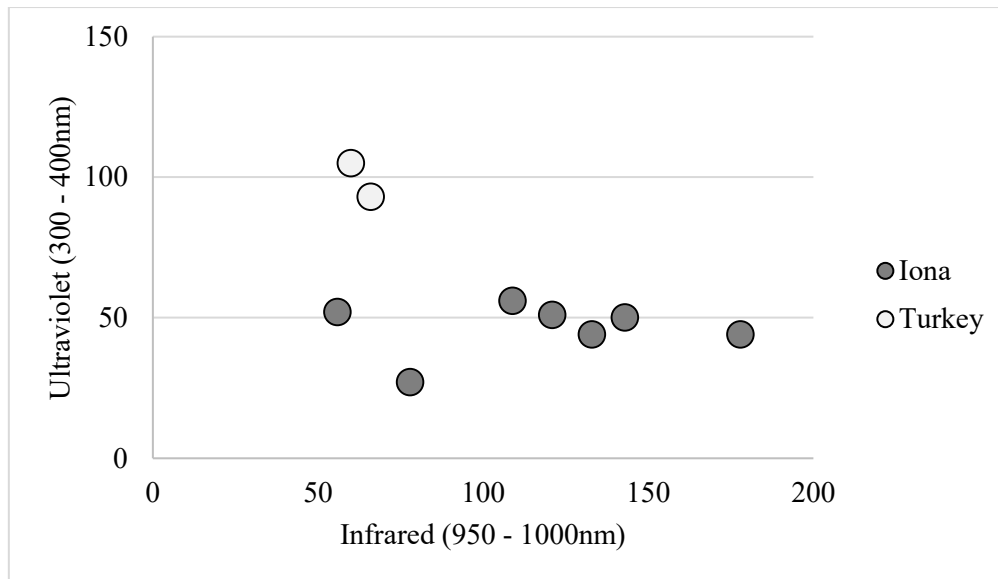
Figure 7.11: Scatter plot of near-ultraviolet and near-infrared reflectance data from glazes on ceramics from Iona and Turkey.

The potential for analysing chemical composition through spectral photography therefore applies to a variety of object types, including metalwork and ceramics. Despite the small sample sizes for both above investigations, spectral photography still provided important insights into the chemical relationships both between the copper-alloy head and lion mount from Iona and between the glazed and unglazed medieval ceramics from Iona and Turkey. Future research combining precise chemical analysis with the more relational spectral photography would allow this technique to advance significantly, but the current technique certainly provides a means of rapid chemical testing in the field on a relative scale.

7.3   PHOTOGRAMMETRY AND RTI OF DIFFICULT MATERIALS

Finally, I have applied the photogrammetric and RTI techniques developed in Chapter 6 to a variety of materials and objects. Some of the first non-glass experiments were a Neolithic potsherd (SF 001) and lithic flake (SF 002) from Cranberry and a lead spindle whorl from Leadketty (SF 03). Both sites were excavated as part of the Strathearn

Environs and Royal Forteviot Project in Perthshire, Scotland in 2016. The potsherd was found in topsoil at Cranberry while the lithic flake came from the upper fill of a postpipe or posthole in a Late Neolithic/Chalcolithic post pit alignment (Wright 2018a). The spindle whorl came from the topsoil of a posthole feature (Wright 2018b). Images for all three objects were captured and processed on-site, using one of the dig tents for a studio (Figure 7.12). All three models were relatively successful, including that of the lithic flake (Appendix E).

Figure 7.12: Image capture conditions at Cranberry, Perthshire 2016.

Figure 7.13: RTI of the Ballyspellan brooch (NMI Unknown #) (Appendix E).

I was also presented with the opportunity to create RTI and 3D photogrammetric models of the Ballyspellan and Hunterston brooches during the dismantling of the Celts exhibit at the National Museum of Scotland in 2016. The Ballyspellan brooch was found in 1806 and dates to the 9th century (Farley and Hunter 2015, 245; Youngs, 1989, 103). The brooch is made of silver, with ten bosses protruding from the terminals and a long pin (25.28cm) (Youngs 1989, 103). It has several lines of ogham text carved into the back of the brooch, which specialists believe are the names of four of the owners (Youngs 1989, 104). The processed RTI of the brooch allowed ogham specialists to examine the text in detail (Figure 7.13, Appendix E).

Figure 7.14: RTI of the Hunterston brooch (NMS X.FC.8) (Appendix E).

The Hunterston brooch is one of the most famous finds from early medieval Scotland. Two workmen discovered it while quarrying stone in Ayrshire in 1830 (Farley and Hunter 2015, 174). The brooch is silver with gold filigree interlace and amber inlays, with intricate interlace on the terminals, hoop, and pinhead. The brooch has a series of runes carved into the back. One side of the runes says 'Melbrigda owns this brooch,' while the other is a design carved to mimic runes, but saying nothing (Clarke et al. 2012, 15; Farley and Hunter 2015, 174). As with the Ballyspellan brooch, captured RTI of the

carvings on both sides allowed specialists to examine them in more detail (Figure 7.14, Appendix E).

Figure 7.15: Difference in positioning of the pinhead between images taken of the front of the Hunterston brooch (top) and those taken of the back (bottom).

Photogrammetric models of both brooches proved reasonably successful using the techniques described for photomacrogrammetry and highly reflective objects (Chapter

6.2.3 and 6.2.4). When changing the position of the brooch, care was taken to keep the

pin and pinhead in the same location to allow for ease of alignment during processing.

Unfortunately, when turning the Hunterston brooch over to capture the back, the pinhead

changed the side of the hoop it rested upon (Figure 7.15). This problem was recognised

only after attempting to align the images for the first time, at which point the objects were

no longer available.

Figure 7.16: Photogrammetric models of the Hunterston (left) (NMS X.FC.8) and Ballyspellan (right) (NMI Unknown #) brooches (Appendix E).

To avoid misalignment, the images were masked differentially to allow separate

models of the front of the brooch, the front of the pinhead, and the back of the brooch that

could then be aligned and merged to create the final model. While Chapter 6.2.2 describes

several problems with masking reflective materials, it provided a better model in this case

due to the changed positioning of the pinhead. There is a slight disparity in the final

model between the front and back of the Hunterston brooch, causing a small gap between

sides in the textured model. Processing in MeshLab closed these gaps, but the technique

for doing so also destroyed the texture. Despite the difficulties in navigating brooch

pinheads, the models themselves were still relatively successful and likely more so than

the results using standard techniques (Figure 7.16, Appendix E).
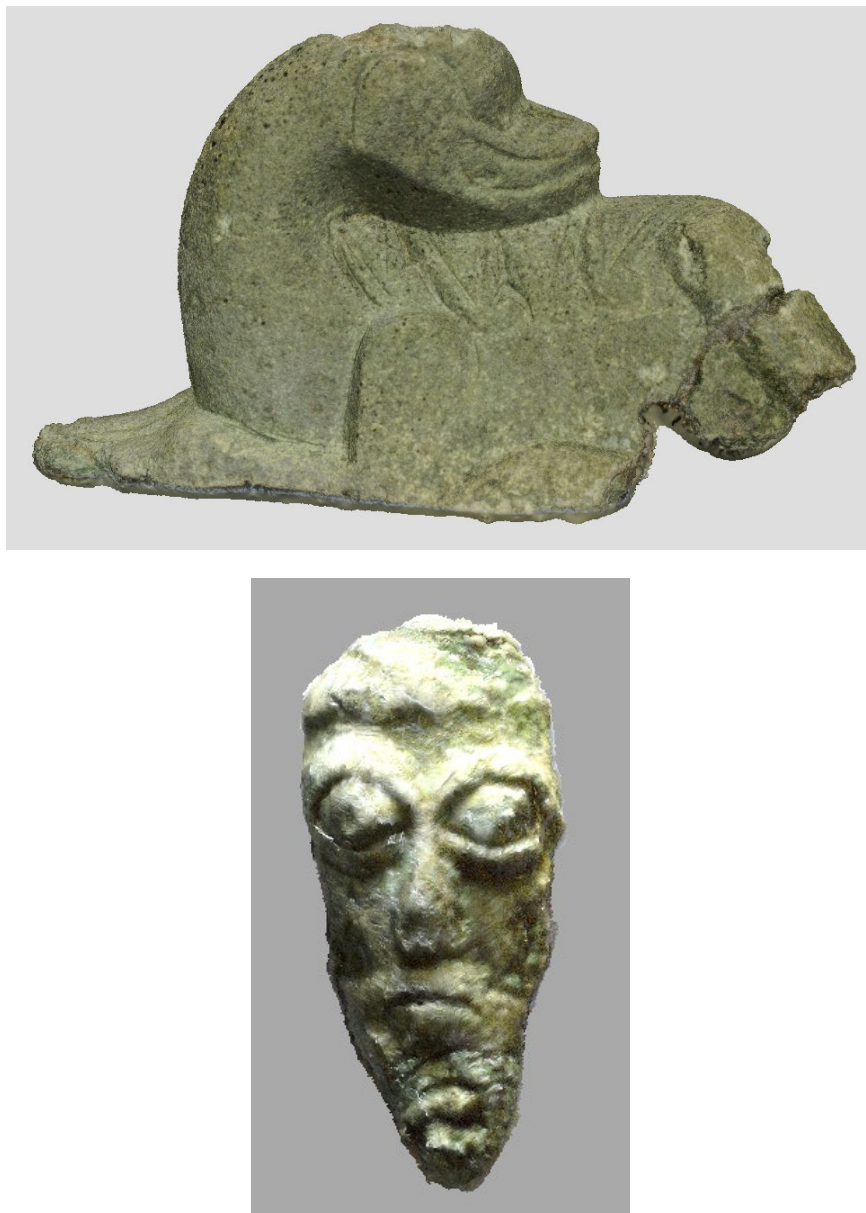
Figure 7.17: Photogrammetric models of the lion (top) (IAM SF 0997) and head (bottom) (IAM SF 0962) figurines from Iona Abbey (Appendix E).

To demonstrate the success of this technique with metal objects, I also created

photogrammetric 3D models of both the lion and head figurines from Iona using the

techniques discussed above for photomacrogrammetry and highly reflective objects

(Figure 7.17, Appendix E) (Chapters 6.2 and 7.2) The lion model captured the entire

object, including elements of the interior of the mount, but the head was more difficult. The thinness of the object results in less overlap between the front and the back, making it difficult for the software to identify matching points to join them together. However, the purpose of these methods is to create either a successful model or to create a more successful model than is currently possible through standard techniques. The model of the lion is successful, while the model of the head figurine still presented more aligned points and better resolution than currently achievable using standard photogrammetric methods.

Figure 7.18: 3D photogrammetric models of faience beads from Castle Craig (top left)(UG, Unknown #) and Newstead (top right) (NMS X.FRA 890) and an amber bead from Culbin Sands (bottom) (NMS X.BIB 27) (Appendix E).
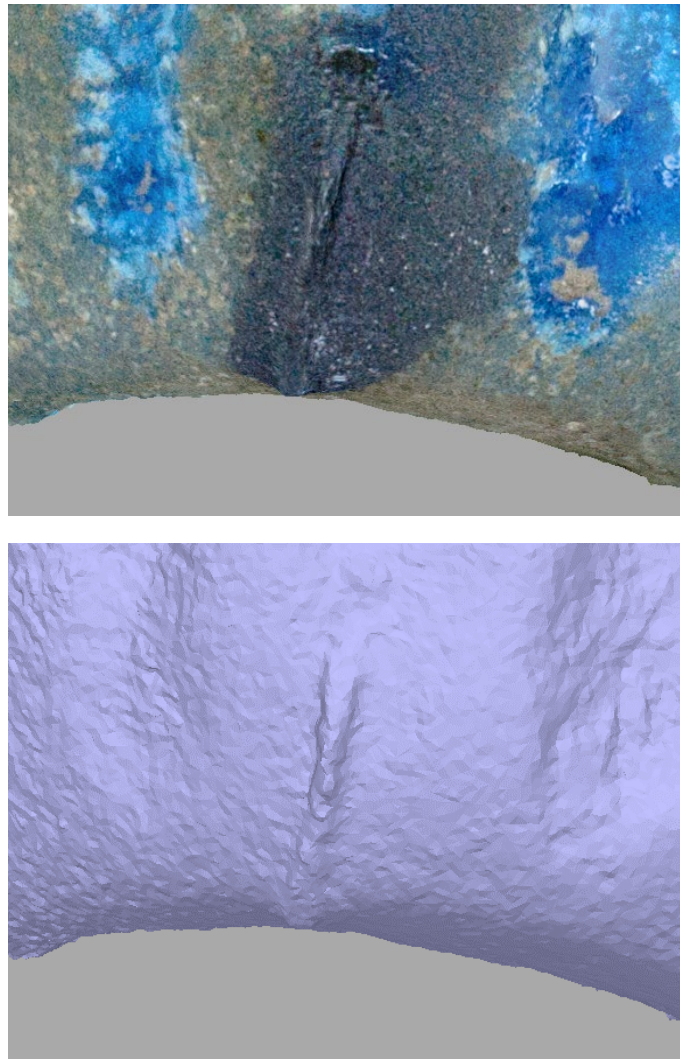
Figure 7.19: Close-up of the dark material on the Newstead faience bead (NMS X.FRA 890) from a textured (top) and untextured (bottom) 3D model (Appendix E).

Finally, I spectrally imaged, reflectance transformation imaged, and photogrammetrically modelled two faience and one amber bead to test the applicability of the techniques to these materials (Appendix E). One faience bead comes from the 2011 excavations at Castle Craig broch and is currently house in the University of Glasgow's department of Archaeology. The other faience bead is from Newstead (NMS, X.FRA 890) and the amber bead is from Culbin Sands (NMS, X.BIB 27). Castle Craig is an early medieval broch in Perthshire, while Newstead is a Roman fort in southern Scotland (Chapter 5.5.7). Beads from Culbin Sands on the Moray Coast lack contextual

information, so their date is less certain (Chapter 4.7) The model of the amber bead captures the cracked nature of the amber and the texture also renders the way in which amber tends to 'glow' (Figure 7.18, Appendix E). The models of the two faience beads also worked well, and that of the faience bead from Newstead captured a previously unnoticed feature: a strip of dark, possibly burnt or melted material at the edge of one of the perforations. The discolouration is visible to the naked eye, but it is difficult to know the strip is raised without using a microscope or viewing the photogrammetric model without a texture (Figure 7.19, Appendix E).

Both photogrammetric modelling and RTI of the faience bead from Newstead also captured the ridges inside the perforation of the bead, providing information about the tool used to create it (Figure 7.20, Appendix E). The photogrammetric model for the amber bead captured the entire perforation as well. The interior of the perforation is visible on some glass beads, particularly those which are broken or fragmentary, but the nature of the tool is less clear, save that it is an iron rod. 3D modelling of perforations for objects of adornment, personal or otherwise, could lead to further insights into their manufacture and trade.
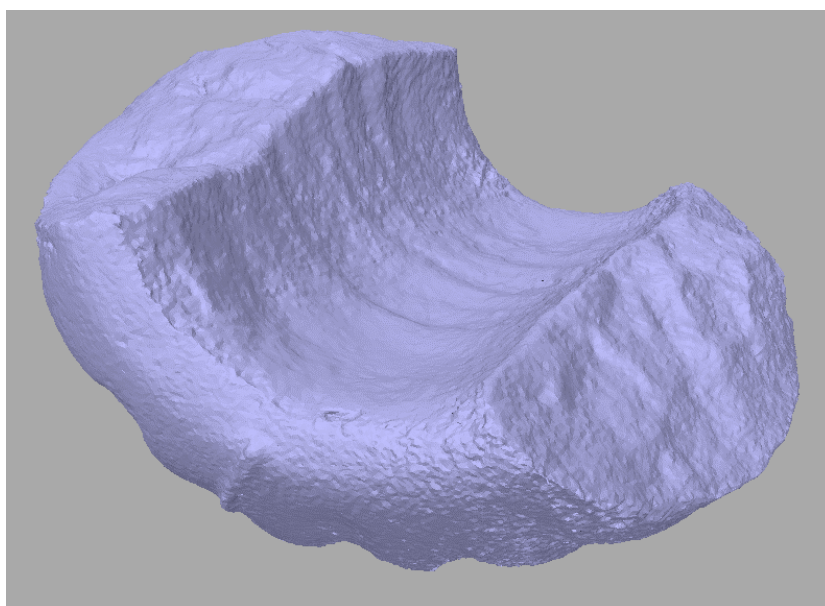
Figure 7.20: 3D model of the perforation of the faience bead from Newstead (NMS X.FRA 890) (Appendix E).

The above examples demonstrate that the techniques described in the previous chapters are beneficial not just for glass beads, but to any archaeological subject a person wishes to study. All objects react to light and we can capture most of these reactions with a digital camera, particularly one that has been converted for near-ultraviolet and near-infrared photography. While the techniques described here may not work for every object, they certainly work for many of the more difficult subjects and materials and significantly improve the results for many more. Furthermore, they are some of if not the most affordable, practical, and portable methods for creating informative visual representations of many archaeological subjects, particularly SRT objects.

8   COMPARING SPECTRAL IMAGING AND OTHER IMAGING TECHNIQUES

Throughout this thesis, I have discussed the cost, benefits, and drawbacks of various archaeological imaging techniques, often in general terms. This chapter serves to summarise that information and critically assess the affordability, practicality, and portability of each of these techniques, including spectral imaging as described throughout this thesis. I will speak specifically about the practicalities of using such techniques for imaging SRT objects as well as more generally in archaeology. The prices quoted here are market prices as of December 2018 within the United Kingdom, because that is where this research was based. Prices may differ between nations and years.

Each of the following methods require access to a computer capable of depicting digital images. Currently, laptops cost as little as £300 or as much as £2000 or more, while desktop computers range between £500 and £2000 or more. The higher the cost, the more versatile the machine and the faster it can process visualisations. The assessment of each technique below includes the costs of the requisite computers, as many £300 laptops do not have enough processing power to render 3D models. This section does not include miscellaneous costs like paper, putty adhesive, or other office supplies due to the varied application of these materials to each circumstance. These costs also do not include the specific materials needed to safely transport the equipment for each technique, as those will also vary depending on circumstances. Instead it focuses on the primary expenses of each technique followed by a critical examination of the practicality and efficiency of each for providing the desired results.

8.1   DIGITAL PHOTOGRAPHY

Digital photography is highly affordable for most archaeological project budgets, and it is usually a technique already accounted for to some degree. It requires a computer and digital camera at its most basic, though some type of photo-editing software is recommended. Gimp is free to download and has some versatility when working with photographs (Gimp 2018), though I recommend a more robust photo-editing software for ease and versatility. Adobe Photoshop or Lightroom Classic CC are industry standards, and subscriptions for each cost £19.97 per month or £49.94 per month for all Adobe products (Adobe 2018). Adobe also has a special photographer's package available, which includes both software and Lightroom CC for £9.98 per month (Adobe 2018). Take care not to confuse Lightroom Classic CC and Lightroom CC; Lightroom Classic CC allows for batch processing and the creation of pre-set filters whereas Lightroom CC is a more user-friendly version of the software with less versatility. Adobe Bridge is also useful for processing raw images, and costs £19.97 per month (Adobe 2018). Students can access all Adobe programs for £16.24 per month while schools and universities can access them for £29.49 per month (Adobe 2018). The computer required for processing digital photographs can be highly affordable, though lower-cost computers often take longer to run more robust programs like the Adobe Suite. A computer intended to run programs such as Adobe Photoshop or Lightroom costs around £500 while a computer that can run Gimp or Inkscape costs closer to £400.

The required camera can be a point-and-shoot or a dSLR. A phone camera could work for archaeological photography, but the quality of point-and-shoot or dSLR cameras is generally much better. Currently, the megapixel ratings of point-and-shoots and dSLRs are similar, so there is no significant difference in quality of the image between camera types. The cost of a point-and-shoot camera ranges between £70 – 100, while a dSLR

currently costs £350 or more. A basic dSLR is enough for digital archaeological photography, as are most point-and-shoot cameras. Additionally, most cameras can store a small number of images on the camera itself, but this quickly fills up, particularly when capturing raw images. Most cameras therefore require SD cards to capture and store images without continually stopping to transfer them to the computer. SD cards range in size and cost from 16 MB (usually included with the camera) to 512 GB (£250). A 32GB SD card is enough for most archaeological photography, and generally costs between £10 – 15. Finally, most archaeological photography benefits significantly from the use of a tripod. Tripods cost between £20 and £900 (Currys 2017; Manfroto 2018a), but the average cost falls between £50 and £200. Most archaeological projects do not require tripods costing more than £80; this thesis did not use any tripods costing more than £35 (Appendix B). The total cost for a camera, computer, SD card, tripod, and photo-editing software can be as little as £400, though the average cost is generally between £700 – 1,650. While more expensive computers, SD cards, and cameras certainly exist, there is little need for them in most digital archaeological photography. This technique is therefore the most affordable of those discussed here, with even the highest average cost still falling well within range for most lower-budget projects.

The equipment for digital photography is highly portable as well. The camera, SD card, and computer (if a laptop) can fit into a backpack or between a camera case and laptop bag. Tripods usually weigh between 0.5 and 3kg and can be carried to site by hand (Currys 2018; Manfroto 2018b). The equipment for digital archaeological photography is compact and relatively light-weight, making it highly portable in field and laboratory settings. One possible drawback is the ruggedness of the equipment – cheaper cameras and laptops or equipment that is not specifically ruggedized can suffer in the field without proper precautions. Protecting the equipment is often as simple as keeping it in its

protective cases when not in use, however, particularly during inclement weather. Additionally, this equipment is the easiest for sourcing repairs, as many camera shops offer such services.

The results of digital archaeological photography can be highly informative. Digital photography creates a visual representation of a specific object, complete with surface features, wear, inclusions, and colour. The resulting digital image generally is considered an accurate representation of the object's surface, colour, and design features according to standard archaeological imaging practices. Photographs also capture information for individual objects rather than averaging them together, even when such objects are grouped into the same image. Digital images are valuable in archaeological research for the same reason photographs have been valuable since their announcement in 1839: they capture significant detail of specific subjects that provide valuable information and are easily sent to other specialists for consultation.

Unfortunately, many archaeological finds are of a size or made of materials that do not photograph well. Surface wear or inclusions on small objects are often too small to capture using a standard zoom lens. Materials like glass, amber, faience, glazed ceramics, lithics, bone, or semi-precious stone are highly reflective, and many are also translucent. Standard photographic practices used on these materials will produce images that are overexposed, do not capture the desired detail, or capture information for other objects that are either reflected in the desired object or situated directly behind it. Standard practices in digital archaeological photography therefore work well for creating digital visual 2D representations of medium or large objects made of opaque, non-reflective materials, but not for objects that do not meet those criteria.

8.2   PHOTOMACROGRAPHY AND PHOTOMICROGRAPHY

Photomacrography and photomicrography allow for the photography of small objects and add comparably little to the cost of standard digital photography. A serviceable macro lens costs roughly £270 - 300 and will solve most size issues (e.g. Canon 2018a; Jessops 2018b; Nikon 2018a), but high-end macro lenses can cost closer to £1300 – 1400 (e.g. Canon 2018b; Sigma 2018). For particularly small objects, a serviceable digital handheld microscope costs roughly £325 (e.g. GT Vision 2018a), though more expensive models can cost closer to £700 (e.g. GT Vision 2018c; GT Vision 2018d). These microscopes connect directly to a computer or laptop and allow the user to capture images for analysis. They can be stabilised with a microscope stand, which has a similar cost to an average camera tripod (DinoLite 2018; GT Vision 2018b). The cost of equipment for photomacrography therefore averages between £1,200 – 2,050, while that for photomicrography averages between £900 – 1,700.

Practically-speaking, macro lenses add little to the equipment needed for standard digital photography described in the previous sub-section, though a camera bag is recommended. Most camera bags have space for an extra lens, which hold a single macro lens safely. Digital handheld microscopes and their stands are often even more portable, fitting into a small box that can slide into a backpack or laptop case without issue. Both macro lenses and digital handheld microscopes run the risk of damage through common culprits like grit, dust, rain or simple carelessness. The effects of these dangers can be minimised through careful packing and regular cleaning. Repairs are relatively simple to source for photomicrography due to the abundance of camera shops, while many digital handheld microscopes come with a limited warranty and can be repaired by the company for a fee thereafter (e.g. DinoLite 2017b).

For subjects or details of subjects smaller than about 10mm, macro lenses and digital microscopes create significantly better digital images than standard digital photography. They allow us to examine and analyse detail that is not visible to human eyes in an affordable way. Some subjects are too large to capture fully through a macro lens or digital microscope, however, and for such subjects this technique is less ideal. If working with subjects of varying size, like vessel sherds, it would be advisable to focus on standard digital photography and photomacrography before exploring digital handheld microscopes. In the case of glass beads, I have found most objects image best using either a macro lens or a digital handheld microscope.

8.3   SPECTRAL PHOTOGRAPHY

The application of digital filters to images like that described in Chapter 4 does not necessarily add an extra cost to that of standard archaeological photography in the visible range; digital filters can be created and applied through photo-editing software like Adobe Photoshop or Lightroom Classic CC (Appendix C). Unfortunately, these settings are not available in current open source software, and they therefore require software like Adobe Photoshop, Bridge, or Lightroom Classic CC. Otherwise, physical visible-range filters can cost as little as £20 for a set of five (red, green, blue, yellow, and orange) (Neewer 2018b). This brings the minimum cost of visible-range filtered photography to roughly £800 (assuming a year-long subscription to Adobe software), but the average cost remains similar to standard photography (£800 – 1,650).

Applying visible-range filters to archaeological photographs allows us to capture, emphasise, and examine object characteristics or features that are not necessarily visible using standard photography. These may be inclusions or bubbles in the object, as demonstrated in Chapter 4, or elements of wear or decoration on the surface. This type of

photography often represents these surface or internal features of an object better than a standard visible-range image. Additionally, this style of photography differs little from standard archaeological photography; it merely limits the representation of the data captured in standard visible-range photography to a much smaller spectrum of light. The image capture technique can even remain the same if digital filters are applied. Visible-range filters in photography capture a two-dimensional image of an object from a single angle, however, and the technique is not ideal for examining the shape of an object or its three-dimensionality. It also does not represent colour data for more than the wavelength represented and is not ideal for any study of an object's colour more generally. Yet, the information gained does provide significant detail in surface and interior features of an object and can lead to a more representative image of the object's shape or decoration than what is currently possible using standard visible-range photography, particularly for SRT objects.

Near-ultraviolet or near-infrared photography, such as that used in Chapter 5, requires a dSLR that has been converted for full spectrum imaging. The conversion replaces the hot mirror with fused silica and costs roughly £250 excluding shipping and delivery (Protech Repairs 2017). This type of spectral photography also requires filters for both the visible and non-visible spectra. Once the camera has been converted, any unfiltered shot will capture the full range of wavelengths from roughly 300 – 1000nm. This means that any image intending to capture the visible spectrum without filters will instead capture the near-ultraviolet, visible, and near-infrared spectrum together. Once the camera has been converted, then, it requires at least four filters to capture each of the spectral ranges between near-ultraviolet and near-infrared: 1) a visible-range filter capturing wavelengths from 400 – 700nm (e.g. Schott S8612); 2) an ultraviolet pass filter capturing wavelengths from 300 – 400nm and from 700 – 800nm (e.g. Hoya 360); 3) an

ultraviolet cut filter eliminating wavelengths from 300 – 400nm (e.g. Hoya HMC UV

cut); and 4) at least one infrared pass filter capturing between 720 – 1000nm (e.g. Neewer

720nm Infrared with a range of 720 – 1000nm or Neewer 950nm Infrared with a range of

950 – 1000nm). The cost of each filter used in this study is listed below (Table 8.1).

Filter	Range	Cost
Schott S8612	400 – 700nm	£65 (UVIROPTICS 2018b)
Hoya 360	300 – 400nm	£50 (UVIROPTICS 2018a)
Hoya HMC UV Cut	400 – 1000nm	£30 (Jessops 2018a)
Neewer 720nm Infrared Neewer 760nm Infrared Neewer 850nm Infrared Neewer 950nm Infrared	720 – 1000nm; 760 – 1000nm; 850 – 1000nm; 950 – 1000nm	£30 for the full set (Neewer 2018a)

Table 8.1: List of filters required for visible- and non-visible-range spectral imaging and their costs.

Non-visible-range spectral photography also requires specialised light sources.

Torches serve this purpose well for many archaeological objects. Full spectrum imaging

requires three torches: one with a xenon or incandescent bulb, one with LEDs, and one

with an ultraviolet bulb or ultraviolet LEDs (Appendix B). Each torch costs roughly £15,

while larger light sources will likely cost more. Given the cost of conversion and

additional costs of filters and torches, the average cost of non-visible-range spectral

photography falls between £1,200 – 2,300.

The primary benefit to spectral photography is in its ability to provide a sample of

information about the object's chemistry. Even a preliminary understanding of the

chemical relationships between objects allows for a more targeted approach in deciding

which objects warrant further chemical testing. If archaeologists imaged more collections

in this manner, the results would provide more information about an object's chemical makeup. There is little change to the portability and practicality of the technique, since the only additional equipment are some filters and torches that easily fit into a backpack or camera bag. Finally, and importantly for this study, spectral photography allows for better imaging of subjects that do not lend themselves well to standard techniques, including SRT objects. Laser and structured light scanners do not capture data for SRT objects well; without photographic filters, the only technology that could be said to create informative visual representations of SRT objects is x-ray computed tomography, the machine for which costs upwards of £71,000. Without the photographic techniques described in this thesis, SRT objects would remain largely visually undocumented.

Infrared and ultraviolet photographs also capture either interior or surface features of an object in more detail or represent such features in a more easily identifiable manner than standard visible-range photographs. Since they use the non-visible range, they also have the additional benefit of not requiring strict control of ambient lighting in a workspace. This style of photography therefore captures more information than standard practices, can determine certain chemical relationships between objects, and often requires less ambient light control than other photographic techniques. Full spectrum imaging still creates a two-dimensional image, however, and is therefore not ideal for capturing data relating to the shape or three-dimensionality of an object. It also generally captures limited colour information for an object and adds further costs due to conversion and the required filters.

8.4   REFLECTANCE TRANSFORMATION IMAGING

While the software for creating and viewing RTI is free, there is an added cost for the RTI spheres required for image capture. Admittedly, RTI spheres need only be red,

black or silver, and passable spheres can be made from snooker balls or ball bearings of various sizes. Officially marketed RTI spheres are only sold as part of a kit, which currently costs roughly £300 not including shipping (Cultural Heritage Imaging 2018b). More make-shift RTI spheres cost as little as £2 for a pack of 100 ball bearings (Simply Bearings 2018). All other costs are the same as standard digital photography. The average cost for RTI therefore falls between £700 – 2,000 (£1100 – 2,400 for photomacrographic RTI). It is also possible to use a microscope for RTI (Chapter 6.1.3), which costs an average of £900 – 2,050. If working exclusively with very small objects, then, it may be more cost effective to invest in a digital handheld microscope rather than a functional dSLR and macro lens. Portability changes little from digital photography, since the added equipment is a maximum of an additional tripod and some reflective spheres the size of snooker balls. The primary benefit of RTI is its ability to capture data for the surface features of an object and its calculation of surface normals. Additionally, the software allows for the manipulation of surface features to deepen grooves or change the texture to emphasise wear, decoration, or surface markings that may not otherwise be visible to the naked eye. The output is still not a three-dimensional image, however, so the technique is still not ideal for representing the shape of an object.

Spectral RTI requires the same additional costs associated with the various types of spectral photography. Visible-range spectral RTI requires the additional cost of photo-editing software like Adobe Photoshop, Bridge, or Lightroom (£120 per year for Photoshop and Lightroom together or £240 per year each for Adobe Bridge, Photoshop, and Lightroom Classic CC individually) (Adobe 2018). Near-ultraviolet or near-infrared RTI requires the extra cost for conversion (£250) and that of filters and torches for each desired wavelength (£45 for near-infrared, £150 for near-ultraviolet). Depending on the type of spectral RTI and quality of the camera and computer desired, the average cost

ranges from £800 – 2,600 (£1,200 – 3,000 for photomacrography and £1,000 – 2,700 for photomicrography). Portability remains similar to standard RTI, since the addition of some filters and small light sources often require little space. If imaging larger objects, however, the required additional lighting and logistics of moving the torch while capturing an image could be substantial enough to require a second team member. Spectral RTI allows for successful reflectance transformation imaging of highly reflective or translucent objects and can also allow for imaging of an object in an open or shared office with minimal or no control over ambient lighting. It does not represent an object's colour as seen by human eyes, however, and only captures the pseudo-three-dimensionality of one side instead of the entire object.

8.5   PHOTOGRAMMETRY

Photogrammetry is the most affordable imaging technique for creating 3D models. Photogrammetry using standard photographic techniques requires a camera (dSLR or point-and-shoot) and photogrammetric modelling software like Agisoft Photoscan. It is possible to create photogrammetric 3D models from mobile phone images, but I recommend at least a point-and-shoot camera to improve alignment and quality. The average camera cost can range from £100 – 500 for photogrammetry, but it can also be significantly higher if more detail is desired or required. A single-use licence for Agisoft Photoscan Standard Edition currently costs $179 USD (£125) or $59 USD (£41) for an educational licence (Agisoft 2018a; Agisoft 2018b). A single-user licence for Agisoft Photoscan Professional Edition costs $3,499 USD (£2,500) or $549 USD (£385) for an educational licence (Agisoft 2018a; Agisoft 2018b). While this is quite an expense, particularly for a non-educational Professional Edition licence, it is generally much more affordable on average than other 3D modelling software and equipment. Finally,

rendering the models in a timely manner requires a relatively robust graphics card and sizable RAM. This pushes the cost for a computer to between £600 – 2,500, depending on the desired processing power. Thus, the average cost for standard photogrammetry falls between £900 – 6,000. Using a macro lens raises the cost to between £1,400 – 6,400, while using a digital handheld microscope brings it to £1,150 – 6,000. The portability of photogrammetry remains similar to standard digital photography, since the primary difference is in the computer and software required to process models rather than in camera equipment.

The primary benefit of photogrammetry is in the ability to represent an object in three dimensions. Photogrammetry captures surface data and measurements of an object and renders the results in 3D to form a visual representation that viewers can rotate and manipulate in several ways. We can alter or eliminate the texture to emphasise surface features or render it as close to reality as possible using data from the images provided. If the object is no longer accessible, we can capture RTI from a photogrammetric model instead. Researchers can calculate certain metrics that may not be possible in reality, such as the volume of certain objects or elements of a building. Photogrammetry also allows for the identification of the finished product of a mould, for example, or the modelling of specific elements of an object to the exclusion of others through either masking or deletion.

Unfortunately, photogrammetry only works for objects that photograph well. Photogrammetry can only work with the data provided by the image, and so cannot render points for overexposed areas of highly reflective materials. The current software also incorrectly aligns particularly symmetrical, translucent, transparent, or smooth objects. This makes it difficult if not impossible to photogrammetrically model most archaeological finds. However, even when the photogrammetric model fails to align or

render with enough detail, the process of acquiring data to create the model still generates 80 – 100 overlapping images of the subject at hand from a variety of angles. This is often significantly more visual representation than currently available for most archaeological finds. Thus, even failed photogrammetric models lead to significant improvements in the visual record available for most archaeological subjects. The same cannot be said of laser or structured light scanning, certainly not to the same degree.

Spectral photogrammetry requires all the above costs stated for photogrammetry as well as the associated costs for spectral photography. If working purely within the visible range of light, the average falls between £1000 – 6,000. If working within the non-visible range, costs increase: £1,200 – 6,300 for near-infrared, £1,300 – 6,400 for near-ultraviolet, or £1,400 – 6,500 for both. Spectral photogrammetry has the primary benefit of creating successful photogrammetric 3D models for materials or objects that fail using the full visible spectrum. For many archaeological finds, full spectrum photogrammetry is the only way to produce a successful photogrammetric 3D model. The primary caveat is that spectral photogrammetry does not capture colour data for an object aside from the specific range used to capture the image.

Spectral photogrammetry is certainly the most expensive of the techniques included in this thesis. Unfortunately, the only open source software for photogrammetric rendering, 123D Catch, is no longer available, leaving Agisoft Photoscan as the primary available software. The cost of a computer is much higher, too, as rendering a photogrammetric 3D model requires more RAM and a better graphics card. Despite this, however, photogrammetric modelling is still the most affordable 3D modelling technique currently on the market.

8.6   STRUCTURED LIGHT SCANNING

Structured light scanners vary widely in price. Cheaper models range from £2,000 – 5,000, but those considered appropriate for professional use range from £10,000 – 20,000 or more (e.g. Artec 2018a; Artec 2018b; Artec 2018c). A computer that can process the model costs an average of £1,000 – 2,000, pushing the average cost of structured light scanning to £11,000 – 22,000. Practically speaking, structured light scanners require their own robust case and padding, and many require an electrical outlet, making them less portable than photography-based imaging techniques. These scanners are also more difficult to repair than a camera, since there are fewer specialists able to do so. Additionally, there are many discontinued structure-light scanners; Artec alone has discontinued 10 of their model series since 2007, averaging roughly one discontinuation per year (Artec 2018d). Their current software also does not support scans created by six of these series, jeopardising the ability to view material created with many Artec structured light scanners within the last decade (Artec 2018d). While this is a single company, it is one of the leading companies on the market for structured light scanners. Considering the rate with which the security of Artec scan data has been jeopardised in the past from an archival standpoint (Chapter 2.2.3), the chance that results may become unreadable is much higher for structured light scanners than for digital cameras.

The primary benefit of structured light scanners is that they capture precise measurements of the object's surface as well as colour and texture information for photorealistic 3D models. They work very well for creating models of buildings or standing stones, for example, and can work well for non-SRT objects. Within archaeology, for example, structured light scanning has provided valuable results for underwater archaeology, human and faunal skeletal remains, and non-SRT archaeological finds (e.g. McPherron et al. 2009; Niven et al. 2009; Roman et al. 2010). Unfortunately,

structured light scanners have difficulty with SRT objects due to apparent challenges of matching the algorithms calculating distance through changes in light to materials that refract light in unpredictable ways. They therefore often fail to model many archaeological objects successfully. This, combined with the cost of equipment and the possible difficulties in archiving and repair, often renders structured light scanners less affordable and practical, both in the field and for archival purposes.

8.7 LASER SCANNING

Laser scanners are certainly the most popular tool for creating 3D models. The scanners themselves range from large scanners mounted on tripods to small, portable, handheld devices (LAGOA n.d.). While there are more affordable models available for $749 USD (£571), close-range professional scanners that can capture enough data from small objects to create a 3D model cost between £3,000 and £80,000 (Matter and Form 2018a; NextEngine 2016; Russell 2016; Schroedter 2016). Coupled with the price of a computer that can run the required software and process the data, the average cost of laser scanning falls between £4,500 and £82,000. Like structured light scanners, laser scanners require their own robust cases and padding. Many also require a tripod like that used for a total station or other survey equipment. Many companies offer repairs of their machines (e.g. Faro 2018a; Matter and Form 2018b; NextEngine 2018), making support easier to access than for structured light scanners. There also appear to be fewer discontinued models of laser scanner, with Faro only listing the FARO Gage, a measuring arm rather than a laser scanner, as discontinued (Faro 2018b).

Laser scanners benefit from using infrared lasers to capture data points, which can penetrate vegetation in landscapes. Well-known examples of its success have been seen in uncovering sites and buildings located vegetation-dense regions such as the complex

urban landscapes at Angkor Wat (Evans et al. 2013) or the Mayan lowlands of the Yucatan (Canuto et al. 2018). Laser scanning of any type is highly accurate and captures large amounts of data in a relatively short time. Additionally, laser scanners only capture the measurements of the surface of a subject rather than the colour or texture. This allows for the visualisation of the surface without the distraction of colour data. Unfortunately, the lack of colour data captured can also be a caveat, particularly in subjects for which colour is a primary characteristic. Laser scanners also do not work well with SRT objects, given both the resolution of the scanner and the variable reactions of reflective, transparent, and translucent materials to light. The cost of the equipment and variable success with objects of different materials makes laser scanners less than ideal for imaging most archaeological objects, despite their success with landscapes, buildings and site trenches.

8.8   X-RAY COMPUTED TOMOGRAPHY

X-ray computed tomography (CT scanning) is perhaps the most precise method for 3D modelling an object currently used in archaeology. The costs associated with x-ray computed tomography vary, because most institutions cannot afford to purchase a system on its own. The average cost of a scientific CT scanner is between £71,000 – 1,000,000 (Microphotonics 2015). The cost of a computer to process the data only increases this amount. X-ray computed tomography is not portable or taken easily into the field. It is possible to send objects to certain institutions for CT scanning, but the cost associated with doing so equates to a plane ticket and lodging for at least one researcher to travel to the nearest laboratory, which is often not in the same country. The cost of obtaining permission to bring objects out of the country will vary, if permission can be obtained at

all. The cost for x-ray computed tomography is therefore high, both monetarily and logistically.

Despite this, the models produced are extremely valuable. Since the technique acquires measurements by capturing slices of the object and stitching them together, it captures all the interior elements of an object in addition to surface features. These can be bubbles, inclusions, perforations, or other features (e.g. Bertini et al. 2014). In archaeology, it has been applied to wooden statues, glass, lithics, ceramics, and other finds (e.g. Anderson and Fell 1995; Bertini et al. 2014; Casali 2006; Morigi et al. 2007; Morigi et al. 2010). It is currently impossible to capture these elements in three dimensions using photogrammetry, structured light scanning, or laser scanning. This marks x-ray computed tomography as one of the best techniques for digitally imaging archaeological finds, including SRT objects. Unfortunately, the logistical and monetary cost coupled with the lack of portability make x-ray computed tomography less suited to many archaeological imaging projects than any other method discussed in this chapter.

8.9   MULTISPECTRAL AND HYPERSPECTRAL IMAGING

The spectral imaging described in Chapters 5 and 6 is multispectral imaging with a dSLR rather than a multispectral camera, and one could argue that using a multispectral camera would be more efficient. Multispectral cameras tend to capture data for a wider spectral range than is currently possible with a converted dSLR. However, they currently cost between £3,000 – 10,000 (e.g. Buzzard Cameras 2018; SILIOS Technologies 2018; Thorlabs 2018a; Thorlabs 2018b). Coupled with a computer and software, this technique has an average cost of £4,500 – 11,500. The technique is highly portable, requiring only the camera and computer for image capture and processing. The benefit of this technique is that it can capture spectral data for a much wider range than a fully converted dSLR

can. This data helps in understanding chemical relationships between different objects and allows us to see details we cannot see with our own eyes. Isolating specific wavelengths of light makes bubbles, inclusions, perforations, striations, colour differences, and surface wear much easier to spot. Unfortunately, multispectral cameras are expensive and provide little additional information to that acquired through spectral imaging with a converted dSLR.

Hyperspectral imaging captures colour data for each wavelength on the spectrum, thereby capturing far more information than a converted dSLR ever will. Hyperspectral cameras also capture data for a much wider spectral range than a dSLR. Hyperspectral cameras costs between £13,000 – 250,000, however, depending on the needs of the project (Keating 2016). Coupled with a computer and imaging software, the full cost of hyperspectral imaging ranges from £14,500 – 251,500. Despite the benefits of highly accurate spectral imaging, the cost of equipment is prohibitively high for most projects and institutions.

8.10 A COMPARATIVE ANALYSIS OF ARCHAEOLOGICAL IMAGING TECHNIQUES

The above sub-sections discuss the benefits, caveats, and costs of major visualisation techniques, including those techniques introduced in this thesis. For ease of comparison, a summary of the costs is provided inTable 8.2. In terms of affordability, only the higher range of average costs for photogrammetry overlap with even the lowest range of costs for laser scanning or multispectral imaging. All other techniques are at least double the highest average cost of any technique described in this thesis. These costs also assume the individual or organisation does not have a computer or camera. If we assume a project already has access to a computer and camera, then the costs for

photography lower to a maximum average of £500 – 1,350 for non-visible-range photography, £500 – 1,650 for non-visible-range RTI, and £500 – 3,800 for non-visible-range photogrammetry. The techniques developed and championed in this thesis therefore open a range of imaging solutions for lower-budget projects and for archaeological subjects that do not lend themselves well to currently recognised standard imaging techniques, such as SRT objects.

Technique	Average Cost (Photography)	Average Cost (Photomacrography)	Average Cost (Photomicrography)
Photography			
Standard	£700 – 1,650	£1,200 – 2,050	£900 – 1,700
Visible-range filtered	£800 – 1,650	£1,300 – 2,050	£1000 – 1,700
Non-visible-range filtered	£1,200 – 2,300	£1,300 – 2,700	£1,050 – 1,750
RTI			
Standard	£700 – 2,000	£1,100 – 2,400	£900 – 2,050
Visible-range filtered	£800 – 2,000	£1,200 – 2,400	£1000 – 2,050
Non-visible-range filtered	£1,200 – 2,600	£1,500 – 3,000	£1,050 – 2,700
Photogrammetry			
Standard	£900 – 6,000	£1,400 – 6,400	£1,150 – 6,000
Visible-range filtered	£1000 – 6,000	£1,500 – 6,400	£1,250 – 6,000
Non-visible-range filtered	£1,200 – 6,500	£1,500 – 6,900	£1,300 – 6,550
Structured Light Scanning	£11,000 – 22,000	-	-
Laser Scanning	£4,500 – 82,000	-	-
X-ray computed tomography	£71,000 – 1,000,000	-	-
Multispectral Imaging	£4,500 – 11,500	-	-
Hyperspectral Imaging	£14,500 – 252,000	-	-

Table 8.2: Average costs of the base equipment required for common digital imaging techniques in archaeology, including computers and cameras.

This is not to say the more expensive techniques are poor techniques; they are valuable technologies that often provide more information than photography can. Yet, even if a project could acquire permission to send a researcher and several objects to a lab with a scientific CT scanner, for example, the cost of travel, housing, and other expenses for a researcher travelling from Glasgow to the Paul Scherrer Institute in Switzerland for a week costs upwards of £1000 for the one-time visualisation of a set number of objects (Paul Scherrer Institute 2016). Photography and photography-based imaging are also more portable and practical in the field, have a wider market for repairs, and have generally well-established methods for archiving the results. For the moment, at least, photography and photography-based imaging techniques are the most affordable, practical, and portable archaeological imaging techniques currently available on the market.

9 PUSHING THE BOUNDARIES OF ARCHAEOLOGICAL IMAGING

This thesis has examined the history of imaging technologies and their relationship to archaeology, identified a need for and developed affordable, practical, and portable techniques for imaging SRT objects, and demonstrated their value in furthering our knowledge about glass beads from Iron Age and Early Medieval Scottish contexts. The techniques developed and employed in this thesis are many, but they all centre on spectral imaging, or the creation of visual representations of a subject through the isolation, capture, and analysis of certain wavelengths of light. Chapter 4 used visible-range spectral photography to 'see' into the matrix of hundreds of glass beads and compare their relative bubble concentrations. The results provide important information about the manufacture and possible short- and long-distance trade of these objects in Iron Age and Early Medieval Scotland. Chapter 5 used non-visible-range spectral photography to capture and analyse the reactions of hundreds of glass objects to infrared and ultraviolet light, which served to elucidate many of the chemical relationships between objects through non-destructive means. The results provided valuable insight into the manufacture and trade of glass in Iron Age and Early Medieval Scotland and allowed for the possible classification of certain objects as belonging to later periods. Chapter 6 demonstrated the value of visible- and non-visible-range spectral photomacrography and photomicrography in improving the results of PTM RTI and SfM photogrammetry for SRT objects. Finally, Chapter 7 provided numerous brief examples of the possible application of these techniques to other archaeological subjects, including objects and trench sections.

The primary contribution of this thesis is demonstrating the value of challenging the standards of current archaeological imaging techniques and pushing the boundaries of

what information they can reveal by developing affordable, portable, and practical techniques for imaging any archaeological subject, especially those neglected by current methods. The conclusions about Iron Age and Early Medieval Scotland drawn in the previous chapters as relating to glass objects would be difficult if not impossible to discover via other means. Given the significant increase in information garnered for glass beads in Chapters 4 and 5 and the brief demonstration of the use of these techniques for other object categories in Chapter 7, we can assert that the changes proposed in approaches to archaeological imaging would provide significant insight into many archaeological subjects from any context, particularly those that are habitually underrepresented and understudied.

9.1 ARCHAEOLOGICAL THEORY AND ARCHAEOLOGICAL IMAGING REVISITED

Chapter 2.2 examined current archaeological imaging practices and their relationship to several contemporary archaeological theories and discourses, namely the objectivity of archaeological imaging, the general requirement that visual representations mimic the human eye as closely as possible, the prescription of standard techniques for creating such visualisations, the championing of new technologies and the effects current approaches to archaeological imaging have on the archaeological record. This section aims to revisit these discourses considering the results provided in Chapters 4 through 7.

9.1.1 ARCHAEOLOGICAL IMAGING AND OBJECTIVITY

Archaeology tends to view photography and other imaging techniques as an objective tool for documenting the results of archaeological investigation and fieldwork. In general, archaeological photography manuals provide instructions and advice on how to take such documentary images of different subjects that capture as much relevant

archaeological information as possible (Cookson 1954, 13; Howell and Blanc 1995, 1; Lyons 2005, 25; Moser and Smiles 2005, 6; Shanks 1997, 73 – 74; Wright 1982, 176). Archaeological imaging functions much like field notes: it is meant to record what an archaeologist has seen to allow them to both remember what they saw and communicate that to other people.

Yet, archaeological imaging can be analytical, too; just because archaeology has used photography as a documentary technique for over a century does not mean it should only ever be considered as such. Biology, ecology, geology, and other sciences regularly use photography as an analytical tool, and through it they know that the colour of a male mandrill's face and a male gelada's chest directly correlates to the animal's position within group hierarchy, for example (Bergman et al. 2009, 796; Setchell et al. 2008, 367; Setchell et al. 2009, 831). Careful photography and image processing allow for the determination of the individual's position through a similar method to that used in Chapter 5: measuring the intensity of red in the mandrill's face by averaging colour data for that area together.

In this thesis, photography has led to the identification of different regional variations in glass bead trade and manufacture in Scotland between 800 BC and AD 800 (Chapter 4), something that was not possible through purely visual analysis. It has also identified significant chemical differences between glass bead collections within Scotland and between Scottish and Anglo-Saxon, Roman, Egyptian, Medieval English, and modern collections (Chapter 5). This research has led to the classification of certain objects likely being modern or at least post-medieval (Chapter 5.6.2) and has highlighted a chemical difference between naturally coloured Scottish glass and naturally coloured Anglo-Saxon glass from this period (Chapter 5.6.6). All conclusions specific to glass and glass beads drawn in this thesis stem from employing photography as an analytical tool, not purely a

documentary one. By treating archaeological photography as we always have, we are limiting the information we can glean from an image to a fraction of what is truly possible. Photography is an analytical tool, and one that archaeology as a discipline has failed to appreciate fully.

The studies presented here also demonstrate the value of intentionally deviating from replicating human vision in archaeological imaging (Chapter 2.2.1). None of the contributions this thesis makes to photographic and imaging techniques replicate human vision; at the very least, they provide a much closer view of the object through photomacrography or photomicrography and at most they delve into light spectra that are invisible to humans. Furthermore, the data recovered and conclusions drawn by the case studies in this thesis are not possible without deviating from replicating human vision in imaging these objects. The conclusions I have drawn here are only possible through challenging the emphasis on realism in archaeological imaging.

In addition to deviating from replicating human vision, these studies also intentionally deviate from the standard, prescribed methods of archaeological photography and photography-based imaging (Chapter 2.2.1). The techniques presented in this thesis do not image an object using perfectly angled LED visible-range lighting and many prefer to emphasise rather than minimise shadows. They use visible- and non-visible-range filters and alter the images in post-processing through white-balancing and exposure adjustment. Nearly all outputs are composite images of multiple visible- or non-visible-range photographs and a significant proportion of the equipment used to generate these images was made of computer paper, paperclips, tape and adhesive putty. Just as the conclusions drawn in this thesis are only possible through challenging the emphasis on realism in archaeological photography, so too are they only possible through challenging the prescribed standards of archaeological imaging.

Finally, these case studies demonstrate that less objective methods still produce important and viable results. Neither bubble concentrations nor chemical composition of glass can be objectively measured through spectral photography alone (Chapters 4.2 and 5.3). It is the identical treatment of the images that allows this thesis to compare the relative similarities and differences between samples and draw informed conclusions from the results. Our analysis therefore need not be truly objective to provide important information that is otherwise difficult or impossible to uncover. Indeed, by employing less-objective techniques in addition to objective ones, we can uncover more information about the past than if we were to limit ourselves to one or the other.

9.1.2 The Value of Older Technologies

Many of the current seminars and publications concerning digital visualisation in archaeology focus on using the latest new technology either to understand the archaeological landscape or to document and visualise an archaeological excavation (e.g. Dellepiane et al. 2006; Doneus and Briese 2006; Doneus et al. 2011; Earl et al. 2008; Earl et al. 2010; Mudge et al. 2005; Mudge et al. 2006; Nylén 2008; Remondino et al. 2009; Remondino 2011). When new techniques appear, many archaeologists discard previously championed methods in favour of the latest new technology. Most of these newly proposed digital techniques emphasise new equipment, new methods, new software, and new algorithms.

The pursuit of new technologies is valuable in archaeology, but the pursuit of new technologies to the detriment of older ones is becoming problematic. First, the rapidity with which technology changes coupled with the limitations of standardised methods and the replication of human vision described above ensure that archaeology rarely will understand and exploit an imaging technology to its fullest before moving on to the latest new piece of equipment. By continually discarding or discrediting older technologies

when new ones arrive, we are allowing the possible information gleaned from them to remain undiscovered and unused.

Second, technology changes rapidly, and each change in technology requires funds to continue to progress. Very little new technology is ever affordable for lower-budget projects, and the specifics of new techniques or of the software developed for them rarely appears in an openly accessible manner. New technologies and techniques are valuable, and we should not abandon our interest in them. However, our current obsession with an emphasis on these techniques is widening the economic gap, and therefore the perceived academic gap, between those projects that can afford the technology and those that cannot (Chapter 2.2.2).

The results of this thesis demonstrate that a technology is not less useful or less innovative merely because it is older or less expensive. The principles of photography are sound and relatively easy to manipulate when understood. In exploring and experimenting with photography, this thesis has uncovered results that have significantly added to our understanding of glass manufacture and trade in Iron Age and Early Medieval Scotland. While it is possible to make these conclusions using newer technologies such as x-ray computed tomography and LA-ICP-MS, these techniques are expensive. The logistics required for conducting a study of this scale using x-ray computed tomography and LA-ICP-MS are also complex, and they are unlikely to garner permission from the museums in which the objects are housed due to the destructive nature of LA-ICP-MS. The argument can be made that current technologies are becoming cheaper by the day, but relying on the capitalist market to reduce the price of a technology for those currently unable to afford it merely passes the responsibility to a third party, one with a vested interest in making a profit. The price of technology lowers because demand lowers, and demand lowers often because the technique is older and seen by many fields as less

objective than the newest technology. Consequently, by the time the price of the current newest technology like x-ray computed tomography lowers to a price range most archaeological projects can afford, the field will have progressed to even newer technologies and relegated x-ray computed tomography to a similarly denigrated status as currently less-valued technologies like photography. The system will continue as it has, along with the widening economic gap between projects and the perceived difference in the inherent value of their results.

By comparison, the techniques proposed here are affordable, portable, practical, non-contact, and produce results comparatively quickly (Chapter 8). They are not new technologies, but they have led to conclusions that, according to current archaeological practice, are not currently possible without expensive, newer technologies. The methods developed in this thesis are not meant to replace newer technologies; rather, they are intended to begin narrowing this divide between higher- and lower-budget projects and the results they can produce. These techniques therefore demonstrate the need to champion exploration and experimentation with older technologies to the same degree we do newer ones, which in turn will provide affordable means of analysis for lower-budget projects in addition to higher-budget ones.

Finally, while archiving does not form a significant discussion throughout this thesis, it would be remiss not to address the topic in relation to newer versus older technologies. Chapter 2.2.3 discusses the difficulties of changes in technology bringing with them changes to archaeological record keeping and archival practices. Many newer technologies continue to create outputs using unusual or new filetypes for which the discipline has not yet developed systematic archival practices or safeguards. The continued emphasis on new technology has created an explosion in data and outputs within the archaeological record that consequently are less likely to securely enter the

archaeological record due to a current lack of standard archival practices that best protect said data. The consequences for creating an abundance of data in new file formats or using new storage methods could be severe, however, and society has seen examples in which data on floppy disks, photographic slides, and even CD-ROMS – all of which were new at one time – have become or are becoming obsolete. Artec has discontinued 10 models since 2007 alone (Artec 2018d). Certain photogrammetric files will not open in any program other than Agisoft Photoscan, for example, and even within this software, there are certain filetypes that only open in the Professional version and not the Standard. Other types of files only open with the software specifically designated for a certain brand's laser or white-light scanner. This is a perpetual problem in archival work, one that likely will never disappear. The archaeological record would likely benefit from techniques that lend themselves better to current archival practices, however, at least until new practices can develop for newer technologies.

9.1.3   Archaeological Imaging and the Archaeological Record

Connected to issues of archival practices, there are problems concerning archaeology's current approaches to archaeological imaging and the selection and retention of information in the archaeological record. Our understanding of the archaeological record as a discipline directly correlates to the degree to which we 'see' elements of that record (Chapter 2.2.3). Famous paintings are famous in large part because they were photographed and widely disseminated. Similarly, objects that photograph well are better-known in the archaeological community than those that do not, such as SRT objects. While there are certainly archaeological photographs of SRT objects, archaeology has concentrated on photographing only the relatively unique objects in an informative manner (e.g. the Hunterston Brooch or the Lycurgus Cup). The lack of

informative images of subjects that do not lend themselves well to current imaging techniques results in the general omission of these objects from the archaeological record.

As a field, we are largely unconscious of this choice, but it is indeed a choice. The omission of these objects from the archaeological record is perpetuated by our continued insistence on employing imaging technologies in prescribed, standard ways to create standard images with a standard aesthetic and by our failure to explore and experiment with the boundaries of current archaeological imaging. Instead, we can consciously choose to investigate currently available technologies for their capacity to document objects using non-standard methods. This thesis has demonstrated several ways in which this type of investigation expands the boundaries of what is currently possible and results in more informative visualisations of SRT objects than is otherwise currently feasible. If challenging the limits of archaeological photography and photography-based imaging produces such informative and beneficial results for SRT objects, it is likely to do so for any archaeological subject currently underrepresented in the archaeological record.

Importantly, archaeology need not explore these boundaries on its own. One important contribution to this thesis and this approach more generally has been that of other disciplines, particularly physics, chemistry, biology, ecology, geology, and art history and conservation. The insights gained here would not be as numerous nor as developed were it not for previous research in each of these fields. Many other fields have spent decades investigating non-standard methods for currently available technologies already and serve as vital inspiration for applying similar methods in archaeological imaging. In beginning to challenge our own imaging standards, then, we would do well to examine the progress other disciplines have made already in employing current technologies in new and innovative ways.

The results of this thesis therefore demonstrate that photographs need not be specifically objective, nor mimic human vision, nor follow specific, prescribed methods of capture to be valuable in archaeological research. This thesis also champions the exploration of and experimentation with older technologies in addition to newer ones and the investigation of creating affordable, portable, and practical techniques that benefit all archaeological research, regardless of their budgetary circumstances. Finally, it recognises and champions the responsibility of archaeology to examine the consequences of current techniques on the archaeological record and to work to eliminate any biases. This proposed approach to archaeological visualisation will result in the recovery of more information and the preservation of more archaeological material than currently possible.

9.2 FUTURE WORK

There are many avenues for future work relating to this thesis, both specifically for glass and glass beads and for archaeological imaging more generally. First, the differences in bubble concentrations between otherwise typologically similar glass beads has not been examined in bead studies before. Photographing more objects would build a corpus of information that may lead to more specific conclusions, such as how or where an object may have been made. Additionally, the control of bubbles exhibited by certain objects warrants further research, particularly in Scotland, as it demonstrates a skill with glass that has not been recognised previously.

Photographing objects that have already been chemically tested would help develop the spectral imaging technique used in Chapter 5 significantly. The primary difficulty in making conclusions from the data presented was in not having enough previously analysed material for specific chemical components. Photographing objects with confirmed chemical compositions would allow us to narrow the possible list of

chemical factors affecting reactions to near-infrared and near-ultraviolet light. Such chemical testing could elucidate whether lead-tin and lead-antimonate yellows differ significantly in their reactions, for example, which would allow researchers to classify yellow glass from this period as Roman or Merovingian in origin with significantly less need of destructive chemical testing. Additionally, capturing data for other contemporary glass bead collections would allow for extensive regional comparison that is not currently available due to the limited number of chemically tested objects.

Spectral photography or RTI of glass and glass beads would improve our knowledge of surface wear significantly without requiring more expensive techniques. Surface wear is seldom examined for glass objects, and further examination could lead to the differentiation between production, use, and post-depositional wear. Unfortunately, while the photogrammetric results were significantly more successful than any other 3D modelling technique except x-ray computed tomography, the detail in the results is too variable to suggest further research into glass beads using photogrammetry. However, further work and experimentation with photogrammetry and photogrammetric software could provide consistently successful photogrammetric results.

All case studies included in this thesis would benefit from collections with contextual and chronological data. Most glass beads in Scottish contexts are stray finds with little to no contextual or chronological information. Imaging collections that differed in where they were found, how they were deposited, and when they were made and used would likely result in significant conclusions about the larger workings of the societies in which they circulated.

On a more general level, we should apply these techniques to other object types, both SRT and non-SRT, to determine the degree to which they are successful for each. Different materials react differently to light and are therefore more or less amenable to

different technologies. While the technologies discussed in this thesis certainly work for glass beads and appear to work for amber, ceramic, metal, faience, and lithic materials, they may differ in their degree of success. It is important to investigate the possible benefits of these techniques with other objects to understand their applicability in archaeology more generally.

These techniques need not be limited to archaeology, either. Specialists could apply them to geological, ecological, biological, art historical, or even mechanical research. Spectral imaging would assist in the identification of precious and semi-precious stone and the quarries it comes from, for example. The photogrammetry techniques can help create models of metal parts of machinery, particularly smaller pieces. While many research teams in these fields have access to more technologically advanced methods, many would also benefit from more affordable and portable techniques.

Finally, there is future work relating to how archaeology views digital imaging. Further research investigating the analytical applications of photography and digital imaging would encourage archaeology to deviate from the standard technique of mimicking what the human eye can see. We should also continue to experiment with imaging archaeological subjects using non-standard methods. Doing so would increase the versatility of digital imaging and encourage further innovation directly pertinent to archaeology. We must also investigate the applications of current technologies in addition to newly developed ones to maximise the tools at our disposal. There are many avenues for future research, then, all of which would benefit archaeology and archaeological imaging.

9.3   CONCLUSION

Archaeological imaging often advocates for the use of expensive, complex imaging technologies that create visualisations closely mimicking that seen by the human eye through standard, prescribed techniques. While this approach is beneficial for archaeological recording, it severely limits the possible applications of archaeological imaging. It contributes to the omission of certain archaeological subjects from the visual archaeological record and to an economic bias that favours the results of projects that can afford the latest new technology over those that cannot.

This thesis has demonstrated the value of pushing the boundaries of archaeological imaging and experimenting with novel approaches to the discipline. The results presented here led to conclusions that are not currently possible through visual comparison and are not currently feasible using other imaging techniques due to logistical, technological, and budgetary restrictions. Thus, to combat the current difficulties faced in archaeological imaging and to exploit the full potential of archaeological imaging techniques, we must approach digital imaging from alternate angles and test the limits of each technology currently available to us. It is our responsibility to create imaging techniques that benefit archaeology as a whole; we must not leave the task to other disciplines nor focus solely on techniques few can afford. Only by exploring and experimenting with currently available imaging technologies in non-standard ways can we realise the true potential of archaeological imaging.

APPENDIX A: CORPUS OF OBJECTS INCLUDED IN THIS THESIS

SCOTTISH BEADS:

Accession #	Site name	Museum	Colours	Bubble Samples	Chemistry Samples	RTI	SFM	Description
B.1914.521/1	Balevullin	Hunterian Museum and Art Gallery, Glasgow	Natural	1				Naturally-green annular bead with black swag design.
ABDUA 15528	Ballater Glenmuick	Marischal Museum, Aberdeen	Cobalt-blue; yellow	2	2			Guido Class 14 black annular bead with yellow rays emanating from the centre.

Accession #	Site name	Museum	Colours	Bubble Samples	Chemistry Samples	RTI	SFM	Description
X.FJ 16	Balmerion	National Museums Scotland, Edinburgh	Yellow	1				Naturally-brown Guido Class 13 bead with yellow spirals.
SF 56	Balure Dun	Kilmartin House Museum, Kilmartin	Natural	1	1	Yes	Yes	Naturally-blue globular bead.
SF 57	Balure Dun	Kilmartin House Museum, Kilmartin	Natural	1	1	Yes		Naturally-blue toggle bead.
SF 58	Balure Dun	Kilmartin House Museum, Kilmartin	Copper-blue	1	1	Yes		Copper-blue toggle bead.
ABDUA 15526	Banff	Marischal Museum, Aberdeen	Natural; white; yellow	3	3			Naturally-brown Guido Class 13 bead with yellow/white spirals.

Accession #	Site name	Museum	Colours	Bubble Samples	Chemistry Samples	RTI	SFM	Description
ABDUA 15531	Buchan	Marischal Museum, Aberdeen	Cobalt-blue; white	2	2			Cobalt-blue globular bead with white swag design.
Unknown #	Castle Craig	University of Glasgow Archaeology Dept.	Cobalt-blue	1		Yes	Yes	Cobalt-blue biconical wound bead. Likely Roman.
Unknown #	Castle Craig	University of Glasgow Archaeology Dept.	NA: Faience bead				Yes	Turquoise-coloured faience melon bead. Likely Roman.
ABDUA 15530	Chapel of Garioch	Marischal Museum, Aberdeen	Yellow	1	1			Black Guido Class 14 bead with yellow whirl design.

Accession #	Site name	Museum	Colours	Bubble Samples	Chemistry Samples	RTI	SFM	Description
CLB 1	Clachbreck	University of Glasgow Archaeology Dept.	Cobalt-blue	1	1			Small cobalt-blue globular bead.
B.1914.521/27	Clarilaw Muir	Hunterian Museum and Art Gallery, Glasgow	Cobalt-blue	1				Cobalt blue bead with opaque red glass marbled into the surface.
X.FJ 13	Clova	National Museums Scotland, Edinburgh	Yellow	1				Naturally-brown Guido Class 13 bead with yellow spirals.
X.FJ 169	Coldingham	National Museums Scotland, Edinburgh	Cobalt-blue	1				Cobalt-blue globular bead.

Accession #	Site name	Museum	Colours	Bubble Samples	Chemistry Samples	RTI	SFM	Description
X.FJ 32	Coulter	National Museums Scotland, Edinburgh	Green	1				Dark green, pressed lozenge-shaped glass bead.
A.1905.2	Craigsfordmains	Hunterian Museum and Art Gallery, Glasgow	White	1				Cobalt-blue glass bead with white spiral eyes.
ABDUA 15507	Culbin Sands	Marischal Museum, Aberdeen	Green; yellow	2	1			Guido Class 13 dark green bead fragment with yellow spirals.
ABDUA 15514	Culbin Sands	Marischal Museum, Aberdeen	Yellow	1	1			Guido Class 13 brown bead fragment with yellow spirals.

Accession #	Site name	Museum	Colours	Bubble Samples	Chemistry Samples	RTI	SFM	Description
ABDUA 15524	Culbin Sands	Marischal Museum, Aberdeen	Cobalt-blue	1	1			Cobalt-blue annular glass bead.
ABDUA 15694	Culbin Sands	Marischal Museum, Aberdeen	Natural; yellow	2	2			Naturally-yellow globular glass bead with opaque yellow core.
ABDUA 15695	Culbin Sands	Marischal Museum, Aberdeen	Yellow	1	1			Annular yellow glass bead.
ABDUA 39481	Culbin Sands	Marischal Museum, Aberdeen	Yellow	1	1			Small yellow glass bead.
ABDUA 39482	Culbin Sands	Marischal Museum, Aberdeen	Cobalt-blue	1	1			Wound cobalt-blue bicone.

Accession #	Site name	Museum	Colours	Bubble Samples	Chemistry Samples	RTI	SFM	Description
ABDUA 39486	Culbin Sands	Marischal Museum, Aberdeen	Cobalt-blue	1	1			Small opaque greyish cobalt-blue bead. Possibly post-medieval.
B.1951.971/31	Culbin Sands	Hunterian Museum and Art Gallery, Glasgow	Copper-blue	1				Long copper-blue bead or glass tube.
Unknown	Culbin Sands	National Museums Scotland, Edinburgh	Yellow	1				Annular yellow glass bead fragment.
X.BIB 10	Culbin Sands	National Museums Scotland, Edinburgh	White; yellow	2	2			Brown Guido Class 13 bead with yellow and white spirals.

Accession #	Site name	Museum	Colours	Bubble Samples	Chemistry Samples	RTI	SFM	Description
X.BIB 11	Culbin Sands	National Museums Scotland, Edinburgh	White; yellow	3	3			Purple Guido Class 13 bead fragment with a white core and yellow, white, and purple spirals.
X.BIB 12	Culbin Sands	National Museums Scotland, Edinburgh	Cobalt-blue	1				Highly corroded/melted cobalt-blue globular bead.
X.BIB 13	Culbin Sands	National Museums Scotland, Edinburgh	Natural; yellow	2	1			Purple Guido Class 13 bead with yellow spirals and naturally-green dots.

Accession #	Site name	Museum	Colours	Bubble Samples	Chemistry Samples	RTI	SFM	Description
X.BIB 14	Culbin Sands	National Museums Scotland, Edinburgh	Natural; yellow	2				Naturally-yellow bead with opaque yellow marbled into the surface.
X.BIB 15	Culbin Sands	National Museums Scotland, Edinburgh	Cobalt-blue; yellow	2	2	Yes	Yes	Cobalt-blue bead with opaque yellow marbled into the surface.
X.BIB 16	Culbin Sands	National Museums Scotland, Edinburgh	Natural; white; yellow	3				Naturally blue-green Guido Class 14 bead fragment with white and yellow whirls.

Accession #	Site name	Museum	Colours	Bubble Samples	Chemistry Samples	RTI	SFM	Description
X.BIB 17	Culbin Sands	National Museums Scotland, Edinburgh	Green; white; yellow	4				Dark green Guido Class 14 bead with yellow and white/dark green reticella whirls.
X.BIB 18	Culbin Sands	National Museums Scotland, Edinburgh	Cobalt-blue; white; yellow	3				Annular bead with cobalt-blue, white, yellow, and red whirls.
X.BIB 19	Culbin Sands	National Museums Scotland, Edinburgh	Cobalt-blue; natural; yellow	3				Cobalt-blue Guido Class 13 bead fragment with yellow spirals and

Accession #	Site name	Museum	Colours	Bubble Samples	Chemistry Samples	RTI	SFM	Description
								naturally green elements.
X.BIB 20	Culbin Sands	National Museums Scotland, Edinburgh	Cobalt-blue; yellow	2				Cobalt-blue Guido Class 13 bead fragment with yellow spirals.
X.BIB 21	Culbin Sands	National Museums Scotland, Edinburgh	Cobalt-blue; white	2				Cobalt-blue and white reticella annular bead.
X.BIB 22	Culbin Sands	National Museums Scotland, Edinburgh	Cobalt-blue	1				Drawn cobalt-blue segmented bead. Likely Norse.

Accession #	Site name	Museum	Colours	Bubble Samples	Chemistry Samples	RTI	SFM	Description
X.BIB 24	Culbin Sands	National Museums Scotland, Edinburgh	Copper-blue	1				Small copper-blue segmented melon bead.
X.BIB 27	Culbin Sands	National Museums Scotland, Edinburgh	NA: Amber bead			Yes	Yes	Short cylinder amber bead.
X.BIB 30	Culbin Sands	National Museums Scotland, Edinburgh	Copper-blue	1				Highly corroded/melted copper-blue globular bead fragment
X.BIB 31	Culbin Sands	National Museums Scotland, Edinburgh	Cobalt-blue	1				Cobalt-blue globular bead fragment.
X.BIB 32	Culbin Sands	National Museums Scotland, Edinburgh	Cobalt-blue	1				Cobalt-blue globular bead fragment.

Accession #	Site name	Museum	Colours	Bubble Samples	Chemistry Samples	RTI	SFM	Description
X.BIB 33	Culbin Sands	National Museums Scotland, Edinburgh	Cobalt-blue	1				Cobalt-blue globular bead fragment.
X.BIB 34	Culbin Sands	National Museums Scotland, Edinburgh	Cobalt-blue	1				Cobalt-blue globular bead fragment.
X.BIB 35	Culbin Sands	National Museums Scotland, Edinburgh	Cobalt-blue	1				Cobalt-blue bead with faceted seed-like shape.
X.BIB 36	Culbin Sands	National Museums Scotland, Edinburgh	Cobalt-blue	1				Cobalt-blue bead with faceted seed-like shape.
X.BIB 37	Culbin Sands	National Museums Scotland, Edinburgh	Copper-blue	1	1		Yes	Copper-blue annular bead.

Accession #	Site name	Museum	Colours	Bubble Samples	Chemistry Samples	RTI	SFM	Description
X.BIB 38	Culbin Sands	National Museums Scotland, Edinburgh	Copper-blue	1				Copper-blue globular bead.
X.BIB 39	Culbin Sands	National Museums Scotland, Edinburgh	Copper-blue	1				Copper-blue globular bead.
X.BIB 40	Culbin Sands	National Museums Scotland, Edinburgh	Cobalt-blue	1				Cobalt-blue thick annular bead.
X.BIB 41	Culbin Sands	National Museums Scotland, Edinburgh	Cobalt-blue	1				Cobalt-blue annular bead.
X.BIB 42	Culbin Sands	National Museums Scotland, Edinburgh	Cobalt-blue	1				Cobalt-blue annular bead.
X.BIB 43	Culbin Sands	National Museums Scotland, Edinburgh	Cobalt-blue	1				Cobalt-blue annular bead.

Accession #	Site name	Museum	Colours	Bubble Samples	Chemistry Samples	RTI	SFM	Description
X.BIB 44	Culbin Sands	National Museums Scotland, Edinburgh	Cobalt-blue	1				Cobalt-blue disc bead.
X.BIB 45	Culbin Sands	National Museums Scotland, Edinburgh	Copper-blue	1				Copper-blue annular bead fragment.
X.BIB 5	Culbin Sands	National Museums Scotland, Edinburgh	Yellow	91	91			String of 91 yellow annular beads.
X.BIB 52	Culbin Sands	National Museums Scotland, Edinburgh	Copper-blue	1				Copper-blue globular bead.
X.BIB 56	Culbin Sands	National Museums Scotland, Edinburgh	Cobalt-blue	11	12			String of 12 cobalt-blue beads.
X.BIB 57	Culbin Sands	National Museums Scotland, Edinburgh	Cobalt-blue; copper-blue	34	36			String of 35 copper-blue beads and one cobalt-blue bead.

Accession #	Site name	Museum	Colours	Bubble Samples	Chemistry Samples	RTI	SFM	Description
X.BIB 58	Culbin Sands	National Museums Scotland, Edinburgh	Green	7				String of 37 green glass beads.
X.BIB 6	Culbin Sands	National Museums Scotland, Edinburgh	White; yellow	2				Amber-coloured bead with yellow and white lines.
X.BIB 70	Culbin Sands	National Museums Scotland, Edinburgh	Copper-blue	1				Cobalt-blue square disc bead fragment.
X.BIB 8	Culbin Sands	National Museums Scotland, Edinburgh	Yellow	1				Deep purple Guido Class 13 bead fragment with yellow spirals.

Accession #	Site name	Museum	Colours	Bubble Samples	Chemistry Samples	RTI	SFM	Description
X.BIB 9	Culbin Sands	National Museums Scotland, Edinburgh	Yellow	1	1	Yes	Yes	Black Guido Class 13 bead fragment with yellow spirals.
B.1914.521/11b	Dryburgh	Hunterian Museum and Art Gallery, Glasgow	Cobalt-blue	1				Wound cobalt-blue bead with greenish tinge. Possibly copper-blue.
Captm 1418	Dun Fhinn	Kilmartin House Museum, Kilmartin	Cobalt-blue	1	1	Yes		Cobalt-blue toggle bead.
SF 22	Earl's Bu	University of Glasgow Archaeology Dept.	Copper-blue	1				Small, cylindrical cobalt-blue bead.

Accession #	Site name	Museum	Colours	Bubble Samples	Chemistry Samples	RTI	SFM	Description
SF 712	Earl's Bu	University of Glasgow Archaeology Dept.	Cobalt-blue	1				Drawn cobalt-blue segmented bead. Likely Norse.
SF 743	Earl's Bu	University of Glasgow Archaeology Dept.	Natural	1				Naturally-green thick annular bead.
SF 881	Earl's Bu	University of Glasgow Archaeology Dept.	Cobalt-blue	1				Cobalt-blue melon bead.
Unknown	Earlston	National Museums Scotland, Edinburgh	Cobalt-blue	1				Cobalt-blue globular bead.

Accession #	Site name	Museum	Colours	Bubble Samples	Chemistry Samples	RTI	SFM	Description
X.FJ 142	Earlston	National Museums Scotland, Edinburgh	Cobalt-blue	1				Large cobalt-blue bead with white spiral protrusions.
X.BK 1	Fendom Sands	National Museums Scotland, Edinburgh	Copper-blue	1				Short cylinder copper-blue bead.
X.BK 2	Fendom Sands	National Museums Scotland, Edinburgh	Green	1				Green barrel-shaped glass bead.
X.BK 157	Fendom Sands	National Museums Scotland, Edinburgh	Cobalt-blue	1				Copper-blue annular bead fragment.
X.BK 158	Fendom Sands	National Museums Scotland, Edinburgh	Cobalt-blue	1				Cobalt-blue (possibly copper-blue) annular bead.

Accession #	Site name	Museum	Colours	Bubble Samples	Chemistry Samples	RTI	SFM	Description
X.BK 159	Fendom Sands	National Museums Scotland, Edinburgh	Copper-blue; green	2				Copper-blue glass tube or long bead with green chunks inlaid.
X.FJ 123	Fetlar	National Museums Scotland, Edinburgh	Yellow	1				Yellow annular bead.
Unknown #	Forteviot	University of Glasgow Archaeology Dept.	Cobalt-blue	1		Yes	Yes	Small cobalt-blue segmented bead. Likely Norse.
Unknown #	Forteviot	University of Glasgow Archaeology Dept.	Natural	1		Yes	Yes	Pressed naturally-blue donut bead.

Accession #	Site name	Museum	Colours	Bubble Samples	Chemistry Samples	RTI	SFM	Description
X.BHB 10	Glenluce Sands	National Museums Scotland, Edinburgh	Natural; yellow	2				Naturally-green Guido Class 13 bead with yellow spirals.
X.BHB 11	Glenluce Sands	National Museums Scotland, Edinburgh	Cobalt-blue	1				Cobalt-blue globular bead.
X.BHB 12	Glenluce Sands	National Museums Scotland, Edinburgh	Cobalt-blue	1	1	Yes	Yes	Cobalt-blue globular bead.
X.BHB 13	Glenluce Sands	National Museums Scotland, Edinburgh	Copper-blue	1				Copper-blue barrel-shaped bead.
X.BHB 14	Glenluce Sands	National Museums Scotland, Edinburgh	Natural	1				Naturally-blue toggle bead.

Accession #	Site name	Museum	Colours	Bubble Samples	Chemistry Samples	RTI	SFM	Description
X.BHB 17	Glenluce Sands	National Museums Scotland, Edinburgh	Cobalt-blue; white; yellow	3	3	Yes	Yes	Cobalt-blue segmented (fused?) bead with white double-swag design on one segment and an unmarvered yellow zone line on the other.
X.BHB 18	Glenluce Sands	National Museums Scotland, Edinburgh	Yellow	1				Cobalt-blue bead with white and yellow raised dots.
X.BHB 19	Glenluce Sands	National Museums Scotland, Edinburgh	White; yellow	2				Small cobalt-blue Guido Class 13 bead

Accession #	Site name	Museum	Colours	Bubble Samples	Chemistry Samples	RTI	SFM	Description
								with yellow dots and white and yellow zone lines.
X.BHB 20.1	Glenluce Sands	National Museums Scotland, Edinburgh	Yellow	1	1			Annular yellow glass bead.
X.BHB 20.2	Glenluce Sands	National Museums Scotland, Edinburgh	Yellow	1	1			Annular yellow glass bead.
X.BHB 20.3	Glenluce Sands	National Museums Scotland, Edinburgh	Yellow	1	1			Annular yellow glass bead.
X.BHB 20.4	Glenluce Sands	National Museums Scotland, Edinburgh	Yellow	1	1	Yes	Yes	Annular yellow glass bead.
X.BHB 20.5	Glenluce Sands	National Museums Scotland, Edinburgh	Yellow	1	1			Annular yellow glass bead.

Accession #	Site name	Museum	Colours	Bubble Samples	Chemistry Samples	RTI	SFM	Description
X.BHB 21	Glenluce Sands	National Museums Scotland, Edinburgh	Yellow	1	1			Annular yellow glass bead.
X.BHB 22	Glenluce Sands	National Museums Scotland, Edinburgh	Yellow	2	2			Annular and globular yellow glass bead.
X.BHB 23.1	Glenluce Sands	National Museums Scotland, Edinburgh	Cobalt-blue	1	1			Cobalt-blue annular bead fragment.
X.BHB 23.2	Glenluce Sands	National Museums Scotland, Edinburgh	Cobalt-blue	1	1			Cobalt-blue annular bead.
X.BHB 23.3	Glenluce Sands	National Museums Scotland, Edinburgh	Cobalt-blue	1	1			Cobalt-blue annular bead.
X.BHB 23.4	Glenluce Sands	National Museums Scotland, Edinburgh	Cobalt-blue	1	1			Cobalt-blue annular bead.

Accession #	Site name	Museum	Colours	Bubble Samples	Chemistry Samples	RTI	SFM	Description
X.BHB 23.5	Glenluce Sands	National Museums Scotland, Edinburgh	Cobalt-blue	1	1			Cobalt-blue annular bead.
X.BHB 23.6	Glenluce Sands	National Museums Scotland, Edinburgh	Cobalt-blue	1	1			Cobalt-blue annular bead.
X.BHB 23.7	Glenluce Sands	National Museums Scotland, Edinburgh	Cobalt-blue	1	1			Cobalt-blue annular bead.
X.BHB 24	Glenluce Sands	National Museums Scotland, Edinburgh	Cobalt-blue	1				Cobalt-blue globular bead.
X.BHB 25	Glenluce Sands	National Museums Scotland, Edinburgh	Cobalt-blue	1				Cobalt-blue globular bead.
X.BHB 26	Glenluce Sands	National Museums Scotland, Edinburgh	Cobalt-blue	1	1			Cobalt-blue bicone.

Accession #	Site name	Museum	Colours	Bubble Samples	Chemistry Samples	RTI	SFM	Description
X.BHB 27	Glenluce Sands	National Museums Scotland, Edinburgh	Cobalt-blue	1	1			Short cobalt-blue bicone.
X.BHB 28	Glenluce Sands	National Museums Scotland, Edinburgh	Cobalt-blue	1				Cobalt-blue bead with faceted seed-like shape.
X.BHB 29	Glenluce Sands	National Museums Scotland, Edinburgh	Cobalt-blue	1				Cobalt-blue bead with faceted seed-like shape.
X.BHB 36	Glenluce Sands	National Museums Scotland, Edinburgh	NA: Amber bead			Yes	Yes	Barrel-shaped amber bead.
X.BHB 51	Glenluce Sands	National Museums Scotland, Edinburgh	Yellow	1				Opaque yellow bead fragment with

Accession #	Site name	Museum	Colours	Bubble Samples	Chemistry Samples	RTI	SFM	Description
								naturally-yellow core.
X.BHB 52	Glenluce Sands	National Museums Scotland, Edinburgh	Yellow	1	1			Yellow globular bead.
X.BHB 53	Glenluce Sands	National Museums Scotland, Edinburgh	Copper-blue	1				Long copper-blue bead or glass tube.
X.BHB 61	Glenluce Sands	National Museums Scotland, Edinburgh	Natural; yellow	4				Naturally-green bead fragments with yellow stripes.
X.BHB 63	Glenluce Sands	National Museums Scotland, Edinburgh	Copper-blue	1				Naturally-blue pinhead (?) fragment.

Accession #	Site name	Museum	Colours	Bubble Samples	Chemistry Samples	RTI	SFM	Description
X.BHB 9	Glenluce Sands	National Museums Scotland, Edinburgh	Natural; yellow	2				Naturally-yellow Guido Class 13 bead with yellow spirals
Unknown #	Glenshee	Northlight Heritage, York	Green	2		Yes	Yes	Tiny triple-segmented (fused?) bead with 2 green segments and one dark green segment.
X.BJ 204	Golspie Links	National Museums Scotland, Edinburgh	Cobalt-blue	1				Short cobalt-blue melon bead.
X.BJ 205	Golspie Links	National Museums Scotland, Edinburgh	Cobalt-blue	1				Small cobalt-blue disc bead.

Accession #	Site name	Museum	Colours	Bubble Samples	Chemistry Samples	RTI	SFM	Description
X.BJ 206	Golspie Links	National Museums Scotland, Edinburgh	Yellow	1				Small yellow thick annular bead.
X.FJ 171	Inveresk	National Museums Scotland, Edinburgh	Cobalt-blue	1				Cobalt-blue long-bead or glass tube.
	Iona Abbey	Iona Abbey Museum	Cobalt-blue; white	3	1			Cobalt-blue long glass bead fragment with cobalt-blue and white reticella lines and spirals.
ABDUA 14350	Jericho	Marischal Museum, Aberdeen	Copper-blue	1	1			Copper-blue wound globular bead.
ABDUA 15505	Jericho	Marischal Museum, Aberdeen	Cobalt-blue;	4	5			Naturally-green pinhead (?) with

Accession #	Site name	Museum	Colours	Bubble Samples	Chemistry Samples	RTI	SFM	Description
			natural; white; yellow					red/yellow and cobalt-blue/white spiral designs.
ABDUA 15536	Kildrummy	Marischal Museum, Aberdeen	White; yellow	2	2			Guido Class 14 black annular bead with yellow and white whirl design.
ABDUA 15538	Kildrummy	Marischal Museum, Aberdeen	Natural; yellow	2	2			Naturally-brown Guido Class 14 bead with yellow whirl designs.

Accession #	Site name	Museum	Colours	Bubble Samples	Chemistry Samples	RTI	SFM	Description
B.1914.524/1	Knowe of Moan	Hunterian Museum and Art Gallery, Glasgow	Cobalt-blue	5				Five drawn cobalt-blue segmented beads, one of which has white lines running between the perforations. Likely Norse.
B.1914.524/14	Knowe of Moan	Hunterian Museum and Art Gallery, Glasgow	Cobalt-blue	1				Wound globular cobalt-blue bead.
B.1914.524/1a	Knowe of Moan	Hunterian Museum and Art Gallery, Glasgow	Cobalt-blue	1				Wound segmented cobalt-blue bead.

Accession #	Site name	Museum	Colours	Bubble Samples	Chemistry Samples	RTI	SFM	Description
B.1914.524/3	Knowe of Moan	Hunterian Museum and Art Gallery, Glasgow	Cobalt-blue; white; yellow	2				Large cobalt-blue glass bead with cobalt-blue and white reticella collars, blue and white reticella lines and raised yellow dots. Likely Irish.
B.1914.524/4	Knowe of Moan	Hunterian Museum and Art Gallery, Glasgow	Cobalt-blue	1				Cobalt-blue collared bead with large central bulge.

Accession #	Site name	Museum	Colours	Bubble Samples	Chemistry Samples	RTI	SFM	Description
B.1914.524/6	Knowe of Moan	Hunterian Museum and Art Gallery, Glasgow	Cobalt-blue; yellow	3				Two globular yellow beads and one cobalt-blue bead from a larger string.
F 128	Loch Eriboll	University of Glasgow Archaeology Dept.	Natural; yellow	2	1	Yes	Yes	Naturally-green Guido Class 13 bead with yellow spirals
X.FJ 163	Meiklelaw Field	National Museums Scotland, Edinburgh	Copper-blue	1				Copper-blue globular bead, probably post-medieval.
X.FJ 164	Meiklelaw Field	National Museums Scotland, Edinburgh	Cobalt-blue	1				Cobalt-blue globular bead.

Accession #	Site name	Museum	Colours	Bubble Samples	Chemistry Samples	RTI	SFM	Description
X.FJ 165	Meiklelaw Field	National Museums Scotland, Edinburgh	Copper-blue	1				Copper-blue globular bead.
X.FJ 167	Meiklelaw Field	National Museums Scotland, Edinburgh	Copper-blue	1				Copper-blue globular bead, probably post-medieval.
ABDUA 15539	Mill of Gellan	Marischal Museum, Aberdeen	Copper-blue; white; yellow	3	4			Black Guido Class 14 bead with yellow, white, and copper-blue whirl design.
ABDUA 15540	Mill of Gellan	Marischal Museum, Aberdeen	Copper-blue; yellow	2	2			Copper-blue Guido Class 14 bead

Accession #	Site name	Museum	Colours	Bubble Samples	Chemistry Samples	RTI	SFM	Description
								fragment with yellow whirl design.
ABDUA 15544	Mill of Gellan	Marischal Museum, Aberdeen	Yellow	1	1			Brown Guido Class 13 bead with yellow spirals.
F.1905.3	Newstead	Hunterian Museum and Art Gallery, Glasgow	Cobalt-blue	1				Cobalt-blue melon bead. Likely Roman. Possibly dark green.
F.1905.4	Newstead	Hunterian Museum and Art Gallery, Glasgow	Natural	1				Naturally-green globular bead.
X.FRA 861	Newstead	National Museums Scotland, Edinburgh	Cobalt-blue	1				Cobalt-blue melon bead.

Accession #	Site name	Museum	Colours	Bubble Samples	Chemistry Samples	RTI	SFM	Description
X.FRA 862	Newstead	National Museums Scotland, Edinburgh	Cobalt-blue	1	1			Cobalt-blue melon bead.
X.FRA 863	Newstead	National Museums Scotland, Edinburgh	Cobalt-blue	1	1			Cobalt-blue melon bead.
X.FRA 864	Newstead	National Museums Scotland, Edinburgh	Cobalt-blue	1	1			Cobalt-blue melon bead.
X.FRA 865 A	Newstead	National Museums Scotland, Edinburgh	Cobalt-blue	1	1			Cobalt-blue melon bead.
X.FRA 868	Newstead	National Museums Scotland, Edinburgh	Cobalt-blue	1				Cobalt-blue melon bead.
X.FRA 869	Newstead	National Museums Scotland, Edinburgh	Cobalt-blue	1	1			Cobalt-blue melon bead.

Accession #	Site name	Museum	Colours	Bubble Samples	Chemistry Samples	RTI	SFM	Description
X.FRA 870	Newstead	National Museums Scotland, Edinburgh	Cobalt-blue	1				Cobalt-blue melon bead.
X.FRA 890	Newstead	National Museums Scotland, Edinburgh	NA: Faience bead			Yes	Yes	Faience melon bead.
X.FRA 895	Newstead	National Museums Scotland, Edinburgh	Natural	1				Naturally-blue bead with cobalt-blue and white reticella-like dots.
X.FRA 897	Newstead	National Museums Scotland, Edinburgh	Cobalt-blue	1				Cobalt-blue annular bead with white swag design.

Accession #	Site name	Museum	Colours	Bubble Samples	Chemistry Samples	RTI	SFM	Description
X.FRA 900	Newstead	National Museums Scotland, Edinburgh	Natural	1				Naturally-green bead with white swag and yellow/other reticella line.
X.FRA 906	Newstead	National Museums Scotland, Edinburgh	Natural	1				Naturally green thick annular bead.
X.FRA 907	Newstead	National Museum Scotland, Edinburgh	Green	1				Dark green long glass tube/bead.
B.1914.521/2	Philiphaugh	Hunterian Museum and Art Gallery, Glasgow	Yellow	1				Annular yellow glass bead.

Accession #	Site name	Museum	Colours	Bubble Samples	Chemistry Samples	RTI	SFM	Description
B.1914.521/26	Plestie	Hunterian Museum and Art Gallery, Glasgow	Yellow	1				Amber-coloured large annular bead with yellow swag design.
SF 15021	Rhynie	University of Glasgow Archaeology Dept.	Cobalt-blue	1	1	Yes	Yes	Coil-wound cobalt-blue glass bead.
X.FJ 199	Rink	National Museums Scotland, Edinburgh	Copper-blue	1				Coil-wound copper-blue long bead.
B.1914.521/3	Ruberslaw	Hunterian Museum and Art Gallery, Glasgow	Green	1				Dark green lozenge-shaped glass bead.

Accession #	Site name	Museum	Colours	Bubble Samples	Chemistry Samples	RTI	SFM	Description
B.1914.521/25	Rule	Hunterian Museum and Art Gallery, Glasgow	Natural	1				Naturally-green thick annular bead.
B.1914.521/14	Rumbleton	Hunterian Museum and Art Gallery, Glasgow	Cobalt-blue; white	2				Copper-blue short cylindrical bead with white double-swag design.
ABDUA 15515	Scotston	Marischal Museum, Aberdeen	Natural; yellow	2	2			Naturally-brown Guido Class 13 bead with yellow spirals.
X.FJ 126	Siccar Point	National Museums Scotland, Edinburgh	Cobalt-blue	1				Cobalt-blue annular bead.

Accession #	Site name	Museum	Colours	Bubble Samples	Chemistry Samples	RTI	SFM	Description
Q.L.1961.10	Smithston	National Museums Scotland, Edinburgh	White; yellow	1				Cobalt-blue Guido Class 13 bead with yellow spirals.
Q.L.1961.9	Smithston	National Museums Scotland, Edinburgh	Natural; Yellow	2				Naturally-brown Guido Class 14 bead with yellow, brown, and white whirls.
X.FJ 161	Soutra	National Museums Scotland, Edinburgh	Cobalt-blue	1				Cobalt-blue annular bead.
B.1951.1304	Todhaugh	Hunterian Museum and Art Gallery, Glasgow	Cobalt-blue; copper-blue	3				Copper-blue globular bead, cobalt-blue globular bead, and copper-

Accession #	Site name	Museum	Colours	Bubble Samples	Chemistry Samples	RTI	SFM	Description
								blue pressed bicone (likely modern).
X.GV 156	Traprain Law	National Museums Scotland, Edinburgh	Green	1				Green cylindrical glass bead.
X.GV 165	Traprain Law	National Museums Scotland, Edinburgh	Cobalt-blue	1				Cobalt-blue globular bead fragment.
X.GV 517	Traprain Law	National Museums Scotland, Edinburgh	Cobalt-blue	1				Naturally-green annular bead.
X.GV 518	Traprain Law	National Museums Scotland, Edinburgh	Cobalt-blue	1				Naturally-green annular bead.
X.GV 519	Traprain Law	National Museums Scotland, Edinburgh	Cobalt-blue	1			Yes	Yellow annular bead.

Accession #	Site name	Museum	Colours	Bubble Samples	Chemistry Samples	RTI	SFM	Description
X.GV 520	Traprain Law	National Museums Scotland, Edinburgh	Cobalt-blue	1	1			Cobalt-blue annular bead fragment.
X.GV 598	Traprain Law	National Museums Scotland, Edinburgh	Yellow	1				Yellow annular bead.
X.GV 768	Traprain Law	National Museums Scotland, Edinburgh	Cobalt-blue; white	2				Cobalt-blue bead with white swag line.
X.GV 767	Traprain Law	National Museums Scotland, Edinburgh	Green	1				Dark green globular glass bead.
X.GV 785	Traprain Law	National Museums Scotland, Edinburgh	Green	1				Dark green globular glass bead.
X.GV 925	Traprain Law	National Museums Scotland, Edinburgh	White	1				Cobalt-blue bead with white spirals.

Accession #	Site name	Museum	Colours	Bubble Samples	Chemistry Samples	RTI	SFM	Description
X.GV 944	Traprain Law	National Museums Scotland, Edinburgh	Cobalt-blue	1				Cobalt-blue globular bead.
X.GV 945	Traprain Law	National Museums Scotland, Edinburgh	Cobalt-blue	1				Cobalt-blue thick annular bead.
X.GV 955	Traprain Law	National Museums Scotland, Edinburgh	Cobalt-blue	1				Cobalt-blue annular bead.
X.GV 1141	Traprain Law	National Museums Scotland, Edinburgh	Yellow	1				Yellow annular bead.
X.GV 1187	Traprain Law	National Museums Scotland, Edinburgh	Cobalt-blue; white	2	2			Cobalt-blue barrel-shaped bead with white swag design.
X.GV 1230	Traprain Law	National Museums Scotland, Edinburgh	Cobalt-blue	1				Cobalt-blue globular bead.

Accession #	Site name	Museum	Colours	Bubble Samples	Chemistry Samples	RTI	SFM	Description
X.GV 1272	Traprain Law	National Museums Scotland, Edinburgh	Cobalt-blue	1				Cobalt-blue disc bead.
X.GV 1274	Traprain Law	National Museums Scotland, Edinburgh	Cobalt-blue; natural; white	3				Naturally-blue bead with cobalt-blue and white reticella swag line and dots.
X.GV 1441	Traprain Law	National Museums Scotland, Edinburgh	Cobalt-blue	1	1			Cobalt-blue thick annular bead.
XI 14-121	Traprain Law	National Museums Scotland, Edinburgh	Yellow	1	1			Yellow annular bead.
XI 14-123	Traprain Law	National Museums Scotland, Edinburgh	Cobalt-blue	1	1			Cobalt-blue globular bead.

Accession #	Site name	Museum	Colours	Bubble Samples	Chemistry Samples	RTI	SFM	Description
XI 14-132	Traprain Law	National Museums Scotland, Edinburgh	Cobalt-blue	1	1			Small cobalt-blue globular bead.
XII 15-116	Traprain Law	National Museums Scotland, Edinburgh	Yellow	1	1			Yellow annular bead.
XII 15-117	Traprain Law	National Museums Scotland, Edinburgh	Yellow	1	1			Yellow annular bead.
XII 15-119	Traprain Law	National Museums Scotland, Edinburgh	Yellow	1	1			Yellow annular bead fragment.
XII 15-121	Traprain Law	National Museums Scotland, Edinburgh	Yellow	1	1			Yellow annular bead.
XII 15-122	Traprain Law	National Museums Scotland, Edinburgh	Yellow	1	1			Yellow annular bead fragment.

Accession #	Site name	Museum	Colours	Bubble Samples	Chemistry Samples	RTI	SFM	Description
XII 15-123	Traprain Law	National Museums Scotland, Edinburgh	Yellow	1	1			Yellow annular bead fragment.
XII 15-132	Traprain Law	National Museums Scotland, Edinburgh	Yellow	1	1			Yellow annular bead fragment.
XII 15-134	Traprain Law	National Museums Scotland, Edinburgh	Cobalt-blue; natural	2	1			Naturally-blue annular bead and cobalt-blue bicone fragment.
XII 15-136	Traprain Law	National Museums Scotland, Edinburgh	Cobalt-blue	2	2			Cobalt-blue globular bead and cobalt-blue glass tube.
XII 15-137	Traprain Law	National Museums Scotland, Edinburgh	Cobalt-blue	1	1			Cobalt-blue globular bead.

Accession #	Site name	Museum	Colours	Bubble Samples	Chemistry Samples	RTI	SFM	Description
Captm 0221.01	Ugadale Point	Kilmartin House Museum, Kilmartin	Cobalt-blue; white	3	2	Yes		Large cobalt-blue glass bead with collars and white and blue reticella raised dots.
Captm 0221.02	Ugadale Point	Kilmartin House Museum, Kilmartin	Cobalt-blue	1	1	Yes		Annular cobalt-blue bead.
Captm 0221.03	Ugadale Point	Kilmartin House Museum, Kilmartin	Cobalt-blue	1	1	Yes		Annular cobalt-blue bead.
ABDUA 15520	Unknown	Marischal Museum, Aberdeen	White; yellow	2	2			Dark green Guido Class 14 bead with white and yellow spiral designs.

Accession #	Site name	Museum	Colours	Bubble Samples	Chemistry Samples	RTI	SFM	Description
ABDUA 15532	Unknown	Marischal Museum, Aberdeen	Cobalt-blue; white	2	2			Cobalt-blue annular bead with white swag design.
ABDUA 15541	Unknown	Marischal Museum, Aberdeen	Cobalt-blue; yellow	2	2			Guido Class 13 cobalt-blue bead with yellow spirals.
ABDUA 15543	Unknown	Marischal Museum, Aberdeen	Yellow	1	1			Brown Guido Class 13 bead with yellow spirals.
ABDUA 15545	Unknown	Marischal Museum, Aberdeen	Green; yellow	2	2			Grey-green Guido Class 13 bead with yellow spirals.

Accession #	Site name	Museum	Colours	Bubble Samples	Chemistry Samples	RTI	SFM	Description
B.1914.521/3f	Unknown	Hunterian Museum and Art Gallery, Glasgow	Yellow	1				Annular yellow glass bead.
X.FJ 158	Unknown	National Museums Scotland, Edinburgh	Cobalt-blue; natural; white	3				Naturally-blue bangle fragment with cobalt-blue and white reticella line.

OTHER SCOTTISH MATERIAL:

Accession #	Site Name	Museum	Bubble Samples	Chemistry Samples	RTI	SFM	Description
SF 001	Cranberry	University of Glasgow Archaeology Dept.				Yes	Neolithic ceramic potsherd.
SF 002	Cranberry	University of Glasgow Archaeology Dept.				Yes	Lithic flake.
SF 003	Leadketty	University of Glasgow Archaeology Dept.				Yes	Lead spindle whorl.
SF 1023	Iona Abbey	Iona Abbey Museum	5	5			Naturally-green window glass sherds.
SF 0962	Iona Abbey	Iona Abbey Museum		1		Yes	Copper-alloy head figurine.
SF 0997	Iona Abbey	Iona Abbey Museum		1		Yes	Copper-alloy lion figurine.
X.FC 8	Hunterston	National Museum of Scotland			Yes	Yes	Silver penannular brooch with gold filigree and amber inlays.

Accession #	Site Name	Museum	Bubble Samples	Chemistry Samples	RTI	SFM	Description
35LL 2EngKU	Kubad-Âbâd	University College London, Archaeology Dept.		2			Glazed ceramic sherd from Kubad-Âbâd, Turkey.
Girişteki Hamam 4	Kubad-Âbâd	University College London, Archaeology Dept.		2			Glazed ceramic sherd from Kubad-Âbâd, Turkey.
SF 613	Iona Abbey	University of Glasgow Archaeology Dept.		1			Medieval ceramic sherd.
SF 595	Iona Abbey	University of Glasgow Archaeology Dept.		2			Medieval glazed ceramic sherd.
SF 509	Iona Abbey	University of Glasgow Archaeology Dept.		1			Medieval ceramic sherd.

Accession #	Site Name	Museum	Bubble Samples	Chemistry Samples	RTI	SFM	Description
SF 427	Trench D	University of Glasgow Archaeology Dept.		1			Medieval ceramic sherd.
SF 411	Trench D	University of Glasgow Archaeology Dept.		1			Medieval ceramic sherd.
SF 420	Trench D	University of Glasgow Archaeology Dept.		1			Medieval ceramic sherd.
SF 501	Iona Abbey	University of Glasgow Archaeology Dept.		1			Medieval ceramic sherd.
SF 510	Iona Abbey	University of Glasgow Archaeology Dept.		2			Medieval glazed ceramic sherd.
SF 523	Iona Abbey	University of Glasgow Archaeology Dept.		2			Medieval glazed ceramic sherd.

Accession #	Site Name	Museum	Bubble Samples	Chemistry Samples	RTI	SFM	Description
SF 538	Iona Abbey	University of Glasgow Archaeology Dept.		1			Medieval ceramic sherd.
SF 548	Iona Abbey	University of Glasgow Archaeology Dept.		2			Medieval glazed ceramic sherd.
SF 553	Iona Abbey	University of Glasgow Archaeology Dept.		1			Medieval ceramic sherd.
SF 592	Iona Abbey	University of Glasgow Archaeology Dept.		2			Medieval glazed ceramic sherd.
SF 593	Iona Abbey	University of Glasgow Archaeology Dept.		2			Medieval glazed ceramic sherd.
SF 594	Iona Abbey	University of Glasgow Archaeology Dept.		1			Medieval ceramic sherd.

Accession #	Site Name	Museum	Bubble Samples	Chemistry Samples	RTI	SFM	Description
SF 596	Iona Abbey	University of Glasgow Archaeology Dept.		1			Medieval ceramic sherd.
SF 625	Iona Abbey	University of Glasgow Archaeology Dept.		1			Medieval ceramic sherd.

IRISH MATERIAL:

Accession #	Site Name	Museum	RTI	SFM	Description
Unknown	Ballyspellan	National Museum of Ireland	Yes	Yes	Silver penannular brooch.

ANGLO-SAXON MATERIAL:

Accession #	Site name	Museum	Colours	Chemistry Samples	Description
1336.70	Faversham	The British Museum	Cobalt-blue	1	Cobalt-blue claw beaker sherd.
1891,0624.3	Kempston	The British Museum	Cobalt-blue	1	Cobalt-blue palm cup sherd.
1893,0716.3	East Shefford	The British Museum	Natural	1	Naturally-brown claw beaker sherd.
1335'70	Faversham	The British Museum	Natural	1	Naturally-green globular beaker sherd.
1902,7-22.85	Droxford	The British Museum	Natural	1	Naturally-brown cone beaker sherd.
1905,0418,10	Sittingbourne	The British Museum	Natural	1	Naturally-brown claw beaker sherd.
1936,0511,48	Howletts	The British Museum	Natural	1	Naturally-brown claw beaker sherd.
1936,5-11,30	Howletts	The British Museum	Natural	1	Naturally-green claw beaker sherd.
1970,4-6,7	Mucking	The British Museum	Natural	1	Naturally-brown claw beaker sherd.
80,2-4,22	Longbridge	The British Museum	Natural	1	Naturally-green cone beaker sherd.

ENGLISH MATERIAL:

Accession #	Site name	Museum	Colours	Chemistry Samples	Description
Wells 2	Wells Cathedral	The British Museum	Natural	1	Naturally-green window glass.
Wells 2A1	Wells Cathedral	The British Museum	Natural	1	Naturally-brown window glass.
Wells 2A4	Wells Cathedral	The British Museum	Natural	1	Naturally-brown window glass.
Wells 2B1	Wells Cathedral	The British Museum	Cobalt-blue	1	Cobalt-blue glass sherd.
Wells 2W2	Wells Cathedral	The British Museum	Natural	1	Naturally-green window glass.
Wells 2Y1	Wells Cathedral	The British Museum	Natural	1	Naturally-brown window glass.
Wells 3	Wells Cathedral	The British Museum	Natural	1	Naturally-brown window glass.
Wells 31	Wells Cathedral	The British Museum	Natural	1	Naturally-brown window glass.
Wells 4	Wells Cathedral	The British Museum	Natural	1	Naturally-brown window glass.
Wells W1	Wells Cathedral	The British Museum	Natural	1	Naturally-green window glass.

EGYPTIAN MATERIAL:

Accession #	Site Name	Museum	Colours	Chemistry Samples	Description
5615-2972 X	Amarna?	The British Museum	Cobalt-blue	1	Glass vessel sherd.
5615-29771 W	Amarna?	The British Museum	Cobalt-blue; copper-blue; white; yellow	4	Glass vessel sherd.
5615-29772 U	Amarna?	The British Museum	Copper-blue	1	Glass vessel sherd.
5615-29775 Z	Amarna?	The British Museum	Cobalt-blue; white; yellow	4	Glass vessel sherd.
5615-29779 V	Amarna?	The British Museum	Cobalt-blue; white; yellow	6	Two glass vessel sherds.
5615-29780 U	Amarna?	The British Museum	Cobalt-blue; white; yellow	3	Glass vessel sherd.
5615-29787 R	Amarna?	The British Museum	Cobalt-blue; white; yellow	3	Glass vessel sherd.
5615-29793 V	Amarna?	The British Museum	Cobalt-blue	1	Glass vessel sherd.
5615-29795 Russel 3	Amarna?	The British Museum	Cobalt-blue	1	Glass vessel sherd.
5615-29796 P	Amarna?	The British Museum	Copper-blue	1	Glass vessel sherd.

Accession #	Site Name	Museum	Colours	Chemistry Samples	Description
REFC 29768 X	Amarna?	The British Museum	Cobalt-blue; copper-blue; white; yellow	8	Three glass vessel sherds.
REFC 29769 V	Amarna?	The British Museum	Cobalt-blue; white; yellow	6	Two glass vessel sherds.
REFC 29770 Y	Amarna?	The British Museum	Cobalt-blue; white; yellow	3	Glass vessel sherd.
REFC 29774 Q	Amarna?	The British Museum	Copper-blue	2	Glass vessel sherd.
REFC 29776 X	Amarna?	The British Museum	Cobalt-blue; white; yellow	9	Four glass vessel sherds.
REFC 29781 S	Amarna?	The British Museum	Cobalt-blue; white; yellow	3	Glass vessel sherd.
REFC 29783 Z	Amarna?	The British Museum	Cobalt-blue; white; yellow	3	Glass vessel sherd.
REFC 29785 V	Amarna?	The British Museum	Cobalt-blue; white; yellow	3	Glass vessel sherd.
REFC 29786 T	Amarna?	The British Museum	Cobalt-blue; copper-blue; white; yellow	4	Two glass vessel sherds.
REFC 29789 Y	Amarna?	The British Museum	Cobalt-blue	2	Glass vessel sherd.
REFC 364 box	Amarna?	The British Museum	Cobalt-blue; white; yellow	6	Two glass vessel sherds.

Accession #	Site Name	Museum	Colours	Chemistry Samples	Description
REFC 3642 T	Amarna?	The British Museum	Cobalt-blue	3	Three glass vessel sherds
REFC 36457 Y	Amarna?	The British Museum	Cobalt-blue; white; yellow	3	Glass vessel sherd.
REFC 36458 W	Amarna?	The British Museum	Cobalt-blue; white; yellow	3	Glass vessel sherd.
REFC 36459 U	Amarna?	The British Museum	Cobalt-blue; white; yellow	3	Glass vessel sherd.
REFC 36461 V	Amarna?	The British Museum	Cobalt-blue; copper-blue; yellow	3	Glass vessel sherd.
REFC 36463 R	Amarna?	The British Museum	Copper-blue; white	4	Four glass vessel sherds.
REFC 66878	Amarna?	The British Museum	Copper-blue	1	Glass vessel sherd.
REFC 66879	Amarna?	The British Museum	Copper-blue	1	Glass vessel sherd.

ROMAN MATERIAL:

Accession #	Site name	Museum	Colours	Chemistry	Description
SVP-6423-115a	San Vincenzo Al Volturno	University College London, Archaeology Dept.	White	1	White tessera.
SVP-6423-115b	San Vincenzo Al Volturno	University College London, Archaeology Dept.	White	1	White tessera.
SVP-6423-115c	San Vincenzo Al Volturno	University College London, Archaeology Dept.	White	1	White tessera.
SVP-6423-116b	San Vincenzo Al Volturno	University College London, Archaeology Dept.	Yellow	1	Yellow tessera.
SVP-6423-116c	San Vincenzo Al Volturno	University College London, Archaeology Dept.	Yellow	1	Yellow tessera.
SVP-6423-117a	San Vincenzo Al Volturno	University College London, Archaeology Dept.	Copper-blue	1	Copper-blue tessera.

Accession #	Site name	Museum	Colours	Chemistry	Description
SVP-6423-117b	San Vincenzo Al Volturno	University College London, Archaeology Dept.	Copper-blue	1	Copper-blue tessera.
SVP-6423-117c	San Vincenzo Al Volturno	University College London, Archaeology Dept.	Copper-blue	1	Copper-blue tessera.
SVP-6423-117d	San Vincenzo Al Volturno	University College London, Archaeology Dept.	Copper-blue	2	Two copper-blue tesserae.
SVP-6423-121a	San Vincenzo Al Volturno	University College London, Archaeology Dept.	Copper-blue	1	Copper-blue tessera.
SVP-6423-121b	San Vincenzo Al Volturno	University College London, Archaeology Dept.	Copper-blue	1	Copper-blue tessera.
SVP-6423-121c	San Vincenzo Al Volturno	University College London, Archaeology Dept.	Copper-blue	1	Copper-blue tessera.
SVP-6423-124c	San Vincenzo Al Volturno	University College London, Archaeology Dept.	Copper-blue	1	Copper-blue tessera.

Accession #	Site name	Museum	Colours	Chemistry	Description
SVP-6423-124d	San Vincenzo Al Volturno	University College London, Archaeology Dept.	Copper-blue	1	Copper-blue tessera.
1866.11.17.252	Unknown	The British Museum	Cobalt-blue; natural; white	5	One naturally-brown, white, and cobalt-blue mosaic Roman glass vessel sherd and one naturally-brown and white mosaic Roman glass vessel sherd.
86.11.17.203	Unknown	The British Museum	Cobalt-blue; natural; white	3	Naturally-brown, white, and cobalt-blue mosaic Roman glass vessel sherd.
7150-56	Belvedere, Baths of Septimius Severus, Rome	The British Museum	Cobalt-blue	1	Cobalt-blue tessera.

Accession #	Site name	Museum	Colours	Chemistry	Description
7150-57	Belvedere, Baths of Septimius Severus, Rome	The British Museum	Copper-blue	1	Copper-blue tessera.
7150-58	Belvedere, Baths of Septimius Severus, Rome	The British Museum	Copper-blue	1	Copper-blue tessera.
7150-63	Belvedere, Baths of Septimius Severus, Rome	The British Museum	Yellow	1	Yellow tessera.
7150-64	Belvedere, Baths of Septimius Severus, Rome	The British Museum	Cobalt-blue	1	Cobalt-blue tessera.

Accession #	Site name	Museum	Colours	Chemistry	Description
7150-65	Belvedere, Baths of Septimius Severus, Rome	The British Museum	Copper-blue	1	Copper-blue tessera.
7150-66	Belvedere, Baths of Septimius Severus, Rome	The British Museum	Copper-blue	1	Copper-blue tessera.
7150-67	Belvedere, Baths of Septimius Severus, Rome	The British Museum	Natural	1	Naturally-green tessera.
7150-87	Domus Augustana, Rome	The British Museum	Cobalt-blue	1	Cobalt-blue tessera.
7150-90	Domus Augustana, Rome	The British Museum	Natural	1	Naturally-yellow tessera.

Accession #	Site name	Museum	Colours	Chemistry	Description
7150-91	Domus Augustana, Rome	The British Museum	Cobalt-blue	1	Cobalt-blue tessera.
7150-93	Domus Augustana, Rome	The British Museum	Natural	1	Naturally-yellow tessera.
7150-94	Domus Augustana, Rome	The British Museum	Cobalt-blue	1	Cobalt-blue tessera.

APPENDIX B: SPECIFIC EQUIPMENT USED IN THIS RESEARCH

All prices current as of December 2018

Camera:	Nikon D3100 dSLR (Nikon 2017)	£240 (discontinued)
Lenses:	Nikon AF-P DX Nikkor 18-55mm (Nikon 2018b) Nikon AF-S Micro Nikkor 40mm (Nikon 2018a)	(included with camera) £270
Microscope:	DinoLite AM4113ZT (GT Vision 2018)	£325
Filters:	Schott S8612 (UVIROPTICS 2018b) Hoya 360 (UVIROPTICS 2018a) Hoya HMC UV Cut (Jessops 2018a) Neewer 720nm Infrared (Neewer 2018a) Neewer 760nm Infrared Neewer 850nm Infrared Neewer 950nm Infrared	£65 £50 £30 £30 for all Neewer
Torches:	LE UV (Lighting Ever 2018) LED (Mountain Warehouse 2018) Maglite Solitaire (Maglite 2018)	£14.50 £5.99 £5.90
Remote Shutter:	Hähnel Remote Shutter Release Pro HRN 280 (Hähnel 2018)	£27
Tripods:	Joby Gorillapod Hybrid (Joby 2018b) Joby Gorillapod Original (Joby 2018a) Vivitar 120 SE	£31.50 £7.75 Discontinued

Laptop:	ASUS Transformer Book T300 Chi (Asus 2018)	£350
		£1200 (Discontinued)
	Dell Inspiron 15 7000 (Dell 2018)	
Software:	Adobe Bridge CC 2018 (Adobe 2018)	£16.24/month for all
	Adobe Lightroom Classic CC 2018 (Adobe 2018)	Adobe
	Adobe Photoshop CC 2018 (Adobe 2018)	
	Agisoft Photoscan Pro 1.4.1 (Agisoft 2018b)	£385
	Agisoft Photoscan Standard 1.4.1 (Agisoft 2018b)	£41
		£0
	Blender v2.79b (Blender 2018)	£0
	DinoCapture 2.0 (DinoLite 2017a)	£0
	MeshLab 2016.12 (MeshLab 2018)	£0
	RTIbuilder 2.0.2 (Cultural Heritage Imaging 2018a)	£0
	RTIViewer 1.1.0 (Cultural Heritage Imaging 2018d)	

APPENDIX C: DIGITAL FILTER SETTINGS USED

Blue Filter:

Reds	-16		Reds	+40	
Oranges	-29		Oranges	+20	
Yellows	-35		Yellows	+3	
Greens	-35		Greens	-21	
Aquas	-9		Aquas	-35	
Blues	+38		Blues	-9	
Purples	+38		Purples	+27	
Magentas	+12		Magentas	+40	

Red Filter: (above, right column)

Green Filter:

Reds	+25
Oranges	+38
Yellows	+40
Greens	+30
Aquas	+38
Blues	0
Purples	0
Magentas	0

APPENDIX D: SAMPLE DATA RECORD FORMS

Bead Summaries

Site ID	502
Bead ID	Culbin Sands-002
Photos	6

Description

Location	National Museums Scotland	Catalogue #	X.BIB 13

Museum Catalogue Description

Seen 2017 ☑ **Bubbles Study** ☑ **Chemistry** ☐ **RTI** ☐ **Photogrammetry**

Diapheneity:
☐ Opaque
✓ Translucent
☐ Transparent

Primary Colour: Dark purple

Colours: 3

Design: Longitudinal spiral, Dots

Marvered: Yes

Manufacture: Wound

Class:

Correlating Classes (AS: Anglo-Saxon; R: Roman; IA: Iron Age):

Notes:

Striations: yes, yellow and deep pink

Length (mm): 10

Diameter (mm): 16

Perforation Diam. 3.5

Profile Shape: Triangular

Longitudinal Shape: Barrel

Parallels: Culbin Sands-012

References:

Bubbles and Spectral Data

Bead ID	**Colour**	**Diapheneity**	**Location**
Culbin Sands-008	Dark blue	Translucent	Core

Design
Base

Marvered
NA

Bubbles
Few

950 NIR
64

UV
22

Notes

Associated Colours
Yellow

New
Next
Previous
First
Last
Search

Site Information

Site_ID	727	Site_Code	BAD

Easting 178270

Northing 685750

OS Grid NR 78270 85750

Site_Name Balure Dun

Lat 56.013234

Other_Names Kilmichael of Inverlussa

Long 5.558746

Canmore ID 290103

Descriptive Location Argyll and Bute

Province Argyll and Bute

Country Scotland

Collection Location Kilmartin House I

Photo Shoots

ID	86	Shutter Speed	Various
Photo Shoot Number	BAD001_01	Exposure compensation	0
Date	12/06/2017	Tripod	Gorillapod Hybrid
Location	Kilmartin House Museum	Remote	☑
Purpose	Photogrammetry	Filter(s)	Hoya HMC UV, S8612
# of Photos	90	Background	white paper
Camera	Nikon D3100	Light box?	white sheet of paper
Lens	AF-S Micro Nikkor 40mm	Capture Method	Camera moves
Lighting	LED torch	Notes	
Aperture	Various		
ISO	Various		

Photo Sets

Photo Set	BAD001_01_1to90_O	Originals	☑
Photo Shoot	BAD001_01	Alteration	☐
Number of Photos	90	Dinolite	☐
Date Created	13/06/2017	Type of Alteration	
File extension	.NEF	Notes	

Projects

Project	CCR001_01_Pg1	Parameters Tested	Seeing if it works with this object
Date	14/07/2016	Notes	Merged chunks worked better than original, but aligning all images and then placing 3 markers yielded best results
Photo Shoot	CCR001_01		
Site	Castle Craig	Errors	Originally didn't line up, but some tweaking helped (see logbook for details)
Subject	Castle Craig-001		
Technique(s)	Photogrammetry, Macrophotography	Logbook	1 Page 132

APPENDIX E: SELECTION OF EXAMPLE FILES AND METADATA FOR THIS THESIS

The enclosed USB drive contains a PowerPoint and PDF file of pivotal image files in this research (Chapter 1.2). The PDF does not have the same functionality as the PowerPoint, but it is included for accessibility purposes. It also contains the processed results for all objects featured as examples in the text plus several further examples. This section contains selected metadata for these examples, including the bubble and spectral data and the parameters of images capture. Successful and unsuccessful attempts feature in this appendix, because the failures informed the techniques that lead to success. Unfortunately, metadata and files cannot be included for all objects examined and imaged in this research due to limitations of space, both within the text and on the USB drive. Nevertheless, this selection provides evidence of all factors discussed in this thesis and serves as a representative sample of this research.

File-naming: The files included in this appendix are named according to various parameters. First, imaging results for the same subject are contained in folders labelled with the museum accession number for the subject (Appendix A) followed by the number given to the subject in the larger database used in this thesis (e.g. BM 1336.70 – FAV001). Different numbering systems result from the tendency for museums and excavations to combine multiple objects under the same accession number, particularly glass beads. Finished, processed photographic, RTI, or photogrammetric files appear in each folder with names corresponding to the number given to the subject for this thesis followed by the number given to the original set of images used to create it, a designation for the type of output generated ('Ph' for photography, 'RTI'' for RTI, and 'Pg' for photogrammetry) and the number of that output generated using that set of images. For example, CS002_1_Ph1 is the first photographic

output generated for the first set of images taken of CS002, while HUN001_2_Pg1 is the first photogrammetric output created from the second set of images of the Hunterston Brooch. All examples correspond to entries in Appendix A.

Please note that some files have been redacted per request of the National Museum of Scotland. The author is currently working with the NMS to make these models available to view on the museum's SketchFab page.

Bubble and Spectral Data Examples:

Object ID	Appendix A #	Material	Colour	Diapheneity	Location	Bubbles	Infrared (950 - 1000nm)	Ultraviolet (300 - 400nm)
Amarna-002	BM 5615-29771 W	Glass	Cobalt-blue	Translucent	Core		54	34
Amarna-002	BM 5615-29771 W	Glass	Copper-blue	Translucent	Design		53	68
Amarna-002	BM 5615-29771 W	Glass	White	Opaque	Design		85	76
Amarna-002	BM 5615-29771 W	Glass	Yellow	Opaque	Design		69	36
Amarna-004	BM 5615-29775 Z	Glass	Yellow	Opaque	Design		99	49
Amarna-004	BM 5615-29775 Z	Glass	Cobalt-blue	Translucent	Core		72	95
Amarna-004	BM 5615-29775 Z	Glass	White	Opaque	Design		68	95
Amarna-004	BM 5615-29775 Z	Glass	White	Opaque	Design		106	140
Balure Dun-001	KHM SF 56	Glass	Light blue	Transparent	Core	Few	53	93
Balure Dun-002	KHM SF 57	Glass	Light blue	Transparent	Core	Few	67	86
Banff-001	MM ABDUA 15526	Glass	Natural yellow	Transparent	Core	Moderate	39	28
Banff-001	MM ABDUA 15526	Glass	White	Opaque	Design	Moderate	94	50
Banff-001	MM ABDUA 15526	Glass	Yellow	Opaque	Design	Many	67	28
Clachbreck-001	UG CLB 1	Glass	Cobalt-blue	Translucent	Core	Moderate	150	80

Object ID	Appendix A #	Material	Colour	Diapheneity	Location	Bubbles	Infrared (950 - 1000nm)	Ultraviolet (300 - 400nm)
Culbin Sands-002	NMS X.BIB.13	Glass	Natural blue	Transparent	Design	Few	91	74
Culbin Sands-002	NMS X.BIB.13	Glass	Yellow	Opaque	Design	Moderate	148	40
Culbin Sands-004	NMS X.BIB.10	Glass	Yellow	Opaque	Design	Few	172	33
Culbin Sands-004	NMS X.BIB.10	Glass	White	Opaque	Design	Few	118	74
Culbin Sands-008	NMS X.BIB.15	Glass	Cobalt-blue	Translucent	Core	Few	64	22
Culbin Sands-008	NMS X.BIB.15	Glass	Yellow	Opaque	Core	Moderate	101	34
Culbin Sands-025	NMS X.BIB.37	Glass	Copper-blue	Translucent	Core	Many	58	40
Culbin Sands-028	NMS X.BIB.40	Glass	Cobalt-blue	Translucent	Core	Many		
Culbin Sands-029	NMS X.BIB.41	Glass	Cobalt-blue	Translucent	Core	Few		
Culbin Sands-030	NMS X.BIB.42	Glass	Cobalt-blue	Translucent	Core	Few		
Culbin Sands-490	NMS X.BIB.70	Glass	Copper-blue	Translucent	Core	Moderate		
Faversham-001	BM 1336.70	Glass	Cobalt-blue	Translucent	Core		68	57
Glenluce Sands-012	NMS X.BHB.11	Glass	Cobalt-blue	Translucent	Core	Moderate		
Glenluce Sands-070	NMS X.BHB.20.4	Glass	Yellow	Opaque	Core	Few	176	41
Glenshee-001	UG Unknown #	Glass	Green	Translucent	Core	Many	101	51
Glenshee-001	UG Unknown #	Glass	Dark green	Translucent	Core	Many	83	51

Object ID	Appendix A #	Material	Colour	Diapheneity	Location	Bubbles	Infrared (950 - 1000nm)	Ultraviolet (300 - 400nm)
Iona-001	IAM SF 0962	Cu-Alloy					117	82
Iona-002	IAM SF 0997	Cu-Alloy					118	67
Kubud Abad-001	UCL Giristeki Hamam 4	Glaze	Copper-blue				169	195
Kubud Abad-002	UCL 35LL 2EngKU	Glaze	Copper-blue				146	77
Loch Eriboll-001	UG F128	Glass	Natural green	Transparent	Core	Few	55	41
Loch Eriboll-001	UG F128	Glass	Yellow	Opaque	Design	Many	161	66
Mill of Gellan-001	MM ABDUA 15539	Glass	Copper-blue	Translucent	Design	Many	43	36
Mill of Gellan-001	MM ABDUA 15539	Glass	White	Opaque	Design	Many	61	64
Mill of Gellan-001	MM ABDUA 15539	Glass	Yellow	Opaque	Design	Many	61	29
Rhynie-001	UG SF 15021	Glass	Cobalt-blue	Translucent	Core	Many	45	35
Sittingbourne-001	BM 1905.0418.10	Glass	Natural brown	Transparent	Core		33	28
Ugadale-001	KHM Captm 0221.01	Glass	Cobalt-blue	Translucent	Core	Moderate	68	17
Ugadale-001	KHM Captm 0221.01	Glass	Cobalt-blue	Transparent	Design	Moderate		
Ugadale-001	KHM Captm 0221.01	Glass	White	Opaque	Design	Many	126	80
Unknown-001	BM 1886.11.17.252	Glass	Natural brown	Transparent	Design		42	32
Unknown-001	BM 1886.11.17.252	Glass	Cobalt-blue	Translucent	Core		35	38

Object ID	Appendix A #	Material	Colour	Diapheneity	Location	Bubbles	Infrared (950 - 1000nm)	Ultraviolet (300 - 400nm)
Unknown-001	BM 1886.11.17.252	Glass	White	Opaque	Design		92	88
Unknown-002	BM 1886.11.17.252	Glass	White	Opaque	Design		103	96
Unknown-002	BM 1886.11.17.252	Glass	Natural brown	Transparent	Core		37	24
Wells Cathedral-003	BM WELLS 2A1	Glass	Natural brown	Translucent	Core		52	40
Wells Cathedral-006	BM WELLS 2A4	Glass	Natural brown	Translucent	Core		60	43

Photo Set and Parameter Examples:

Photo Shoot	Date	Purpose	Photos	Camera	Lens	Lighting	Aperture	ISO	Shutter Speed	Filter	Background
AM001_1	14/12/2017	Spectral Photography	15	Nikon D3100	Nikon AF-S 40mm Micro	LE UV; LED; Maglite Solitaire	F20	200	1/6	S8612; Hoya HMC UV; Hoya U-360; Neewer 950nm	white paper
AM002_1	14/12/2017	Spectral Photography	26	Nikon D3100	Nikon AF-S 40mm Micro	LE UV; LED; Maglite Solitaire	F20	200	1/6	S8612; Hoya HMC UV; Hoya U-360; Neewer 950nm	white paper
BAD001_3	12/06/2017	RTI	37	Nikon D3100	Nikon AF-S 40mm Micro	LE UV	F20	200	1/4	S8612; Hoya U-360	white paper
BAD002_3	12/06/2017	RTI	35	Nikon D3100	Nikon AF-S 40mm Micro	LE UV	F16	200	1	S8612; Hoya U-360	white paper
BAL001_1	27/09/2016	RTI	47	Nikon D3100	Nikon AF-S 40mm Micro	LED	F22	200	1/2	S8612; Hoya HMC UV	white paper

Photo Shoot	Date	Purpose	Photos	Camera	Lens	Lighting	Aperture	ISO	Shutter Speed	Filter	Background
BAL001_2	27/09/2016	Photogrammetry	168	Nikon D3100	Nikon AF-S 40mm Micro	LED	F22	200	1/2	S8612; Hoya HMC UV	white paper
BNF001_1	24/10/2017	Spectral Photography	14	Nikon D3100	Nikon AF-S 40mm Micro	LE UV; LED; Maglite Solitaire	F20	200	1/8	S8612; Hoya HMC UV; Hoya U-360; Neewer 950nm	white paper
CCR001_1	06/07/2016	Photogrammetry	95	Nikon D3100	Nikon AF-S 40mm Micro	Natural and LED torches	F29	200	Various	None	white paper
CLB001_7	13/06/2017	Spectral Photography	3	Nikon D3100	Nikon AF-S 40mm Micro	LE UV; LED; Maglite Solitaire	F16	200	1/6	S8612; Hoya HMC UV; Hoya U-360; Neewer 950nm	white paper
CNC001_1	30/05/2017	Spectral Photography	3	Nikon D3100	Nikon AF-S 40mm Micro	LE UV; LED; Maglite Solitaire	F5	100	Various	S8612; Hoya HMC UV; Hoya U-360; Neewer 950nm	white paper

Photo Shoot	Date	Purpose	Photos	Camera	Lens	Lighting	Aperture	ISO	Shutter Speed	Filter	Background
CS002_1	21/08/2017	Spectral Photography	11	Nikon D3100	Nikon AF-S 40mm Micro	LE UV; LED; Maglite Solitaire	F22	200	1.6	S8612; Hoya HMC UV; Hoya U-360; Neewer 950nm	white paper
CS004_1	21/08/2017	Spectral Photography	10	Nikon D3100	Nikon AF-S 40mm Micro	LE UV; LED; Maglite Solitaire	F22	200	1.6	S8612; Hoya HMC UV; Hoya U-360; Neewer 950nm	white paper
CS008_1	21/08/2017	Photogrammetry	90	Nikon D3100	Nikon AF-S 40mm Micro	LED	F16	200	Various	S8612; Hoya HMC UV	white paper
CS008_2	21/08/2017	Photogrammetry	100	DinoLite AM4113ZT	DinoLite AM4113ZT	DinoLite AM4113ZT LED lights					white paper
CS008_3	21/08/2017	RTI	48	Nikon D3100	Nikon AF-S 40mm Micro	UV Torch	F20	200	1	S8612; Hoya U-360	white paper
CS025_1	21/08/2017	Photogrammetry	111	DinoLite AM4113ZT	DinoLite AM4113ZT	DinoLite AM4113ZT LED lights					white paper

Photo Shoot	Date	Purpose	Photos	Camera	Lens	Lighting	Aperture	ISO	Shutter Speed	Filter	Background
CS028_1	05/06/2014	Documentary	6	iPhone 4s	iPhone 4s	Maglite	F2.4	50	1/50		white paper
CS029_1	05/06/2014	Documentary	6	iPhone 4s	iPhone 4s	Maglite	F2.4	50	1/50		white paper
CS030_1	05/06/2014	Documentary	7	iPhone 4s	iPhone 4s	Maglite	F2.4	50	1/40		white paper
CS490_1	05/06/2014	Documentary	7	iPhone 4s	iPhone 4s	Maglite	F2.4	160	1/20		white paper
CS493_1	21/08/2017	Spectral Photography	5	Nikon D3100	Nikon AF-S 40mm Micro	LE UV; LED; Maglite Solitaire	F22	200	1.6	S8612; Hoya HMC UV; Hoya U-360; Neewer 950nm	white paper
CS493_2	21/08/2017	Photogrammetry	147	DinoLite AM4113ZT	DinoLite AM4113ZT	DinoLite AM4113ZT LED lights					white paper
CS493_3	21/08/2017	Photogrammetry	72	DinoLite AM4113ZT	DinoLite AM4113ZT	DinoLite AM4113ZT LED lights					white paper
CS493_4	21/08/2017	RTI	44	Nikon D3100	Nikon AF-S 40mm Micro	UV Torch	F20	200	1	S8612; Hoya U-360	white paper
FAV001_1	14/12/2017	Spectral Photography	29	Nikon D3100	Nikon AF-S 40mm Micro	LE UV; LED; Maglite Solitaire	F20	200	1/8	S8612; Hoya HMC UV; Hoya U-360;	white paper

Photo Shoot	Date	Purpose	Photos	Camera	Lens	Lighting	Aperture	ISO	Shutter Speed	Filter	Background
										Neewer 950nm	
GL001_04	04/02/2016	Photogrammetry	22	Nikon D3100	AF-P DX Nikkor 18-55mm	Ambient fluorescent	f/5.6	1000	1/80	None	Coloured web on white paper
GL001_11	12/02/2016	Photogrammetry	28	Nikon D5300	Nikon AF-S 40mm Micro	Ambient fluorescent	F36	640	1.6	None	white table
GL001_13	12/02/2016	Photogrammetry	28	Nikon D5300	Nikon AF-S 40mm Micro	Ambient fluorescent	F36	640	2	None	Coloured web on white paper
GL001_30	19/09/2016	Photogrammetry	109	DinoLite AM4113ZT	DinoLite AM4113ZT	DinoLite AM4113ZT LED lights				None	white paper
GL001_31	19/09/2016	Photogrammetry	57	DinoLite AM4113ZT	DinoLite AM4113ZT	DinoLite AM4113ZT LED lights				None	white paper
GL001_32	25/8/2016	RTI	81	DinoLite AM4113ZT	DinoLite AM4113ZT	DinoLite AM4113ZT LED lights				None	White paper

Photo Shoot	Date	Purpose	Photos	Camera	Lens	Lighting	Aperture	ISO	Shutter Speed	Filter	Background
GL001_34	13/06/2017	Spectral Photography	3	Nikon D5300	Nikon AF-S 40mm Micro	LE UV; LED; Maglite Solitaire	F16	200	1/2	S8612; Hoya HMC UV; Hoya U-360; Neewer 950nm	white paper
GS012_1	05/06/2014	Documentary	4	iPhone 4s	iPhone 4s	Maglite Solitaire	F2.4	125	1/20		white paper
GS070_1	21/08/2017	Photogrammetry	92	DinoLite AM4113ZT	DinoLite AM4113ZT	DinoLite AM4113ZT LED lights					white paper
GS070_2	21/08/2017	Spectral Photography	5	Nikon D3100	Nikon AF-S 40mm Micro	LE UV; LED; Maglite Solitaire	F22	200	1.6	S8612; Hoya HMC UV; Hoya U-360; Neewer 950nm	white paper
GS070_3	21/08/2017	Bubbles	1	DinoLite AM4113ZT	DinoLite AM4113ZT	DinoLite AM4113ZT LED lights					white paper
GS070_4	21/08/2017	RTI	43	Nikon D3100	Nikon AF-S 40mm Micro	LE UV	F20	200	1	S8612; Hoya U-360	white paper

Photo Shoot	Date	Purpose	Photos	Camera	Lens	Lighting	Aperture	ISO	Shutter Speed	Filter	Background
HUN001_1	27/09/2016	RTI	42	Nikon D3100	Nikon AF-S 40mm Micro	LED	F20	200	0.8	S8612; Hoya HMC UV	white paper
HUN001_2	27/09/2016	Photogrammetry	224	Nikon D3100	Nikon AF-S 40mm Micro	LED	Various	200	Various	S8612; Hoya HMC UV	white paper
IOA001_1	31/05/2017	Photogrammetry	81	Nikon D3100	Nikon AF-S 40mm Micro	LED	F16	100	1/13	S8612; Hoya HMC UV	white paper
IOA001_2	31/05/2017	Spectral Photography	6	Nikon D3100	Nikon AF-S 40mm Micro	LE UV; LED; Maglite Solitaire	F16	100	Various	S8612; Hoya HMC UV; Hoya U-360; Neewer 950nm	white paper
IOA002_1	31/05/2017	Photogrammetry	184	Nikon D3100	Nikon AF-S 40mm Micro	LED	F16	100	1/8	S8612; Hoya HMC UV	white paper
IOA002_2	31/05/2017	Spectral Photography	4	Nikon D3100	Nikon AF-S 40mm Micro	LE UV; LED; Maglite Solitaire	F16	100	Various	S8612; Hoya HMC UV; Hoya U-360; Neewer 950nm	white paper

Photo Shoot	Date	Purpose	Photos	Camera	Lens	Lighting	Aperture	ISO	Shutter Speed	Filter	Background
IOA003_1	18/05/2017	Spectral Photography	8	Nikon D3100	Nikon AF-S 40mm Micro	LE UV; LED; Maglite Solitaire	F5	100	Various	S8612; Hoya HMC UV; Hoya U-360; Neewer 950nm	white paper
KA001_1	13/12/2017	Spectral Photography	14	Nikon D3100	Nikon AF-S 40mm Micro	LE UV; LED; Maglite Solitaire	F20	200	1/8	S8612; Hoya HMC UV; Hoya U-360; Neewer 950nm	white paper
KA002_1	13/12/2017	Spectral Photography	10	Nikon D3100	Nikon AF-S 40mm Micro	LE UV; LED; Maglite Solitaire	F20	200	1/8	S8612; Hoya HMC UV; Hoya U-360; Neewer 950nm	white paper
LEB001_01	23/03/2016	Photogrammetry	37	Nikon D3100	Nikon AF-S 40mm Micro	Ambient fluorescent	F18	100	1.3	Jessops Circular Polariser	white paper
LEB001_03	23/03/2016	Photogrammetry	28	Nikon D3100	Nikon AF-S 40mm Micro	Desk lamp	F22	400	1	Jessops Circular Polariser	white paper

Photo Shoot	Date	Purpose	Photos	Camera	Lens	Lighting	Aperture	ISO	Shutter Speed	Filter	Background
LEB001_05	24/03/2016	Photogrammetry	72	Nikon D3100	Nikon AF-S 40mm Micro	Ambient fluorescent	F18	800	1	Jessops Circular Polariser	white paper
LEB001_06	24/03/2016	Photogrammetry	19	Nikon D3100	Nikon AF-S 40mm Micro	Ambient fluorescent and RTI AP PRO Series LED torch with paper as diffuser	F18	100	1.3	Jessops Circular Polariser	white paper
LEB001_10	24/03/2016	RTI	55	Nikon D3100	Nikon AF-S 40mm Micro	(RTI AP PRO Series LED torch	F18	100	1/2		white paper
LEB001_11	29/04/2016	Photogrammetry	95	Nikon D3100	Nikon AF-S 40mm Micro	Ambient fluorescents and cold light	F25	100	1/3	None	white paper
LEB001_15	07/03/2017	Photogrammetry	48	Nikon D80	Nikon AF-S 40mm Micro	Halogen lamp	F9	200	0.8	Neewer 720nm	white paper

Photo Shoot	Date	Purpose	Photos	Camera	Lens	Lighting	Aperture	ISO	Shutter Speed	Filter	Background
LEB001_17	14/03/2017	RTI	42	Nikon D80	Nikon AF-S 40mm Micro	Maglite Solitaire	F7.1	200	Various	Neewer 950nm	white paper
LEB001_19	13/06/2017	Spectral Photography	3	Nikon D3100	Nikon AF-S 40mm Micro	LE UV; LED; Maglite Solitaire	F16	200	1/2	S8612; Hoya HMC UV; Hoya U-360; Neewer 950nm	white paper
MG001_1	24/10/2017	Spectral Photography	14	Nikon D3100	Nikon AF-S 40mm Micro	LE UV; LED; Maglite Solitaire	F20	200	1/8	S8612; Hoya HMC UV; Hoya U-360; Neewer 950nm	white paper
NE078_1	21/08/2017	Photogrammetry	67	Nikon D3100	Nikon AF-S 40mm Micro	LED	F16	200	1/6	S8612; Hoya HMC UV	white paper
NE078_2	21/08/2017	Photogrammetry	85	DinoLite AM4113ZT	DinoLite AM4113ZT	DinoLite AM4113ZT LED lights					white paper
NE078_3	21/08/2017	Photogrammetry	85	DinoLite AM4113ZT	DinoLite AM4113ZT	DinoLite AM4113ZT LED lights					white paper

Photo Shoot	Date	Purpose	Photos	Camera	Lens	Lighting	Aperture	ISO	Shutter Speed	Filter	Background
NE078_6	21/08/2017	RTI	33	Nikon D3100	Nikon AF-S 40mm Micro	LE UV	F20	200	1	S8612; Hoya U-360	white paper
RO001_1	14/01/2016	Photogrammetry	25	Samsung Galaxy S6	Samsung Galaxy S6	LED	F1.9	Various	Various		white paper
RO002_10	24/03/2017	RTI	34	Nikon D3100	Nikon AF-S 40mm Micro	LED	F18	100	0.6		white paper
RO002_2	29/01/2016	Photogrammetry	83	iPhone 4s	iPhone 4s	LED	F2.4	Various	Various		white paper with drawn targets
RO002_29	14/03/2017	RTI	39	Nikon D80	Nikon AF-S 40mm Micro	Maglite Solitaire	F7.1	200	1/2	Neewer 720nm	white paper
RY001_05	15/08/2016	Photogrammetry	56	Nikon D3100	Nikon AF-S 40mm Micro	Cold light	F22	200	1/25	None	white paper
RY001_10	19/09/2016	Photogrammetry	167	DinoLite AM4113ZT	DinoLite AM4113ZT	DinoLite AM4113ZT LED lights					white paper

Photo Shoot	Date	Purpose	Photos	Camera	Lens	Lighting	Aperture	ISO	Shutter Speed	Filter	Background
RY001_13	22/08/2016	Photogrammetry	53	DinoLite AM4113ZT	DinoLite AM4113ZT	DinoLite AM4113ZT LED lights				None	white paper
RY001_19	13/06/2017	Spectral Photography	3	Nikon D3100	Nikon AF-S 40mm Micro	LE UV; LED; Maglite Solitaire	F16	200	1/2	S8612; Hoya HMC UV; Hoya U-360; Neewer 950nm	white paper
SIT001_1	14/12/2017	Spectral Photography	23	Nikon D3100	Nikon AF-S 40mm Micro	LE UV; LED; Maglite Solitaire	F20	200	1/8	S8612; Hoya HMC UV; Hoya U-360; Neewer 950nm	white paper
U001_1	14/12/2017	Spectral Photography	25	Nikon D3100	Nikon AF-S 40mm Micro	LE UV; LED; Maglite Solitaire	F20	200	1/8	S8612; Hoya HMC UV; Hoya U-360; Neewer 950nm	white paper
U002_1	14/12/2017	Spectral Photography	21	Nikon D3100	Nikon AF-S 40mm Micro	LE UV; LED; Maglite Solitaire	F20	200	1/8	S8612; Hoya HMC UV; Hoya U-360;	white paper

Photo Shoot	Date	Purpose	Photos	Camera	Lens	Lighting	Aperture	ISO	Shutter Speed	Filter	Background
										Neewer 950nm	
UP001_1	12/06/2017	RTI	48	Nikon D3100	Nikon AF-S 40mm Micro	LE UV	F16	200	Various	S8612; Hoya U-360	white paper
UP001_2	12/06/2017	Spectral Photography	5	Nikon D3100	Nikon AF-S 40mm Micro	LE UV; LED; Maglite Solitaire	F20	200	1/6	S8612; Hoya HMC UV; Hoya U-360; Neewer 950nm	white paper
WC003_1	14/12/2017	Spectral Photography	9	Nikon D3100	Nikon AF-S 40mm Micro	LE UV; LED; Maglite Solitaire	F20	200	0.6	S8612; Hoya HMC UV; Hoya U-360; Neewer 950nm	white paper
WC003_2	14/12/2017	Spectral Photography	8	Nikon D3100	Nikon AF-S 40mm Micro	LE UV; LED; Maglite Solitaire	F20	200	0.6	S8612; Hoya HMC UV; Hoya U-360; Neewer 950nm	white paper

Photo Shoot	Date	Purpose	Photos	Camera	Lens	Lighting	Aperture	ISO	Shutter Speed	Filter	Background
WC006_1	14/12/2017	Spectral Photography	9	Nikon D3100	Nikon AF-S 40mm Micro	LE UV; LED; Maglite Solitaire	F20	200	0.6	S8612; Hoya HMC UV; Hoya U-360; Neewer 950nm	white paper
WC006_2	14/12/2017	Spectral Photography	9	Nikon D3100	Nikon AF-S 40mm Micro	LE UV; LED; Maglite Solitaire	F20	200	0.6	S8612; Hoya HMC UV; Hoya U-360; Neewer 950nm	white paper

REFERENCES CITED

3D Digital. 2015. *History of 3D Scanners*. [Online]. [Accessed 26 October 2016].
Available from:
https://web.archive.org/web/20161027153616/http://3ddigitalcorp.com/history-3d-scanners.html/

Abraham, S. 2013. In Search of Craft and Society: The Glass Beads of Early Historic
Tamil South India. In: Abraham, S., Gullapalli, P., Raczek, T., and Rizvi, U. eds.
Connections and Complexity: New Approaches to the Archaeology of South Asia. Walnut
Creek, California: Left Coast Press, pp.239 – 261.

Abraham, S. and Christie, H. 2010. *The Indian Ocean and the Indo-Pacific Bead:
Mapping a Key Artifact Category from the Pattanam Excavations.* 20th Conference of the
European Association for South Asian Archaeology and Art, 4 – 9 July, Vienna.

Absolute Data Services Ltd. 2017. *Dino-Lite UK - Introducing the Dino-Lite Digital
Microscope. Dino-Lite UK*. [Online]. [Accessed 7 September 2017]. Available at:
http://www.dinolite-uk.com/index.php/introducing/

Adobe. 2018. *Discover the Creative Cloud Experience*. [Online]. [Accessed 29 March
2018]. Available from:
https://web.archive.org/web/20180329092811/https://www.adobe.com/uk/creativecloud/plans.html?promoid=P3KMQYMW&mv=other/

Aerts, A., Janssens, K. and Adams, F. 1999. Trace-Level Microanalysis of Roman Glass
from Khirbet Qumrân, Israel. *Journal of Archaeological Science.* **26**, pp.883 – 891.

Agisoft. 2018a. *Online Store*. [Online]. [Accessed 30 March 2018]. Available from:

https://web.archive.org/web/20180330194827/http://www.agisoft.com/buy/online-store/

Agisoft. 2018b. *Online Store*. [Online]. [Accessed 20 April 2018]. Available from:

https://web.archive.org/web/20180420102138/http://www.agisoft.com:80/buy/online-store/educational-license/

Agisoft. 2017. *Agisoft Photoscan User Manual: Professional Edition Version 1.3*.

[Online]. [Accessed 6 May 2018]. Available from:

https://web.archive.org/web/20180506143315/http://www.agisoft.com/pdf/photoscan-pro_1_3_en.pdf/

Agua, F., Conde, J., Kobylinska, U., Kobilinski, Z., Garcia-Heras, M. and Villegas, M.

2017. Chemical-Physical Characterisation of Early Iron Age Glass Beads from Central

Europe. *Boletín de la Sociedad Española de Cerámica y Vidrio*. **56**(3), pp.119 – 130.

Amateur Photographer. 2013. *Focal Length Explained*. [Online]. [Accessed 12 September

2017]. Available at:

https://web.archive.org/web/20170912032758/http://www.amateurphotographer.co.uk:80/technique/camera_skills/focal-length-explained-3-4178/

Anderson, T. and Fell, C. 1995. Analysis of Roman Cremation Vessels by Computerized

Tomography. *Journal of Archaeological Science*. **22**(5), pp.609 – 617.

Apple. 2018. *Mac App Store: Pixelmator Pro*. [Online]. [Accessed 24 April 2018].

Available from: https://itunes.apple.com/us/app/pixelmator-pro/id1289583905?mt=12/

Archaeology Data Service. 2018a. *Guides to Good Practice.* [Online]. [Accessed 29 December 2018]. Available from: https://web.archive.org/web/20181229113225/http://guides.archaeologydataservice.ac.uk/g2gp/Main/

Archaeology Data Service. 2018b. *Data Selection: Preservation Intervention Points.* [Online]. [Accessed 22 December 2018]. Available from: https://web.archive.org/web/20181222190913/http://guides.archaeologydataservice.ac.uk/g2gp/ArchivalStrat_1-3

Arnold, D. 2005. Unlearning the Images of Archaeology. In: Smiles, S. and Moser, S. eds. *Envisioning the Past: Archaeology and the Image.* Oxford: Blackwell Publishing, pp.92 – 114.

Artec. 2018a. *Artec Spider High Resolution 3D Scanner: Industrial 3D Scanner for Small Objects*. [Online]. [Accessed 24 June 2018]. Available at: https://web.archive.org/web/20180624010536/https://www.artec3d.com/portable-3d-scanners/artec-spider/

Artec. 2018b. *Artec Eva 3D Object Scanner: Structured-Light Scanning Device*. [Online]. [Accessed 29 October 2018]. Available at: https://web.archive.org/web/20181029021405/https://www.artec3d.com/portable-3d-scanners/artec-eva/

Artec. 2018c. *Industrial 3D Scanner – Space Spider: 3D Scanning in High Resolution*. [Online]. [Accessed 24 June 2018]. Available at:

https://web.archive.org/web/20180624010536/https://www.artec3d.com/portable-3d-scanners/artec-spider#specifications/

Artec. 2018. *Support for Discontinued Scanners.* [Online]. [Accessed 17 December 2018]. Available from:

https://web.archive.org/web/20181217142249/https://artecgroup.zendesk.com/hc/en-us/articles/360000446173-Support-for-discontinued-scanners

van Asperen de Boer, J. 1968. Infrared Reflectography: A Method for the Examination of Paintings. *Applied Optics* **7**(9), p.1711.

Asus. 2018. *Asus Transformer Book 12.5" 2-In-1 Laptop/Tablet Intel Core M 4GB RAM, 128GB SSD.* [Online]. [Accessed 28 December 2018]. Available from:

https://web.archive.org/web/20181229135659/https://uk.store.asus.com/asus-transformer-book-t300chi-ms-fl097t-12-5-convertible-tablet-laptop-intel-core-m-5y10-processor-4gb-ram-128gb-ssd-windows-10-90nb07g1-m06500.html/

Atkinson, G. 1883. Glass Beads and Jet Ornaments. *The Journal of the Royal Historical and Archaeological Association of Ireland.* **6**(54), pp.69 – 71.

Atkinson, K. 1969. Some Recent Developments in Non-Topographic Photogrammetry. *The Photogrammetric Record.* **6**(34), pp.357 – 378.

Aziz, I. 2013. Comparing Point Counting & Image Analysis in Sandstone North Carnarvon Basin, Australia. *2nd International Conference on Geological and Environmental Sciences.* **52**(5), pp.20 – 24.

Backhouse, P. 2006. Drowning in Data? Digital Data in a British Contracting Unit. In: Evans, T. and Daly, P. eds. *Digital Archaeology: Bridging Method and Theory.* London: Routledge, pp.50 – 58.

Baeten, V., Pierna, J. and Dardenne, P. 2007. Hyperspectral Imaging Techniques: An Attractive Solution for the Analysis of Biological and Agricultural Materials. In: Grahn, H. and Geladi, P. eds. *Techniques and Applications of Hyperspectral Image Analysis*. John Wiley & Sons, Ltd., pp.289 – 311.

Balas, C., Papadakis, V., Papadakis, N., Papadakis, A., Vazgiouraki, E. and Themelis, G. 2003. A Novel Hyper-Spectral Imaging Apparatus for the Non-Destructive Analysis of Objects of Artistic and Historic Value. *Journal of Cultural Heritage.* **4**(Supplement 1), pp.330 – 337.

Bard, K., Fattovich, R., Manzo, A. and Perlingieri, C. Archaeological Investigations at Bieta Giyorgis (Aksum), Ethiopia: 1993 – 1995 Field Seasons. *Journal of Field Archaeology*. **24**(4), pp.387 – 403.

Basa, K. 1991. *The Westerly Trade of Southeast Asia From C. 500 BC to C. 500 AD with Special Reference to Glass Beads*. Ph.D. Dissertation, University of London.

Bateman, J. 2005. Wearing Juninho's Shirt: Record and Negotiation in Excavation Photographs. In: Smiles, S. and Moser, S. eds. *Envisioning the Past: Archaeology and the Image.* Oxford: Blackwell Publishing, pp.194 – 203.

Bayer, B. 1976. *Color Imaging Array*. US3971065.

Beale, G., Beale, N., Dawson, I. and Minkin, L. Making Digital: Visual Approaches to the Digital Humanities. In: Ng, K., Bowen, J. and McDaid, S. eds. *EVA 2013: Electronic Visualisation and the Arts, United Kingdom, 29 – 31 July 2013.* BCS, The Chartered Institute for IT, pp.240 – 247.

Beck, H. 1928. Classification and Nomenclature of Beads and Pendants. *Archaeologia.* **77,** pp.1 – 76.

Behdad, A. 2013. The Orientalist Photograph. In: Behdad, A. and Gartlan, L. (eds.). *Photography's Orientalism: New Essays on Colonial Representation.* Los Angeles: Getty Publications, pp.11 – 32.

Bellina, B. 2003. Beads, Social Change, and Interaction between India and South-East Asia. *Antiquity.* **77**(296), pp.285 – 297.

Bergman, T., Ho, L. and Beehner, J. 2009. Chest Color and Social Status in Male Geladas (*Theropithecus gelada*). *International Journal of Primatology.* **30**, pp.791 – 806.

Bernardini, F., Rushmeier, H., Martin, I., Mittleman, J. and Taubin, G. 2002. Building a Digital Model of Michelangelo's Florentine Pieta. *IEEE Computer Graphics and Applications.* **22**(1), pp.59 – 67.

Bertini, M. 2012. *Novel Application of Micro- and Non-Destructive Analytical Techniques for the Analysis of Iron Age Glass Beads from North-Eastern Scotland.* Unpublished Ph.D. Thesis. University of Aberdeen.

Bertini, M., Mokso, R., and Krupp, E. 2014. Unwinding the Spiral: Discovering the Manufacturing Method of Iron Age Scottish Glass Beads. *Journal of Archaeological Science*. **43**, pp.256–266.

Bertini, M., Shortland, A., Milek, K., and Krupp, E. 2011. Investigation of Iron Age north-eastern Scottish glass beads using element analysis with LA-ICP-MS. *Journal of Archaeological Science* **38**(10), pp.2750 – 2766.

Biek, L. and Bayley, J. 1979. Glass and other Vitreous Materials. *World Archaeology* **11**(1), pp.1 – 25.

Binford, L. 1962. Archaeology as Anthropology. *American Antiquity*. **28**(2), pp.217 – 225.

Black, G. 1891. Report on the Archaeological Examination of the Culbin Sands, Elginshire, Obtained under the Victoria Jubilee Gift of His Excellency Dr. R. H. Gunning. *Proceedings of the Society of Antiquaries of Scotland*. **25,** pp.484 – 511.

Blender. 2018. *Blender.* [Online]. [Accessed 29 December 2018]. Available from: https://web.archive.org/web/20181229141819/https://www.blender.org/

Boehler, W. and Heinz, G. 1999. Documentation, Surveying, Photogrammetry. *XVII CIPA Symposium, Recife, Brazil*.

Boehler, W. and Marbs, A. 2004. 3D Scanning and Photogrammetry for Heritage Recording: A Comparison. In: Anders, B. ed. *Proceedings of the Twelfth International Conference on Geoinformatics*. Gävle: Gävle University Press, pp.291 – 298.

Boespflung, X., Long, B. and Occhietti, S. 1995. CAT-Scan in Marine Stratigraphy: A Quantitative Approach. *Marine Geology.* **122**(4), pp.281 – 301.

Bohren, C. and Huffman, D. 2008. *Absorption and Scattering of Light by Small Particles*. John Wiley & Sons.

Bohrer, F. 2005. Photography and Archaeology: The Image as Object. In: Smiles, S. and Moser, S. eds. *Envisioning the Past: Archaeology and the Image.* Oxford: Blackwell Publishing, pp.182 – 191.

Bourke, E. 1994. Glass Vessels of the First Nine Centuries AD in Ireland. *The Journal of the Royal Society of Antiquaries of Ireland.* **124**(1994), pp.163 – 209.

Bradley, M. 2006. Archaeological Survey in a Digital World. In: Evans, T. and Daly, P. eds. *Digital Archaeology: Bridging Method and Theory.* London: Routledge, pp.35 – 49.

Brugmann, B. 2004. *Glass Beads from Anglo-Saxon Graves: A Study of the Provenance and Chronology of Glass Beads from Early Anglo-Saxon Graves, Based on Visual Examination*. Oxford: Oxbow Books.

Bruker. 2017. *S1 Titan.* [Online]. [Accessed 26 September 2017]. Available from: https://web.archive.org/web/20170926152424/https://www.bruker.com/products/x-ray-diffraction-and-elemental-analysis/handheld-xrf/s1-titan-series/overview.html/

Burke, P. 2001. *Eyewitnessing.* London: Reakton Books.

Buzzard Cameras. 2018. *Buzzard Six Multispectral Camera*. [Online]. [Accessed 3 September 2018]. Available from:

https://web.archive.org/web/20180903210935/https://buzzard.camera/buy/six/

Callander, J. 1911. Notice of the Discovery of Two Vessels of Clay on the Culbin Sands, the First Containing Wheat and the Second from a Kitchen-Midden, with a Comparison of the Culbin Sands and the Glenluce Sands and of the Relics Found on Them. *Proceedings of the Society of Antiquaries of Scotland*. **45**, pp.158 – 181.

Callmer, J. 1977. *Trade Beads and Bead Trade in Scandinavia, ca. 800-1000 A.D.* Rudolph Habelt Verlag.

Campana, D. 1977. Making Stereo-Photomacrographs for Archaeological Studies. *Journal of Field Archaeology.* **4**(4), pp.435 – 440.

Campbell, E. 2007. *Continental and Mediterranean Imports to Atlantic Britain and Ireland, AD 400-800*. York: Council for British Archaeology.

Campbell, E. 2018a. *Email from Ewan Campbell,* 6 April.

Campbell, E. 2018b. *Conversation with Ewan Campbell*, 25 April.

Campbell, E. and Lane, A. 1993. Excavations at Longbury Bank, Dyfed, and Early Medieval Settlement in South Wales. *Medieval Archaeology.* **37,** pp.15 – 77.

Campbell, E. and MacIver, C. 2017. *Excavations at Iona Abbey 2017: Data Structure Report.* University of Glasgow.

Campbell, E. and Maldonado, A. 2016. *Russell Trust Excavations on Iona Led by Charles Thomas, 1956-1963: Data Structure Report for Historic Environment Scotland.* University of Glasgow.

Cannon, A. 1989. The Historical Dimension in Mortuary Expressions of Status and Sentiment. *Current Anthropology.* **30**, pp.437 – 458.

Canon. 2018a. *Canon EF-M 28mm f/3.5 Macro IS STM Lens.* [Online]. [Accessed 14 December 2018]. Available from:

https://web.archive.org/web/20181214134034/https://store.canon.co.uk/canon-ef-m-28mm-f-3-5-macro-is-stm-lens/1362C005/

Canon, 2018b. *Canon EF 180mm f/3.5L Macro USM Lens.* [Online]. [Accessed 29 December 2018]. Available from:

https://web.archive.org/web/20181229151935/https://store.canon.co.uk/canon-ef-180mm-f-3-5l-macro-usm-lens/2539A014/

Canuto, M., Estrada-Belli, F., Garrison, T., Houston, S., Acuña, J., Kováč, M., Marken, D., Nondédéo, P., Auld-Tomas, L., Castanet, C., Chatelain, D., Chiriboga, C., Drápela, T., Lieskovský, T., Tokovinine, A., Velasquez, A., Fernánsez-Díaz, J. and Shrestha, R. 2018. Ancient Lowland Maya Complexity as Revealed by Airborne Laser Scanning of Norther Guatemala. *Science.* **361**(6409).

Casali, F.2006. X-Ray and Neutron Digital Radiography and Computed Tomography for Cultural Heritage. In: Bradley, D. and Creagh, D., eds. *Physical Techniques in the Study of Art, Archaeology, and Cultural Heritage.* Amsterdam: Elsevier, pp.41 – 123.

Chabrillat, S., Goetz, A., Krosley, L. and Olsen, H. 2002. Use of Hyperspectral Images in the Identification and Mapping of Expansive Clay Soils and the Role of Spatial Resolution. *Remote Sensing of Environment.* **82**(2), pp.431 – 445.

Chaichian, M., Rojas, H. and Tureanu, A. 2014. *Basic Concepts in Physics*. Heidelberg: Springer.

Chandler, J. 1999. Effective Application of Automated Digital Photogrammetry for Geomorphological Research. *Earth Surface Processes and Landforms.* **24**(1), pp.51 – 63.

CheekyTorchGlass. 2009. *Glass Art: Easy Air Bubble Inclusions*. [Online]. [Accessed 11 September 2017]. Available at: https://www.youtube.com/watch?v=oooF0S0Japg/

Christens-Barry, W. Boydston, K., France, F., Knox, K., Easton Jr., R. and Toth, M. 2009. Camera System for Multispectral Imaging of Documents. *Proceedings of SPIE, the International Society for Optical Engineering, Society of Photo-Optical Instrumentation Engineers.* **7249**(8).

Christie, H. 2011. *Glass Bead Distribution Analysis: A New Approach to Understanding the Early History of Southeast Asia*. Unpublished B.A. Honours Thesis. St. Lawrence University.

Christie, H. 2014. *Got Swag? Investigating Beads and Bead Trade in Scotland During the First Millennium AD*. Unpublished M.Litt. Dissertation. University of Glasgow.

Chrys Art Glass. 2015a. *How to Make a 'Champagne' Glass Bead with Bubbles.* [Online]. [Accessed: 11 September 2017]. Available at: https://www.youtube.com/watch?v=mi9c3_-nyVw/

Chrys Art Glass. 2015b. *How to Make an Encased Bubble Lampwork Glass Bead*. [Online]. [Accessed 11 September 2017]. Available at: https://www.youtube.com/watch?v=x6vQGh-DPFI/

Clarke, D., Blackwell, A. and Goldberg, M. 2012. *Early Medieval Scotland: Individuals, Communities, and Ideas*. Edinburgh: National Museums Scotland.

Clemente Conte, I. and Goméz Romero, F. 2008. Microwear Analysis of Retouched Glass Fragments from Fortlet Miñana, Azul, Argentina, 1860–1863. *International Journal of Historical Archaeology*. **12**(3), pp.248 – 262.

Cnudde, V. and Boone, M. 2013. High-Resolution X-Ray Computed Tomography in Geosciences: A Review of the Current Technology and Applications. *Earth-Science Reviews*. **123**, pp.1 – 17.

Conlon, V. 1973. *Camera Techniques in Archaeology*. London: John Baker.

Connolly, C. 1953. Brain Morphology and Taxonomy. *Anthropological Quarterly*. **26**(2), pp.35 – 65.

Cookson, M. 1954. *Photography for archaeologists*. London: Max Parrish.

Cosentino, A. 2014. Identification of Pigments by Multispectral Imaging: A Flowchart Method. *Heritage Science*. **2**(1), pp.8.

Costall, A. 1997. Things, and Things Like Them. In: Molyneaux, B., ed. *The Cultural Life of Images*. London: Routledge, pp.49 – 61.

Cultural Heritage Imaging. 2010. *Guide to RTIViewer.* Cultural Heritage Imaging and Visual Computing Lab.

Cultural Heritage Imaging. 2018a. *Process: RTIBuilder Download.* [Online]. [Accessed 1 July 2018]. Available from:

https://web.archive.org/web/20180701191217/http://culturalheritageimaging.org:80/What _We_Offer/Downloads/Process/

Cultural Heritage Imaging. 2018b. *RTI Highlight Capture Starter Kit.* [Online]. [Accessed 3 July 2018]. Available from:

https://web.archive.org/web/20180703234619/http://culturalheritageimaging.org:80/What _We_Offer/Downloads/rti_kits.html/

Cultural Heritage Imaging. 2018c. *RTI Lighting Array.* [Online]. [Accessed: 27 March 2018]. Available from:

http://culturalheritageimaging.org/What_We_Offer/Gear/Lighting_Array/

Cultural Heritage Imaging. 2018d. *RTIViewer Download.* [Online]. [Accessed 2 May 2018]. Available from:

https://web.archive.org/web/20180502142901/http://culturalheritageimaging.org:80/What _We_Offer/Downloads/View/index.html/

Currys. 2017. *PRIMAPHOTO PHKP001 Tripod – Black.* [Online]. [Accessed 16 October 2017]. Available from:

https://web.archive.org/web/20171016165014/http://www.currys.co.uk:80/gbuk/cameras-and-camcorders/photography-accessories/camera-stands/primaphoto-phkp001-tripod-black-10140431-pdt.html/

Currys. 2018. *Search: Tripods*. [Online]. [Accessed 29 December 2018]. Available from: https://www.currys.co.uk/gbuk/tripod/photography-accessories/camera-stands/346_3210_30312_xx_ba00011847-bv00309587/1_20/price-asc/xx-criteria.html/

Dale, L., Thewis, A., Boudry, C., Rotar, I., Dardenne, P., Baeten, V. and Peirna, A. 2013. Hyperspectral Imaging Applications in Agriculture and Agro-Food Product Quality and Safety Control: A Review. *Applied Spectroscopy Reviews.* **48**(2), pp.142 – 159.

Daguerre, L. 1838. *Boulevard du Temple*. [Photograph].

Day, R. 1887. Ornaments in Glass from Egypt to Illustrate Those Found in Ireland. *The Journal of the Royal Historical and Archaeological Association of Ireland.* **8**(71/72), pp.112 – 114.

Degryse, P., Schneider, J., Poblome, J., Waelkens, M., Haack, U., and Muchez, P. 2005. A Geochemical Study of Roman to Early Byzantine Glass from Sagalassos, South-West Turkey. *Journal of Archaeological Science.* **32**(2), pp.287 – 299.

Dejneka, M. and Gomez, S. 2012. *Fining Agents for Silicate Glasses.* US 8158543 B2. 2012-04-17.

Delft University of Technology. 2018. *Pricelist 2018*. [Online]. [Accessed 9 October 2018]. Available from: https://www.tudelft.nl/en/faculty-of-applied-sciences/business/facilities/reactor-institute-delft/research-instruments/inaa/pricelist-2018/

Dell. 2018. *Inspiron 15 7000 Gaming Laptop.* [Online]. [Accessed 16 January 2018]. Available from:

https://web.archive.org/web/20180116025156/http://www.dell.com:80/en-uk/shop/laptops-notebooks-and-2-in-1-laptops/inspiron-15-7000-gaming-laptop/spd/inspiron-15-7577-laptop/

Dellepiane, M., Corsini, M., Callieri, M., and Scopigno, R. 2006. High Quality PTM Acquisition: Reflection Transformation Imaging for Large Objects. In: Arnold, D., Niccolucci, F., Ioannides, M. and Mania, K. *Proceedings of the 7th International Conference on Virtual Reality, Archaeology and Intelligent Cultural Heritage.* Aire-la-Ville, Switzerland: Eurographics Association, pp.179 – 186.

Díaz-Guardamino, M. and Wheatley, D. 2013. Rock Art and Digital Technologies: The Application of Reflectance Transformation Imaging (RTI) and 3D Laser Scanning to the Study of Late Bronze Age Iberian Stelae. *MENGA: Journal of Andalusian Prehistory*. **3**(4), pp.187 – 203.

DinoLite. 2017a. *Downloads.* [Online]. [Accessed 4 February 2017]. Available from: https://web.archive.org/web/20170204114631/http://www.dinolite.us/downloads/

DinoLite. 2017b. *Returns, Repairs, and Replacements.* [Online]. [Accessed 10 April 2017]. Available from: https://web.archive.org/web/20170410080316/http://www.dinolite.us:80/warranty/

DinoLite. 2018. *DinoLite Stands.* [Online]. [Accessed 29 December 2018]. Available from: https://web.archive.org/web/20181229151650/https://www.dinolite.us/products/accessories/dino-lite-stands/

Ditchburn, R. 1991. *Light*. New York: Dover Publications.

Doneus, M. and Briese, C. 2006. Full-Waveform Airborne Laser Scanning as a Tool for Archaeological Reconnaissance. *BAR International Series*. **1568**, pp.99 – 106.

Doneus, M., Verhoeven, G., Fera, M., Briese, C., Kucera, M. and Neubauer, W. 2011. From Deposit to Point Cloud – A Study of Low-Cost Computer Vision Approaches for the Straightforward Documentation of Archaeological Excavations. *Geoinformatics CTU FCE.* **6**(2011), pp.81-88.

Dorrell, P. 1989. *Photography in Archaeology and Conservation*. Cambridge: Cambridge University Press.

Dorrell, P. 1994. *Photography in Archaeology and Conservation*. 2nd ed. Cambridge: Cambridge University Press.

Dussubieux, L. 2001. *L'apport de l'ablation laser couplée à l'ICP-MS à la caractérisation des verres : application à l'étude du verre archéologique de l'Océan Indien*. Unpublished Ph.D. Dissertation. Orléans.

Dussubieux, L., Kusimba, C., Gogte, V., Kusimba, S., Gratuze, B., and Oka, R. 2008. The Trading of Ancient Glass Beads: New Analytical Data from South Asian and East African Soda-alumina Glass Beads. *Archaeometry.* **50**(5), pp.797 – 821.

Dussubieux, L. and Gratuze, B. Non-Destructive Characterization of Glass Beads: An Application to the Study of Glass Trade between India and Southeast Asia. *9th International Conference of the European Association of Southeast Asian Archaeologists, Sigtuna, May 27th-June 2nd 2002*. pp.135 – 148.

Dussubieux, L., Gratuze, B. and Blet-Lemarquand, M. 2010. Mineral Soda Alumina Glass: Occurrence and Meaning. *Journal of Archaeological Science.* **xxx**, pp.1 – 10.

Earl, G. 2006. At the Edges of the Lens: Photography, Graphical Constructions, and Cinematography. In: Evans, T. and Daly, P. eds. *Digital Archaeology: Bridging Method and Theory*. London: Routledge, pp.191 – 209.

Earl, G., Beale, G., Martinez, K. and Pagi, H. 2010. Polynomial Texture Mapping and Related Imaging Technologies for the Recording, Analysis and Presentation of Archaeological Materials. *International Archives of Photogrammetry, Remote Sensing and Spatial Information Sciences.* **38**(Part 5), pp.218 – 223.

Earl, G., Keay, S. and Beale, G. 2008. Computer Graphic Modelling at Portus: Analysis, Reconstruction and Representation of the Claudian and Trajanic Harbours. In: Lasaponara, R. and Masini, N. eds. *Proceedings of the 1st International EARSeL Workshop Program, Rome.* Consiglio Nazionale di Ricerca. pp. 165 – 172.

Eder, J. 1945. *History of Photography*. New York: Dover Publications, Inc.

Elzinga, C., Salzer, D., Willoughby, J. and Gibbs, J. 2009. *Monitoring Plant and Animal Populations: A Handbook for Field Biologists.* Malden, Massachusetts: Blackwell Science.

d'Errico, F., Vanhaeren, M. and Wadley, L. 2008. Possible Shell Beads from the Middle Stone Age Layers of Sibudu Cave, South Africa. *Journal of Archaeological Science.* **35**, pp.2675 – 2685.

Esco Optics. 2017. Fused Silica / Fused Quartz. [Online]. [Accessed 27 February 2017]. Available at:

https://web.archive.org/web/20170227124303/http://escooptics.com:80/pages/materials-fused-silica-quartz/

Estes, J., Jensen, J. and Tinney, L. 1977. The Use of Historical Photography for Mapping Archaeological Sites. *Journal of Field Archaeology.* **4**(4), pp.441 – 447.

Evans, A. and Donahue, R. 2008. Laser Scanning Confocal Microscopy: A Potential Technique for the Study of Lithic Microwear. *Journal of Archaeological Science.* **35**(8), pp.2223 – 2230.

Evans, D., Fletcher, R., Pottier, C., Chevance, J., Soutif, D., Tan, B., Im, S., Ea, D., Tin, T., Samnang, K., Cromarty, C., Greef, S. Hanus, K., Bâty, P., Shimoda, I. and Boornazian, G. 2013. Uncovering Archaeological Landscapes at Angkor Using Lidar. *Proceedings of the National Academy of Sciences.* **110**(31), pp.12595 – 12600.

Farley, J. and Hunter, F. 2015. *Celts: Art and Identity*. London: The British Museum Press.

Faro. 2018a. *Maintenance.* [Online]. [Accessed 17 December 2018]. Available from:

https://web.archive.org/web/20181217145143/https://www.faro.com/support/maintenance/

Faro. 2018b. *Search: Discontinued.* [Online]. [Accessed 17 December 2018]. Available from:

https://web.archive.org/web/20181217150333/https://www.faro.com/search/?key=discontinued

The Field Museum. 2018. *Archaeological Science: Policies*. [Online]. [Accessed 27 February 2018]. Available from: https://www.fieldmuseum.org/science/research/area/archaeological-science/archaeological-science-policies/

Fischer, C. and Kakoulli, I. 2006. Multispectral and Hyperspectral Imaging Technologies in Conservation: Current Research and Potential Applications. *Studies in Conservation.* **51**(Supplement 1), pp.3 – 16.

Fisher, L. 2009. *Photography for Archaeologists Part II: Artefact Recording*. British Archaeological Jobs Resource.

Flynn, B. 2007. The Morphology of Space in Virtual Heritage. In: Cameron, F. and Kenderdine, S. eds. *Theorizing Digital Cultural Heritage: A Critical Discourse.* London: The MIT Press, pp.19-34.

Forte, M., Issavi, J., Onsurez, L. and Lercari, N. 2012. 3D Archaeology at Çatalhöyük. *International Journal of Heritage in the Digital Era.* **1**(3), pp.351 – 378.

Francis, P. 1988. Glass Beads in Asia Part I. Introduction. *Asian Perspectives.* **28**, pp.1 – 21.

Francis, P. 1990. Glass Beads in Asia Part Two: Indo-Pacific Beads. *Asian Perspectives.* **29**(1), p.1 – 23.

Francis, P. 1991. Beadmaking at Arikamedu and Beyond. *World Archaeology*. **23**(1), pp.28 – 43.

Francis, P. 2002. *Asia's Maritime Bead Trade:300 BC to the Present*. Honolulu: University of Hawai'i Press.

Freeman, M. 1985. *The Encyclopedia of Practical Photography*. London: Macdonald & Co.

Freestone, I. 2009. Scientific Analysis of Glazed Tile from the Seljuq Palace of Kubad Âbâd, Lake Beyşehir, Turkey. In: McCarthy, B., Chase, E., Cort, L., Douglas, J. and Jett, P., eds. *Scientific Research on Historic Asian Ceramics: Proceedings of the Fourth Forbes Symposium at the Freer Gallery of Art*. Washington DC: Archetype Publications with the Freer Gallery of Art, pp.3 – 8.

Freestone, I. 2015. The Recycling and Reuse of Roman Glass: Analytical Approaches. *Journal of Glass Studies*. **57**(2015), pp.29 – 40.

Freestone, I. 2018. *Emails from Ian Freestone*. 25 – 28 February.

Freestone, I., Hughes, M. and Stapleton, C. 2008. Composition and Production of Anglo-Saxon Glass. In: Evison, V. I., and Freestone, I. (eds) *Catalogue of Anglo-Saxon Glass in the British Museum*. UK: The British Museum, pp.29 – 46.

Friedland, T. 2016. Macro, Close-up, and Micro Photography: What's the Diff? [Online]. [Accessed 14 December 2018]. Available at: https://web.archive.org/web/20181214131634/https://www.picmonkey.com/blog/macro-close-up-and-micro-photography-whats-the-diff/

Friedman, A. and Ross, D. 2003. *Mathematical Models in Photographic Science*. Berlin: Springer.

Frizot, M. 1998. *A New History of Photography*. Koln: Könemann.

Gajski, D., Solter, A., and Gašparović, M. 2016. Applications of Macro Photogrammetry in Archaeology. *The International Archives of the Photogrammetry, Remote Sensing, and Spatial Information Sciences.* **41**(B5), pp.263 – 266.

Gan, F. 2009. The Silk Road and Ancient Chinese Glass. In: Gan, F. ed. *Ancient Glass Research along the Silk Road*. New Jersey: World Scientific, pp.41 – 108.

Gan, F., Cheng, H., Hu, Y., Ma, B., and Gu, D. 2009. Study on the Most Early Glass Eye-Beads in China Unearthed from Xu Jialing Tomb in Xichuan of Henan Province, China. *Science in China Series E: Technological Sciences.* **52**(4), pp.922 – 927.

Garrison, E. 2003. *Techniques in Archaeological Geology.* Berlin: Springer-Verlag.

Gathercole, P. 1984. A Consideration of Ideology. In: Spriggs, M. ed. *Marxist Perspectives in Archaeology.* Cambridge: Cambridge University Press, pp.149 – 154.

Gawler, J., Sanders, M., Bull, J., du Boulay, G. and Marshall, J. 1974. Computer Assisted Tomography in Orbital Disease. *The British Journal of Opthamology.* **58**(6), pp.571 – 587.

Geertz, C. 1972. Deep Play: Notes on the Balinese Cockfight. *Daedalus.* **101**(1), pp.1 – 37.

Giachetti, A., Ciortan, I., Daffara, C., Pintus, R. and Gobbetti, E. 2017. Multispectral RTI Analysis of Heterogenous Artworks. In: Fellner, D. ed. *The 14th Eurographics Workshop on Graphics and Cultural Heritage 2017*. Goslar: Eurographics Association, pp.19 – 28.

Gigahertz-Optik. 2017. *Reflection, Transmission, and Absorption*. [Online]. [Accessed 22 October 2017]. Available at: https://web.archive.org/web/20171022233142/http://light-measurement.com:80/reflection-absorption/

Gimp. 2018. *Gimp*. [Online]. [Accessed 15 April 2018]. Available from: https://web.archive.org/web/20180415024826/https://www.gimp.org/

Glotzbach, J., Schafer, R., and Illgner, K. 2001. A Method of Color Filter Array Interpolation with Alias Cancellation Properties. *Proceedings 2001 International Conference on Image Processing*. **1,** pp.141 – 144.

Goetz, A., Vane, G., Solomon, J., and Rock, B. 1985. Imaging Spectrometry for Earth Remote Sensing. *Science*. **228**(4704), pp.1147 – 1153.

Golowzcynski, M. 2016. *Digital Camera Sensors Explained.* [Online]. [Accessed 10 September 2017]. Available at: https://web.archive.org/web/20170910182807/http://www.whatdigitalcamera.com:80/technical-guides/technology-guides/sensors-explained-11457/

Gomez, R., & Del Re, N. 2005. Hyperspectral Imaging: Gem Identification and Authentication. *Proceedings of SPIE – The International Society for Optical Engineering*. **5655,** pp.325 – 332.

Green, J., Baker, P., Richards, B., and Squire, D. 1971. Simple Underwater Photogrammetric Techniques. *Archaeometry.* **13**(2), pp.221 – 232.

Grün, A., Remondino, F., and Zhang, L. 2004. Photogrammetric Reconstruction of the Great Buddha of Bamiyan, Afghanistan. *The Photogrammetric Record.* **19**(107), pp.177 – 199.

Grussenmeyer, P., Landes, T., Voegtle, T. and Ringle, K. 2008. Comparison Methods of Terrestrial Laser Scanning, Photogrammetry and Tacheometry Data for Recording of Cultural Heritage Buildings. *The International Archives of the Photogrammetry, Remote Sensing and Spatial Information Sciences.* **36**, pp.213 – 218.

GT Vision. 2018a. *GXM-Dino-Lite AM4113ZT Pro Digital Microscope, 10X-50X & 230X Magnification, 1.3megapixels.* [Online]. [Accessed 29 October 2018]. Available from:

https://web.archive.org/web/20181229151917/https://www.gtvision.co.uk/epages/es141397.sf/en_GB/?ObjectPath=/Shops/es141397/Products/4031/

GT Vision. 2018b. *Microscope Stands*. [Online]. [Accessed 29 December 2018]. Available from:

https://web.archive.org/web/20181229152507/https://www.gtvision.co.uk/epages/es141397.sf/en_GB/?ViewAction=View&ObjectID=30686983&PageSize=60&OrderBy=ListPrice&OrderDesc=0/

GT Vision. 2018c. *GXM - Dino-Lite AM4815ZTL EDGE-Extended Dynamic Range*. [Online]. [Accessed 29 December 2018]. Available from:

https://web.archive.org/web/20181229151909/https://www.gtvision.co.uk/epages/es141397.sf/en_GB/?ObjectPath=/Shops/es141397/Products/0596/

GT Vision. 2018d. *GXM-Dino-Lite AD7013MTL, 20X-90X Magnification, 5 megapixels.* [Online]. [Accessed 29 December 2018]. Available from: https://web.archive.org/web/20181229151850/https://www.gtvision.co.uk/epages/es141397.sf/en_GB/?ObjectPath=/Shops/es141397/Products/9180/

Guha, S. 2002. The Visual in Archaeology: Photographic Representation of Archaeological Practice in British India. *Antiquity*. **76**(2006), pp.93 – 100.

Guido, M. 1978. *Prehistoric and Roman Glass Beads in Britain and Ireland*. London: The Society of Antiquaries of London.

Guido, M. 1999. *The Glass Beads of Anglo-Saxon England c. AD 400-700: A Preliminary Visual Classification of the More Definitive and Diagnostic Types.* Suffolk: Boydell Press for The Society of Antiquaries of London.

Hähnel. 2018. *HRN 280 Pro for Nikon.* [Online]. [Accessed 28 December 2018]. Available from: https://web.archive.org/web/20181229140454/https://www.hahnel.ie/irish-shop/hrn-280-pro-for-nikon/

Hall, M. and Yablonsky, L. 1998. Chemical Analysis of Sarmatian Glass Beads from Pokrovka, Russia. *Journal of Archaeological Science*. **25**(1995), pp.1239 – 1245.

Harrison, R. 2000. 'Nowadays with Glass': Regional Variation in Aboriginal Bottle Glass Artefacts from Western Australia. *Archaeology in Oceania.* **35**(1), pp.34 – 47.

Hecht, J. 2010. Short History of Laser Development. *Optical Engineering.* **49**(9): pp.091002-1 – 091002-23.

Heck, M., Rehren, T. and Hoffman, P. 2003. The Production of Lead-Tin Yellow at Merovingian Schleitheim (Switzerland). *Archaeometry.* **45**(1), pp.33 – 44.

von Helmholtz, H. 1896. *Handbuch der Physiologischen Optik.* 2nd ed. Hamburg: Verlag von Leopold Voss.

Henderson, J. 1985. The Raw Materials of Early Glass Production. *Oxford Journal of Archaeology.* **4**(3), pp.26 – 291.

Henderson, J., McLoughlin, S. and McPhail, D. 2004. Radical Changes in Islamic Glass Technology: Evidence for Conservatism and Experimentation with New Glass Recipes from Early and Middle Islamic Raqqa, Syria. *Archaeometry.* **46**(3), pp.439 – 468.

Hermann, E. 2017. *Lee Filters: Resin vs Pro Glass.* [Online]. [Accessed 7 September 2017]. Available at:

https://web.archive.org/web/20170907131737/http://ericherrmann.com:80/news/lee-filters-resin-vs-pro-glass/

Historic England. 2018. *3D Laser Scanning for Heritage: Advice and Guidance on the Use of Laser Scanning in Archaeology and Architecture.* [Online]. [Accessed 28 December 2018]. Available from:

https://web.archive.org/web/20181229142525/https://historicengland.org.uk/images-books/publications/3d-laser-scanning-heritage/heag155-3d-laser-scanning/

Historic Environment Scotland. 2018. *Applied Digital Documentation in the Historic Environment.* Edinburgh: Historic Environment Scotland.

Hodder, I. 1982. *Symbols in Action: Ethnoarchaeological Studies of Material Culture.* Cambridge: Cambridge University Press.

Hodder, I. 1999. *The Archaeological Process: An Introduction.* Oxford: Blackwell.

Hounsfield, G. 1973. Computerized Transverse Axial Scanning (Tomography): Part 1. Description of the System. *The British Journal of Radiology.* **46**(552), pp.1016 – 1022.

House, K., Mazumder, P., Peterson, I., and Schiefelbein, S. 2009. *Method of Increasing the Effectiveness of a Fining Agent in a Glass Melt.* US 7584623 B2. 2009-09-08.

Howell, C. and Blanc, W. 1992. *A Practical Guide to Archaeological Photography*. Institute of Archaeology, University of California.

Hoya Optics. 2017a. *Ultraviolet Transmitting, Visible Absorbing Filters*. [Online]. [Accessed 11 September 2017]. Available at: https://web.archive.org/web/20170911060934/http://www.hoyaoptics.com:80/color_filter/uv_transmitting.htm/

Hoya Optics. 2017b. *UV & IR Cut Filter*. [Online]. [Accessed 24 October 2017]. Available at: https://web.archive.org/web/20171024042554/http://www.hoyafilter.com:80/hoya/products/generalfilters/uvircut/

Huggett, J. 2004. Archaeology and the New Technological Fetishism. *Archaeologia e Calcolatori.* **15**, pp.81 – 92.

Huggett, J. 2015. A Manifesto for an Introspective Digital Archaeology. *Open Archaeology.* **1**(1), pp.86 – 95.

Hunter, F. 2013. Hillfort and Hacksilber: Traprain Law in the Late Roman Iron Age and Early Prehistoric Period. In: Hunter, F. and Painter, K. eds. *Late Roman Silver: The Traprain Treasure in Context.* Edinburgh: Society of Antiquaries of Scotland, pp.3 – 10.

Huntington, R. and Metcalf, P. 1979. *Celebrations of Death.* Cambridge: Cambridge University Press.

Indraningsih, R. 1985. Research on Prehistoric Beads in Indonesia. *Bulletin of the Indo-Pacific Prehistory Association.* **6**: pp.133 – 141.

Inkscape. 2018. *Inkscape.* [Online]. [Accessed 31 March 2018]. Available from: https://web.archive.org/web/20180331000207/https://inkscape.org/en/

Instituto Nazionale di Fisica Nucleare. 2018. *Price List*. [Online]. [Accessed 9 October 2018]. Available from: http://chnet.infn.it/en/price-list/

Ives, R. 1941. Photographing Translucent, Transparent, and Multicolored Artifacts. *American Antiquity.* **6**(3), pp.263 – 265.

James, S. 1997. Drawing Inferences: Visual Reconstructions in Theory and Practice. In: Molyneaux, B. ed. *The Cultural Life of Images: Visual Representations in Archeology.* London: Routledge, pp. 22 – 48.

Janssens, K., Aerts, A., Vincze, L., Adams, F., Yang, C., Utui, R., Malmqvist, K., Jones, K., Radke, M., Garbe, S., Lechtenberg, F., Knöchel, A., and Wouters, H. 1996. Corrosion Phenomena in Electron, Proton and Synchrotron X-ray Microprobe Analysis of Roman Glass from Qumran, Jordan. *Nuclear Instruments and Methods in Physics Research Section B: Beam Interactions with Materials and Atoms.* **109/110**(1996): pp.690 – 695.

Jeffrey, S. 2005. The Missing Dimension: Future Directions in Digital Recording of Early Medieval Sculptured Stone. In: Foster, S. ed. *Able Minds and Practised Hands: Scotland's Early Medieval Sculpture in the 21st Century.* New York: Routledge, pp.353 – 366.

Jeffrey, S. 2015. Challenging Heritage Visualisation: Beauty, Aura and Democratisation. *Open Archaeology 2015.* **1**, pp.144 – 152.

Jenkins, F. and White, H. 1981. *Fundamentals of Optics 4th ed.* Auckland: McGraw-Hill.

Jessops. 2018a. *Hoya 52mm Revo SMC UV Filter.* [Online]. [Accessed 24 April 2018]. Available from: https://www.jessops.com/p/hoya/52mm-revo-smc-uv-filter-89412/

Jessops. 2018b. *Nikon AF-S 40mm Micro f/2.8 DX G Lens.* [Online]. [Accessed 24 April 2018]. Available from: https://www.jessops.com/p/nikon/af-s-40mm-micro-f-2-8-dx-g-lens-82003/

Jewitt, L. 1870. *Grave-Mounds and Their Contents: A Manual of Archaeology, as Exemplified in the Burials of the Celtic, The Romano-British, and the Anglo-Saxon Periods.* London: Groombridge and Sons.

Joby. 2018a. Gorillapod Original. *Joby*. [Online]. [Accessed 19 April 2018]. Available from: https://web.archive.org/web/20180419060755/https://joby.com/gorillapod-original/

Joby. 2018b. Gorillapod Hybrid. *Joby*. [Online]. [Accessed 25 September 2017]. Available from:

https://web.archive.org/web/20170925004821/https://joby.com/gorillapod-hybrid/

Johnson, G. 1909. *Photographic Optics and Colour Photography: Including the Camera, Kinematograph, Optical Lantern, and the Theory and Practice of Image Formation*. London: Ward and Company.

Kanungo, A. 2004. *Glass Beads in Ancient India: An Ethnoarchaeological Approach*. John and Erica Hedges, Limited.

Katsuhiko, O. and Gupta, S. 2000. The Far East, Southeast and South Asia: Indo-Pacific Beads in Yayoi Tombs as Indicators of Early Maritime Exchange. *South Asian Studies*. **16**, pp.73 – 88.

Keating, A. 2016. *Email to Andrew Keating of Gilden Photonics*. 9 March.

Kitzler-Åhfelt, L. 2015. Picture-Stone Workshops on Viking Age Gotland – A Study of Craftworker's Trade. In: Heizmann, W. and Oehrl, S., eds. *Bilddenkmäler zur germanischen Götterund Heldensage.* Berlin: De Gruyter, pp.397 – 462.

Kitzler-Åhfelt, L. 2002. *Work and Worship: Laser Scanner Analysis of Viking Age Rune Stones.* Unpublished Ph.D. Dissertation, Stockholm University.

Koutsoudis, A., Vidmar, B., Ionnakis, G., Arnaoutoglou, F., Pavlidis, G., and Chamzas, C. 2014. Multi-Image 3D Reconstruction Data Evaluation. *Journal of Cultural Heritage*. **15**(1), pp.73 – 79.

Kurz, T., Buckley, S., and Howell, J. 2012. Close Range Hyperspectral Imaging Integrated with Terrestrial LIDAR Scanning Applied to Rock Characterisation at Centimetre Scale. *ISPRS - International Archives of the Photogrammetry, Remote Sensing and Spatial Information Sciences*. **39B5**: pp.417 – 422.

Kurz, T., Buckley, S., and Howell, J. 2013. Close-Range Hyperspectral Imaging for Geological Field Studies: Workflow and Methods. *International Journal of Remote Sensing*. **34**(5), pp.1798 – 1822.

LAGOA. 2014. *What's the Right 3D Scanner for You?* [Online]. [Accessed: 14 April 2016]. Available from:
https://web.archive.org/web/20160414013511/http://home.lagoa.com/2014/04/whats-the-right-3d-scanner-for-you/

Lankton, J. and Dussubieux, L. 2006. Early Glass in Asian Maritime Trade: A Review and an Interpretation of Compositional Analyses. *Journal of Glass Studies*. **48**, pp.121 – 144.

Lankton, J.W., Dussubieux, L. and Rehren, T. 2009. A Study of Mid-First Millennium CE Southeast Asian Specialized Glass Beadmaking Traditions. In: Bacus, E., Glover, I., and Sharrock, P. eds. *Interpreting Southeast Asia's Past: Monument, Image and Text*. Singapore: NUS Press, pp.335 – 356.

Latour, B. and Lowe, A. 2010. The Migration of the Aura, or How to Explore the Original through its Facsimiles. In: Bartscherer, T. ed. *Switching Codes*. Chicago: University of Chicago Press, pp.275 – 298.

Lau, D., Villis, C., Furman, S. and Livett, M. 2008. Multispectral and Hyperspectral Image Analysis of Elemental and Micro-Raman Maps of Cross-Sections from a 16th Century Painting. *Analytica Chimica Acta.* **610**(1), pp.15 – 24.

Ledley, R., Chiro, G., Luessenhop, A. and Twigg, H. 1974. Computerized Transaxial X-Ray Tomography of the Human Body. *Science.* **186**(4160), pp.207 – 212.

Lee, I. 2009. Glass and Bead Trade on the Asian Sea. In: Gan, F. ed. *Ancient Glass Research along the Silk Road*. New Jersey: World Scientific, pp.165 – 182.

Legnaioli, S. Lorenzetti, G., Cavalcanti, G., Grifoni, E., Marras, L., Tonazzini, A., Salerno, E., Pallecchi, P., Giachi, G. and Palleschi, V. 2013. Recovery of Archaeological Wall Paintings Using Novel Multispectral Imaging Approaches. *Heritage Science.* **1**, pp.33.

Lerma, J., Savarro, S., Cabrelles, M. and Villaverde, V. 2010. Terrestrial Laser Scanning and Close-Range Photogrammetry for 3D Archaeological Documentation: The Upper Palaeolithic Cave of Papalló as a Case Study. *Journal of Archaeological Science.* **37**(3), pp.499 – 507.

Liang, H. 2012. Advances in Multispectral and Hyperspectral Imaging for Archaeology and Art Conservation. *Applied Physics.* **A 106**(2), pp.309 – 323.

Lighting Ever. 2018. *21 LEDs UV Torch, Backlight, 395nm Ultra Violet, Batteries Included Mini Flashlight.* [Online]. [Accessed 29 December 2018]. Available from: https://web.archive.org/web/20181229131138/https://www.lightingever.co.uk/21-led-uv-led-torch.html/

Lin, S., Douglass, M., Holdaway, S. and Floyd, B. 2010. The Application of 3D Laser Scanning Technology to the Assessment of Ordinal and Mechanical Cortex Quantification in Lithic Analysis. *Journal of Archaeological Science.* **37**(4), pp.694 – 702.

Linton, H. 1876. Notice of a Collection of Flint Arrow-Heads and Bronze and Iron Relics from the Site of an Ancient Settlement Recently Discovered in the Culbin Sands in Findhorn, Near Morayshire. *Proceedings of the Society of Antiquaries of Scotland.* **11,** pp.543 – 546.

Lobb, M., Krawiec, K., Howard, A., Gearey, B. and Chapman, H. A New Approach to Recording and Monitoring Wet-Preserved Archaeological Wood Using Three-Dimensional Laser Scanning. *Journal of Archaeological Science.* **37**(12), pp.2995 – 2999.

Lyons, C. 2005. The Art and Science of Antiquity in Nineteenth-Century Photography. In: Lyons, C. Papadopoulos, J., Stewart, L., and Szegedy-Maszak, A. eds. *Antiquity & Photography: Early Views of Ancient Mediterranean Sites.* London: Thames & Hudson, pp.22 – 65.

MacLeod, S. 2008. *Basics Photography 05: Post Production Colour.* Lausanne: AVA Publishing.

Maglite. 2018. *Maglite Solitaire Flashlight.* [Online]. [Accessed 29 December 2018]. Available from:

https://web.archive.org/web/20181229131010/http://www.maglite.com/shop/flashlights/compact-flashlights/maglite-solitaire-1-cell-aaa-flashlight.html/

Maiman, T. 1960. Optical and Microwave-optical Experiments in Ruby. *Physics Review Letters.* **4**(11): pp.564 – 566.

Malpas, P. 2007. *Basics Photography 03: Capturing Colour*. Lausanne: AVA Publishing.

Malzbender, T., Gelb, D., and Wolters, H. 2001. Polynomial Texture Maps. In: Pocock, L. ed. *Proceedings of the 28th Annual Conference on Computer Graphics and Interactive Techniques*. New York: Association for Computing Machinery, pp.519 – 528.

Manfroto. 2018a. *Search: Tripods*. [Online]. [Accessed 29 December 2018]. Available from:

https://web.archive.org/web/20181229153807/https://www.manfrotto.co.uk/products/photo-tripods/tripod-with-heads?dir=asc&is_ajax=1&limit=36&order=price&p=2/

Manfroto. 2018b. *190go! MS Carbon Tripod kit 4-Section with XPRO 3-way head.* [Online]. [Accessed 14 December 2018]. Available from:

https://web.archive.org/web/20181214122508/https://www.manfrotto.co.uk/190-go-cf-4-sec-ms-kit-3wxp/

Mannion, M. 2015. *Glass Beads from Early Medieval Ireland*. Oxford: Archaeopress Publishing Ltd.

Mansurov, N. 2009. *What is a DSLR (Digital SLR) Camera?* [Online]. [Accessed 4 September 2017]. Available at: https://photographylife.com/what-is-a-dslr/

Mansurov, N. 2017. *Glass vs Resin Filters - Are There Any Differences in Sharpness? Photography Life.* [Online]. [Accessed 8 September 2017]. Available from: https://photographylife.com/glass-vs-resin-filters/

Marshall, C., Speth, J., & Payne, S. 1997. Induced Optical Absorption in Gamma, Neutron and Ultraviolet Irradiated Fused Quartz and Silica. *Journal of Non-Crystalline Solids.* **212**(1), pp.59 – 73.

Mathewson, A. 1877. Notes on the Age of the Settlements on the Sands of Culbin. *Proceedings of the Society of Antiquaries of Scotland.* **12**, pp.302 – 305.

Matter and Form. 2014. *A Brief History of 3D Scanning.* [Online]. [Accessed 9 October 2018]. Available from: https://matterandform.net/blog/a-brief-history-of-3d-scanning/

Matter and Form. 2018a. *Matter and Form 3D Scanner V2 +Quickscan.* [Online]. [Accessed 10 October 2018]. Available from: https://matterandform.net/store/checkout/

Matter and Form. 2018b. *Matter and Form 3D Scanner V2 User Manual*. [Online]. [Accessed 29 December 2018]. Available from: https://web.archive.org/web/20181229144803/https://matterandform.net/downloads/MFStudio_User-Manual_EN.pdf?2018-05-14/

Maxwell, J. 1862. On the Theory of the Three Primary Colours. Notices of the *Proceedings of the Royal Institute of Great Britain.* **3**, pp.370 – 374.

McDowell, G. 2009. How Does A Digital Camera Work? [Online]. [Accessed 25 August 2017]. Available at:

https://web.archive.org/web/20170825083346/http://www.makeuseof.com:80/tag/technology-explained-how-does-a-digital-camera-work/

McFadgen, B. 1971. An Application of Stereophotogrammetry to Archaeological Recording. *Archaeometry.* **13**(1), pp.71 – 81.

McPherron, S., Gernat, T. and Hublin, J. 2009. Structured Light Scanning for High-Resolution Documentation of In-Situ Archaeological Finds. *Journal of Archaeological Science.* **36**(1), pp.19 – 24.

MeshLab. 2018. *MeshLab.* [Online]. [Accessed 12 December 2018]. Available from:

https://web.archive.org/web/20181212150101/http://www.meshlab.net/

Messiga, B. and Riccardi, M. 2001. A Petrological Approach to the Study of Ancient Glass. *Periodico di Mineralogia.* **70**(1), pp.57 – 70.

Meyer, J. 2013. What is a macro lens? Magnification and Minimum Focus Distance Explained. *TechRadar*. [Online]. [Accessed 1 March 2017]. Available at:

https://web.archive.org/web/20180301232142/http://www.techradar.com/how-to/what-is-a-macro-lens-magnification-and-minimum-focus-explained/

Michels, S. 2018. Re-framing Photography – Some Thoughts. In: Michels, S. and Helff, S. eds. *Global Photographies: Memory – History – Archives.* Bielefeld: Transcript-Verlag, pp.9 – 17.

Microphotonics. 2015. *How much does a Micro-CT scanner cost?* [Online]. [Accessed 22 September 2017]. Available at:

https://web.archive.org/web/20170922062502/http://www.microphotonics.com:80/how-much-does-a-micro-ct-scanner-cost/

Milentijevic, I. 2018. *The Science of Infrared Hotspots*. [Online]. [Accessed 20 December 2018]. Available from:

https://web.archive.org/web/20181220153036/https://kolarivision.com/the-science-of-infrared-hotspots/

Moffitt, F. 1967. *Photogrammetry*. Scranton, PA: International Textbook Company.

Molina, G., Odin, G., Pradell, T., Shortland, A. and Tite, M. 2014. Production technology and Replication of Lead Antimonate Yellow Glass from New Kingdom Egypt and the Roman Empire. *Journal of Archaeological Science.* **41**, pp.171 – 184.

Morigi, M., Casali, F., Berdondini, A., Bettuzzi, M., Bianconi, D., Brancaccio, R., Catellani, A., D'Errico, V., Pasini, A., Rossi, A., Labanti, C. and Scianna, N. 2007. X-Ray 3D Computed Tomography of Large Objects: Investigation of an Ancient Globe Created by Vincenzo Coronelli. *O3A: Optics for Arts, Architecture, and Archaeology.* **6618**.

Morigi, M., Casali, F., Bettuzzi, M., Brancaccio, R. and d'Errico, V. 2010. Application of X-ray Computed Tomography to Cultural Heritage Diagnostics. *Applied Physics.* **A 100**(3), pp.653 – 661.

Moser, S. and Smiles, S. 2005. Introduction: The Image Question. In: Smiles, S. and Moser, S. eds. *Envisioning the Past: Archaeology and the Image.* Oxford: Blackwell Publishing, pp.1 – 12.

Mountain Warehouse. 2018. Fun 9 LED Gift Torch. [Online]. [Accessed 28 December 2018]. Available from:

https://web.archive.org/web/20181229140701/https://www.mountainwarehouse.com/camping/equipment/torches-lanterns/fun-9led-gift-torch-p5604.aspx/purple/

Mudge, M., Malzbender, T., Schroer, C., & Lum, M. 2006. New Reflection Transformation Imaging Methods for Rock Art and Multiple-Viewpoint Display. In: Arnold, D., Niccolucci, F., Ioannides, M. and Mania, K. eds. *Proceedings of the 7th Annual Symposium on Virtual Reality, Archaeology and Cultural Heritage.* Aire-la-Ville, Switzerland: Eurographics Association, pp.195 – 202.

Mudge, M., Voutaz, J.-P., Schroer, C., & Lum, M. 2005. Reflection Transformation Imaging and Virtual Representations of Coins from the Hospice of the Grand St. Bernard. In: Mudge, M., Ryan, N. and Scopigno, R. eds. *Proceedings of the 6th International Symposium on Virtual Reality, Archaeology and Cultural Heritage*. Aire-la-Ville, Switzerland: Eurographics Association, pp.29 – 39.

Neblette, C. 1952. *Photography: Its Materials and Processes*. 5th ed. London: Macmillan & Co.

Neewer. 2014a. *Neewer - IR760 FILTER 52MM*. [Online]. [Accessed 20 December 2017]. Available at:

https://web.archive.org/web/20171220152953/http://www.neewer.com:80/imaging-products/filters/10000318.html/

Neewer. 2014b. *Neewer - IR850 FILTER 52MM*. [Online]. [Accessed 21 December 2017]. Available at:

https://web.archive.org/web/20171221165137/http://www.neewer.com:80/imaging-products/filters/10000319.html/

Neewer. 2014c. *Neewer - IR950 FILTER 52MM*. [Online]. [Accessed 20 December 2017]. Available at:

https://web.archive.org/web/20171220152958/http://www.neewer.com:80/imaging-products/filters/10000324.html/

Neewer. 2018a. Neewer 4 Pieces 52MM Infrared X-Ray IR Filter Set: IR720, IR760, IR850, IR950 with Filter Carrying Pouch for NIKON D7100 D700 D5200 D5100 D500 D3300 D3200 D3000 D90 D80 DSLR Cameras. [Online]. [Accessed 24 April 2018]. Available from: https://www.amazon.com/Neewer-Pieces-Infrared-X-Ray-Filter/dp/B015XMSUB0/ref=sr_1_2?s=electronics&ie=UTF8&qid=1523619637&sr=1-2&keywords=neewer+52mm+infrared+filter/

Neewer. 2018b. Neewer 52 mm Colour Filter Set for Nikon D7100 D7000 D5200 D5100 D5000 D3300 D3200 D3000 D90 D80 DSLR Cameras – Includes: 5x 52 mm Color Filter Blue/Yellow/Orange/Red/Green) and 1x 52 mm Center Pinch Lens Cover with Hat Belt and Filter Carrying Case. [Online]. [Accessed 24 April 2018]. Available from: https://www.amazon.co.uk/Neewer%C2%AE-Colour-Filter-D7100-D7000-D5200-D5100-D5000-D3300-D3200-D3000-D90-D80-DSLR-

Cameras/dp/B00ZF3YU8U/ref=sr_1_1?s=electronics&ie=UTF8&qid=1523615347&sr=1
-1&keywords=neewer+52mm+colour+filter+set/

Newhall, B. 2006. *The History of Photography: From 1839 to the Present.* New York:
Bulfinch Press.

Newport Corporation. 2017. *Technical Note: Optical Materials*. [Online]. [Accessed 18
October 2017]. Available at:

https://web.archive.org/web/20171018085111/https://www.newport.com/n/optical-
materials/

NextEngine. 2016. *Products*. [Online]. [Accessed 28 October 2016]. Available from:

https://web.archive.org/web/20161028150556/http://www.nextengine.com:80/products

NextEngine. 2018. *Customer Support.* [Online]. [Accessed 17 December 2018].
Available from:

https://web.archive.org/web/20181217145723/http://www.nextengine.com/support/fast-
service/

Nicholson, P. and Henderson, J. 2000. Glass. In: Nicholson, P. and Shaw, I. ed. *Ancient
Egyptian Materials and Technology.* Cambridge: Cambridge University Press, pp.195 –
224.

Nikon. 2017. *D3100.* [Online]. [Accessed 25 July 2017]. Available from:

https://web.archive.org/web/20170725173059/http://www.europe-
nikon.com:80/en_GB/product/discontinued/digital-cameras/2015/d3100/

Nikon. 2018a. *AF-S DX Micro Nikkor 40mm f/2.8G*. [Online]. [Accessed 14 December 2018]. Available from:

https://web.archive.org/web/20181214133319/https://www.nikon.co.uk/en_GB/product/nikkor-lenses/auto-focus-lenses/dx/single-focal-length/af-s-dx-micro-nikkor-40mm-f-2-8g/

Nikon. 2018b. *AF-P DX Nikkor 18 – 55mm f/3.5 – 5.6G.* [Online]. [Accessed 29 December 2018]. Available from:

https://web.archive.org/web20181229150654/http://www.nikon.co.uk/en_GB/product/nikkor-lenses/auto-focus-lenses/dx/af-p-dx-nikkor-18-55mm-f-3-5-5-6g/

NitonUK. 2018. *Online conversation with Sales Representative*, 27 February.

Niven, L., Steele, T., Finke, H., Gernat, T. and Hublin, J. 2009. Virtual Skeletons: Using Structured Light Scanner to Create a 3D Faunal Comparative Collection. *Journal of Archaeological Science*. **36**(9), pp.2018 – 2023.

Noordam, J. and van den Broek, W. 2007. Clustering and Classification in Multispectral Imaging for Quality Inspection of Postharvest Products. In: Grahn, H. and Geladi, P. eds. *Techniques and Applications of Hyperspectral Image Analysis*. Chichester: John Wiley & Sons, Ltd, pp.43–67.

Nylén, E. 1978. The Recording of Unexcavated Finds: X-ray Photography and Photogrammetry. *World Archaeology*. **10**(1), p.88–93.

Opitz, R. 2015. Three Dimensional Field Recording in Archaeology: An Example from Gabii. In: Olson, B. and Caraher, W., eds. *Visions of Substance: 3D Imaging in*

Mediterranean Archaeology. Grand Forks, North Dakota: The Digital Press at The University of North Dakota, pp.73 – 86.

Optical Society of America. 1968. *The Science of Color*. Washington, D.C.: Optical Society of America.

Padfield, J., Saunders, D. and Malzbender, T. 2005. Polynomial Texture Mapping: A New Tool for Examining the Surface of Paintings. *ICOM Committee for Conservation Triennial Meeting*. pp.504 – 510.

Papadopoulos, J. 2005. Antiquity Depicted. In: Lyons, C. Papadopoulos, J., Stewart, L., and Szegedy-Maszak, A. eds. *Antiquity & Photography: Early Views of Ancient Mediterranean Sites.* London: Thames & Hudson, pp.104 – 147.

Paquin, R. 1995. Properties of Metals. In: Bass, M., van Stryland, E., Williams, D. and Wolfe, W. eds. *Handbook of Optics: Devices, Measurements and Properties, Volume II.* New York: McGraw Hill, pp.35.1 – 35.78.

Park, B., and Lu, R. 2015. *Hyperspectral Imaging Technology in Food and Agriculture*. New York: Springer.

Paul Scherrer Institute. 2016. *Frequently Asked Questions.* [Online]. [Accessed: 15 April 2016]. Available from: https://www.psi.ch/sls-techno-trans-ag/frequently-asked-questions/

Pawlowicz, Leszek. 2015. Creating a Portable Dome-RTI System for Imaging Lithics [Online]. [Accessed 27 March 2018]. Available from:

https://culturalheritageimaging.wordpress.com/2015/05/26/creating-a-portable-dome-rti-system-for-imaging-lithics/

Paynter, S. 2006. Analyses of Colourless Roman Glass from Binchester, County Durham. *Journal of Archaeological Science*. **33**(8), pp.1037 – 1057.

Peed, A. 1987. *Transmission of Wratten Filters*. [Online]. [Accessed 20 June 2016]. Available at: http://www.astrosurf.com/luxorion/Documents/transmission-wratten-filters.pdf/

Petrovic, A., Siebert, J. and Rieke, P. 1982. Soil Bulk Density Analysis in Three Dimensions by Computed Tomography Scanning 1. *Soil Science Society of America Journal*. **46**(3), pp.445 – 450.

Philipp, H. 1966. Optical Transitions in Crystalline and Fused Quartz. *Solid State Communications*. **4**(1), pp.73 – 75.

Phillips, J. 2005. "To Make the Dry Bones Live": Amédee Forestier's Glastonbury Lake Village. In: Smiles, S. and Moser, S. eds. *Envisioning the Past: Archaeology and the Image*. Oxford: Blackwell Publishing, pp. 72 – 91.

Phillips, P. 1955. American Archaeology and General Anthropological Theory. *Southwestern Journal of Anthropology*. **11**(3), pp.246 – 250.

Phillips, P. and Willey, G. 1953. Method and Theory in American Archaeology: An Operational Basis for Culture-Historical Integration. *American Anthropologist*. **55**(5): pp.615 – 633.

Pilarska, M. 2016. *False Colour Photogrammetry: Mapping Pigments in 3D*. Unpublished M.Sc. Dissertation. Glasgow School of Art.

Pinney, C. 2003. Introduction: "How the Other Half…". In: Pinney, C. and Peterson, N., eds. *Photography's Other Histories*. Durham: Duke University Press, pp.1 – 17.

Pirard, E. 2016. Multispectral Imaging of Ore Minerals in Optical Microscopy. *Mineralogical Magazine.* **68**(2), pp.323 – 333.

Protech Repairs. 2017. *Email to Protech Repairs,* 21 April.

Ramli, Z., Hassan Shuhaimi, N. and Abdul Rahman, N. 2009. Beads Trade in Peninsula Malaysia: Based on Archaeological Evidences. *European Journal of Social Sciences.* **10**(4), pp.585 – 593.

Rapantzikos, K. and Balas, C. 2005. Hyperspectral Imaging: Potential in Non-Destructive Analysis of Palimpsests. IEEE International Conference on Image Processing 2005. [Online]. [Accessed 20 April 2017]. Available from: https://ieeexplore.ieee.org/stamp/stamp.jsp?tp=&arnumber=1530131/

RCAHMS. 1982. *Argyll: An Inventory of the Monuments 4: Iona*. Edinburgh: Her Majesty's Stationery Office.

Rehren, T. 1997. Ramesside Glass-Colouring Crucibles. *Archaeometry*. **39**(2), pp.355 – 368.

Rehren, T. 2000. Rationales in Old World Base Glass Compositions. *Journal of Archaeological Science*. **27**, pp.1225 – 1234.

Rehren, T. 2001. Aspects of the Production of Cobalt-blue Glass in Egypt. *Archaeometry.* **43**(4), pp.483 – 489.

Rekrei. 2018. *Rekrei: A Summary.* [Online]. [Accessed 29 December 2018]. Available from: https://web.archive.org/web/20181229130010/https://projectmosul.org/about/

Remondino, F., El-Hakim, S., Girardi, S., Rizzi, A., Benedetti, S., and Gonzo, L. 2009. 3D Virtual Reconstruction and Visualization of Complex Architectures—The 3D-ARCH Project. *Proceedings of ISPRS International Workshop 3D-ARCH 2009 "3D Virtual Reconstruction and Visualization of Complex Architectures".* [Online]. [Accessed 24 April 2017]. Available from: https://pdfs.semanticscholar.org/cf87/2fdcede5f3860ff7928e6d0aaa6e4c58e74d.pdf/

Remondino, F. 2011. Heritage Recording and 3D Modeling with Photogrammetry and 3D Scanning. *Remote Sensing* **3**(6), p.1104 – 1138.

Renishaw. 2018. *A Basic Overview of Raman Spectroscopy.* [Online]. [Accessed 25 April 2018]. Available from: https://web.archive.org/web/20180425115315/http://www.renishaw.com:80/en/a-basic-overview-of-raman-spectroscopy--25805/

Richmond, I. 1950. Excavations at the Roman Fort of Newstead, 1947. *Proceedings of the Society of Antiquaries of Scotland.* **84**, pp.1 – 38.

Riggs, C. Shouldering the Past: Photography, Archaeology, and Collective Effort at the Tomb of Tutankhamun. *History of Science.* **55**(3): pp.336 – 363.

Robertshaw, P., Wood, M., Melchiorre, E., Popelka-Filcoff, R. and Glascock, M. 2010. Southern African Glass Beads: Chemistry, Glass Sources and Patterns of Trade. *Journal of Archaeological Science.* **37**, pp.1898 – 1912.

Roman, G., Inglis, C. and Rutter, J. 2010. Applications of Structured Light Imaging for High-Resolution Mapping of Underwater Archaeological Sites. *OCAENS'10 IEEE Sydney*. Pp.1 – 9.

Rowse, D. 2006. ISO Settings in Digital Photography. Digital Photography School. [Online]. [Accessed 9 August 2017]. Available at: https://web.archive.org/web/20170809202635/http://digital-photography-school.com:80/iso-settings/

Russell, M. 2016. *Email to Mark Russell of FARO,* 12 April.

Rutsky, R. 1999. *High Techne: Art and Technology from the Machine Aesthetic to the Posthuman.* Minneapolis: University of Minnesota Press.

Saitowitz, S. and Sampson, C. 1992. Glass Trade Beads from Rock Shelters in the Upper Karoo. *The South African Archaeological Bulletin.* **47**(156), pp.94 – 103.

Salonia, P., Negri, A., Valdarnini, L., Scolastic, S., and Bellucci, V. 2005. Quick Photogrammetric Systems Applied to Documentation of Cultural Heritage: The Example of Aosta Roman City Wall. *CIPA 2005 XX International Symposium, Torino, Italy.* [Online]. [Accessed 24 April 2017]. Available from: http://95.110.228.56/documentArchive/TechincalArticles/[ENG]_2003_quick%20photog

rammetric%20systems%20applied%20to%20documentation%20of%20cultural%20herita
ge%20the%20example%20of%20aosta%20roman%20city%20wall.pdf/

Santana Quintero, M. and Eppich, R. 2016. Introduction – Current Trends in Cultural
Heritage and Documentation. In: Stylianidis, E. and Remondino, F. eds. *3D Recording,
Documentation, and Management of Cultural Heritage*. Dunbeath, Scotland: Whittles
Publishing, pp.1 – 13.

Sayre, E. and Smith, R. 1973. Analytical Studies of Ancient Egyptian Glass. *Cairo Solid
State Conference, Cairo, United Arab Republic, 21 Apr 1973.* pp.2 – 22. [Online].
[Accessed 12 October 2018]. Available from:
https://inis.iaea.org/collection/NCLCollectionStore/_Public/05/124/5124330.pdf?r=1&r=
1/

Schott. 2017. *Bandpass Filters/NIR Cutoff Filters*. [Online]. [Accessed 2 June 2017].
Available at:
https://web.archive.org/web/20170602232317/http://www.schott.com:80/advanced_optics
/english/products/filteroverviewdetail-bandpass-bg-a.html/

Schroedter, E. 2016. *Email to Eva Schroedter of Creaform,* 11 April.

Scogings, D. 1978. The Experimental Recording of Petroglyphs and Archaeological Sites.
The Photogrammetric Record. **9**(51), pp.327 – 341.

Setchell, J., Charpentier, M., Abbott, K., Wickings, E. and Knapp, L. 2009. Is Brightest
Best? Testing the Hamilton-Zuk Hypothesis in Mandrills. *International Journal of
Primatology.* **30**: pp.825 – 844.

Setchell, J., Smith, T., Wickings, E. and Knapp, L. 2008. Social Correlates of Testosterone and Ornamentation in Male Mandrills. *Hormones and Behavior.* **54**, pp.365 – 372.

Shackley, M. 2011. X-Ray Fluorescence (XRF) Analysis in Archaeology. In: Shackley, M. ed. *X-Ray Fluorescence Spectrometry (XRF) in Geoarchaeology.* New York: Springer, pp.7 – 44.

Shanks, M. 1997. Photography and Archaeology. In: Molyneaux. B. ed. *The Cultural Life of Images: Visual Representation in Archaeology.* London: Routledge, pp.73 – 107.

Shelby, J. 2005. *Introduction to Glass Science and Technology*. Cambridge: Royal Society of Chemistry.

Shortland, A. 2002. The Use and Origin of Antimonate Colorants in Early Egyptian Glass. *Archaeometry.* **44**(4), pp.517 – 530.

Sigma. 2018. *APO Macro 180mm F2.8 EX DG OS HSM*. [Online]. [Accessed 29 December 2018]. Available from:
https://web.archive.org/web/20181229151926/https://www.sigmaphoto.com/apo-macro-180mm-f28-ex-dg-os-hsm/

Silios Technologies. 2018. *Cameras*. [Online]. [Accessed 9 October 2018]. Available from: https://www.silios.com/cms-pricing/

Silver, M. 2016. Conservation Techniques in Cultural Heritage. In: Stylianidis, E. and Remondino, F. eds. *3D Recording, Documentation, and Management of Cultural Heritage*. Dunbeath, Scotland: Whittles Publishing, pp.15 – 105.

Silvestri, A., Molin, G., and Saviulo, G. 2005. Sand for Roman Glass Production: An Experimental and Philological Study on Source of Supply. *Archaeometry.* **48**(3), pp.415 – 432.

Simmons, H. 1969. *Archaeological Photography*. London: University of London Press, Ltd.

Simply Bearings. 2018. *2mm Diameter Grade 100 Hardened 52100 Chrome Steel Ball Bearings*. [Online]. [Accessed 24 April 2018]. Available from: https://simplybearings.co.uk/shop/p35908/2mm-Diameter-Grade-100-Hardened-52100-Chrome-Steel-Ball-Bearings/product_info.html/

van der Sleen, W. 1973. *A Handbook on Beads*. York, Pennsylvania: George Shumway Publisher.

Smirniou, M. and Rehren, T. 2011. Direct Evidence of Primary Glass Production in Late Bronze Age Amarna, Egypt. *Archaeometry*. **53**(1), pp.58 – 80.

Smith, B. 2009. *Macro Photography for Beginners - Part 1*. [Online]. [Accessed 14 December 2018]. Available at: https://web.archive.org/web/20181214132021/https://digital-photography-school.com/macro-photography-for-beginners-part-1/

South, S. 1968. Photography in Historical Archaeology. *Historical Archaeology*. **2**, pp.73 – 113.

StellarNet, Inc. 2018. *Price List: Modular Spectrometers, Systems, Light Sources, Accessories, Software, & Services*. [Online]. [Accessed on 27 February 2018]. Available from: https://www.stellarnet.us/price-list/#raman785vial/

Szegedy-Maszak, A. 2005. Introduction. In: Lyons, C. Papadopoulos, J., Stewart, L., and Szegedy-Maszak, A. eds. *Antiquity & Photography: Early Views of Ancient Mediterranean Sites.* London: Thames & Hudson, pp.2 – 23.

Taylor, J., McManus, P., Murch, G., Rochat, R. and Weiman, N. 1991. *Display-Based Color System*. US4985853. 1991-01-15.

Tetley, C. and Young, S. 2007. Digital Infrared and Ultraviolet Imaging Part 1: Infrared. *Journal of Visual Communication in Medicine.* **30**(4), pp.162 – 171.

Tetley, C. and Young, S. 2008. Digital Infrared and Ultraviolet Imaging Part 2: Ultraviolet. *Journal of Visual Communication in Medicine.* **31**(2), pp.51 – 60.

The Physics Classroom. 2017a. *Light Absorption, Reflection, and Transmission*. [Online]. [Accessed 30 August 2017]. Available at: https://web.archive.org/web/20170830113928/http://www.physicsclassroom.com:80/class/light/Lesson-2/Light-Absorption,-Reflection,-and-Transmission/

The Physics Classroom. 2017b. *Natural Frequency*. [Online]. [Accessed 18 September 2017]. Available at: https://web.archive.org/web/20170918022503/http://www.physicsclassroom.com:80/Class/sound/u11l4a.cfm/

ThorLabs. 2018a. *1.4 Megapixel Scientific Cameras for Microscopy*. [Online]. [Accessed 9 October 2018]. Available from:

https://www.thorlabs.com/newgrouppage9.cfm?objectgroup_id=6592/

ThorLabs. 2018b. *8 Megapixel Scientific-Grade Cameras for Microscopy*. [Online]. [Accessed 9 October 2018]. Available from:

https://www.thorlabs.com/newgrouppage9.cfm?objectgroup_id=6540/

Tisato, F. and Parraman, C. 2014. An Investigation into the Micro Surface of Artworks Using Alternative Lighting Techniques. In: Segovia, M. V. O., Urban, P. and Allebach, J. P., eds. *Measuring, Modeling, and Reproducing Material Appearance*. USA: Society for Imaging Science and Technology and SPIE. [Online] [Accessed 29 October 2018]. Available from: https://www.spiedigitallibrary.org/conference-proceedings-of-spie/9018/901808/An-investigation-into-the-micro-surface-of-artworks-using-alternative/10.1117/12.2041209.full/

Tite, M., Pradell, T. and Shortland, A. 2008. Discovery, Production and Use of Tin-Oxide Opacifiers in Glasses, Enamels, and Glazes from the Late Iron Age Onwards: A Reassesment. *Archaeometry*. **50**(1), pp.67 – 84.

Trigger, B. 2006. *A History of Archaeological Thought.* Cambridge: Cambridge University Press.

Tringham, R. 2010. Forgetting and Remembering the Digital Experience and Digital Data. In: Borić, D. ed. *Archaeology and Memory.* Oxford: Oxbow Books, pp.68 – 104.

Turgeon, L. 2001. French Beads in France and Northeastern North America during the Sixteenth Century. *Historical Archaeology.* **35**(4), p.58 – 82.

Ulm, S., Vernon, K., Roberston, G. and Nugent, S. 2009. Historical Continuities in Historical Continuities in Aboriginal Land-Use at Bustard Bay, Queensland: Results of Use-Wear and Residue Analysis of Aboriginal Glass Artefacts. *Australasian Historical Archaeology.* **27**, pp.111 – 119.

University of Missouri Research Reactor. 2018. *Standard Rates for Archaeological and Geological Specimens by Neutron Activation*. [Online]. [Accessed 9 October 2018]. Available from: http://archaeometry.missouri.edu/StandardRates_NAA.html/

University of South Florida. 2018. *College of Arts and Sciences: Price List.* [Online]. [Accessed 27 February 2018]. Available from:
http://facilities.cas.usf.edu/geoanalysis/pricing/

UVIROPTICS. 2018a. *Hoya U-360 52mm (+ other sizes) x 2mm UV-Bandpass, Ultraviolet, Dual Band IR, Camera Filter*. [Online]. [Accessed 24 April 2018]. Available from: https://www.etsy.com/uk/listing/262984286/hoya-u-360-52mm-other-sizes-x-2mm-uv?ga_order=most_relevant&ga_search_type=all&ga_view_type=gallery&ga_search_query=hoya%20360&ref=sr_gallery-1-1/

UVIROPTICS. 2018b. *Schott S8612 52mm x 1mm thick UV/IR Cut Filter Visual Bandpass IR Suppress Hot Mirror*. [Online]. [Accessed 24 April 2018]. Available from:
https://www.etsy.com/uk/listing/287221717/schott-s8612-52mm-x-1mm-thick-uvir-cut?gpla=1&gao=1&&utm_source=google&utm_medium=cpc&utm_campaign=shopping_uk_en_gb_a-craft_supplies_and_tools-other&utm_custom1=1a9456ba-bf4d-4ba5-

b2ec-

61fe4cec645d&gclid=Cj0KCQjwqsHWBRDsARIsALPWMEN9a54XG3_bm1j5hbxbK1

LbB6WRQh0SBXgcaXNF6ImFbufDdDtHVykaAjdbEALw_wcB/

Verhoeven, G. 2016. Basics of Photography for Cultural Heritage Imaging. In:
Stylianidis, E. and Remondino, F. eds. *3D Recording, Documentation, and Management
of Cultural Heritage*. Dunbeath, Scotland: Whittles Publishing, pp.127 – 251.

Vinegar, H. and Wellington, S. Tomographic Imaging of Three-Phase Flow Experiments.
Review of Scientific Instruments. **58**(1), pp.96 – 107.

Voorips, A. 1984. Data Catchment Analysis and Computer Carrying Capacity: Notes on
Theory and Practice of the Use of Computer Systems in Archaeology. In: Mertlew, R. ed.
Information Systems in Archaeology. Gloucester: Alan Sutton, pp.45 – 53.

Walsh, P. 2012. Rise and Fall of the Post-Photographic Museum: Technology and the
Transformation of Art. In: Cameron, F. and Kenderdine, S. eds. *Theorizing Digital
Cultural Heritage: A Critical Discourse*. London: The MIT Press, pp.19 – 34.

Ward, C. 2015. *The Science of Shutters: How Camera Shutters Work*. [Online].
[Accessed 14 February 2018]. Available at:

https://web.archive.org/web/20180214012446/https://www.premiumbeat.com/blog/how-
camera-shutters-work/

Weber, G., Strivay, D., Martinot, L. and Garnir, H. 2002. Use of PIXE–PIGE Under
Variable Incident Angle for Ancient Glass Corrosion Measurements. *Nuclear Instruments*

and Methods in Physics Research Section B: Beam Interactions with Materials and Atoms. **189**(2002), pp.350 – 357.

Weitz, A. 2015. *A Guide to Filters for Lenses. B&H Explora*. [Online]. [Accessed 8 September 2017]. Available at:

https://www.bhphotovideo.com/explora/photography/buying-guide/guide-filters-lenses/

Westoby, M., Brasington, J., Glasser, N., Hambrey, M. and Reynolds, J. 2012. 'Structure-from-Motion' Photogrammetry: A low-cost, effective tool for geoscience applications. *Geomorphology.* **179**(2012), pp.300 – 314.

Wheadon, R. 1968. *The Principles of Light and Optics*. London: Longmans.

Whitehouse, D. 2000. Ancient Glass from ed-Dur (Umm al Qaiwain, U.A.E.) 2. Glass Excavated by the Danish Expedition. *Arabian Archaeology and Epigraphy.* **11**, pp.87 – 128.

Whittlesey, J. 1966. Photogrammetry for the Excavator. *Archaeology.* **19**(4), pp.273 – 276.

Wilkie, L. 1996. Glass-Knapping at a Louisiana Plantation: African-American Tools? *Historical Archaeology.* **30**(4), pp.37 – 49.

Willey, G. and Phillips, P. 1955. Method and Theory in American Archaeology II: Historical-Developmental Interpretation. *American Anthropologist.* **55**: pp.723 – 819.

Willey, G. and Phillips, P. 1958. *Method and Theory in American Archaeology*. London: The University of Alabama Press.

Williams, J. 2015. *Trapping Air Bubbles*. [Online]. [Accessed 11 September 2017]. Available at: https://www.youtube.com/watch?v=7hUz89_yLMg/

Wright, D. 2018a. *Conversation with Dene Wright*, 17 December.

Wright, D. 2018b. *Email from Dene Wright*, 17 December.

Wright, R. 1982. Archaeological Photography. In: Dever, W., and Lance, H. eds. *A Manual of Field Excavation: Handbook for Field Archaeologists.* New York: Hebrew Union College, pp.175 – 195.

Wright, W. 1958. *The Measurement of Colour*. London: Hilger & Watts.

Young, T. 1802. The Bakerian Lecture: On the Theory of Light and Colours. *Philosophical Transactions of the Royal Society of London.* **92**, pp.12 – 49.

Youngs, S. 1989. *'The Work of Angels': Masterpieces of Celtic Metalwork, 6th – 9th Centuries AD*. London: British Museum Publications Ltd.

Zhao, Z. and Li, K. 2006. A Photo-Modeling Approach to Restituting 3D Model Data from Single 2D Imagery for Rapid Prototyping of Artifact Products. *International Journal of Automation and Computing.* **3**(1), pp.69 – 75.

Zollikofer, C., Ponce de León, M., and Martin, R. 1998. Computer-Assisted Paleoanthropology. *Evolutionary Anthropology: Issues, News, and Reviews.* **6**(2), pp.41 – 54.

Zubrow, E. 2006. Digital Archaeology. In: Evans, T. and Daly, P., eds. *Digital Archaeology: Bridging Method and Theory*. London: Routledge, pp.10 – 31.